PAN ARCHIVES OF ACOUSTICS
Vol. **37**, No. 3, pp. 253–260 (2012)

DOI: 10.2478/v10168-012-0033-4

Multimodal Ultrasonic Imaging for Breast Cancer Detection

Jorge CAMACHO, Luis MEDINA, Jorge F. CRUZA, José M. MORENO, Carlos FRITSCH

Ultrasound for Medical and Industrial Applications Group (UMEDIA)
Spanish National Research Council (CSIC)
La Poveda (Arganda), 28500 Madrid, Spain; e-mail: j.camacho@csic.es

(*received January 20, 2012; accepted May 15, 2012*)

Ultrasound is used for breast cancer detection as a technique complementary to mammography, the standard screening method. Current practice is based on reflectivity images obtained with conventional instruments by an operator who positions the ultrasonic transducer by hand over the patient's body. It is a non-ionizing radiation, pain-free and not expensive technique that provides a higher contrast than mammography to discriminate among fluid-filled cysts and solid masses, especially for dense breast tissue. However, results are quite dependent on the operator's skills, images are difficult to reproduce, and state-of-the-art instruments have a limited resolution and contrast to show micro-calcifications and to discriminate between lesions and the surrounding tissue. In spite of their advantages, these factors have precluded the use of ultrasound for screening.

This work approaches the ultrasound-based early detection of breast cancer with a different concept. A ring array with many elements to cover 360° around a hanging breast allows obtaining repeatable and operator-independent coronal slice images. Such an arrangement is well suited for multi-modal imaging that includes reflectivity, compounded, tomography, and phase coherence images for increased specificity in breast cancer detection. Preliminary work carried out with a mechanical emulation of the ring array and a standard breast phantom shows a high resolution and contrast, with an artifact-free capability provided by phase coherence processing.

Keywords: ultrasound imaging, ultrasound tomography, breast cancer.

1. Introduction

Ultrasonic imaging is a common practice for medical diagnosis in many specialties from more than three decades. For early breast cancer detection, it is a technique that currently complements the information provided by a previous mammography, the standard screening technique. The aim of screening is detection of small and pre-invasive tumors in asymptomatic women to achieve a high rate of treatment success. However, since mammography measures tissue density, it produces a high level of false negatives in women with dense breasts and, since it uses ionizing radiation, the interval between examinations must be no less than one year, giving rise to the so-called interval cancer (Berry *et al.*, 2005).

Current ultrasound practice is based on echography, where the operator positions by hand the transducer over the patient's body. Ultrasound has many advantages over other imaging techniques like X-rays, TAC, MRI, PET, etc. because it uses non-ionizing radiation, provides high-contrast real-time images, equipment is less expensive, and its application is pain-free. Furthermore, with regard to mammography, ultrasound images allow a cleaner distinction between fluid-filled cysts and solid masses. But, in spite of their advantages, current ultrasound technology and procedures have limitations that, following international guidelines, have precluded its use as a screening tool for breast cancer. The main reasons are the sensitivity dependence on the operator skills, the difficulty for imaging and registering the whole breast, and the lack of resolution to detect micro-calcifications (Teh, Wilson, 1998).

The first two limitations are due to the operational procedure. Images are taken by hand from different orientations, which makes it difficult to obtain repeatable results in a historical perspective. Also, the detection and location of a tumor greatly depends on the operator's experience. Moreover, reflectivity ultrasound images display differences in the acoustic impedance of tissues, which may be subtle, with low specificity

for tumor distinction from the surrounding healthy tissue. This way, ultrasound is just used as a complementary technique to mammography (Nothacker *et al.*, 2009).

However, some recent developments try to overcome these limitations with automatic imaging systems based on ring transducers with a large amount of elements. The ring array surrounds a hanging breast immersed in a water-bath (Stozka *et al.*, 2004; Waag *et al.*, 2006; Duric *et al.*, 2007). With this circular geometry, slice images at coronal planes are acquired. Moving the ring array vertically one can obtain a volumetric image (Fig. 1a). This arrangement avoids the problems associated with scanning the transducer by hand, so that the images are repeatable. The circular geometry provides an increased resolution which may be determined by the signal bandwidth instead of the aperture size. This is useful to improve the detection of micro-calcifications.

a)

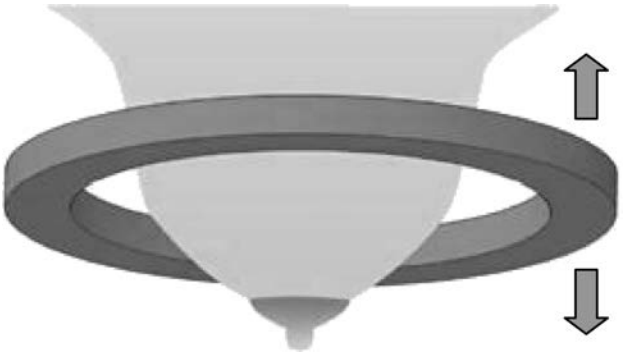

b)

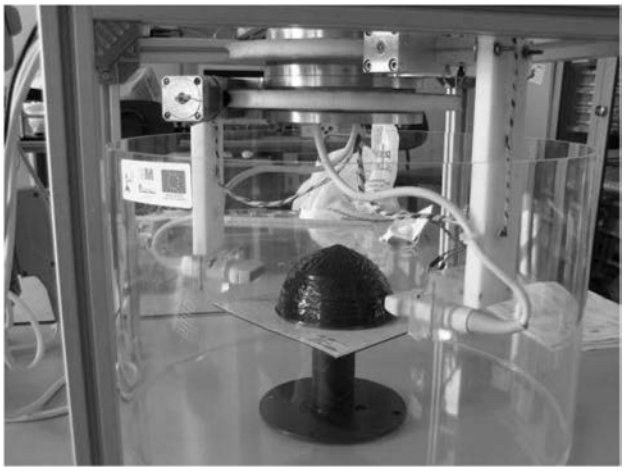

Fig. 1. a) Concept for breast imaging in real-time based on a circular array with thousands of elements, b) experimental arrangement with mechanically rotated conventional arrays.

On the other hand, other imaging modalities may provide increased specificity for breast cancer detection, as it has been shown with ultrasound velocity transmission tomography (Li *et al.*, 2008). One of its advantages is that it provides quantitative data of the whole breast, and transmission measurements are independent of echo images.

A recent achievement of our group provides an improved resolution and contrast for ultrasonic images by means of *phase coherence processing* (Camacho *et al.*, 2009). Furthermore, this technique complements the others by suppressing grating lobes, sidelobes, and reverberation artifacts.

This work presents a low-cost arrangement to experiment with different imaging modalities. A standard breast-mimic phantom that includes low and high scatterer density cysts and micro-calcifications is used for imaging. To avoid the expenses of a ring array with thousands of elements standard 128-element arrays have been used for this preliminary study. The arrays are mechanically rotated to emulate a circular aperture (Fig. 1b). Commercial equipment with pulse-echo and transmission capability is used for the experiments. This arrangement allows easy testing of different ultrasound imaging modalities at the expense of a rather large acquisition time.

2. Imaging modalities with circular arrays

Conventional echography uses linear or slightly curved arrays of N independent transducer elements. Beam steering and focusing is carried out by electronic means, using a set of fixed delays for the individual excitations and dynamically changing the delays for the signals received by every element. This is the standard *phased array* technique that provides images in real time and, in practice, the only ultrasonic imaging modality used for diagnostic purposes. However, with a circular array surrounding the inspected body, several other modalities are possible, in particular: *synthetic aperture*, *transmission tomography*, and *phase coherence imaging*. All these methods, described in this section, are being implemented in the present system and are the basis of our multi-modal approach. Finally, in section 5, first results with *phased array image compounding* and *phase coherence imaging* are presented.

2.1. Phased array and image compounding

Phased array image quality is limited by several factors. First, while dynamic focusing is applied in reception, focusing in emission is performed at a single depth to keep a relatively high frame rate. Thus, resolution is better at the focus proximities.

Second, the lateral resolution Δx improves with the aperture size D:

$$\Delta x = k\frac{\lambda}{D}z, \tag{1}$$

where k is a constant (≈ 1), λ is the wavelength, and z is depth. Therefore, the larger the aperture, the better the resolution. But, to avoid grating lobe artifacts,

the distance d between elements must be kept below $\lambda/2$, so that a high number N of elements and associated electronic channels is required to obtain a large aperture $D = N \cdot d$.

Third, the sidelobes level limits the contrast and dynamic range of phased-array images. Apodization techniques help to reduce their impact at the expense of some losses in the lateral resolution (Szabo, 2004). On the other hand, a single phased array image composed of L scan-lines over a length z can be acquired and processed in a time,

$$T_P = \frac{2z}{c} L. \tag{2}$$

For $z = 150$ mm, $c = 1.5$ mm/μs, and $L = 150$, the acquisition time is $T_P = 30$ ms and the frame rate that can be reached is 33 images/s (real-time imaging).

The phased array technique can be advantageously used in a circular geometry. A large set of sector images with active apertures at different angular positions can be averaged in the overlapping region to form the final image (Fig. 2). This process is known as *image compounding* and has been previously used with conventional arrays, getting contrast improvements and clutter reductions (Jespersen *et al.*, 1998).

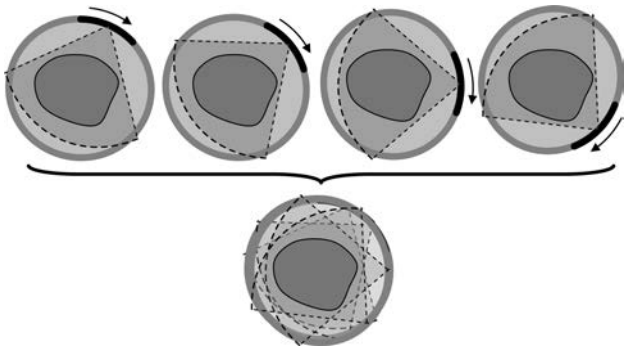

Fig. 2. Compound image built from sector phased array images with a circular array geometry.

A time $T_C = n \cdot T_P$ is required to acquire a single compound slice image built from $n$phased array images taken at $360°/n$ angular intervals. This takes about 0.5 s per slice image with the above parameters and $n = 16$. By vertically moving the ring array a set of 120 slices can be obtained in 60 seconds, which is a rather high time interval for the clinical use. However, since the results are obtained in real-time, the operator can set the vertical position of the ring array for zooming and looking for details. This is useful for *in-situ* diagnostics and deciding whether further explorations or proofs are necessary.

2.2. Synthetic aperture techniques

Another approach is based on *synthetic apertures*. The "gold standard" is *the synthetic transmit aperture* or STA. A single or a reduced set of elements generate an omnidirectional wavefront. The whole N-elements aperture is used in reception, and a *low-resolution image* is obtained by compensating the time-of-flight differences from the emitter to every imaged point and back to each receiver element. This process is repeated N times, changing the position of the emitter. Adding together the low-resolution images yields an image focused in emission and reception with a high resolution and contrast (Trots *et al.*, 2010). The cost of this technique is the huge data volume generated and the requirements for a high performance hardware. The current technology does not allow obtaining the STA gold standard in real time (Jensen *et al.*, 2005).

Various approaches that are based on the effective aperture concept allow reducing the number of emissions, so that the frame rate can be increased with regard to the phased array technique, while preserving a high resolution and dynamic range, at the cost of a reduced signal-to-noise ratio (Nikolov, Behar, 2005). Some of these alternatives also reduce the number of receiving elements, which achieves real-time imaging with the use of GPUs (Romero *et al.*, 2009).

Synthetic aperture techniques can also be applied in a circular geometry (Fig. 3) with further resolution improvements. The combined effect around 360° approaches the radial resolution Δz of every partial image. In fact, given by the transducer bandwidth B:

$$\Delta z \approx \frac{c}{2B} \approx \lambda. \tag{3}$$

Differently from (1), this equation yields a depth-independent resolution. Moreover, for $z{>}D$ (that is, $F\# > 1$), Eq. (3) yields a better resolution than (1). To this purpose, the image is progressively formed in a rectangular grid using the analytic signal to preserve the phase information, so that constructive and destructive interferences take place at building the final image.

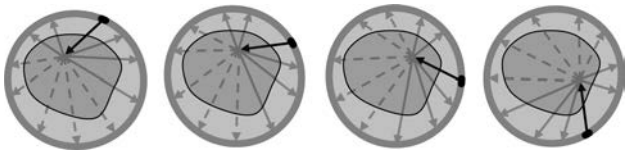

Fig. 3. STA imaging: a small aperture is used for omnidirectional emission and a large one for reception. The analytical signal corresponding to the time-of-flight from the emitter to every image pixel and to every receiving element is obtained. Then, the emitter aperture is moved by an angular interval and the process repeated. The final image results by averaging all the partial images.

The acquisition time for every low-resolution image is,

$$T_S = \frac{2z}{c}. \tag{4}$$

With the parameters given, each low-resolution image is acquired in 0.2 ms. Taking these images at 0.5° intervals around the circle, the acquisition time for a slice is 144 ms (composition of 720 low-resolution images). To get the full volume of 120 slices, a total time lower than 18 seconds is required. This is a good figure for the clinical use.

However, there are also other associated costs. The computing time and data volume have not been considered in the previous calculation. In a circular image of a 150 mm diameter with the resolution of 0.1 mm there are about 1.8 Mpixels. Using receiving apertures of $N = 256$ elements, every partial image requires processing 460 MS (complex samples) with the delay-and-sum algorithm. A slice composed from 720 low-resolution images requires processing of around 330 GS, and the whole volumetric image amounts for 40 TS. Processing and storing this huge information volume can take much longer than the acquisition time, even if a specialized hardware is used to accelerate the process.

On the other hand, at 0.5° intervals in a ring transducer of a 100 mm radius, the distance between emitters is about 0.9 mm, which represents 6λ for a 5 MHz frequency transducer. As the inter-element distance must be kept below $\lambda/2$ to avoid grating lobes, the number of array elements should be $N \approx 4200$. As a solution of this problem, techniques based on the effective aperture concept could be explored to obtain an equivalent dense circular aperture with fewer electronic channels but the same high number of array elements.

Phase coherence processing which suppresses grating lobes, as it is explained below, may be a better alternative. If the inter-element pitch is increased from $\lambda/2$ to approximately 2λ, the number of elements and associated electronic channels is reduced by four (for example, to 1024 channels). This is beneficial to lower the implementation costs, as well as to reduce the data volume involved in the acquisitions.

2.3. Transmission tomography

Finally, the third imaging modality is transmission *tomography*. In this case, two opposing apertures are used in a through-transmission mode, one acting as the emitter and the other as receiver (Fig. 4). The emitter is created by a reduced set of array elements to produce a fan-beam illuminating the inspected body. The time-of-flight from emission to reception is recorded at every element of the opposite receiving aperture. This is repeated many times changing the angular position to cover the 360° circumference, keeping both apertures in opposite sides.

Computed tomography algorithms, modified to take into account ultrasound refraction with changes in the propagation velocity, are applied to obtain velocity images (Quan, Huang, 2007).

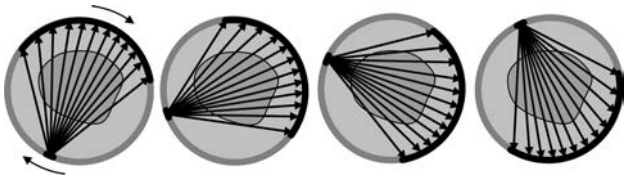

Fig. 4. Ultrasound transmission tomography arrangement with fan-beams.

Basically, for straight-ray paths, a rectangular grid is defined with M cells small enough to consider constant the propagation velocity within the cell. If the total number of rays generated around the circle is N, the time-of-flight of the ray i is,

$$T_i = \sum_{j=1}^{M} l_{ij} b_j, \tag{5}$$

where b_j is the inverse of the sound velocity at cell j (*slowness*), and l_{ij} is the length of the ray i when crossing the cell j, which is frequently set to one if the ray crosses the cell or to zero if it does not. This is a system of N equations with M unknowns $\{b_j\}$, where usually $N > M$, that can be solved by the least squares method. Numerical techniques to avoid the ill-conditioned equations (the values of T_i are large and those of l_{ij} are small) must be applied and a subset of equations can be used (Duric *et al.*, 2005). In order to take into account the ray bending due to refraction, an iterative procedure is followed, progressively refining the slowness values found for every cell (Li *et al.*, 2008).

Acquisition time for ultrasound tomography depends only on the number of emissions if parallel receiving channels are available. For 360° emissions (at intervals of 1°) with a ring array of 200 mm diameter, a single slice can be acquired in less than 60 ms. This way, the volumetric data of 120 slices would take about 7 seconds, which is a very good figure for the clinical use.

2.4. Phase coherence imaging

Phase coherence imaging (PCI) yields an image of the phase concentration of the received signals after application of the focusing delays (*aperture data*). PCI can be used with the phased array, as well as with the synthetic aperture modalities by providing, at every pixel, a coherence factor with values in the range [0, 1] (Camacho *et al.*, 2009).

Basically, it measures the focus quality so that, when the received signals originated at the focus, the coherence factor approaches unity, while for the out-of focus signals it tends to zero. This way PCI is insensitive to side and grating lobes, as well as to reverberations, since these indications are produced in regions far away from the focus. By the way, this reduces the main-lobe width, which also improves resolution.

PCI image itself is useful to show weak reflectors immersed in clutter (like micro-calcifications), since the coherence factor does not depend on the reflected signal amplitudes and, the clutter, originated by unresolved scatterers in the range cell, is simultaneously reduced. Besides, PCI improves the resolution and contrast of the phased array and synthetic aperture images by weighting the output of these beamformers.

Its operation does not require additional acquisition time when jointly used with the phased array or with synthetic aperture techniques, since a specific hardware can obtain the coherence factors in real-time.

3. Experimental arrangement

A first experimental arrangement is presented in Fig. 1b, where a cylindrical tank, two independent arms holding linear 128-element arrays of 5 MHz (Prosonic, Korea) and a breast phantom (Gammex-RMI, USA) are shown. Independent circular movement is provided by means of worm and wheel attachments driven by stepper motors that offer a high mechanical resolution (0.1°) and low hysteresis. The motors were individually controlled by our own designed drivers with the USB interface. Both array arms can be independently and freely moved with the limitation that their relative angular distance cannot be less than 30° because they lie in the same plane. Figure 5 shows a schematic representation.

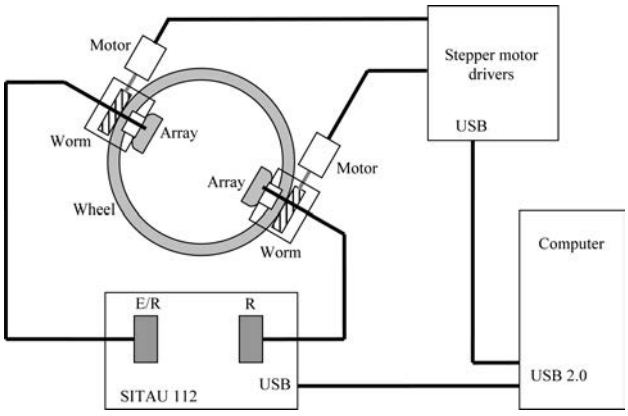

Fig. 5. Schematic representation of the experimental arrangement.

A phased array SITAU 112 system (Dasel, Spain), with 128 pulse-echo and transmission channels in parallel, was used to acquire and process the ultrasonic data. This instrument is connected to a computer by means of an USB-2.0 interface. The computer receives and further processes data provided by the ultrasonic equipment with programs written in MATLAB (The Mathworks, USA) that also control motor movements.

This arrangement can be used to emulate a ring array composed of thousands of elements at low-cost, but without high frame-rate capabilities. However, since the arrays are linear, the emulated geometry is not circular but polygonal. This has little importance as long as the accurate position of every element is known. This requires a calibration procedure that, anyway, must be also followed for circular arrays to compensate for possible manufacturing gaps and tolerances. Furthermore, a polygonal ring composed of independent linear arrays may be less expensive than a single circular array. Also, such an arrangement is easier and cheaper to maintain if dead elements appear by simple substitution of the damaged array.

4. Calibration procedure

Precise knowledge of all operating parameters is essential to obtain high quality images. In particular, the sound velocity in the coupling medium (water) must be accurately evaluated, as well as the positions of all the array elements with regard to a reference coordinate system. Since the mechanics is precise, circular movement can be assumed, although with an unknown radius.

The calibration takes place in two steps. First, the sound velocity is evaluated using a phantom composed of two parallel 0.1 mm diameter copper wires ($\lambda/3$ at 5 MHz). The distance between the wires is accurately known and a base plate assures their vertical position. This phantom is set alone in an arbitrary position of the tank filled with water.

Using a single element of an array in pulse-echo, a search is performed to find the angular position where the time interval between both wire echoes is at maximum. In this situation the element and wires are aligned, and the sound velocity is obtained as double the wire distance divided by the time interval among echoes.

The second step determines the element positions. To this purpose, it is enough to find the radius R to the array center and the angle β formed by the radius and the normal to the array (Fig. 6). At this stage it is assumed that the nominal array mechanical characteristics are accurate enough (possible deviations lower than $\lambda/10$).

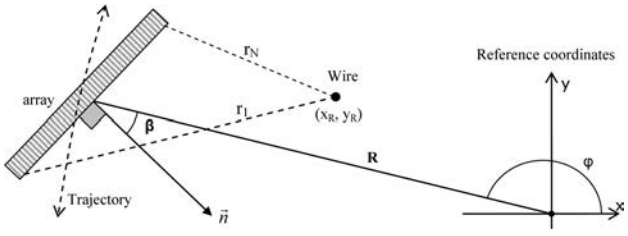

Fig. 6. Arrangement for the calibration of the array element positions.

To this purpose a single 0.1 mm copper wire normal to the array plane is put at an arbitrary position. Its unknown coordinates with regard to the absolute

reference are (x_R, y_R), assumed at the circumference centre. The distance from element i to the wire is:

$$r_i^2 = (x_i - x_R)^2 + (y_i - y_R)^2 = \left(\frac{ct_i}{2}\right)^2, \qquad (6)$$

where t_i is the measured round time-of-flight to the target and c is the sound velocity. On the other hand, the element coordinates are given by:

$$x_i = R\cos\varphi + \left(i - \frac{N-1}{2}\right) d\cos\left(\varphi - \beta - \frac{\pi}{2}\right),$$
$$y_i = R\sin\varphi + \left(i - \frac{N-1}{2}\right) d\sin\left(\varphi - \beta - \frac{\pi}{2}\right), \qquad (7)$$
$$\leq i \leq N,$$

where φ is the absolute angular position of the array centre, which is accurately known, N is the array number of elements and d is the distance between elements.

Substitution of (7) in (6) provides a set of N nonlinear equations with 4 unknowns (R, β, x_R, y_R) which can be solved by numerical methods. However, although the equation system is over-dimensioned, the measurements of the round trip time of flight are quite related to yield accurate results. But, repeating the measurements in several angular positions (changing φ) and the wire position (changing x_R, y_R) provides a larger variability on the t_i values, which yields better results for R and β. It was found experimentally that using 8 angular positions of the array (every 45°) and 4 positions of the reflector (one at every quadrant) repeatable results are obtained. By taking just the time of flight to the extreme elements, the system is composed of 64 equations with 10 unknowns and is solved by numerical methods. This procedure considers R and β constants independent of the angular position of the array. Care was taken to avoid array displacements when rotating due to, for example, the cable tension.

5. First results

Preliminary experiments were conducted to assess the performance of the proposed arrangement. Up to now, only three imaging modalities were used: phased array, image compounding and phase coherence processing. Algorithms for transmission tomography and synthetic aperture techniques are under development.

A standard medical-grade breast phantom designed to train operators for biopsies was used for the experiments (Gammex-RMI, USA). It includes reflectors and high and low scatterer density objects to mimic microcalcifications, masses and cysts. A schematic representation of the phantom at the image plane is shown in Fig. 7.

Images were obtained in the phased array mode from 36 angular positions (at 10° intervals), using the full 128-element aperture for every position. Figure 8 shows four of the phased array images (at angular positions of 0°, 80°, 140°, and 240°), which give partial views of the breast phantom.

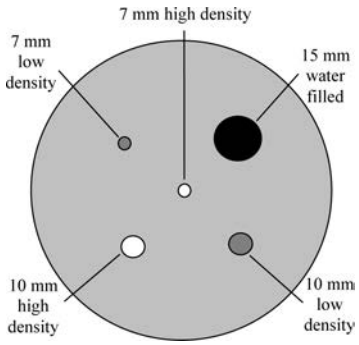

Fig. 7. Scheme of the breast phantom with high and low density scatterers' cylindrical objects.

It can be appreciated that clutter and sidelobes are rather high in the phased array imaging mode, thus, limiting the reliable detection of lesions. The diagnostics is not easy, since only a partial region of the breast phantom is seen. Finally, if taken by hand, it is difficult to reproduce any of these images.

However, when combining the 36 phased array images acquired with the circular arrangement, a full 360° view is obtained (Fig. 9). Image is shown with a 50 dB dynamic range. It can be appreciated that cysts and masses are clearly identified, as well as microcalcifications. Also, their positions are easily determined.

The resolution agrees with the theoretically expected one. Furthermore, the contrast to noise ratio (CNR) improves by image compounding, as it has been previously found by other researchers.

However, some of the reflectors that mimic microcalcifications are not well resolved over the clutter floor. Also, around the centre of the image, there are some artifacts that are due to reverberations between the "skin" and the transducer. These could be confused with tissue structures in a real examination.

Figure 10 shows a detail of the central region. At left (compounded image), the reverberation artifacts are clearly visible. Also, some of the microcalcifications show a low contrast with regard to the clutter floor level. At right, the phase coherence image of the same region is shown, where the artifacts have been suppressed and the micro-calcifications are made more evident, with a high contrast and resolution.

On the other hand, the phase coherence image alone shows a darker central region. This is due to the single focus in emission of the phased array technique, which was set halfway between the phantom centre and the perimeter in this experiment (25 mm from the center). As the emitted beam is narrow in this region, the range cell becomes thinner, which increases the scatterers coherence and hence, the phase coherence value. With synthetic aperture techniques, where emission and reception focusing is applied at all

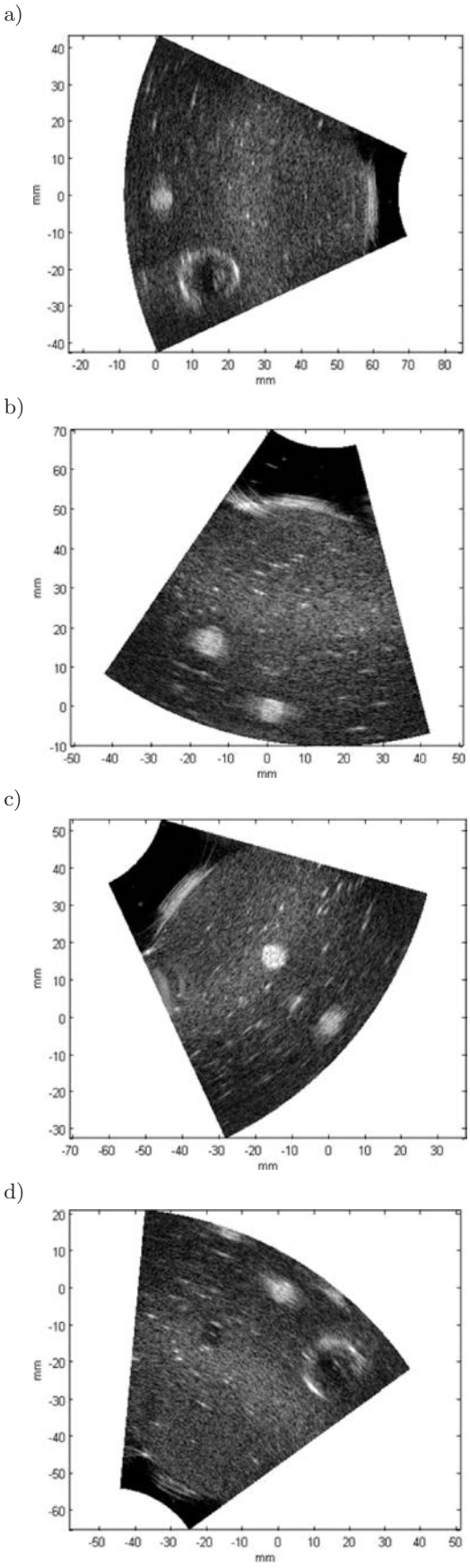

Fig. 8. Four phased array images, taken at angular positions 0°, 80°, 140°, and 240°.

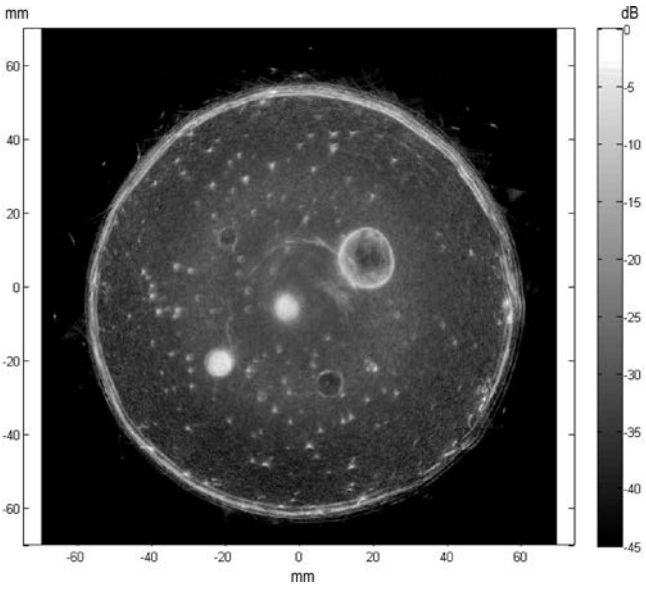

Fig. 9. Compound image of the breast phantom.

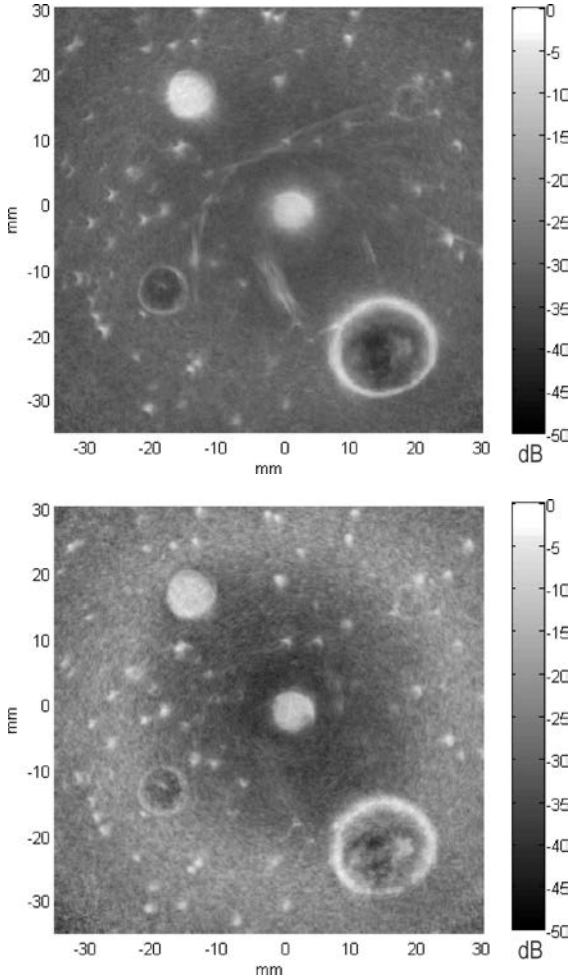

Fig. 10. Top: detail around the centre of the compound image, showing the artifacts and low-contrast to detect some micro-calcifications, bottom: phase coherence image of the same region, where the artifacts have been suppressed and the micro-calcifications get highlighted.

the imaged points, it is expected to achieve a lower clutter (better contrast) and higher resolution.

6. Conclusions

This work has been carried out to test the possibilities of ultrasound for detecting breast cancer by means of a circular geometry and multiple imaging modalities. Preliminary results with a low-cost, low frame-rate mechanical moving hardware and a standard breast phantom have been obtained using phased array, compound, and phase coherence imaging modalities. This arrangement has shown the capabilities for detecting cysts, solid masses, and micro-calcifications. A calibration procedure was required to accurately obtain the operational parameters (sound velocity in the coupling medium and position of the array elements).

It has been demonstrated that, with conventional phased array technology, slice images with reduced clutter and improved contrast-to-noise ratio are obtained by compounding many sector images taken from different angular positions. Further, phase coherence images are artifact free and provide an increased resolution and contrast. The phase coherence image information complements that of the compound image, and both can be combined by a simple multiplication.

These results indicate that a ring array surrounding a suspended breast is a good choice to improve sensitivity, resolution, and contrast for breast cancer detection. Furthermore, it provides volumetric information by taking many image slices. These images are repeatable to follow up the patient evolution after successive examinations at the prescribed periods. Also, the acquisition time for different modalities and volumetric imaging has been estimated, ranging from a few seconds to around one minute.

Acknowledgment

This work was jointly supported by the projects DPI-2010-17648 of the Spanish Ministry for Science and Innovation and S2009/DPI-1802 of the Community of Madrid. Part of this work was presented at Tecniacústica-2011 (26–28 Oct, Cáceres, Spain).

References

1. Berry D.A., Cronin K.A., Plevritis S.K., Fryback D.G., Clarke L., Zelen M., Mandelblatt J.S., Yakovlev A.Y., Habbema J.D., Feuer E.J. (2005), *Effect of screening and adjuvant therapy on mortality from breast cancer*, N. Engl. J. Med, **353**, 17, 1784–1792.
2. Camacho J., Parrilla M., Fritsch C. (2009), *Phase Coherence Imaging*, IEEE Trans. on UFFC, **56**, 5, 958–974.
3. Duric N., Littrup P., Babkin A., Chambers D., Azevedo S., Pevzner R., Tokarev M., Holsapple E., Rama O., Duncan R. (2005), *Development of ultrasound tomography for breast imaging: Technical assessment,* Med. Phys., **32**, 5, 1375–1386.
4. Duric N., Littrup P., Poulo L., Babkin A., Pevzner R., Holsapple E., Rama O., Glide C. (2007), *Detection of breast cancer with ultrasound tomography: First results with the Computed Ultrasound Risk Evaluation (CURE) prototype*, Med. Phys., **34**, 773.
5. Jensen J.A., Holm O., Jensen L.J., Bendsen H., Nikolov S.I., Tomov B.G., Munk P., Hansen M., Salomonsen K., Hansen J., Gormsen K., Pedersen H.M., Gammelmark K.L. (2005), *Ultrasound Research Scanner for Real-Time Synthetic Aperture Data Acquisition*, IEEE Trans. UFFC, **52**, 5, 881–891.
6. Jespersen S.K., Wilhjelm J.E., Sillesen H. (1998), *Ultrasound Spatial Compound Scanner for Improved Visualization in Vascular Imaging*, Proc. 1998 IEEE Ultrasonics Symposium, 1623–1626.
7. Li C., Duric N., Huang L. (2008), *Breast Imaging Using Transmission Ultrasound: Reconstructing Tissue Parameters of Sound Speed and Attenuation*, 2008 Conf. on Biomed. Engineering and Informatics, 708–712.
8. Nikolov M., Behar V. (2005), *Analysis and optimization of synthetic aperture ultrasound imaging using the effective aperture approach*, Int. J. Information Theory & Applications, 12, 257–265.
9. Nothacker M., Duda V., Hahn M., Warm M., Degenhardt F., Madjar H., Weinbrenner S., Albert U.S. (2009), *Early detection of breast cancer: benefits and risks of supplemental breast ultrasound in asymptomatic women with mammographically dense breast tissue*, BMC Cancer, **9**, 335,
10. Quan Y., Huang L. (2007), *Sound-speed tomography using first-arrival transmission ultrasound for a ring array*, Proc. SPIE Medical Imaging, 6513, 651306-1-9.
11. Romero D., Martinez–Graullera O., Martin C.J., Higuti R.T., Octavio A. (2009), *Using GPUS for beamforming acceleration on SAFT imaging*, Proc. IEEE Ultrason. Symp., 1334–1337
12. Stozka R., Widmann H., Müller T.O. (2004), *Prototype of a new 3D ultrasound computer tomography system: transducer design and data recording*, Med. Imag, 5373, 70–79.
13. Szabo T.L. (2004), *Diagnostic ultrasound imaging*, Elsevier Academic Press.
14. Teh W., Wilson A.R.M. (1998), *The role of ultrasound in breast cancer screening. A Consensus Statement by the European Group for Breast Cancer Screening*, European Journal of Cancer, **34**, 4, 449–450.
15. Trots I., Nowicki A., Lewandowski M., Tasinkevych Y. (2010), *Multi-Element Synthetic Transmit Aperture in Medical Ultrasound Imaging*, Archives of Acoustics, **35**, 4, 687–699.
16. Waag R.C., Fedewa R.J. (2006), *A Ring Transducer System for Medical Ultrasound Research*, IEEE Trans. on UFFC, **56**, 5, 958–974.

PAN ARCHIVES OF ACOUSTICS
Vol. **37**, No. 3, pp. 261–268 (2012)

DOI: 10.2478/v10168-012-0034-3

Application of Acoustic Emission Method to Determine Critical Stress in Fibre Reinforced Mortar Beams

Zbigniew RANACHOWSKI, Daria JÓŹWIAK–NIEDŹWIEDZKA,
Andrzej M. BRANDT, Tomasz DĘBOWSKI

Institute of Fundamental Technological Research, Polish Academy of Sciences
Pawińskiego 5B, 02-106 Warszawa, Poland; e-mail: {zranach, djozwiak, abrandt, tdebow}@ippt.pan.pl

(*received March 12, 2012; accepted May 16, 2012*)

The objective of this investigation was to test the effectiveness of the Acoustic Emission (AE) measurements in determining the critical stresses during four-point bending of mortar beams. Within the measuring procedure the parameter σ_{cr}/σ_{300} was calculated and analysed. Additionally, the influence of cement replacement by high calcium fly ash (HCFA) on the process of crack healing was discussed. Mortar beams with different content of HCFA and reinforced by steel microfibres were prepared for tests. After curing in standard conditions the beams were subjected to four-point bending test in order to introduce the pre-cracking. Thereafter the beams were cured in the lime water and loaded after 56 and 112 days in the same way as for the first time. Additionally the microstructure of mortars was studied in a stereo optical microscope as well in an electron scanning microscope including the Energy Dispersive X-ray analysis (EDX). The results of microstructural characterization of mortar containing HCFA from lignite combustion are presented. The applied load level slightly exceeded the critical stress, producing intense crack growth processes however did not significant affected the load capacity of the beams. During the consecutive loading the decreasing tendency of σ_{cr}/σ_{300} ratio was noted. The obtained results confirm that the latter parameter can be applied as a measure of the composite degradation level for the elements carrying the repeated loads of amplitude close to the critical stress of the structure and also that the cement replacement with HCFA influences the process of crack healing.

Keywords: critical stress, Acoustic Emission, microcracking, self-healing, concrete microstructure, fly ash.

1. Introduction

The concrete structures are subjected to static or dynamic load and environmental interaction what collectively evoke the continuous processes of structural degradation. These processes include: loss of load bearing capacity, evolution of crack systems, deflections and deformations. The cumulation of defects imply the growth of cracks leading to the catastrophic loss of structural integrity. The effects of formation and propagation of defects significantly influence the strength and durability of concrete elements (Golewski, Sadowski, 2007; Marks M. *et al.*, 2012).

During exploitation of real structures the opposite effect to crack growth is also observed. The phenomenon of self-healing (self-regeneration, autogenous healing) in cementitious composite materials was discovered many years ago. First test results on the self-healing of cracks in concrete were published by Abrams (1917). The large study of the effect mentioned above delivered (Kasperkiewicz, Stroeven, 1991) who tested plain concrete beams with a central notch and recorded Crack Opening Displacement (COD). The results proved considerable influence of initial value of the preliminary crack width and only in fine microcracks appreciable healings were observed: for COD exceeding 0.3 mm only approx. 10% of recovery was stated. In recent papers (Qjan *et al.*, 2010) these results have been confirmed. Mor *et al.* (1989) measured crack healing in lightweight concrete. Schiess, Reuter (1992) observed influence of crack healing on permeability of reinforced concrete elements. Cracks caused by freeze/thaw cycles were healed in tests by Jacobsen, Sellevold (1996), Reinhardt, Jooss (2003) determined progress of healing in relation to temperature and crack width.

Şahmaran *et al.* (2008) observed crack healing in concrete with high volume of standard fly ash of Class F, while Wenhui *et al.* (2008) confirmed the influence of damage degree on healing of cracks in concrete.

Possibility of self- healing of cracks in the elements subjected to water flow was confirmed by Hosoda *et al.* (2009). Several investigations concerned self-healing in high performance concretes (Granger *et al.*, 2009) – the results of self-healing in ultra high performance concrete with water to cement ratio $w/c = 0.2$ were modelled. After curing period of 20 weeks in water, healing was observed after load-deflection curves and acoustic emission records. Comparative tests with concretes of w/c equal to 0.35 and 0.48 did not show any self-healing.

On the basis of the research cited above it may be concluded that self-healing is reported to definitely exist in cementitious composites and to influence their strength, rigidity and density, although this high potential is not explicitly employed in any design code of practice. It is believed that the self-healing of microcracks in elements subjected to bending is particularly important from practical viewpoint, because in most cases the concrete and reinforced concrete elements are used in that state of stress (Gray, 1984; Hannant, Edgington, 1975; Hannant, Keer, 1983). At the preliminary stage of degradation the damages in the bulk of the concrete elements are possible to detect only with the application of sophisticated techniques, including acoustic methods (Hoła, 1999; Ohtsu, 1996; Yuyama, Ohtsu, 2000). The most common example is using Acoustic Emission for crack formation monitoring in mechanically loaded objects (Arrington, Evans, 1977; Ouyang *et al.*, 1991). In the research presented in (Ruesch, 1959; Ranachowski *et al.*, 2009) a remarkable progress of AE signal activity was reported related to the increase of mechanical load applied to compressed or flexured specimens made of materials with brittle matrix. Due to auxiliary tensometric measurements it could be noted that at certain stress level applied to an element a local increase of volume of damaged section is recorded due to the crack growth. The effect appears when ca. 75% of ultimate stress was exceeded. Thus the stress level mentioned above, related to remarkable AE signal activity increase was named a critical stress.

In the paper a possibility of application of AE method to determine the critical stresses in bending mortars with different compositions and also the experimental results of self-healing process in the beams under bending are presented. The mortars were reinforced with steel microfibers. The cement paste was partially replaced with HCFA to examine mechanical properties of such a composite material. The previous research described in (Tsimas, Moutsatsou–Tsima, 2005; Jóźwiak–Niedźwiedzka *et al.*, 2011) let the authors to conclude that high calcium fly ash is a valuable addition to mortars and concretes. Dispersed steel microfibers were added in order to assess the growth of cracks in a relatively brittle material. The microfibers also simulated ordinary steel reinforcement generally applied in real constructions.

It is expected that the self-healing process, if quantified in a reliable way, might be explicitly employed in design codes of practice for concrete structures. Self-healing of cracks in the reinforced concrete elements under bending may reduce permeability of external layers that provide cover for steel reinforcement against corrosive environment. Therefore, certain positive influence on durability of civil engineering structures may be expected even if only partial recovery of strength would be possible.

2. Experimental research

2.1. Materials and preparation of specimens

In all mixtures ordinary Portland Cement CEMI 42.5R (PC) and high-calcium fly ash with content of CaO of over 22% were used. Chemical composition of PC and HCFA are presented in Table 1.

Table 1. Chemical composition of Portland Cement and High Calcium Fly Ash.

Constituent (% by mass)	CEM I 42.5R	HCFA
SiO_2	22.2	39.2
Al_2O_3	5.3	23
Fe_2O_3	3.0	4.95
$\Sigma\ SiO_2 + Al_2O_3 + Fe_2O_3$	30.5	67.15
CaO	66.3	22.4
SO_3	2–6	3.07
$CaO_{\ free}$	1.3	1.46
MgO	1.3	1.27
Loss on ignition	0.2	1.85
Glassy phase content	–	64.23

Unprocessed HCFA was applied and it contained mainly spherical particles with predominant grain size between 20 and 60 μm and conglomerate both, spherical and irregular shape, size from 60 to 80 μm. The morphology of the HCFA particles is presented in Fig. 1.

The HCFA, a by-product of lignite burning, is captured by electrostatic precipitators. It has a form of a very fine powder, originating from the presence of highly active constituents, such as reactive lime, reactive silica and alumina. It has CaO content within the range from 10 to 40% and therefore so-called self-setting is observed, and for this reason high calcium fly ash is considered as a pozzolanic and hydraulic material (Tsimas, Moutsatsou–Tsima, 2005). HCFA also contains significant amounts of calcium aluminate glass which is more soluble than the glass in low-

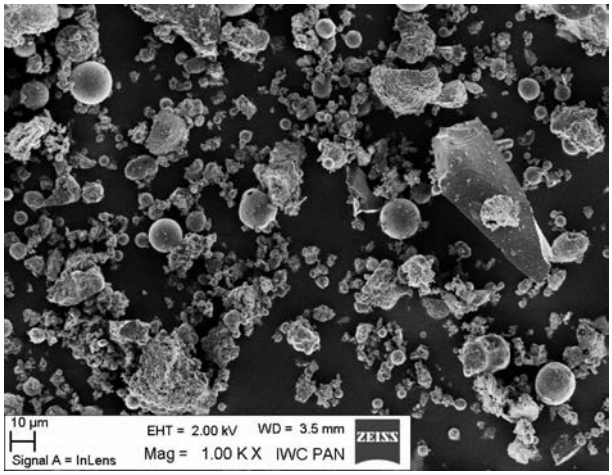

Fig. 1. SEM micrograph showing the morphology of the HCFA particles.

calcium fly ash and may slowly release calcium and aluminum into solution.

As for fine aggregate, standard siliceous sand 0–2 mm according to PN-EN 196-1 was used. The water/binder (cement + high calcium fly ash) ratio was held constant equal to 0.4. Steel microfibres Dramix OL6/.16 were used with volume fraction 1%. These microfibres are 6 mm long and 0.16 mm in diameter, made with high-carbon steel with minimum tensile strength equal to 2000 N/mm^2. The mix proportions of mortar are shown in Table 2. Mortar denoted as R-0% was the reference composition without fly ash. Other mortars R-30 and R-60 had 30 and 60% of Portland cement replaced by fly ash, respectively.

Table 2. Mortar mixture proportions in [kg/m^3].

Constituents	Mix ID		
	R-0%	R-30%	R-60%
Cement	1000	700	400
Siliceous Sand (0–2.0 mm)	600		
High Calcium Fly Ash	0	300	600
Water	400		
Fibers, 1% vol.	78.6		

The constituents were first mixed with water in a kind of Hobart mixer for 1 min thoroughly. Then fibres were added and the mixture was mixed again for 1 min. Coupon specimens with the dimensions 240 × 320 × 40 mm were cast and cured 1 day in the moulds under sealed conditions. Then the coupons were cured in the lime water for another 27 days. When the time of pre-cracking arrived, each coupon was sawn into six beams with the dimensions of 220×40×40 mm.

2.2. Pre-cracking of specimens and program of tests

The beams were loaded in four-point bending test where the support span was set up for 200 mm with the middle loading span equal to 66.7 mm, what is presented in Fig. 2.

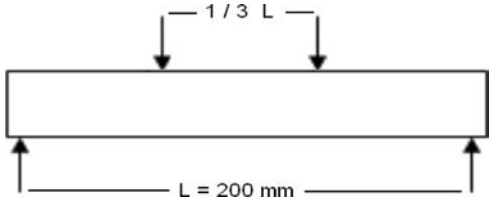

Fig. 2. Specimen under loading with two concentrated forces.

All beams were loaded up to maximum deflection equal to 0.3 mm. This deflection was arbitrarily selected in order to obtain central crack in the beam of appropriate width for self healing. The deflection did not cause the crucial loss of beam stiffness, however its level guaranteed the excess of the critical stress in central cross-section of the sample. The tests were repeated at selected dates to register healing process in time; the test program is given in Table 3. The acoustic emission events were recorded in order to monitor crack propagation.

Table 3. The testing program.

	Denotation	Age since precracking [days]
Casting	–	−28
Precracking	A	0
Loading #1	B	56
Loading #2	C	112

2.3. Acoustic Emission measurements

Acoustic emission effects were registered and recorded in order to monitor the progress of cracking process during loading. Registration of AE signals was performed with a wideband AE sensor of type WD PAC. A custom-made AE analyser included high-pass filter with roll-off frequency of 15 kHz, 60 dB amplifier and fast 12 bit A/D converter to store the source signal in a PC disk. AE signals of duration longer that 100μs and which amplitudes exceeded 1 mV were recognized due to applied software. The AE sensor was placed in the central part of the loaded beam at it lateral surface and coupled with the beam body with a silicone grease. All the 18 records of AE activity described below have revealed the excess of the critical load. At that level of stress the significant increase of AE event rate was noted. The parameter describing the flexural stress induced in beam loaded in four-point bending σ_{fl} was calculated after the formula recommended by the ASTM C1018-94 for the case where middle span equals 1/3 of the support span:

$$\sigma_{fl} = P\,L/(b\,h^2) \quad [\text{MPa}], \tag{1}$$

where P – loading force [N], L – support span [mm], b – beam width, h – beam height [mm].

Using the formula (1) the following parameters were calculated: 1 – σ_{300}, denoting flexural stress level at 300 μm deflection and 2 – σ_{cr}, denoting flexural stress level at critical load, whereas $\sigma_{cr} < \sigma_{300}$.

2.4. Microscopic tests methods

The evaluation of the microstructure was performed using stereomicroscope and back scattered electron microscope (BSE). The stereomicroscope Nikon SMZ 800 and colour video camera SONY DXC 950P were used for determination of the microstructural changes in the specimens at the micro scale (magnification 63 times). In the higher magnification the specimens were examined using Scanning Electron Microscope (SEM), BSE together with Energy Dispersive X-ray analysis (EDX). The specimens were analyzed after 1st loading (total 57 days of curing) in the SEM-EDX mode on the polished surface and after 2nd loading and additional 28 days of curing in the lime water (total 170 days of curing) – in the stereomicroscope. Parallel with microscopic observations after 170 days of maturity period the SEM analysis has been executed on the split surface of the specimen.

Additionally, certain samples were analysed using Laser Scanning Confocal Microscope of LEXT type equipped with a MPALON object – lens of 20 X magnification. Pictures made with the latter equipment were taken of surfaces polished in the same way as for the SEM analysis.

3. Results of measurements and their analysis

Typical experimental results obtained during pre-cracking and after curing in lime water during 56 and 112 days respectively, are shown in Figs. 3, 4 and 5. The onset of the critical crack was marked with 'x' at these Figures. The load rate was set to 25 N/s however due to differences in stiffness within the elements of the loading machine and the concrete beam the deflection measured by the gage placed below the beam was of non-linear character. Therefore in Figs. 3–5 the load and AE events sum versus time is placed with additional marker of measured deflection at the moment when a critical stress had been reached. The analysis of the results had revealed that the consecutive loadings were of minor importance to the loss of stiffness of examined beams. It is possible that a self-healing during a relatively long periods of curing was responsible for the effect of stiffness recovery. At this moment it seems impossible to separate the variation of stiffness due to cracking and to healing. However more distinct variations of stiffness were found out after comparison of the beams made of different mixes.

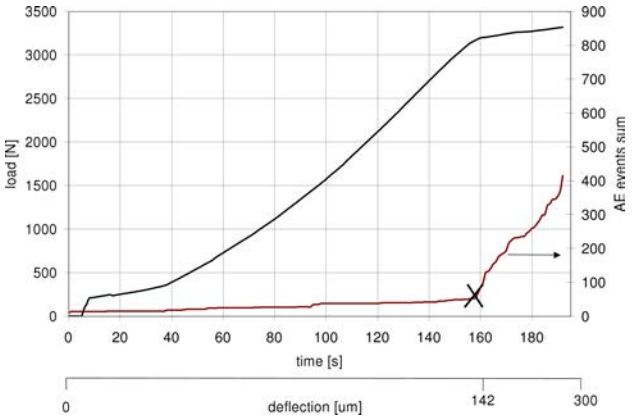

Fig. 3. Load vs. time and AE events sum vs. time recorded during pre-cracking in the beam made of a mix without HCFA admixture. A critical crack growth was detected after the deflection of 142 μm was reached.

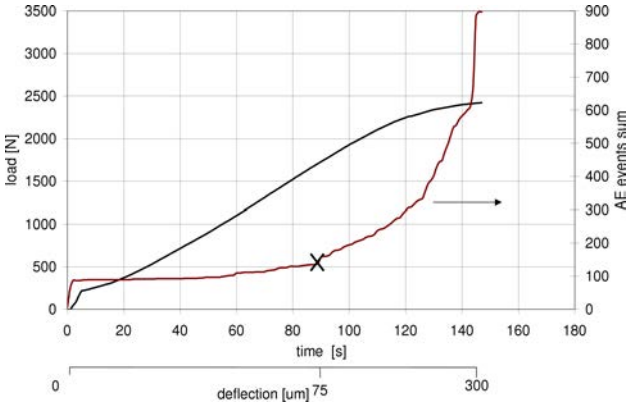

Fig. 4. Load vs. time and AE events sum vs. time recorded in the beam after 56 days of curing, made of a mix with 30% HCFA admixture. A critical crack growth was detected after the deflection of 75 μm was reached.

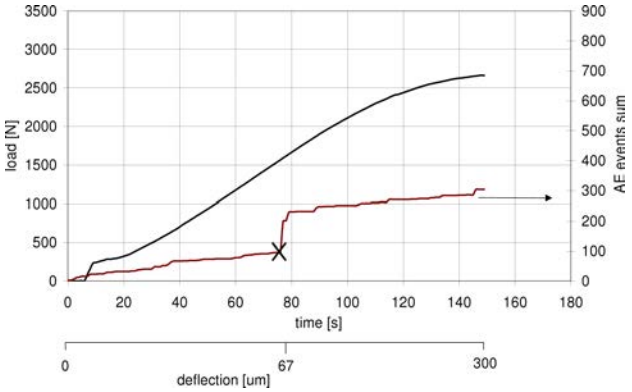

Fig. 5. Load vs. time and AE events sum vs. time recorded in the beam after 112 days of curing, made of a mix with 60% HCFA admixture. A critical crack growth was detected after the deflection of 67 μm was reached.

It can be assumed that crack growth did not affected seriously the mechanical strength of the inves-

tigated beams because the capacity of carrying the load was partly realized by the system of micro reinforcement. Therefore the beams were good models of a real reinforced elements used in civil engineering. The quantitative analysis of mechanical strength of the investigated beams was made in the following way. The results of two samples of each set (i.e. R-0%, R-30% and R-60%) presenting the lowest and the highest value of σ_{300} parameter were rejected and the other were averaged. The standard deviation calculated for the remaining 4 members did not exceeded 20% of the mean value. The mean values of flexural stress σ_{300} calculated for three types of mixes and its changes due to consecutive loadings are presented in Table 4 and the critical value of flexural strength are presented in Table 5.

Table 4. Mean values of flexural strength σ_{300} calculated for three types of mixes and its changes due to consecutive loadings.

Mix ID	σ_{300} measured at precracking [MPa]	σ_{300} measured at loading #1 [MPa]	σ_{300} measured at loading #2 [MPa]
R-0%	8.2	8.5	8.3
R-30%	7.5	7.8	7.7
R-60%	7.1	7.2	7.2

Table 5. Mean values of flexural stress σ_{cr} calculated for three types of mixes and its changes due to consecutive loadings.

Mix ID	σ_{cr} measured at precracking [MPa]	σ_{cr} measured at loading #1 [MPa]	σ_{cr} measured at loading #2 [MPa]
R-0%	7.3	6.6	6.7
R-30%	6.4	6.7	4.7
R-60%	6.8	6.7	4.9

The comparison of the data presented in Table 4 let the authors to conclude that a slight increase of flexural strength in examined mixes was observed after 56 days of curing (prolonged curing was not so effective). That effect may be explained by the increasing cohesion between the fibres and matrix during maturing. The other effect is that mortars with 30% (by weight) substitution of cement by HCFA admixture presented ca. 8% lower value of flexural stress than that with no admixture. 60% substitution of cement by HCFA resulted in ca. 15% decrease of the flexural stress. The critical value of flexural strength is influenced significantly and decreasing by the number of loadings. That means that σ_{cr} reflects the structure degradation due to crack growth. To demonstrate the latter tendency in the Table 6. σ_{cr} was laid as a ratio of the corresponding value of σ_{300}. That ratio is proposed to be used as a clear measure of stage of structural degradation.

Table 6. The measure of structural degradation expressed as a ratio of σ_{cr}/σ_{300} calculated for data presented in Tables 4 and 5.

Mix ID	σ_{cr}/σ_{300} precracked beams	σ_{cr}/σ_{300} loading #1	σ_{cr}/σ_{300} loading #2
R-0%	0.90	0.77	0.81
R-30%	0.86	0.86	0.60
R-60%	0.93	0.93	0.67

4. Microscopic observations

Figure 6 presents an example of the general view of the observed cracking surface, taken with the use of optical microscopy. The separate mortar constituents are visible: fine aggregate – sand, spherical particles of high calcium fly ash, and steel fibres (the latter visible as white needles). Steel fibres tend to stop crack propagation. The image of the observed main crack taken in the confocal laser scanning microscope (Fig. 7) demonstrates the depth of the crack propagation which arrives to about 400 μm.

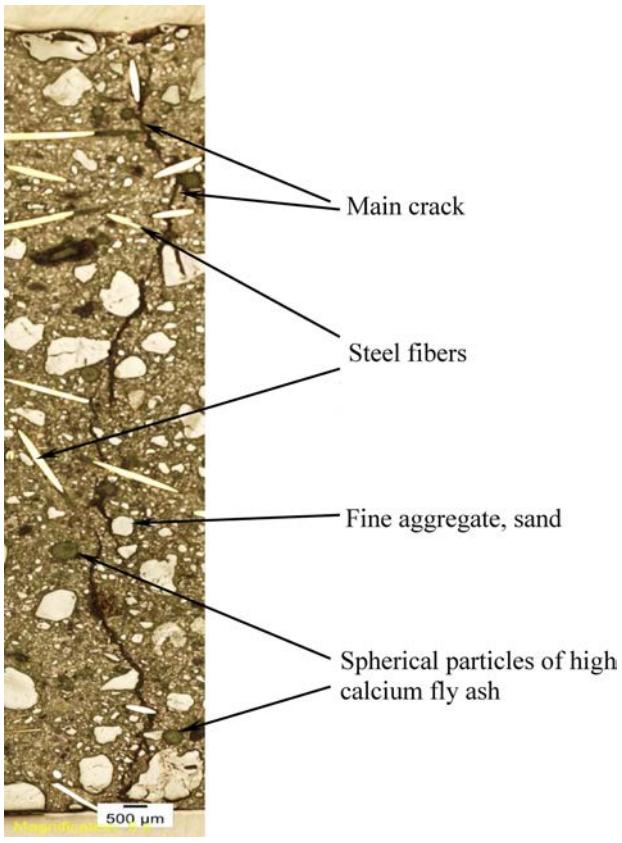

Fig. 6. Microphotograph of the observed cracking surface, mix of R-60% type, thin white 'needles' are images of microfiber fragments.

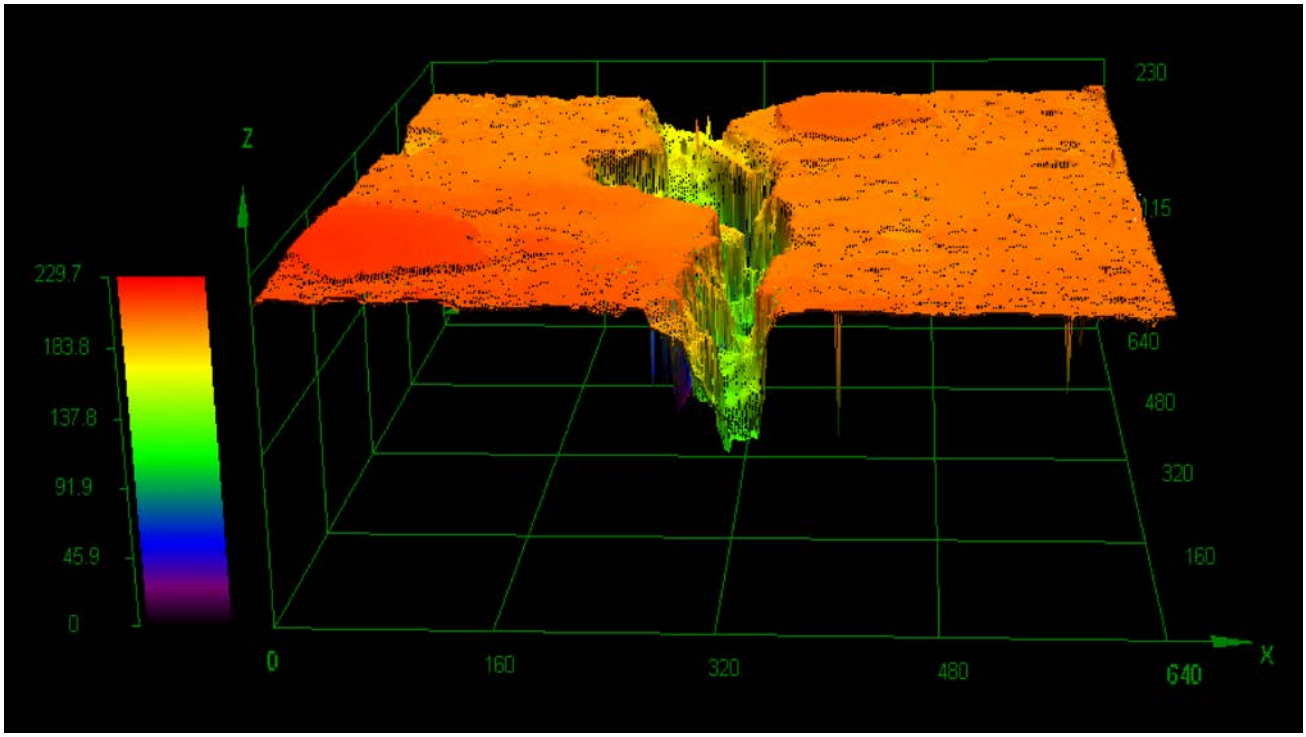

Fig. 7. Image created of data recorded with confocal laser scanning microscope, demonstrating the real depth of cracked concrete matrix, arriving to 400 μm. The color mapping was used to present the local depression of the surface.

Figure 8 presents an example of the crack system consisting of the main crack which propagates through the whole specimen (width about 100 μm) and the fine microcrack (width about less than 30 μm) which is parallel to the main crack.

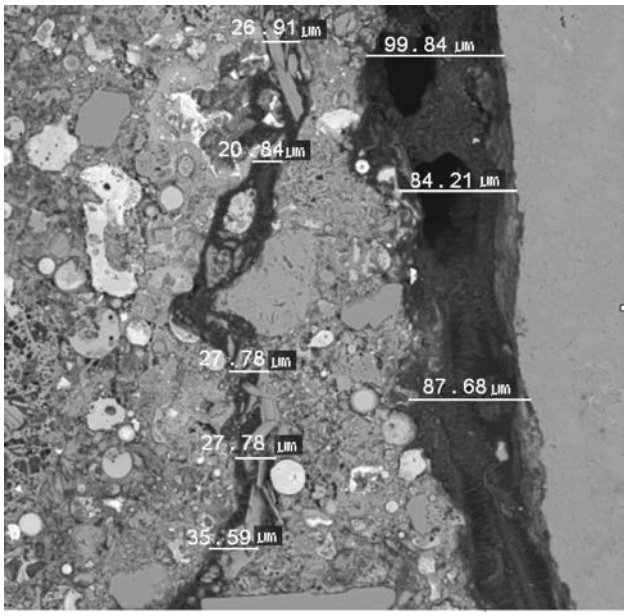

Fig. 8. Microphotograph of the crack system consisting of the single microcrack, (central part of the cross-section) and the main crack, situated to the right from the microcrack.

5. Conclusions

In the paper the mechanical testing of mortar elements with high calcium fly ashes was presented. HCFA were used as a partial cement replacement in mortar beams to increase the self-healing phenomenon in cracks and to tighten the structure of concrete. The beams were subjected to 4-point bending until opening of a system of microcracks and cracks. After specific period of time the beams structure was analyzed using stereomicroscope and SEM.

With regard to the main findings of the present work, these are summarized as follows:

- Limited increase of stiffness of specimens after 56 and 112 days of curing due to crack healing is shown on load- deflection curves. Considering the data presented in Table 6 the relative recovery of stiffness due to crack healing, (i.e. initial to final stiffness level) can be estimated to 60–80%. The highest effect of healing was measured in mix with no HCFA admixture.
- Due to good bond between the micro reinforcement and the matrix the process of crack growth was successfully blocked,
- The analysis of the recorded Acoustic Emission activity has revealed that the HCFA admixture decreased the overall beam stiffness measured under bending and also that the critical stress level, possible to determine with the application

of acoustic method is close to the stage of degradation processes induced by multiple loading of reinforced concrete object.

More information on load-deflection behaviour of tested beams is presented in Jóźwiak–Niedźwiedzka *et al.* (2012).

Acknowledgment

The experimental work concerning SEM-BSE analysis presented in this study was conducted in the Charles Pankow Concrete Materials Laboratory at Purdue University. The authors gratefully acknowledge the support at that part of the presented investigation.

The authors are thankful to Bekaert Poland Sp. z o.o. for complimentary supply of microfibers.

The results presented in the paper have been obtained within the project "Innovative cement binders and concretes with addition of high calcium fly ash" (project no POIG.01.01.02-24-005/09 with the Polish Ministry of Science and Higher Education) in the framework of the Operational Programme Innovative Economy 2007–2013.

References

1. Abrams D.A. (1917), *Effects of rate of application of load on the compressive strength of concrete*, Amer. Soc. For Testing of Materials, Proc. 17, part II, 364–377.
2. Arrington M., Evans B.M. (1977), *Acoustic emission testing of high alumina cement concrete*, NDT Int., **10**, 2, 81–87.
3. Golewski G., Sadowski T. (2007), *Analysis of brittle damages in concrete composites* [in Polish], Proc. of Cracow University of Technology, Civil Engineering, **1-B**, 4, 55–62.
4. Granger S., Pijaudier G., Loukili A., Marlot D., Lenain J.C. (2009), *Monitoring of cracking and healing in an ultra high performance cementitious material using the time reversal technique*, Cem. & Concr. Res., **39**, 296–302.
5. Gray R.J. (1984), *Autogeneous healing of fibre/matrix interfacial bond in fibre-reinforced mortar*, Cem. & Concr. Res., **14**, 315–317.
6. Hannant D.J., Edgington J. (1975), *Durability of steel fibre concrete*, [in:] Proc. RILEM Symp. "Fibre reinforced cement and concrete", Lancaster; Construction Press, 159–169.
7. Hannant D.J., Keer J.G. (1983), *Autogeneous healing of thin cement based sheets*, Cem. & Concr. Res., **13**, 533–538.
8. Hoła J. (1999), *Acoustic Emission investigation of failure of high-strength concrete*, Archives of Acoustics, **24**, 2, 233–244.
9. Hosoda A., Komatsu S., Ahn T., Kishi T., Ikeno S., Kobayashi K. (2009), *Self healing properties with various crack widths under continuous water leakage*, in: Concr. Repair, Rehab. and Retrofit., II, Alexander *et al.* [Eds.], Taylor and Francis, 221–227.
10. Jacobsen S., Sellevold E.J. (1996), *Self healing of high strength concrete after deterioration by freeze/thaw*, Cem. & Concr. Res., **26**, 1, 55–62.
11. Jóźwiak–Niedźwiedzka D., Gibas K., Glinicki M.A., Nowowiejski G. (2011), *Tightness of the concretes with high calcium fly ash admixture in relation to diffusion of aggressive agents* [in Polish: *Drogi i Mosty*], Journal of Polish Institute of Roads and Bridges, 3, 39–61.
12. Jóźwiak–Niedźwiedzka D., Brandt A.M., Ranachowski Z. (2012), *Self-healing of cracks in fibre reinforced mortar beams made with high calcium fly ash*, Cement, Wapno, Beton (www.cementwapnobeton.pl), **1**, 38–49.
13. Kasperkiewicz J., Stroeven P. (1991), *Observations on crack healing in concrete*, [in:] Proc. Int. Symp. "Brittle Matrix Composites 3" Warszawa, Appl. Sc. Publ., 164–173.
14. Marks M., Jóźwiak–Niedźwiedzka D., Glinicki M.A. (2012), *Automatic categorization of chloride migration into concrete modified with CFBC ash*, Computers and Concrete, **9**, 5, 375–387.
15. Mor A., Monteiro P.J.M., Hester W.T. (1989), *Observations of healing of cracks in high-strength lightweight concrete*, Cem. Concr. and Aggr., **11**, 2, 121–125.
16. Ohtsu M. (1996), *The history and development of acoustic emission in concrete engineering*, Magazine of Concrete Res., **48**, 321–330.
17. Ouyang C.S., Landis E., Shah S.P. (1991), *Damage assesment in concrete using quantitative acoustic emission*, J. Eng. Mech., **117**, 11, 2681–2698.
18. Qjan S.Z., Zhou J., Schlangen E. (2010), *Influence of curing condition and precracking time on the self-healing behavior of Engineered Cementitious Composites*, Cem. & Concr. Comp., **32**, 686–693.
19. Ranachowski P., Rejmund F., Ranachowski Z., Pawełek A., Piątkowski A. (2009), *Comparison of Acoustic Emission and Structure Degradation in Compressed Porcelain and Corrundum Materials*, Archives of Acoustics, **34**, 4, 566–676.
20. Reinhardt H.W., Jooss M. (2003), *Permeability and self-healing of cracked concrete as a function of temperature and crack width*, Cem. & Concr. Res., **33**, 981–985.
21. Ruesch H. (1959), *Physical problems in the testing of concrete*, Zement, Kalk, Gips, **12**, 1, 1–9.
22. Şahmaran M., Keskin S.B., Ozerkan G., Yaman I.O. (2008), *Self-healing of mechanically-loaded*

self consolidating concretes with high volumes of fly ash, Cem. & Concr. Comp., **30**, 872–879.

23. Schiessl P., Reuter C. (1992), *Massgebende Einflussgrössen auf die Wasserdurchlässigkeit von gerissenen Stahlbetonbauteilen*, Ann. Report, Institüt für Bauforschung, Aachen, 223–228.

24. Tsimas S., Moutsatsou–Tsima A. (2005), *High-calcium fly ash as the fourth constituent in concrete: problems, solutions, and perspectives*, Cem. Concr. Comp., **27**, 231–237.

25. Wenhui Zhong, Wu Yao (2008), *Influence of damage degree on self-healing of concrete*, Constr. & Build. Materials, **22**, 1137–1142.

26. Yuyama S., Ohtsu M. (2000), *Acoustic Emission evaluation in concrete* [in:] Kishi T., Ohtsu M., Yuyama S. [Eds.], Acoustic Emission-Beyond the Millennium, Elsevier, 187–213.

PAN ARCHIVES OF ACOUSTICS
Vol. **37**, No. 3, pp. 269–278 (2012)

DOI: 10.2478/v10168-012-0035-2

Pulsed Focused Nonlinear Acoustic Fields from Clinically Relevant Therapeutic Sources in Layered Media: Experimental Data and Numerical Prediction Results

Tamara KUJAWSKA

Department of Ultrasound, Institute of Fundamental Technological Research, Polish Academy of Sciences
Pawińskiego 5B, 02-106 Warsaw, Poland; e-mail: tkujaw@ippt.pan.pl

(*received March 1, 2012; accepted May 18, 2012*)

In many therapeutic applications of a pulsed focused ultrasound with various intensities the finite-amplitude acoustic waves propagate in water before penetrating into tissues and their local heating. Water is used as the matching, cooling and harmonics generating medium. In order to design ultrasonic probes for various therapeutic applications based on the local tissue heating induced in selected organs as well as to plan ultrasonic regimes of treatment a knowledge of pressure variations in pulsed focused nonlinear acoustic beams produced in layered media is necessary. The main objective of this work was to verify experimentally the applicability of the recently developed numerical model based on the Time-Averaged Wave Envelope (TAWE) approach (WÓJCIK *et al.*, 2006) as an effective research tool for predicting the pulsed focused nonlinear fields produced in two-layer media comprising of water and tested materials (with attenuation arbitrarily dependent on frequency) by clinically relevant axially-symmetric therapeutic sources. First, the model was verified in water as a reference medium with known linear and nonlinear acoustic properties. The measurements in water were carried out at a 25°C temperature using a 2.25 MHz circular focused (f/3.0) transducer with an effective diameter of 29 mm. The measurement results obtained for 8-cycle tone bursts with three different initial pressure amplitudes varied between 37 kPa and 113 kPa were compared with the numerical predictions obtained for the source boundary condition parameters determined experimentally. The comparison of the experimental results with those simulated numerically has shown that the model based on the TAWE approach predicts well both the spatial-peak and spatial-spectral pressure variations in the pulsed focused nonlinear beams produced by the transducer used in water for all excitation levels complying with the condition corresponding to weak or moderate source-pressure levels. Quantitative analysis of the simulated nonlinear beams from circular transducers with $ka \gg 1$ allowed to show that the axial distance at which sudden accretion of the 2nd or higher harmonics amplitude appears is specific for this transducer regardless of the excitation level providing weak to moderate nonlinear fields. For the transducer used, the axial distance at which the 2nd harmonics amplitude suddenly begins to grow was found to be equal to 60 mm. Then, the model was verified experimentally for two-layer parallel media comprising of a 60-mm water layer and a 60-mm layer of 1.3-butanediol (99%, Sigma-Aldrich Chemie GmbH, Steinheim, Germany). This medium was selected because of its tissue-mimicking acoustic properties and known nonlinearity parameter B/A. The measurements of both, the peak- and harmonic-pressure variations in the pulsed nonlinear acoustic beams produced in two-layer media (water/1.3-butanediol) were performed for the same source boundary conditions as in water. The measurement results were compared with those simulated numerically. The good agreement between the measured data and numerical calculations has shown that the model based on the TAWE approach is well suited to predict both the peak and harmonic pressure variations in the pulsed focused nonlinear sound beams produced in layered media by clinically relevant therapeutic sources. Finally, the pulsed focused nonlinear fields from the transducer used in two-layer media: water/castor oil, water/silicone oil (Dow Corning Ltd., Coventry, UK), water/human brain and water/pig liver were predicted for various values of the nonlinearity parameter of tested media.

Keywords: therapeutic ultrasound, circular focused transducers, pulsed nonlinear acoustic pressure beams, layered media, numerical modeling and experiments.

1. Introduction

A majority of currently used therapeutic ultrasonic techniques employs circular focused transducers generating pulsed acoustic pressure waves with various intensity penetrating into tissues after passing through a water layer. The water layer prior tissues is used as the matching and cooling medium. Besides, water is

a weakly attenuating medium, therefore the secondary waves with harmonic frequencies are there easily generated causing an increase of nonlinear waveform distortion. An absorption of the nonlinearly distorted tone bursts increases with increasing of number of harmonics generated. A concentration of energy of pulsed nonlinear waves inside tissues and increase of their absorption lead to a local heating of tissues in the area of the beam focus. In order to design ultrasonic probes for various therapeutic applications based on a tissue heating as well as to select the safe ultrasonic regime of treatment a prediction of both the pressure variations in the pulsed focused nonlinear acoustic beams and heat sources distributions induced in tissues due to these fields is required (Kujawska *et al.*, 2011b).

However, there is a lack of papers published (according to the knowledge of authors), which address the pulsed nonlinear focused beams from axially-symmetric acoustic sources in layered media with arbitrary dependence of attenuation on frequency. This work presents experimental verification of the numerical model based on the Time-Averaged Wave Envelope (TAWE) approach by comparing the measured spatial peak- and harmonic- pressure variations in the pulsed nonlinear sound beams from a circular focused transducer in two-layer media: water/tested material with those simulated numerically. A description of the TAWE approach to the numerical solution of the second order nonlinear differential wave equation for axially-symmetric sources is presented in (Wójcik *et al.*, 2006). The numerical solver, being the computer implementation of the model, accounts for the effects of diffraction, absorption, nonlinear interaction of harmonics as well as of transmission and reflection at the media interfaces.

This paper is organized as follows. First, both the source and media boundary condition parameters, required for the nonlinear propagation model as the input data, are described. Then, detailed description of the experimental setup and measurement methodology in water and in two-layer media is given. Next, the results of measurements in water (as a reference medium with known linear and nonlinear acoustic properties) as well as in two-layer media: water/1.3-butanediol are presented and compared with those simulated numerically for the source boundary conditions determined experimentally. Finally, pressure distributions of the harmonic components in the pulsed focused nonlinear sound beams produced in two-layer media comprising of water and tested fluids (castor oil, DC-710 silicone oil, Dow Corning Ltd., Coventry, UK) or tissues (pig liver, human brain) were predicted for various nonlinearity parameters of the tested medium.

2. Numerical model

The numerical model used in this work was presented in (Wójcik *et al.* 2006; 2008). The model describes (in frequency domain) nonlinear waveform distortion of a pulsed finite-amplitude sinusoidal wave generated from an axially-symmetric acoustic source and propagating in a dissipative fluid with an attenuation arbitrarily dependent on a frequency. The model developed is computationally efficient due to application of the Time-Averaged Wave Envelope (TAWE) approach to the numerical solution of the second order differential nonlinear wave equation for sources with axial symmetry. The model was extended to multilayer media *via* introduction to the model equations the terms accounting for the effects of transmission and reflection at the media interfaces. The computer implementation of the extended model was a new effective research tool for investigation and quantitative analysis of the pulsed nonlinear fields generated from the single-element circular planar or focused acoustic sources in layered attenuating media with arbitrary frequency-dependence of attenuation.

The model requires a number of input parameters related to the source geometry and working conditions as well as to the acoustic properties of the media of propagation. The source boundary condition parameters required for the model include the transducer centre frequency f_0, effective radius a_{eff}, focal length F, source-pressure amplitude P_0, radiating aperture apodization function $P_0(r) = P_0 f(r)$, initial tone burst waveform $P(t)$ and pulse repetition frequency (PRF).

The source boundary condition parameters used in numerical simulations were determined experimentally by using the comparison-fitting method. The radial pressure distribution $P(r)$ was measured in water by the needle hydrophone at the axial distance of 5 mm from the transducer face and fitted to the simulated one by adjusting the source-pressure amplitude P_0, effective radius a_{eff} and index m in the radiating aperture apodization function introduced to the model in a form of the analytical function

$$P_0(r) = P_0\,|1 - (r/a_{\text{eff}})^m|.$$

For the transducer used, the optimal apodization function, which produced in water at the axial distance of 5 mm the radial pressure distribution best fitted to the measured one, was found when the effective radius of the source was equal to 14.5 mm and exponent m was equal to 10 for all excitation levels used.

The initial tone burst pressure-time waveform $P(t)$ used in the numerical simulations was also determined by the comparison-fitting method and introduced to the numerical model in the form of polynomial function:

$$P(t) = [1 - |(t - t_c)/(t_b - t_e)|^q] \cdot \sin[\omega(t - t_c)]$$

for $t_b \le t \le t_e$; $P(t) = 0$ for $t \notin (t_b, t_e)$. Here t_c, t_b and t_e are dimensionless times determining the midpoint,

Table 1. The acoustic parameters of tested media.

Medium	Density [kg/m^3]	Sound velocity [m/s]	Absorption coefficient [Np/(m · Hz^b)]	b	B/A	T [°C]	Literature
Distilled water	997	1497	$0.025 \cdot (10^{-6})^b$	2	5.2	25	[2]
1.3-butanediol	1005	1530	$1.27 \cdot (10^{-6})^b$	2	10.5	25	[3]
Castor oil	969	1452	$5.8 \cdot (10^{-6})^b$	1.667	5–13	25	[9]
DC-710 Silicone oil	1102	1378	$7.3 \cdot (10^{-6})^b$	1.79	5–13	25	[9]
Pig liver	1060	1590	$7.8 \cdot (10^{-6})^b$	1	5–9	25	[4]
Human brain	1040	1562	$5 \cdot (10^{-6})^b$	1.08	7	37	[4]

beginning and end of the initial tone burst, respectively, t is dimensionless time and q is integer related to the envelope function of the tone burst. The space and time were normalized regarding to 2π (see Eq. (2) in Wójcik *et al.*, 2006). The pressure-time waveform $P(t)$ that best reproduced the waveform of the initial tone burst measured on the acoustic axis close to the transducer surface comprised of 8 cycles and enabled determining the optimal initial tone burst waveform for the index q equal to 8.

The acoustic parameters of media required for the model include their density ρ, sound velocity c, attenuation coefficient α_1, power index b determining the dependence of attenuation on frequency $\alpha(f) = \alpha_1 \cdot f^b$ and nonlinearity parameter B/A. The density, sound velocity and frequency-dependent attenuation law used in numerical simulations for tested media considered in this work were available from the literature and are quoted in Table 1. The value of the nonlinearity parameter B/A for these media was assumed to be varying between 5 and 13. These values cover the range of the B/A typical for most physiological fluids and soft tissues.

Similarly to the commonly used KZK nonlinear propagation model the model based on the TAWE approach has limitations. The limitation of the model used was determined in (Baker *et al.*, 1988; Nachef *et al.*, 1995) showing that the model equations provide very good prediction of the measured sound fields from planar circular sources in water when the source-pressure level is weak to moderate, i.e. when the ratio of the shock formation (discontinuity) distance ($l_D = \rho_0 c_0^2 \lambda_0/(2 + B/A)\pi P_0$) to the Rayleigh distance ($R_0 = \pi a^2/\lambda_0$) is larger than 0.3 ($l_D/R_0 > 0.3$). In case of a planar transducer with a diameter and centre frequency the same as for the transducer used here fulfillment of this condition means that the pressure amplitude on its surface should be above the value providing the linear propagation mode but below 214 kPa. Physically, this condition means that a shock is formed only in the transition- or far-field region of the acoustic beam. However, therapeutic applications of ultrasound involve the focused beams in which shock is formed in the near-field region of the beam. So, the experimental investigation of focused beams in water and in two-layer media (comprising of water and the tested medium) provides an opportunity to verify the applicability of the numerical model based on the TAWE approach as the effective research tool for predicting of the peak- and harmonic- pressure variations in the pulsed focused nonlinear beams, produced by therapeutic transducers in layered attenuating media.

3. Experimental setup for measurements in water

First, the model was verified in water as a reference medium with known linear and nonlinear acoustic properties. All measurements were carried out at a 25°C temperature using a 2.25 MHz frequency, circular focused (f-number 3) transducer with a 29 mm effective diameter. The experimental setup used for the measurements is shown in Fig. 1. The Arbitrary Function Generator (Ritec Advanced Measurement System RAM-10000, Warwick, RI, USA) produced 2.25 MHz, 8-cycle tone bursts with 1 kHz pulse repetition frequency (PRF). This signal was applied to the piezoelectric transducer used (Olympus-NDT Inc.,

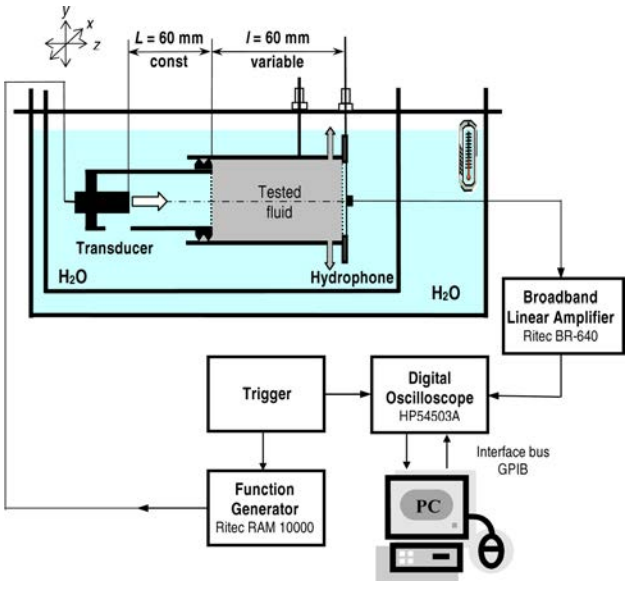

Fig. 1. Schematic diagram of the experimental setup.

Waltham, MA, USA) which generated tone bursts with the initial pressure amplitude varied from 37 kPa to 117 kPa. The pressure-time waveforms were recorded by the 0.513 mm, broadband bilaminar, PVDF membrane hydrophone (Unisyn, formerly Sonora, SN S5-259, Longmont, CO) with an integrated preamplifier. The hydrophone output was amplified additionally by 20 dB with a linear broadband amplifier (Ritec BR-640, Warwick, RI, USA). The signals recorded by hydrophone were captured by 8 bit, 200 Ms per s digital storage oscilloscope (HP54503A, Hewlett Packard, Colorado Springs, CO, USA), averaged over 16 consecutive waveforms, to maximize signal-to-noise-ratio, digitized, and then transferred to a personal computer (PC) for FFT (spectral) processing.

4. Methodology of measurements in water

The transmitting transducer was mounted in the *xyz*-axis positioning system driven by three stepper motors allowing its motion in the x, y and z directions with steps adjustable from 0.1 to 5 mm by PC. The transducer generated tone bursts with initial pressure amplitude of three different levels $P_0 = 37$, 103 and 113 kPa and corresponding to the weak and moderate nonlinear propagation condition. The measuring hydrophone was fixed.

The measurement results were compared with those simulated numerically for the source boundary conditions determined experimentally. As noted above, the radiating aperture apodization function was described by the analytical function $P_0(r) = P_0\,|1 - (r/a_{\text{eff}})^{10}|$, where the effective aperture radius a_{eff} was found to be 14.5 mm. When this function was assumed the radial pressure distribution calculated at the axial distance of 5 mm from the transducer face was best fitted to the measured one at the same distance. The initial pressure-time waveform of the generated tone bursts was described by the polynomial function

$$P(t) = [1 - |(t - t_c)/(t_b - t_e)|^8 \cdot \sin[\omega(t - t_c)]$$

for $t_b \le t \le t_e$; $P(t) = 0$ for $t \notin (t_b, t_e)$. This function provided the best fitting between the simulated and measured waveform of the tone bursts generated by the transducer used.

5. Measurement results in water

The measurement results were compared with those simulated numerically using the model based on the TAWE approach. Figure 2 shows the axial peak-compression (P^+), peak-rarefaction (P^-) and peak-peak (P_{pp}) pressure variations in the pulsed focused nonlinear sound beams in water calculated for 8-cycle tone bursts with the initial pressure amplitude varied from 50 kPa to 200 kPa that corresponded to the weak or moderate source-pressure levels.

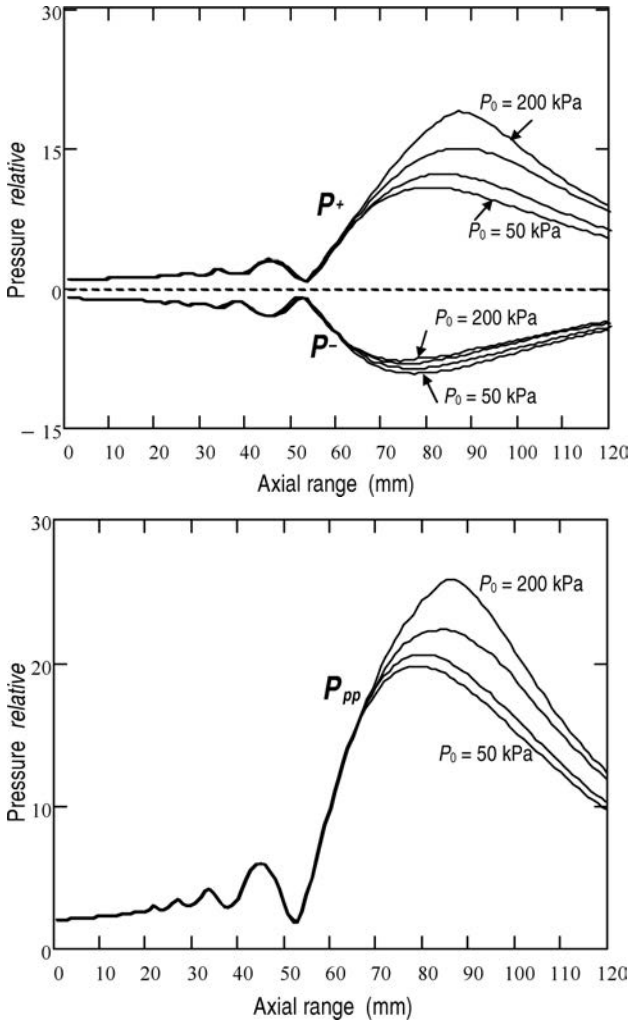

Fig. 2. Axial variations of the peak-compression (P^+), peak-rarefaction (P^-) and peak-peak (P_{pp}) pressure amplitude in pulsed focused nonlinear beams generated from the transducer used in water. Numerical simulations for 2.25 MHz 8-cycle tone bursts with the initial pressure amplitude varied from 50 to 200 kPa with a 50 kPa increment are shown.

These results indicate a correlation between the source-pressure amplitude and the focal plane position in the focused nonlinear beams. The higher is the source-pressure amplitude the closer to the geometric focus the true focal plane is positioned. The reason of this phenomena is the presence of a large amount of harmonics in the focal plane of the nonlinear beams.

The comparison of the measured and simulated axial peak-peak pressure variations in the pulsed focused nonlinear beams in water for three different levels of transducer excitation, providing the initial pressure amplitude of the generated tone bursts equal to 37, 103 and 113 kPa is shown in Fig. 3. The obtained results have shown a very good agreement between the measurement data and the numerical predictions up to the axial distance of about 90 mm (focal distance for the nonlinear propagation mode) where the dis-

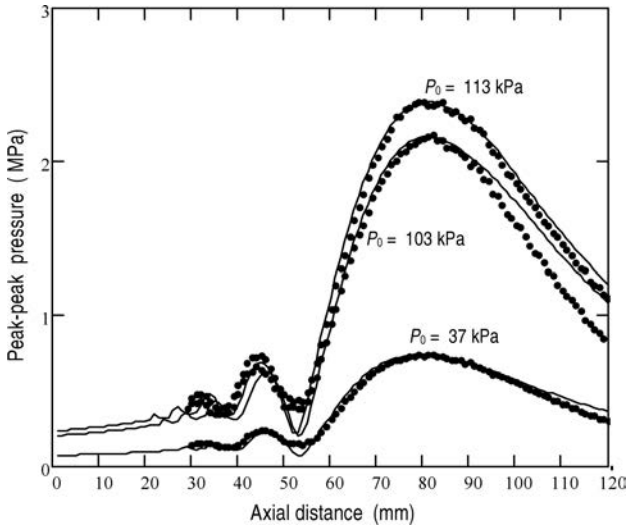

Fig. 3. Axial peak-peak pressure variations in the pulsed focused nonlinear acoustic beams produced by the transducer used generating in water 8-cycle tone bursts with the initial pressure amplitude varied between 0.037 and 0.113 MPa. Measurement data (points) and numerical simulations (solid lines) obtained for the source boundary conditions determined experimentally.

crepancy begins to be visible. Probable reason for this discrepancy is that the true plane wave conditions beyond the focal plane are not fulfilled.

Figure 4 illustrates the axial pressure variations of the fundamental (1st), 2nd and 3rd harmonics calculated for the tone bursts with the initial pressure amplitude varied from 50 kPa to 200 kPa generated from the transducer used here and propagating in water. It is evident from Fig. 4 that the axial distance from the transducer surface at which sudden growth of the second or higher harmonics amplitude appear is specific for this transducer regardless of the source-pressure.

The axial pressure variations of the fundamental and 2nd harmonics, measured for the tone bursts with various initial pressure amplitude (37 kPa and 113 kPa) generated from the transducer used here and propagating in water, are shown in Fig. 5 in comparison with those calculated under experimental boundary conditions. The distributions of predicted and measured pressure amplitudes of both the fundamental and 2nd harmonic components are virtually identical up to the axial distance of 90 mm (focal distance for the nonlinear propagation mode) where the discrepancy begins to be visible. Although the exact reason for this discrepancy is difficult to determine, it is conceivable that the true plane wave conditions are not fulfilled beyond the focal distance.

The quantitative analysis of the axial pressure variations of the fundamental and higher harmonics in weak to moderate nonlinear beams, produced in water by circular planar or focused transducers with $ka \gg 1$, has shown that the axial distance at which sudden growth of the 2nd or higher harmonics amplitude occurs is constant and specific for each transducer regardless of the source-pressure level. For the transducer considered here the axial distance at which sudden accretion of the 2nd harmonics amplitude occurs was found to be 60 mm.

This characteristic feature of the weak and moderate pulsed nonlinear acoustic beams generated from axially-symmetric sources in water was used to develop an alternative semi-empirical method for determination of the nonlinearity parameter B/A of clinically relevant media (Kujawska *et al.*, 2011a, 2011c).

Good agreement between measurement data and theoretical predictions in water confirmed applicability of the numerical model based on the TAWE method as an effective research tool for predicting of the 3D (2D space + time) pulsed nonlinear acoustic pressure fields produced by circular focused sources in water.

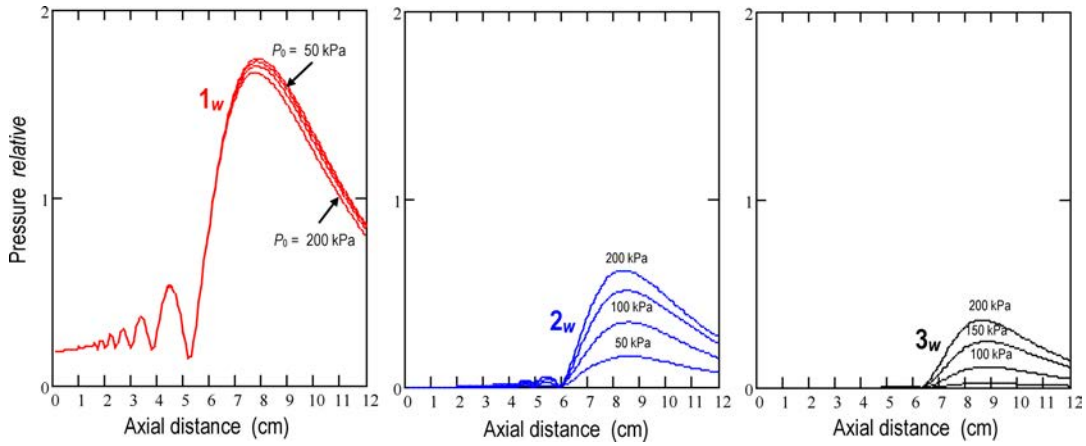

Fig. 4. Axial pressure variations of the fundamental (1_w), 2nd (2_w) and 3rd (3_w) harmonics in the pulsed focused nonlinear acoustic beams produced by the transducer used generating in water 2.25 MHz 8-cycle tone bursts with the initial pressure amplitude varied between 50 kPa and 200 kPa with an increment of 50 kPa.

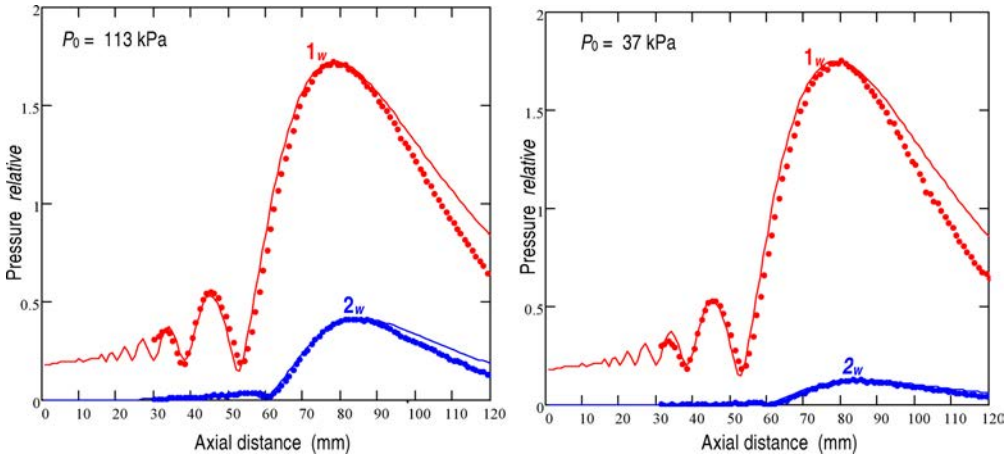

Fig. 5. Axial pressure variations of the fundamental (1_w) and 2nd (2_w) harmonic amplitudes in the pulsed focused nonlinear acoustic beams produced by the transducer used generating in water 8-cycle tone bursts with the initial pressure amplitude of 113 kPa (left) and 37 kPa (right). Numerical simulation (solid lines) and measurement (points) results.

6. Experimental setup for measurements in two-layer media

Next, the model was verified experimentally for two-layer parallel media comprising of a 60-mm water layer and a 60-mm layer of 1.3-butanediol (99%, Sigma-Aldrich Chemie GmbH, Steinheim, Germany) selected because of its tissue-mimicking acoustic properties and known nonlinearity parameter B/A. The thickness of the water layer was chosen to be equal to the axial distance at which sudden accretion of the 2nd harmonics amplitude occurs for the tone bursts propagating in water in order to maximize nonlinear effects in 1.3-butanediol. The path-length that tone bursts propagate through a 1.3-butanediol was chosen to be equal also to 60 mm, however for strongly attenuating media in which harmonics are quickly suppressed this path-length may be chosen shorter.

All measurements in the two-layer media: water/1.3-butanediol were carried out at a 25 °C temperature using the experimental setup shown in Fig. 1. In order to determine experimentally the harmonic pressure variations in the pulsed nonlinear acoustic beam produced in the two-layer media the two-chamber coaxial design was immersed in the larger, temperature controlled water tank. The fixed length ($L = 60$ mm) chamber was filled with distilled water. Its proximal end was sealed by the 2.25 MHz transducer used. The distal end boundary was made from acoustically transparent 20-μm thick Mylar film. The diameter of the fixed-length chamber was slightly smaller than that of the variable-length one, so the fixed-length chamber could be moved coaxially in such a way that it varied the length of the second chamber. The second chamber had independent inlets, so some volume of the 1.3-butanediol could be removed when the first chamber was moved towards the hydrophone. The distal end of the variable-length chamber was also sealed with 20-μm thick Mylar film. The xyz micromanipulator was PC controlled and allowed recording of the pressure-time waveforms versus axial distance. The sensitive element of the stationary broadband bilaminar membrane hydrophone (Sonora, SN S5-259) used to record the $P(t)$ waveforms was positioned at the axial distance of 1.7 mm behind the 2nd chamber Mylar window. The maximal path-length of the two chambers was 120 mm (fixed-length chamber 60 mm and variable-length chamber 60 mm). So, the data presented in the next section were recorded starting at the axial distance of 120 mm from the transducer face and ending at the axial distance of 80 mm, which was in the vicinity of the focal plane of the source for the linear propagation mode.

7. Measurement results in two-layer media

The measurement results in the two-layer media comprising of a 60 mm water layer and a 60 mm layer of 1.3-butanediol were compared with the results predicted numerically for the assumed source boundary conditions determined experimentally. Figure 6 shows the comparison between the measured axial pressure distributions of the fundamental (1st), 2nd and 3rd harmonics in the pulsed nonlinear acoustic beam produced in the two-layer configuration of media and their numerical predictions obtained using the TAWE approach for the transducer used. In Fig. 6 the fundamental, 2nd and 3rd harmonic components measured along the beam axis are plotted for the axial distance varying from 80 mm to 120 mm. The agreement between the simulation and measurement results at the axial distances up to 90 mm (focal distance for the nonlinear propagation mode) is very good, however at the distances larger than 90 mm the discrepancy begins to be visible. The exact reason for this discrepancy is difficult to determine. It is likely that the discrepancy

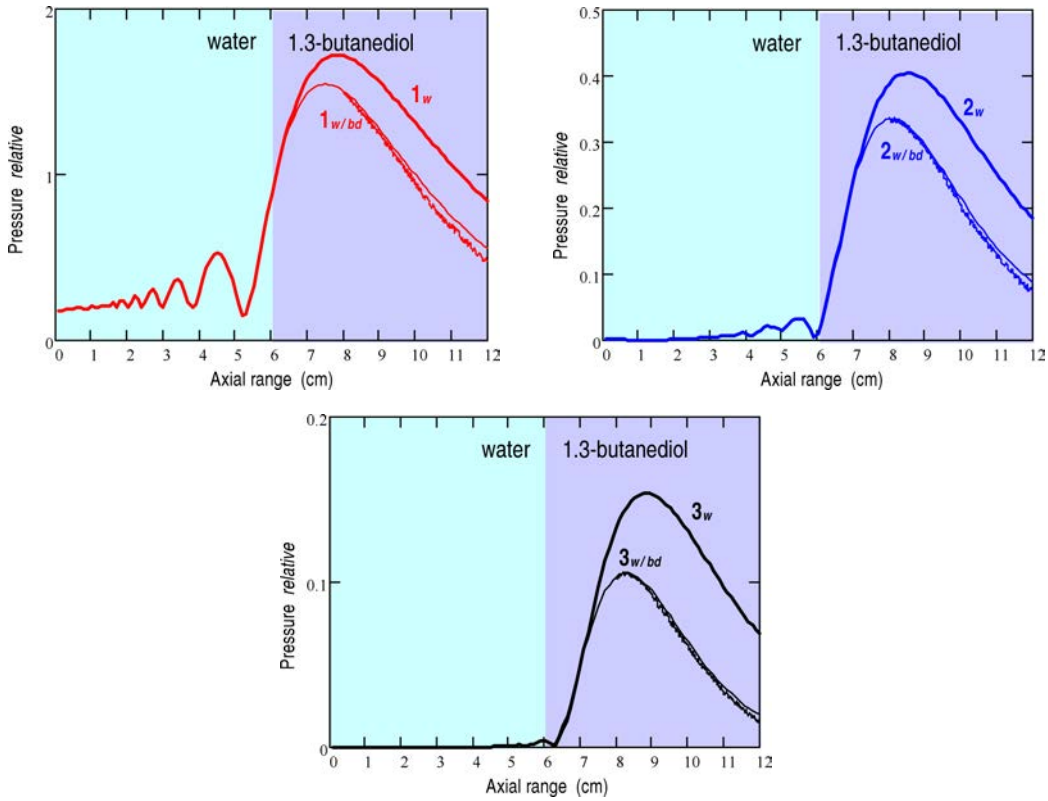

Fig. 6. Axial pressure variations of the fundamental (1), 2nd (2) and 3rd (3) harmonics in the pulsed focused nonlinear beam produced by the transducer used in water (thick lines, subscripts w) and in two-layer media comprising of a 60-cm water layer and a 60-cm layer of 1.3-butanediol (thin lines, subscripts w/bd). Calculation (solid lines) and measurement (points) results for 2.25 MHz 8-cycle tone bursts with the initial pressure amplitude of 117 kPa are shown.

is due to the fact that the plane wave conditions beyond the focal plane are not met. The results presented in Fig. 6 demonstrate that the nonlinear propagation model based on the TAWE approach is capable of predicting the pulsed nonlinear acoustic pressure fields from axially-symmetric sources in layered media with attenuation arbitrarily dependent on frequency. So, the model can be used as an effective research tool for prediction of both the 3D acoustic pressure variations and heat sources distributions (induced due to these fields) in pulsed focused nonlinear beams produced by clinically relevant therapeutic sources in layered media comprising of physiological fluids and tissues.

Figures 7, 8, 9 and 10 show the axial pressure variations of the fundamental (1st), 2nd and 3rd harmonic components in the pulsed nonlinear beams generated

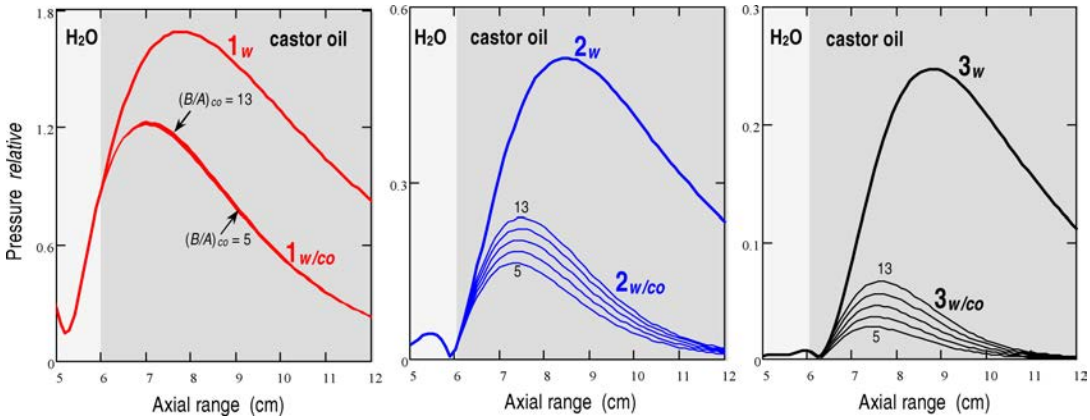

Fig. 7. Axial pressure variations of the fundamental (1st), 2nd (2) and 3rd (3) harmonics in the pulsed focused nonlinear beam produced by the transducer used generating 8-cycle tone bursts with the initial pressure amplitude of 0.15 MPa in water (subscripts w) and in two-layer media (subscripts w/co) comprising of a 6-cm water layer and a 6-cm layer of castor oil whose value of the $(B/A)_{co}$ assumed in calculations was varied between 5 and 13 with an increment of 2. Pressure variations are shown at the axial range between 5 cm and 12 cm.

from the transducer used and calculated for 8-cycle tone bursts with the initial pressure of 150 kPa propagating in water or in two-layer media: 6-cm water/6-cm tested medium (castor oil, silicone oil, pig liver and human brain, respectively) whose value of the B/A parameter assumed in calculations was varied between 5 and 13 with various increments.

The linear and nonlinear acoustic parameters assumed in calculations for media considered are quoted in Table 1.

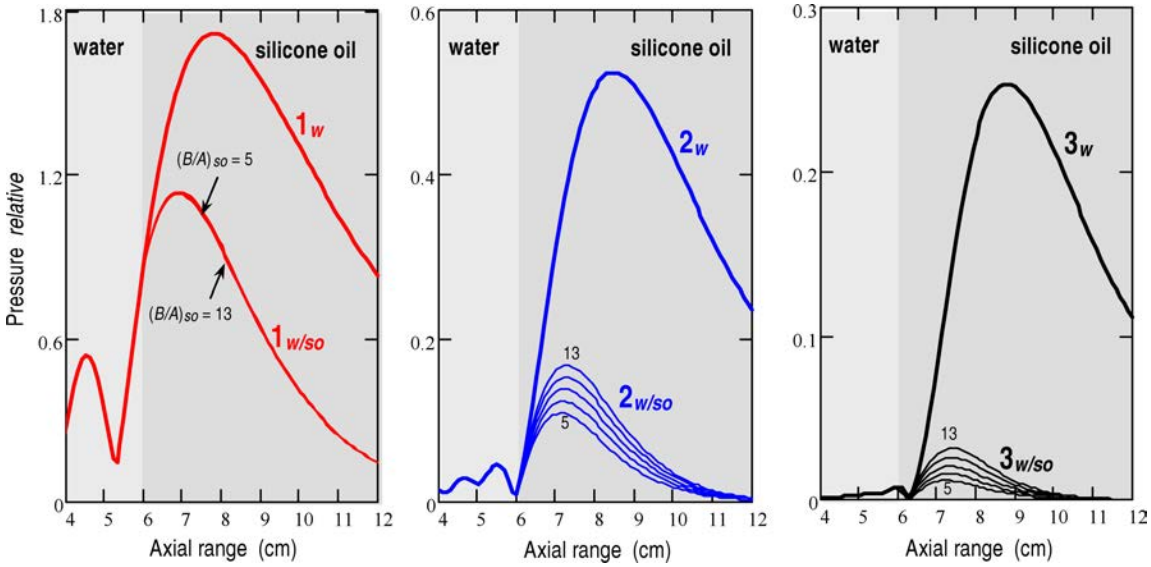

Fig. 8. Axial pressure variations of the fundamental (1), 2nd (2) and 3rd (3) harmonics in the pulsed focused nonlinear beam produced by the transducer used generating 8-cycle tone bursts with the initial pressure amplitude of 0.15 MPa in water (subscripts w) and in two-layer media (subscripts w/so) comprising of a 6-cm water layer and a 6-cm layer of silicone oil. The nonlinearity parameter $(B/A)_{so}$ assumed in calculations for silicone oil was varied between 5 and 13 with an increment 2. Pressure variations of harmonics are shown at the axial range between 4 cm and 12 cm.

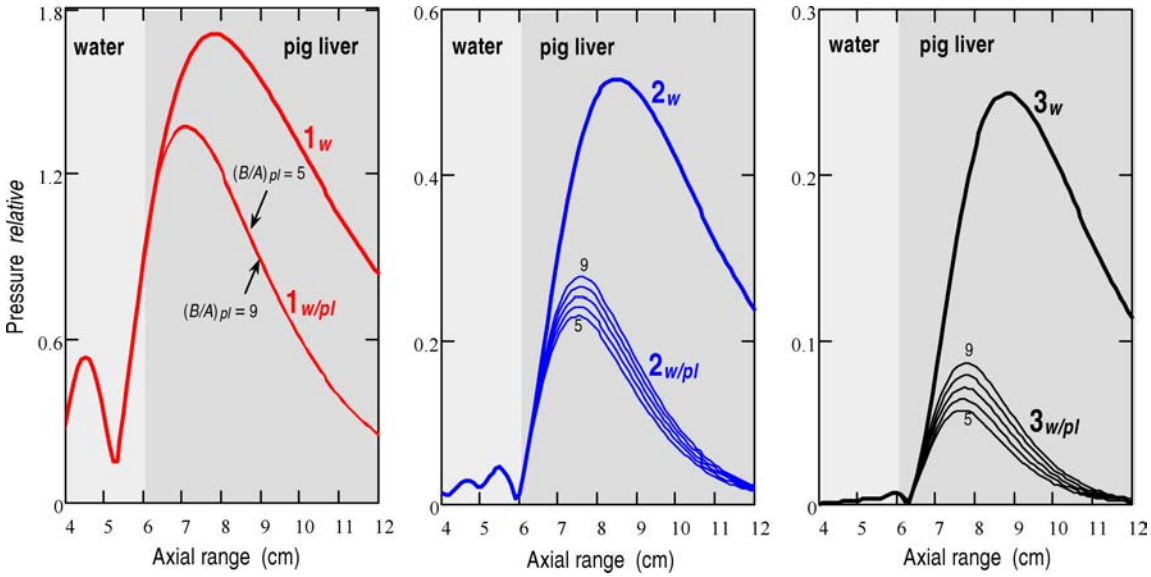

Fig. 9. Axial pressure variations of the fundamental (1), 2nd (2) and 3rd (3) harmonics in the pulsed focused nonlinear beam produced by the transducer used generating 8-cycle tone bursts with the initial pressure amplitude of 0.15 MPa in water (subscripts w) and in two-layer media (subscripts w/pl) comprising of a 6-cm water layer and a 6-cm layer of pig liver whose value of the $(B/A)_{pl}$ assumed in calculations was varied between 5 and 9 with an increment 1.

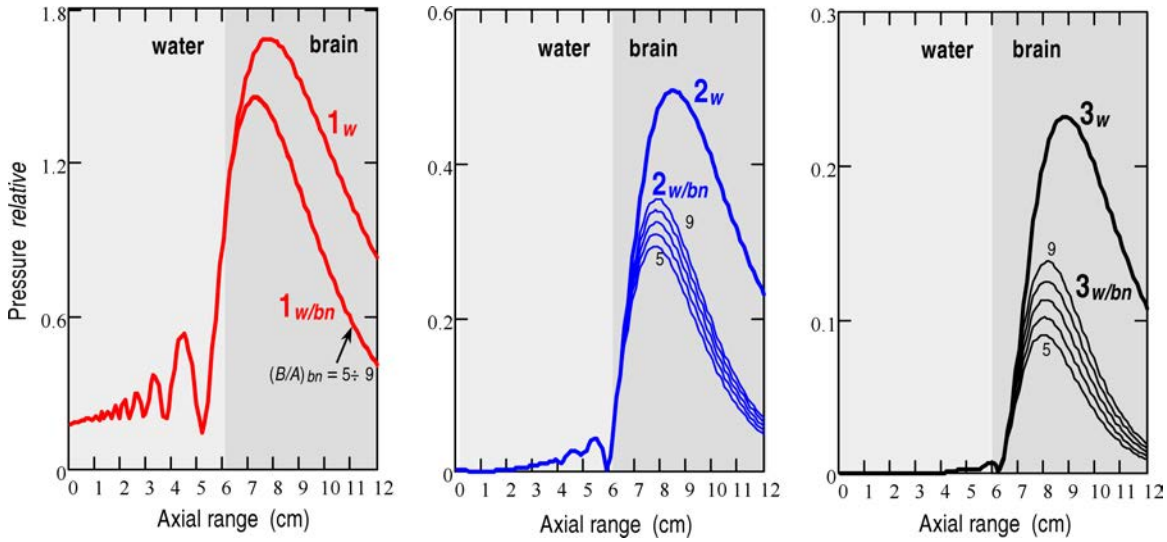

Fig. 10. Axial pressure variations of the fundamental (1), 2nd (2) and 3rd (3) harmonics in the pulsed focused nonlinear beam from the transducer used generating 8-cycle tone bursts with the initial pressure amplitude of 0.15 MPa in water (subscripts w) and in two-layer media (subscripts w/bn) comprising of a 6-cm water layer and a 6-cm layer of human brain whose value of the $(B/A)_{bn}$ assumed in calculations was varied between 5 and 9 with an increment 1.

8. Conclusions

The results of the measurements of pulsed focused nonlinear acoustic fields in water and in two-layer media: water/1.3-butanediol produced by the 2.25 MHz circular focused (f-number 3) transducer with diameter of 29 mm were compared with the numerical predictions obtained using the Time-Averaged Wave Envelope (TAWE) approach to the numerical solution of the second order nonlinear differential wave equation for axially-symmetric sources (Wójcik *et al.*, 2006). The comparison of the experimental results and numerical predictions has shown that the TAWE approach is capable of predicting fairly well both the spatial-peak and spatial-spectral pressure distributions in pulsed focused nonlinear beams produced in layered biological media by clinically relevant therapeutic sources.

Discrepancies between the theoretically predicted axial pressure distributions and those determined experimentally are visible beyond the focal plane. It is conceivable that the true plane wave conditions are not fulfilled in this region. The data presented verified the applicability of the TAWE method as an effective research tool for prediction both the pulsed focused nonlinear acoustic pressure fields and heat sources distributions from clinically relevant therapeutic probes in layered media comprising of physiological fluids and tissues. Such effective research tool is indispensable for planning noninvasive ultrasonic therapies in layered soft tissues and especially inside a brain when the nonlinear pulsed waves have to pass through a skull bone strongly attenuating ultrasonic waves.

Acknowledgment

This work was supported by the Ministry of Science and Higher Education from means on the statutory activity and by the National Science Centre from the Grant 2011/01/B/ST7/06735.

References

1. Baker A.C., Anastasiadis K., Humphrey V.F. (1988), *The nonlinear pressure field of a plane circular piston: theory and experiment*, J. Acoust. Soc. Am., **84**, 1483–1487.
2. Beyer R.T. (1997), *The B/A parameter*, [in:] Nonlinear acoustics, Hamilton M.F., Blackstock D.T. [Eds.], Academic Press, NY, pp. 25–37.
3. Chavrier F., Lafon C., Birer A., Barriere C., Jacob X., Cathignol D. (2006), *Determination of the nonlinear parameter by propagating and modelling finite amplitude plane waves*, J. Acoust. Soc. Am., **119**, 5, 2639–2644.
4. Duck F.A. (1990), *Physical Properties of Tissue*, Academic Press, London.
5. Kujawska T., Nowicki A., Lewin P.A. (2011a), *Determination of nonlinear medium parameter B/A using model assisted variable-length measurement approach*, Ultrasonics, **51**, 997–1005.
6. Kujawska T., Secomski W., Krawczyk K., Nowicki A. (2011b), *Thermal effects induced in liver tissues by pulsed focused ultrasonic beams from annular array transducer*, Archives of Acoustics, **36**, 937–944.
7. Kujawska T., Wójcik J., Nowicki A. (2011c), *Determination of the B/A of biological media by measuring and modeling nonlinear distortion of pulsed acoustic wave in two-layer system of media*, [in:] Acousti-

cal Imaging, vol. 30, 295–303, M. Andre *et al.* [Eds.], Springer Science & Business Media B.V.

8. Nachef S., Cathignol D., Tjøtta J.N., Berg A.M., Tjøtta S. (1995), *Investigation of a high intensity sound beam from a plane transducer. Experimental and theoretical results*, J. Acoust. Soc. Am., **98**, 4, 2303–2323.
9. National Physical Laboratory, Kaye&Laby, Tables of Physical & Chemical Constants, Medical Ultrasonics, http://www.kayelaby.npl.co.uk.
10. Wójcik J., Nowicki A., Lewin P.A., Bloomfield P.E., Kujawska T., Filipczyński L. (2006), *Wave envelopes method for description of nonlinear acoustic wave propagation*, Ultrasonics, **44**, 310–329.
11. Wójcik J., Kujawska T., Nowicki A., Lewin P.A. (2008), *Fast prediction of pulsed nonlinear acoustic fields from clinically relevant sources using Time-Averaged Wave Envelope approach: comparison of numerical simulations and experimental results*, Ultrasonics, **48**, 707–715.

PAN ARCHIVES OF ACOUSTICS
Vol. **37**, No. 3, pp. 279–286 (2012)

DOI: 10.2478/v10168-012-0036-1

Application of Artificial Neural Networks for Defect Detection in Ceramic Materials

Tahir Cetin AKINCI[(1)], H. Selcuk NOGAY[(1)], Ozgur YILMAZ[(2)]

[(1)] *Department of Electrical & Electronics Engineering*
Faculty of Engineering, Kirklareli University
Kirklareli-Turkey; e-mail: cetinakinci@hotmail.com, selcuknogay@kirklareli.edu.tr

[(2)] *Department of Computer Education & Instructional Technology*
Hasan Ali ucel Education Faculty, Istanbul University
Fatih, Istanbul-Turkey; e-mail: oyilmaz@istanbul.edu.tr

(*received October 28, 2011; accepted June 6, 2012*)

In this study, an artificial neural network application was performed to tell if 18 plates of the same material in different shapes and sizes were cracked or not. The cracks in the cracked plates were of different depth and sizes and were non-identical deformations. This ANN model was developed to detect whether the plates under test are cracked or not, when four plates have been selected randomly from among a total of 18 ones. The ANN model used in the study is a model uniquely tailored for this study, but it can be applied to all systems by changing the weight values and without changing the architecture of the model. The developed model was tested using experimental data conducted with 18 plates and the results obtained mainly correspond to this particular case. But the algorithm can be easily generalized for an arbitrary number of items.

Keywords: impulse noise, ANN, defect detection, ceramic materials.

1. Introduction

The use of ceramic materials is an indispensable part of our daily lives, occurring both as a part of artistic forms and a part of industrial processes (Bayazit, Bayazit, 2010). Ceramics are obtained by mixing inorganic industrial raw materials in certain ratios, shaping the end product, and hardening it by cooking. They are among the oldest tools used by mankind (Kucuk, Akinci, 2006) and were used since ancient times, especially for the production of kitchen utensils and the production of them still form the greatest production sector pertaining to ceramics (Bayazit, Bayazit, 2010).

Today, the ceramics industry forms the basis of many other industrial areas (Kucuk, Akinci, 2006). Ceramic materials are preferred for their certain advantages, such as resistance to high temperatures, lightness compared to metal materials, abundance of raw material sources, and resistance to wear, low coefficients of friction and high resistance. In recent years, special ceramics have found application fields in areas like computers, electronics and space research (Sawitz, 1999a; 1999b; Kubik, 2006; Uludag, 1998; SMPISTC, 2001).

The brittle nature of ceramic materials is their most important disadvantage. Since the compositions of ceramic materials contain metal oxides, silicates, carbides, nitrides, borides, glass etc, which can all be found in nature in abundance, their crystalline structures are very complex (MEGEP, 2007; Kamilov *et al.*, 1998). Amorphous structures or amorphous/crystalline joint structures may also be formed (Popovskaya, Bobkova, 2002; Samborski, Sadowski, 2005). Their material properties are based on their bond structures. They generally have low satiety and ductility, are hard and brittle. Sine they don't contain free electrons, they isolate electricity and heat well (Revel, Rocchi, 2006; De Andrade *et al.*, 1998; 1999). Because of the structure of their atomic bonds, they are chemically stable and have high melting points. The abundance in raw materials, the ease of their processing, the simplicity of their production, their low costs, the ease of their use, their hardness and resistance to heat increase their fields of use. Beside these, the most important problem in ceramic materi-

als is the brittleness and deformation property of those materials. The greatest disadvantages of ceramics and porcelains used in industry and as kitchen utensils are breaking and cracking.

Mechanical failure in ceramic materials mostly stem from structural imperfections. These structural imperfections are surface cracks, pores, residues and large particles that are formed during production (De Andrade *et al.*, 1998; 1999; Ranachowski, Rejmund, 2008).

All ceramic materials are brittle. Their observed tensile strength is about 0.70 MPa. In some special ceramics, a value of 7000 MPa can be reached through A12O3 fibers. The impact resistances of hard ceramics are low because of their ionic collective bonds (SMP-ISTC, 2001; Uludag, 1998; MEGEP, 2007).

In some ceramics, through stacking or storing mistakes, grain boundaries with small angles or twin grain boundaries may be form. However, the surfaces of ceramic particles are much more important since their breaking surface may be exposed (Uludag, 1998). Since these break and cracks are not visible in enamelled ceramics, such deformations have to be detected through special methods. In this study, the cracks formed in ceramic pales were detected through impact noise. To obtain impact noise, it is necessary to apply a fixed impact A pendulum was used for this purpose.

The impulse noise generated by the measuring system was then digitized and transferred to the signal processing unit (a personal computer PC) as the input data fort it developed the ANN algorithm. Pendulums have a quite interesting dynamic system. They are such physical devices that make angular movements and cause the same effects by forming the same movements (Ranachowski, Rejmund, 2008; Bevivino, 2009; Kater, 1996).

Using Fig. 1 one can begin deriving the equation of motion for the pendulum. Equation (1) becomes, by use of

$$\mathbf{\Gamma} = \mathbf{r} \times \mathbf{F}, \tag{1}$$

$$-\text{damping}_{\text{force}} = \text{gravity}_{\text{force}} + \text{driving}_{\text{force}} = I\ddot{\theta}, \tag{2}$$

$$-bvr\sin\theta + -mgr\sin\theta + Fr\sin\theta = I\ddot{\theta}. \tag{3}$$

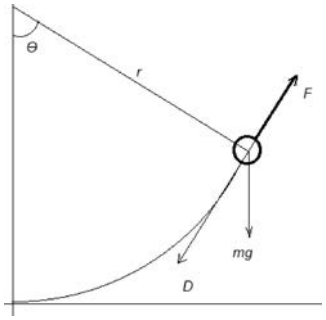

Fig. 1. Scheme of a pendulum (Akinci, 2011).

Let the damping and driving forces be parallel to the motion of the pendulum. Let the driving force be a function of time. Let $D = bv$, so the damping force is dependent on the velocity, v or $r\dot{\theta}$. Rearranging and substituting gives:

$$mr^2\ddot{\theta} + br^2\dot{\theta} + mrg\sin\theta = F(t)r, \tag{4}$$

$$\ddot{\theta} + \frac{b}{m}\dot{\theta} + \frac{g}{r}\sin\theta = \frac{F(t)}{mr}. \tag{5}$$

Equation (5) is a second order differential equation describing the dynamical system of interest (Bevivino, 2009; Kater, 2008; Akinci, 2011). The paper is organized as follows. In the next section a brief introduction to the ANN algorithm is given. In Sec. 3, the experimental setup is shown and in Sec. 4, the selected parameters of the developed ANN are explained. In Secs. 5 and 6, the training and testing ANN are briefly commented, respectively. And finally, a discussion of the obtained results is given in Sec. 7.

2. Artificial Neural Network (ANN)

Artificial Neural Networks (ANN) are complex computational or mathematical models developed in order to process information in the way inspired by the nature of biological neural networks. They are usually adaptive systems for non-linear data processing, used intensively for modelling complex relations between inputs and outputs, pattern recognition, etc.

There are many of different types of ANN models. The most popular of them include the multilayer perceptron, which is generally trained with the back propagation algorithm. In Fig. 1 two layers feed forward network for general application of ANN is illustrated. Back propagation is a training method for multilayer feed forward networks. Such an ANN model network proposed for this study, including three layers of perceptrons is shown in Fig. 2. In this study, thirty-five number of neuron was used in the hidden layer, sixteen input parameters and five output parameters were used in the input layer as shown in Tables 1 and 2, respectively (Hagan *et al.*, 1996; Akinci, 2011; Box, Jenkins, 1970).

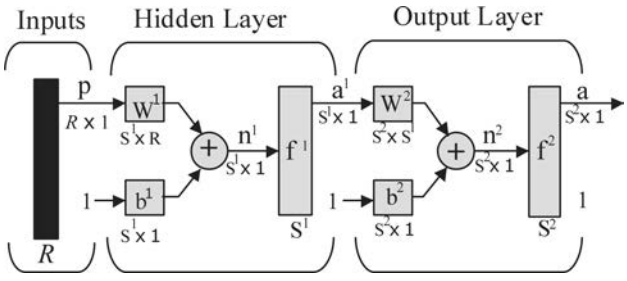

Fig. 2. Two-layer feed forward network.

By the algorithmic approach known as the Levenberg-Marquardt back propagation algorithm,

the error is decreased repeatedly. Some ANN models employ supervisory training while others are referred to as none-supervisory or self-organizing training. However, the vast majority of ANN models use supervisory training (Fig. 3). The training phase may consume a lot of time. In the supervisory training, the actual output of ANN is compared with the desired output. The training set consists of presenting input and output data to the network. The network adjusts the weighting coefficients, which usually begin with a random set, so that the next iteration will produce a closer match between the desired and the actual output. The training method tries to minimize the current errors for all the processing elements. This global error reduction is created over time by continuously modifying the weighting coefficients until the ANN reaches the user defined performance level. This level signifies that the network has achieved the desired statistical accuracy for a given sequence of inputs. When no further training is necessary, the weighting coefficients are frozen for the application. After a supervisory network performs well on the training data, then it is important to see what can it do with data which it had not seen before. If a system does not give reasonable outputs for this test set, the training period is not over. Indeed, this testing is critical to insure that the network has not simply memorized a given set of data, but has learned the general patterns involved within the application (Hagan *et al.*, 1996; Akinci, 2011; Box, Jenkins, 1970).

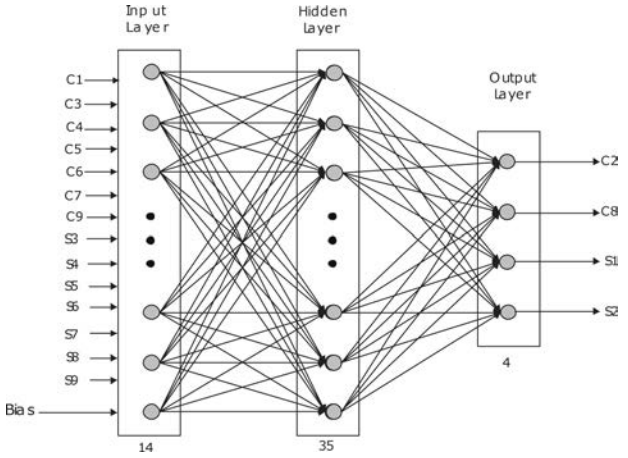

Fig. 3. Proposed ANN model.

The back-propagation learning algorithm is presented below in brief. For each neuron in the input layer, the neuron outputs are given by

$$n_i = o_i, \tag{6}$$

where n_i is the input of neuron i, and o_i the output of this neuron. Again for each neuron in the output layer, the neuron inputs are given by

$$n_k = \sum_{j=1}^{N_j} w_{kj} o_j, \qquad k = 1, 2, 3, ..., N_k, \tag{7}$$

where w_{kj} is the connection weight between neuron j and neuron k, and N_j, N_k the number of neurons in the hidden layer and output layer, respectively. The neuron outputs are given by

$$o_k = \frac{1}{1 + \exp\left[-\left(n_k + \theta_k\right)\right]} = f_k\left(n_k, \theta_k\right), \tag{8}$$

where θ_k is the threshold of neuron k, and the activation function f_k is a sigmoidal function. For the neurons in the hidden layer, the inputs and outputs are given by relationships similar to those given in Eqs. (2) and (3), respectively.

The connection weights of the feed-forward network are derived from the input–output patterns in the training set by the application of the generalized delta rule. The algorithm is based on minimization of the error function on each pattern p by the use of the steepest descent method. The sum of squared errors E_p that is the error function for each pattern is given by

$$E_P = \frac{1}{2} \sum_{k=1}^{N_k} (t_{pk} - o_{pk})^2, \tag{9}$$

where t_{pk} is the target output for the output neuron k, and o_{pk} is the calculated output for the output neuron k. The overall measure of the error for all the input-output patterns is given by

$$E = \sum_{p=1}^{N_p} E_p, \tag{10}$$

where N_p is the number of input-output patterns in the training set. When an input pattern p with the target output vector t_p is presented, the connection weights are updated by using the following equations:

$$\Delta w_{kj} = \eta \delta_{pk} o_{pj} + \alpha \Delta w_{kj}(p-1), \tag{11}$$

$$\delta_{pk} = (t_{pk} - o_{pk}) o_{pk} (1 - o_{pk}), \tag{12}$$

where η is the learning rate, and α is the momentum constant. Again, the connection weights between input the layer neuron i and the hidden layer neuron j can be updated by using the following equations:

$$\Delta w_{ji} = \eta \delta_{pk} o_{pj} + \alpha \Delta w_{ji}(p-1), \tag{13}$$

$$\delta_{pj} = o_{pj}(1 - o_{pj}) \sum_{k=1}^{N_k} \delta_{pk} w_{kj}. \tag{14}$$

It is important to note that the threshold θ of each neuron is learned in the same way as that for the other weights. The threshold of a neuron is regarded as a modifiable connection weight between that neuron and a fictitious neuron in the previous layer which always has an output value of unity (Hagan *et al.*, 1996; Aydogmus, 2009; Bose, 2002).

In order to use the ANN simulator for any application, the number of neurons in the layers, type of activation function (purelin, tansig, logsig), the number of patterns, and the training rate must first be chosen.

The ANN designing process involves five steps. These are gathering the input data, normalizing the data, selecting the ANN architecture, training the network, and validation-testing the network.

3. The measurement system and data acquisation

In this study, a pendulum was used to produce a stable impulse. The Impact Pendulum is an improved pendulum model used for creating equal magnitudes of impacts (Kamilov *et al.*, 1998). Through a little plastic hammer attached to the end of the Impact Pendulum it was provided to have equal magnitudes of impact hits without any damages to the ceramic plate and it was intended to analyse the sound coming from the plate. The measurement and data acquisition can be represented as shown in Fig. 4.

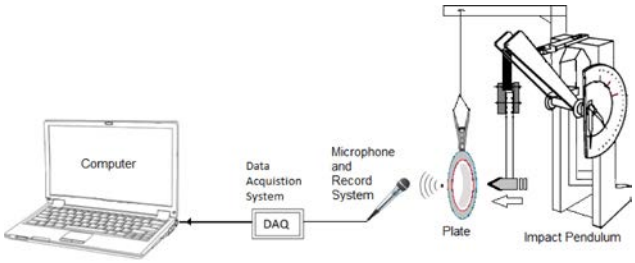

Fig. 4. Data acquisition and measurement systems (Akinci, 2011).

In the study, the POE 2000 type Impact Pendulum was used and the effect to hit the ceramic plate with the same magnitude was achieved. Here, using the Impact Pendulum, the sound coming out as a result of applying equal impacts on the same type and model of plates with or without cracks (in good condition) was transferred to the data collection system, then from the data collection system to the computer and the data processing stage was started. In this study, the sound system model Onyx 800R is used. The output audio data of the amplifier is transmitted to the computer at a sampling rate of 0.0000125 seconds via the Advantech 1716L Multifunction PCI card and the data analysis is performed using Matlab (Fig. 5).

Ten ceramic plates, including those in good condition and those that have different cracks, were determined and plates with impacts of equal magnitudes were applied. The differences of the sounds from the ceramic plates in the same impact are shown in Fig. 5.

The assessments of the time-amplitude graphics of the cracked and good plates are given in Fig. 5. Ac-

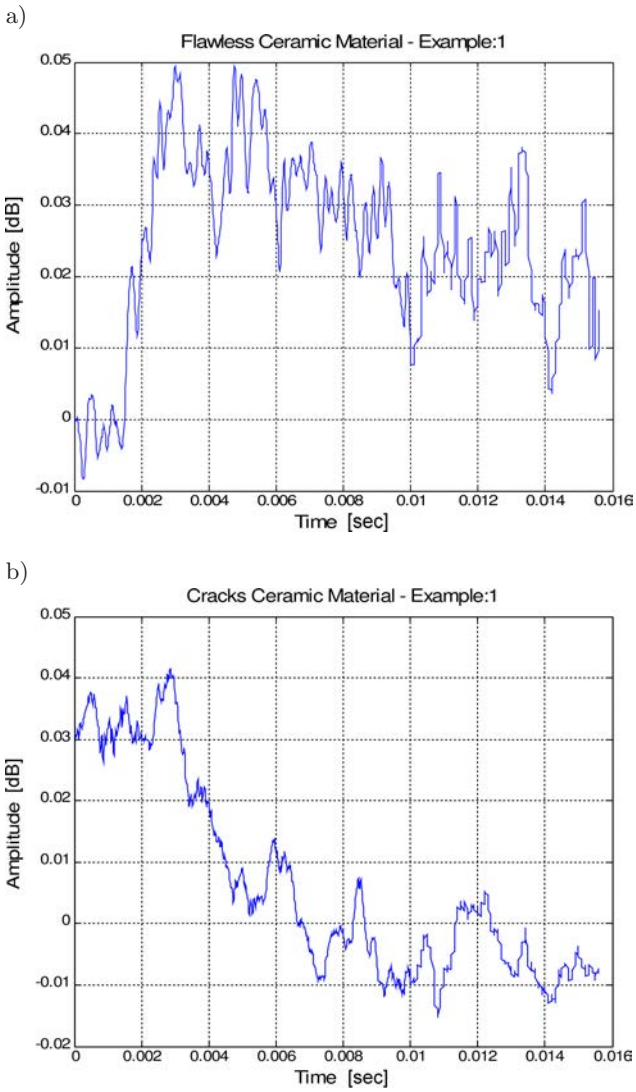

Fig. 5. Noise plot of undamaged and cracked plates (Akinci, 2011): a) undamaged plate, b) cracked plate.

cording to this graphic, there is a sound absorption through the crack openings in the cracked plate after the impact and the vibration does not continue; on the contrary, the vibration in the plate in good condition continues for a longer period on the same level. This situation shows a similar trend in other graphics though it changes according to the size and shape of the cracks in the plates. Here, only one of the five tests was examined. The cracked plates made of different material were used in each experiment.

A summary of the data set used in the study is presented in Table 1. It is also possible to see the input and output data, and the maximum and minimum values for intact and cracked plates in this table. In the study, intact plates were named with "s" and the cracked ones were named with "c". The numbers following the letters (s or c) denote the plate numbers.

Before further processing the measured data were normalized for convenience.

Table 1. Data Set Summary.

	Maximum value	Minimum value	Symbol
Input	0.0415	−0.0153	c1
	0.0128	−0.0358	c3
	0.0214	−0.0351	c4
	0.0315	−0.0159	c5
	0.0345	−0.0429	c6
	0.5260	−0.1970	c7
	0.0338	−0.0053	c9
	0.0447	−0.0180	s3
	0.0560	−0.0094	s4
	0.0440	−0.0202	s5
	0.0314	−0.0167	s6
	0.0400	−0.0344	s7
	0.0380	−0.0507	s8
	0.0437	−0.0139	s9
Output	0.0063	−0.0318	c2
	0.0495	−0.0084	s1
	0.0349	−0.0196	c8
	0.0379	−0.0103	s2

4. Selecting the ANN architecture

The number of layers and the number of processing elements per layer are important decisions for selecting the ANN architecture. Choosing these parameters to a feed forward back propagation topology is the art of the ANN designer. There is no quantifiable best answer to the layout of the network for any particular application. There are only general rules picked up over time and followed by most researchers and engineers applying this architecture to their problems. The first rule states that if the complexity in the relationship between the input data and the desired output increases, then the number of the processing elements in the hidden layer should also increase. The second rule says that if the process being modelled is separable into multiple stages, then additional hidden layer(s) may be required. The result of the tests has showed that the optimal number of neurons in the hidden layer can be chosen as 35 and the activation function has been chosen as a hyperbolic tangent sigmoid function for all the layers.

5. Training the network

In this study ANN was trained with the back propagation (Levenberg-Marquardt) training algorithm. In the training process of this study, the actual output of ANN was compared with the desired output. The training set consists of fourteen input and four output data to the ANN model. The number of data was 1024; 90% of this data were used for training. The network adjusted the weighting coefficients that began with the random set. The training process has been stopped when the error has become stable. The ANN simulator has been trained through the 61 epochs as shown in Fig. 6.

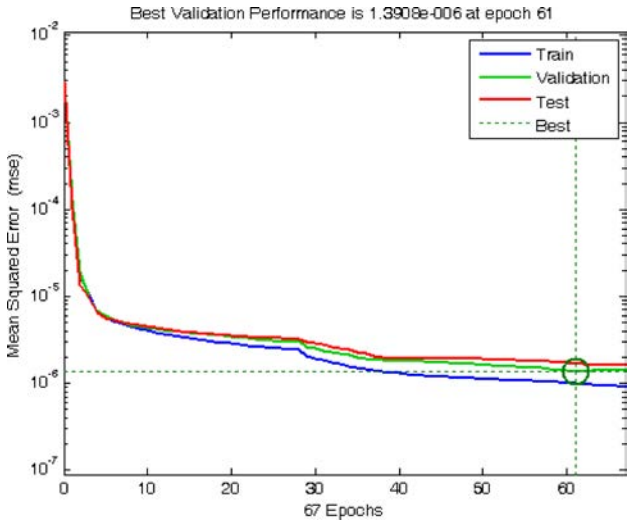

Fig. 6. Training process of the developed ANN algorithm.

6. Testing the network

In the test, an unknown input pattern has been presented to the ANN, and the output has been calculated. A linear regression between the ANN output and target is performed. After the ANN test in step, founded regression coefficients for C2, C8, S1 and S2 outputs ($R = 0.98389$, $R = 0.99348$, $R = 0.99286$ and $R = 0.99669$, respectively) reveals a good agreement between the target and ANN output values. The results of regression analyses are shown in Fig. 7. These coefficient shows that the target and ANN output values were very related to each other.

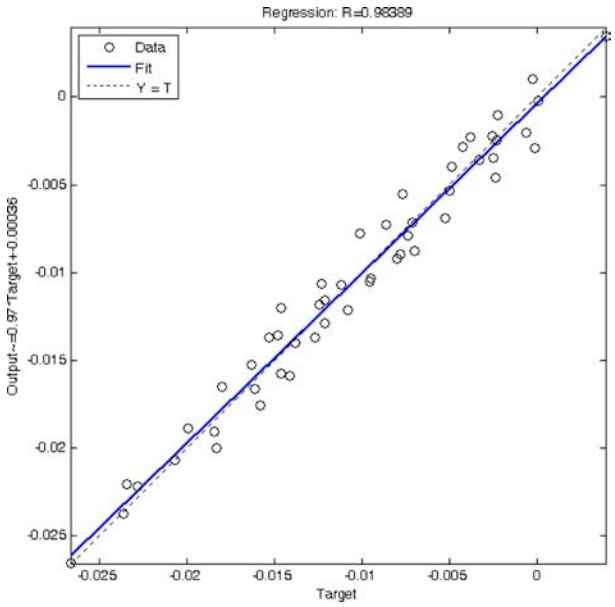

Fig. 7. Regression results of the system for C2.

7. Results and discussions

There are many different statistical methods in the literature. The most common methods mean absolute error (MAE), mean squared error (MSE), root mean squared error (RMSE), and mean absolute percentage error (MAPE). Those were used in this study as seen in Table 2.

With the ANN prediction model developed, the intactness of any four of the 18 plates, of which 9 was cracked, was predicted. Since the prediction was performed basing on the sound data at hand, the details of the deformations can be interpreted by checking the depth of the crack. In the study, only the conditions of the plates with the code numbers C2 and C8 from among the cracked plates and S1 and S2 from among the intact plates were predicted. After all, the real goal of this study is not finding cracked plates but examining the cracks or determining the properties of the cracks. For this purpose, the impact noises that all plates produced as a result of the test conducted through the pendulum were recorded. The goal is to make a right prediction. When Table 2 is examined, it can be clearly seen how low are the values denominating the error. The regression values for every output are proofs of the success of the prediction model. For example, the output of S2 from Table 2 was predicted with a correctness of 99.6%. This means that, through the predicted curve of the S2 plate, an idea can be obtained about how intact is this plate compared to other plates besides identifying the plate as cracked.

Since four outputs were used in the system, it is possible to obtain separate curves for each output. A three-dimensional chart showing all outputs at once can be seen in Figs. 8a and 8b. Even though these three-dimensional charts obtained only from test data look the same, there are error differences between them, albeit small ones. For example, when we look at the last curve of the first output curve line in both of the curves, we can see that the last data indicate a falling trend in the target chart, whereas they are slightly vertex in the output chart.

When separate curves are drawn for every output, they are as shown in Figs. 9–12. Among them Fig. 9 is a chart comparing the true value to the predicted one obtained only for the C2 output.

The proximity of the two curves in Fig. 10 shows the success of the system. The system determines the crack level or intactness of the plate according to the similarity between the true chart and the predicted one. In other words, when one looks as in Fig. 10, where the crack curve of the plate with code number C2 is the target curve that corresponds to the prediction curve of the system, one can say that the plate with the code number C2 is deformed or cracked.

In Fig. 10, the intactness curve of the plate with code number S1 was used. Here, similarly to Fig. 9, the intactness curve of the plate was used to check whether the plate was intact. When the output of the ANN prediction model is compared to the intactness curve in Fig. 10, their proximity can be easily seen. In that case, it can be said that the plate with the code number S1 is intact.

Table 2. Performance of the system.

Output	MAPE	MAE	MSE	RMSE	R
C2	0.227133323	0.001073978	0.00000161381	0.00127035	0.98389
C8	0.154625299	0.000962429	0.00000151338	0.00123019	0.99348
S1	0.159036303	0.001305272	0.00000258198	0.00160685	0.99286
S2	1.705792685	0.00082323	0.00000102769	0.00101375	0.99669

a) b)

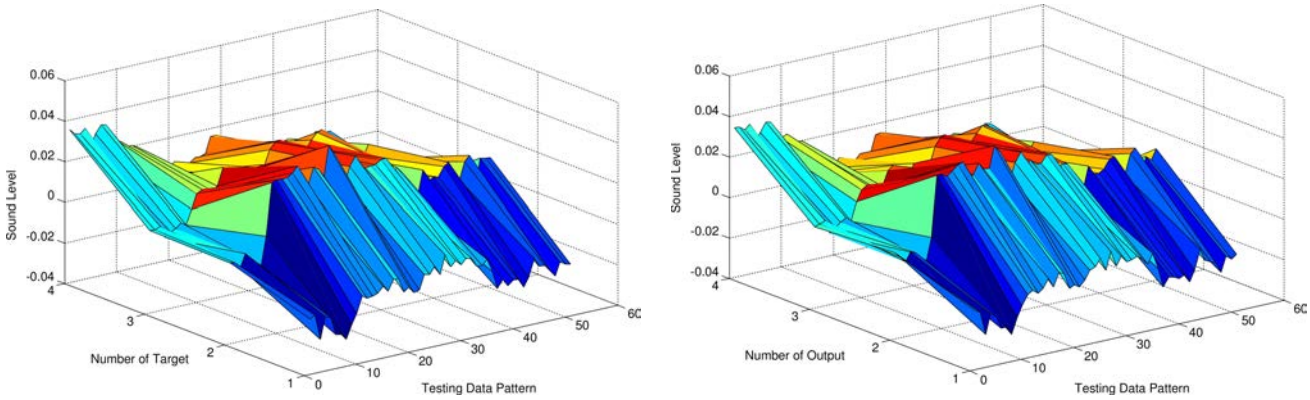

Fig. 8. Variation of the ANN testing data (a) output, (b) target.

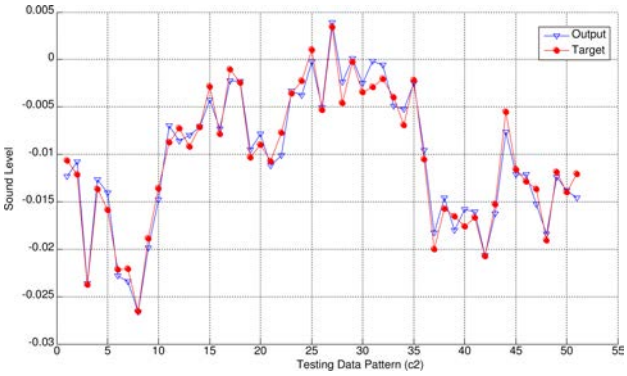

Fig. 9. Comparison of the testing data with the target ones.

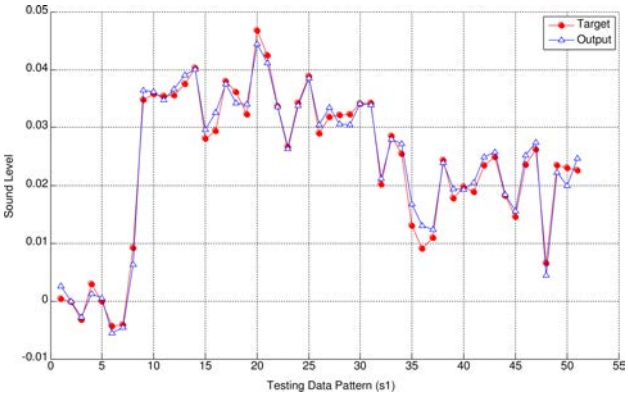

Fig. 10. Comparison of the testing data with the target ones.

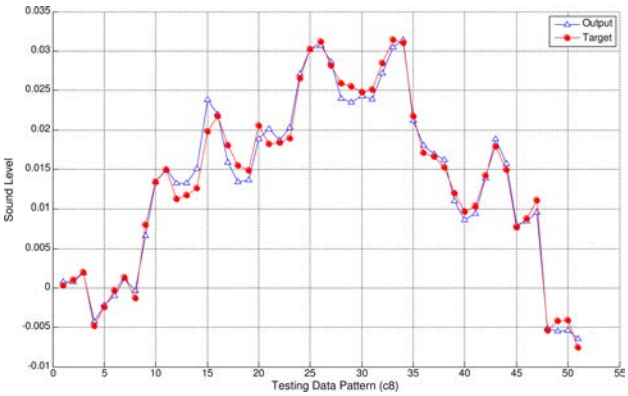

Fig. 11. Comparison of the testing data with the target ones.

Comparison of the testing data with the target ones are shown Fig. 11. In Fig. 12, just like in Fig. 10, the intactness curve of the plate with code number S2 was compared to the output of the ANN and the intactness of the plate was confirmed. In order to determine the wear conditions of the plates, the intactness and crack data from the plates of the same kind are needed. With those curves, it is possible to obtain prediction models and data sets that allow one to check the physical conditions of the plates and calculate the lifespan of them.

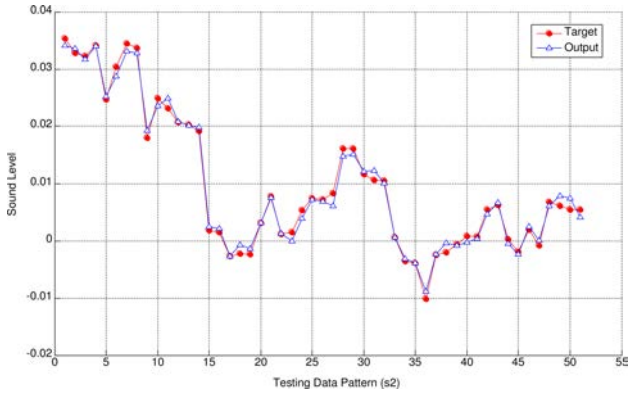

Fig. 12. Comparison of the testing data with the target ones.

8. Conclusions

In this study, a multi-layered artificial neural network model was developed in order to determine the deformation condition (whether cracked or not) of a ceramic material. Experimental applications were performed in order to obtain a data set that would be used in the ANN model. As a result of these experiments, the data set to be used in the training and testing of the ANN model was trained with the impact noises of impacts applied on 18 ceramic plates, 9 of which were cracked

The following results have been obtained:

- The deformation level of a ceramic material was measured.
- A data set was formed from the data obtained according to different deformation conditions.
- A multi-layered ANN model was developed. Using 90% of the data set that was formed, the ANN model as trained with the Back propagation learning algorithm. With the other 10% of the data set, the success of the system was tested.
- At the end of the test, the deformation conditions of the cracked or intact plates were predicted with a success rate of 98.38% for the plate with code number C2, 99.34% for the plate with code number C8, 99.28% for the plate with code number S1, and 99.66% for the plate with code number S2.

As a result of the study, it was found that the experimental results for intact and cracked plates and the ANN outputs were very consistent with each other.

References

1. Akinci T.C. (2011), *The Defect Detection in Ceramic Materials Based on Time-Frequency Analysis by Using the Method of Impulse Noise*, Archieves on Accoustic, **36**, 1, 77–85.
2. Aydogmus Z. (2009), *A neural network-based estimation of electric fields along high voltage insulators*, Expert Systems with Applications, **36**, 8705–8710.

3. Bayazit M., Bayazit E. (2010), *Evaluation of Ceramic Materials on Art*, Journal of Applied Sciences Research-INSInet Publication, **6**, 6, 790–795.
4. Bevivino J. (2009), *The Path From the Simple Pendulum to Chaos*, Dynamics at the Horsetooth, **1**, 1–24.
5. Bose B.K. (2002), *Modern power electronics and AC drivers*, Prentice Hall PTR, USA, p. 625–689.
6. Box G.E.P., Jenkins G. (1970), *Time Series Analysis, Forecasting and Control*, *Golden-Day, San Francisco,* CA.
7. Ceramics and Glass Technology, (2007), Republic of Turkey Ministry of National Education, [MEGEP], p. 340–355.
8. De Andrade R.M., Paone N., Revel G.M. (1998), *Non Destructive Thermal Detection of Delamination in Ceramic Tile*, Proc. ENCIT 98, pp. 727–731, Rio de Janeiro.
9. De Andrade R.M., Esposito E., Paone N., Revel G.M. (1999), *Non-destructive Techniques for Detection of Delamination in Ceramic Tile: A Laboratory Comparison Between Ir Thermal Cameras and Laser Doppler Vibrometers*, Proc. SPIE, **3585**, 367–377.
10. Hagan T.M., Demuth H.B., Beale M. (1996), *Neural Network Design*, PWS Publishing Company, Boston, 2–44.
11. Kamilov S., Karabaeva M., Abdurrahmanov M. (1998), *Studies of Structure of Ceramic Materials Containing Molibdenum Particles Within the Framework of Theory of Non-Homogeneous Systems*, TUBITAK, Tr. J. of Physics, **22**, 777–781.
12. Kater H. (1818), *An account of experiments for determining the length of the pendulum vibrating seconds in the latitude of London*, Phil. Trans. R. Soc. (London), **104**, 33, 109, [Retrieved (2008)-11-25].
13. Kubik J. (2006), *Durability of monuments* [in Polish: *Trwałość zabytków*], Studia z zakresu Fizyki Budowli. Sekcja Fizyki Budowli KILiW PAN, Łódź.
14. Kucuk H., Akinci T.C. (2006), *Roughness of Ceramic Materials by the Method of Determining Noise Impact*, Conference For Computer Aided Engineering And System Modelling, Abant Palace Hotel, Bolu-Turkey.
15. Maldague X.P.V. (2001), *Theory and Practice of Infrared Technology for Nondestructive Testing*, pp. 238–250, John Wiley & Sons, New York.
16. Popovskaya N.F., Bobkova N.M. (2002), *Mullite-Tialite Ceramic Materials Based on Chemically Precipitated Mixtures (A Review)*, Glass and Ceramics, **59**, 7–8, 234–236, DOI: 10.1023/A:1020979228914.
17. Ranachowski P., Rejmund F. (2008), *Mechanical-Acoustic Examination of Ceramic Material*, Proceedings of the 7th Int. Conference EEEIC 08, Cottbus, pp. 11–13.
18. Revel G.M., Rocchi S. (2006), *Defect detection in ceramic materials by quantitative infrared thermography*, 8th Conference on Quantitative Infrared Thermography – QIRT'2006, Padova, Italy.
19. Samborski S., Sadowski T. (2005), *Experimental Investigations and Modelling of Porous Ceramics, Solid Mechanics and ıts Applications*, IUTAM Symposium on Multiscale Modelling of Damage and Fracture Processes in Composite Materials Proceedings of the IUTAM Symposium held in Kazimierz Dolny, Poland.
20. Sawitz M. (1999), *Commercialisation of Advanced Ceramics,* Part I, Am. Ceram. Soc. Bull., **78**, 1, 53–56.
21. Sawitz M. (1999), *Commercialisation of Advanced Structural Ceramics*, Part II, Am. Ceram. Soc. Bull., **78**, 3, 52–56.
22. Stone and Mineral Products Industry Special Trade Commission Report [SMPISTC], (Ceramic Coating Materials, Ceramic Health Care Products, Technical Ceramics), DPT: 2552 – ÖÝK: 568, ISBN 975-19-2807-9, Ankara 2001 Turkey.
23. Uludag K. (1998), *Ceramic Art of Identity Problem*, Journal of Art in Turkey, **33**, 36–38.

PAN ARCHIVES OF ACOUSTICS
Vol. **37**, No. 3, pp. 287–294 (2012)

DOI: 10.2478/v10168-012-0037-0

Theoretical Studies of Nonlinear Generation Efficiency in a Bubble Layer

Anna BARANOWSKA

Faculty of Applied Physics and Mathematics
Gdańsk University of Technology
Narutowicza 11/12, 80-233 Gdańsk, Poland; e-mail: anbar@mif.pg.gda.pl

(*received October 25, 2011; accepted June 13, 2012*)

The aim of the paper is a theoretical analysis of propagation of high-intensity acoustic waves throughout a bubble layer. A simple model in the form of a layer with uniformly distributed mono-size spherical bubbles is considered. The mathematical model of the pressure wave's propagation in a bubbly liquid layer is constructed using the linear non-dissipative wave equation and assuming that oscillations of a single bubble satisfy the Rayleigh-Plesset equation. The models of the phase sound speed, changes of resonant frequency of bubbles and damping coefficients in a bubbly liquid are compared and discussed. The relations between transmitted and reflected waves and their second harmonic amplitudes are analyzed. A numerical analysis is carried out for different environmental parameters such as layer thicknesses and values of the volume fraction as well as for different parameters of generated signals. Examples of results of the numerical modeling are presented.

Keywords: nonlinear acoustics, bubble layer, transmitted and reflected waves.

1. Introduction

The nonlinear wave generation inside layers plays a very important role in practice of production of parametric sonars, where the key problem is the efficiency of their nonlinear generation. The known mathematical models of this problem consist of a set of two differential equations. The first of them, the linear non-dissipative wave equation, describes acoustic pressure changes in the bubble layer (see, for example, Druzhinin *et al.*, 1996; Vanhille, Campos–Pozuelo, 2008). The second one is an equation, which allows to predict the bubble radius changes, or equivalently, the bubble volume variations. To complete their models, some authors use the Zabolotskaya and Soluyan approach, in which the bubble volume variation changes are applied (see e.g., Hamilton, Blackstock, 1998; Vanhille, Campos–Pozuelo, 2008). Another option in the theoretical analysis is the application of the Rayleigh–Plesset equation which allows to analyze radius changes of a bubble (see, for example Leighton, 2008). Our model of bubble oscillations is based on the Rayleigh–Plesset equation. It is worth noting that in the Vanhille and Druzhin models and similar ones, it is assumed that the differences between values of density in the bubble layer and outside of it are small. Moreover, they take into account only the viscous damping constant. The model proposed by the author of this paper (Baranowska, 2011) allows to analyze the problem in a more general form. For example, it permits to include not only the viscous damping constant but also the total damping coefficient and different values of the sound speed and density inside and outside the bubble layer. In this paper, we assume that the density differences are small and the model presented in Sec. 2 takes into consideration this fact and, as a consequence, we obtain a simplified version of the general model.

It should also be mentioned that a correct choice of physical parameters is very important in the process of theoretical investigations as they influence the accuracy and the correctness of the results. One of them is the sound speed. It is possible to find many papers on modeling and measurements of this parameter in different media (for example Hamilton, Blackstock, 1998; Perelomova, Wojda, 2010). There exist a few formulae for the prediction of the behavior of this parameter in a bubbly medium. Among others there is a model proposed by Ye and Ding (1995) where the influence of multiple scattering of waves on the sound

speed is incorporated. Another one, simpler but nevertheless very popular and commonly used, is a model proposed by Commander and Prosperetti (1989). However, it does not include higher-order bubble interactions and can be used rather when the gas volume fraction is small or the frequencies of sounding signals are far from the resonance of the bubbles.

In this paper we present the results of a numerical study of the nonlinear propagation of high intensity waves in a bubbly liquid layer. The transmitted and reflected waves as a function of the incident wave frequency in relation to the bubble's resonance frequency as well as their concentration and layer thicknesses are studied. The efficiency of the generation of second harmonic components is examined and examples of computations are presented. In our work, we have considered two cases of bubble layers. In the first one, the layers are filled with bubbles of size which assures that they are at resonance with the sounding signals. In the second case, the bubble's resonance frequency is far from the sounding signals. We used the Commander and Prosperetti model to compute the phase sound speed in the bubble layer. The values of this parameter obtained by this model for higher values of the volume fraction and resonance frequency differ from those obtained by using the Ye and Ding model. However, this fact did not influence the final results of the numerical calculations significantly.

2. Mathematical model

We assume that a liquid layer (region II) of single size spherical bubbles distributed uniformly is placed between $x = 0$ and $x = L$. Figure 1 sketches out the problem studied in this paper. The density and sound speed inside the bubble layer are ρ_L and c_L, correspondingly. These parameters outside this layer are ρ_0 and c_0, respectively. Because of small differences between the density of water at the equilibrium state and in the medium with bubbles we can put $\rho_L = \rho_0$. The media outside the layer are considered to be linear liquids. In region I the acoustic field is the sum of the incident wave p_i and reflected one p_r. In region III propagates only the transmitted wave p_t.

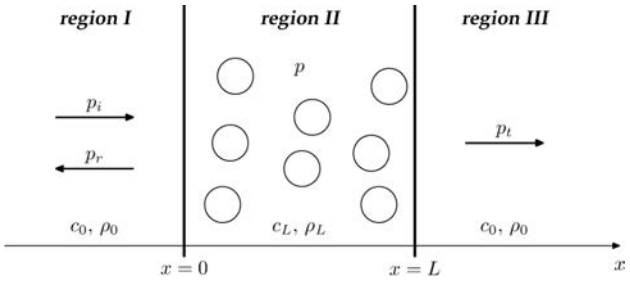

Fig. 1. Sketch of the problem.

The equation for the acoustic pressure p in the bubble layer is given in the following form (Druzhinin *et al.*, 1996; Hamilton, Blackstock, 1998; Karpov *et al.*, 2003; Baranowska, 2011):

$$\frac{\partial^2 p}{\partial x^2}(x,t) - \frac{1}{c_L^2}\frac{\partial^2 p}{\partial t^2}(x,t) = -\rho_0 \frac{\partial^2 \beta}{\partial t^2}(x,t), \tag{1}$$

where β is the local fraction of the volume occupied by the gas. Assuming a constant number N of air bubbles per unit volume, the volume fraction is given by

$$\beta(x,t) = \frac{4}{3}\pi R^3(x,t)N, \tag{2}$$

where R is the instantaneous radius of the bubbles.

The instantaneous bubble radius $R(t)$ driven by the incident signal acoustic pressure $P(t)$ is calculated using the Rayleigh–Plesset equation:

$$R\frac{\mathrm{d}^2 R}{\mathrm{d}t^2} + \frac{3}{2}\left(\frac{\mathrm{d}R}{\mathrm{d}t}\right)^2 = \frac{1}{\rho_0}\left[p_g\left(\frac{R_0}{R}\right)^{3\gamma} + p_v - p_{\mathrm{stat}} - \frac{2\sigma}{R} - P(t) - \rho_0\delta_t\omega R\frac{\mathrm{d}R}{\mathrm{d}t}\right], \tag{3}$$

where p_v is the gas and vapor pressure inside a bubble, p_{stat} is the ambient static pressure, R_0 is the equilibrium bubble radius, ω is the angular frequency, γ is the polytropic exponent of the gas, σ is the coefficient of surface tension, $p_g = 2\sigma/R_0 + p_{\mathrm{stat}} - p_v$ and δ_t is the damping coefficient for the bubble. It should be noted here that the bubble radius R and pressure P in the Rayleigh–Plesset equation (3) are only functions of the time variable t. In fact, we consider them as functions of two coordinates: the time coordinate t and the one-dimensional coordinate x putting $p(x,t)$ instead of $P(t)$.

To complete the formulation of our problem, initial and boundary conditions are defined. The initial conditions for $x \neq 0$ are as follows:

$$\begin{aligned} p(x,0) &= 0, & \frac{\partial p}{\partial t}(x,0) &= 0, \\ R(x,0) &= R_0, & \frac{\partial R}{\partial t}(x,0) &= 0. \end{aligned} \tag{4}$$

The boundary conditions are defined in the following way. The medium outside the layer is regarded as linear and non dispersive, therefore we can assume that the incident, reflected and transmitted waves have the forms

$$\begin{aligned} p_i(x,t) &= p_i(t - x/c_0), \\ p_r(x,t) &= p_r(t + x/c_0), \\ p_t(x,t) &= p_t(t - x/c_0). \end{aligned} \tag{5}$$

At the layer boundaries the pressure should be continuous, which, at $x = 0$ and $x = L$, gives

$$\begin{aligned} p(0,t) &= p_i(0,t) + p_r(0,t), \\ p(L,t) &= p_t(L,t). \end{aligned} \tag{6}$$

Taking into account the continuity of velocity or, equivalently, the pressure gradient, for $x = 0$, we have

$$\frac{\partial p_i}{\partial x}(0,t) + \frac{\partial p_r}{\partial x}(0,t) = \frac{\partial p}{\partial x}(0,t). \tag{7}$$

Taking the time derivative of (6), using (7) and the relation $\partial p_r/\partial t = c_0 \partial p_r/\partial x$ together with the analogous relation for the incident wave p_i, we eliminate the reflected wave. Finally the boundary condition for $x = 0$ is

$$\frac{\partial p}{\partial t}(0,t) - c_0 \frac{\partial p}{\partial x}(0,t) = 2\frac{\partial p_i}{\partial t}(0,t). \tag{8}$$

A similar consideration at $x = L$ leads to

$$\frac{\partial p}{\partial t}(L,t) + c_0 \frac{\partial p}{\partial x}(L,t) = 0. \tag{9}$$

Assuming a harmonic incident signal, we define for $x = 0$

$$p_i(0,t) = P_A \sin(\omega t). \tag{10}$$

We are looking for the solution of the system of Eqs. (1), (3) with initial and boundary conditions (4), (8), (9) for $x \in [0, L]$ and $t \in [0, T_{\max}]$. The finite-difference method was employed to solve equation (1), while Eq. (3) was solved using the classical fourth order Runge–Kutta method. As the result of numerical calculations we obtain the acoustic pressure $p_{i,n} = p(x_i, t_n)$ and the bubble radius $R_{i,n} = R(x_i, t_n)$ at the nodal points $x_i = i\Delta x$, $t_n = n\Delta t$, where $\Delta x = L/N_x$, $\Delta t = T_{\max}/N_t$, $i = 0, 1, \ldots, N_x$ and $n = 0, 1, \ldots, N_t$. After the calculation of $p_{i,m}$ and $R_{i,m}$ for $m \le n$, we can compute $R_{i,n+1}$ and the pressure $p_{i,n+1}$, i.e. we can compute the bubble radius and the pressure at time $t = t_{n+1}$ if we know the values of these functions for $t \le t_n$.

3. Phase sound speed, resonant frequency and damping coefficient

The phase speed of acoustic waves c_L is calculated on the basis of the dispersion relation including the effective complex wave number κ in a gas-liquid mixture. To describe the procedure of calculation, first we write the square of the complex wave number using the Ye and Ding formula (Ye, Ding, 1995):

$$\kappa^2 = k^2 + 4\pi A \left(1 - i\frac{2\pi B}{k}\right), \tag{11}$$

where

$$A = \int_0^\infty \frac{n(a)a\,\mathrm{d}a}{\omega_0^2/\omega^2 - 1 + i\delta_t}, \qquad B = \int_0^\infty \frac{n(a)a^2\,\mathrm{d}a}{\left(\omega_0^2/\omega^2 - 1 + i\delta_t\right)^2} \tag{12}$$

and $k = \omega/c_0$ is the acoustic wave number, ω_0 is the resonance angular frequency of a bubble, $n(a)$ is the number of bubbles per unit volume with radii a in the $da = 1$ μm range.

Now, we set

$$\frac{\kappa}{k} = u - iv, \tag{13}$$

where the quantities u and v are obtained using Eq. (11). Finally, the phase speed c_L is given by

$$c_L = \frac{c_o}{u}. \tag{14}$$

If the higher order term $2\pi B/k$ in Eq. (11) is ignored, we obtain the Commander and Prosperetti formula (Commander, Prosperetti, 1989):

$$\kappa^2 = k^2 + 4\pi \int_0^\infty \frac{n(a)a\,\mathrm{d}a}{\omega_0^2/\omega^2 - 1 + i\delta_t}. \tag{15}$$

In this paper we consider a bubble population with the same equilibrium radius R_0, i.e. $n(a) = N\delta(a - R_o)$ where δ denotes the Dirac delta function. After some calculations we obtain:

$$\kappa^2 = k^2 + \frac{3\beta_0/R_0^2}{\omega_0^2/\omega^2 - 1 + i\delta_t}, \tag{16}$$

where the gas volume fraction at equilibrium is given by

$$\beta_0 = \frac{4}{3}\pi R_0^3 N. \tag{17}$$

The phase sound speed depends on the bubble size distribution, the frequency of the sounding signal, the bubble resonance frequency and the bubble damping coefficient. The resonance angular frequency ω_0 of a bubble with radius R_0 can be determined using the formula (Commander, Prosperetti, 1989):

$$\omega_0^2 = \frac{p_0}{\rho_0 R_0^2}\left(\mathrm{Re}\,\Phi - \frac{2\sigma}{p_0 R_0}\right), \tag{18}$$

with

$$\Phi = \frac{3\gamma}{1 - 3(\gamma-1)iz[(i/z)^{1/2}\coth(i/z)^{1/2} - 1]}, \tag{19}$$

where $z = D/(\omega R_0^2)$ and D is the gas thermal diffusivity. The quantity p_0 is the undisturbed pressure in the bubble and is given by $p_0 = P_0 + 2\sigma/R_0$, where P_0 denotes the equilibrium pressure in the liquid. The damping coefficient δ_t is the sum of three components: the viscous damping constant, the damping constant due to thermal effects and the acoustic radiation damping constant:

$$\delta_t = \frac{4\mu}{\rho_0 \omega R_0^2} + \frac{p_0}{\rho_0 R_0^2 \omega^2}\mathrm{Im}\,\Phi + \frac{\omega R_0}{c_0}, \tag{20}$$

where μ is the coefficient of molecular viscosity of seawater.

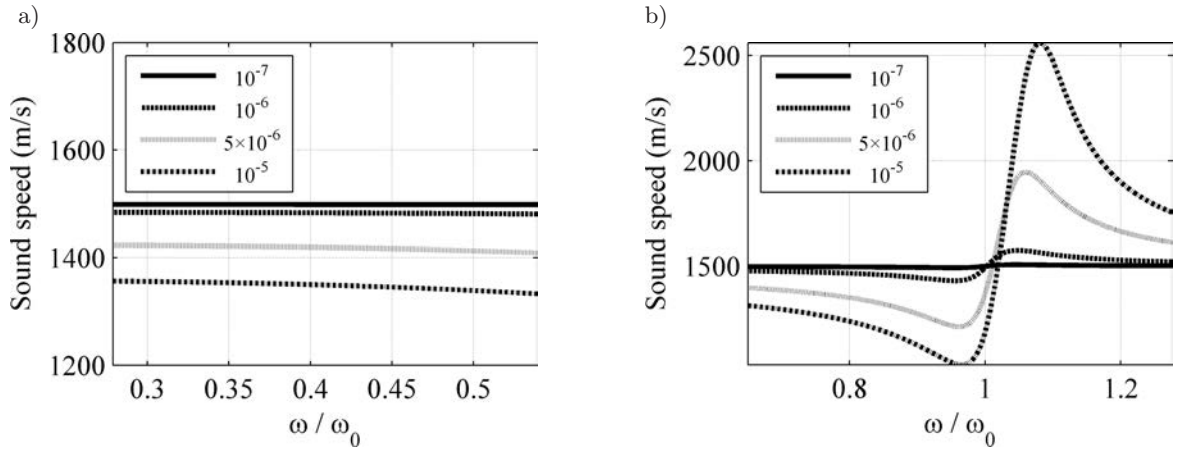

Fig. 2. The phase sound speed as function of signal frequency normalized by the bubble resonance frequency for different values of bubble radii and volume fractions: a) $R_0 = 40$ μm, b) $R_0 = 100$ μm.

We have analyzed signals which frequencies f are in the region from 20 kHz to 40 kHz. The results of the numerical investigations presented here are for two values of the bubble radius. In the first case, the bubble population is not resonant with the incident wave ($R_0 = 40$ μm) and in the second one this population is resonant with the incident wave ($R_0 = 100$ μm). Figure 2 depicts the phase sound speed as function of signal frequency normalized by the bubble resonance frequency. The curves show the results obtained for different values of bubble radius and volume fraction. For the frequency $f = 30$ kHz and radius $R_0 = 40$ μm, the resonance frequency equals $f_0 = 73.1$ kHz. Similarly, for $R_0 = 100$ μm we obtain $f_0 = 31.9$ kHz. We put here $c_0 = 1500$ m/s, $\rho_0 = 1000$ kg/m^3, $P_0 = 100$ kPa, $\sigma = 0.07$ N/m, $\mu = 0.001$ Ns/m^2 and $\gamma = 1.4$. The sound speed changes are large when the source frequency is not far from the resonance one. Near the resonance frequency of the bubbles, when the sounding frequency increases above or decreases below the resonance frequency of a single sized bubble population, the acoustic impedance in the layer becomes essentially different from that obtained in the case of a pure liquid. One of the results is an increase of the reflection coefficient.

4. Results of numerical investigations

The first step of our theoretical analysis was the study of influence of frequency and layer thickness on the transmitted and reflected waves. Figure 3 depicts the first and second harmonic amplitudes of transmitted waves normalized by the pressure $P_A = 40$ kPa calculated numerically assuming that a harmonic wave is propagated in the bubble layer. We put the sound speed $c_0 = 1500$ m/s and density $\rho_0 = 1000$ kg/m^3. The values of the speed c_L, which depend on the sound frequency were calculated using the Commander and Prosperreti model. The numerical calculations were made for different values of volume fraction assuming

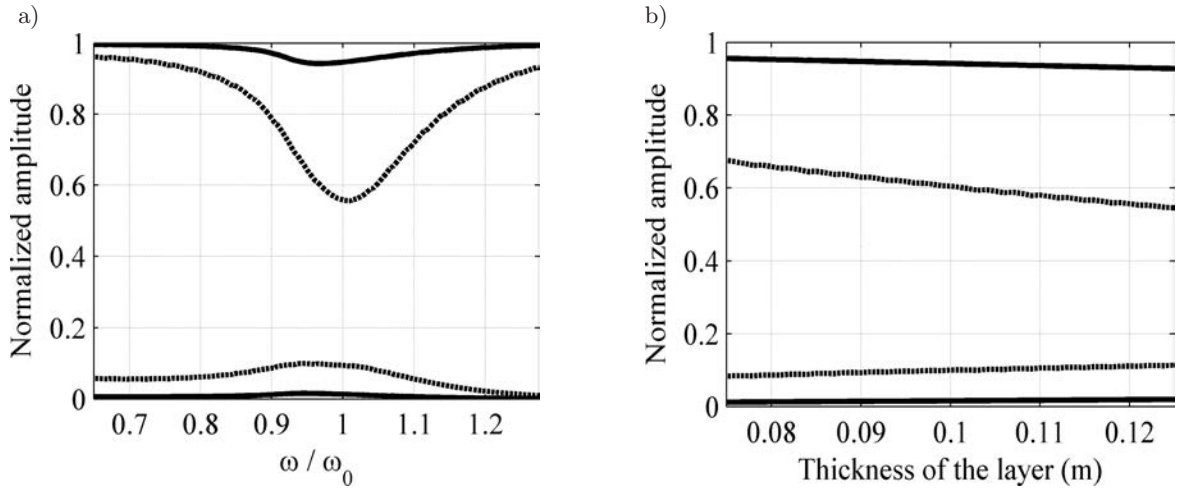

Fig. 3. The first and the second harmonic amplitudes of the transmitted waves normalized by the pressure P_A for volume fractions $\beta_0 = 10^{-7}$ (solid line) and $\beta_0 = 10^{-6}$ (dashed line): $P_A = 40$ kPa, $R_0 = 100$ μm; a) $L = 0.1$ m, b) $f = 30$ kHz.

that the bubble radius is $R_0 = 100$ μm. The pressure amplitudes of the transmitted wave as function of signal frequency normalized by the bubble resonance frequency for the layers of thickness $L = 0.1$ m are presented in Fig. 3a. The result obtained for the same pressure amplitudes as a function of layer thickness for the incident wave frequency $f = 30$ kHz is given in Fig. 3b. The pressure amplitudes of the reflected wave obtained for the volume fraction $\beta_0 = 10^{-7}$ are presented in Fig. 4. The values of the remaining physical and numerical parameters are the same as used earlier.

The values of the volume fraction have a great influence on the pressure distribution inside the layer. For this reason, the effect of this parameter on the nonlinear generation was more thoroughly examined. Figure 5 shows normalized amplitudes of the first and second harmonics in the transmitted wave as function of volume fraction calculated for different values of the bubble radius. Figure 5a shows the result obtained for $R_0 = 100$ μm. In this case the amplitude of the first harmonic decreases very quickly, while the amplitude of the second one increases for small values of the volume fraction and then it stabilizes. An example of the results of calculations obtained for bubble radius not resonant presents Fig. 5b. Figure 6 presents the first and the second harmonic amplitudes of the transmitted and reflected waves normalized by pressure P_A as functions of volume fraction for $R_0 = 40$ μm, $L = 0.1$ m, $f = 30$ kHz and $P_A = 20$ kPa.

The distributions normalized by pressure P_A of the first and the second harmonic amplitudes of the transmitted and reflected waves at frequency $f = 30$ kHz, amplitude $P_A = 20$ kPa and bubble radius $R_0 = 40$ μm for different layer thicknesses and different values of volume fraction are represented in Fig. 7. Figure 8 shows similar results obtained for $R_0 = 100$ μm.

The last step of our theoretical investigations was devoted to a theoretical analysis of the relationship

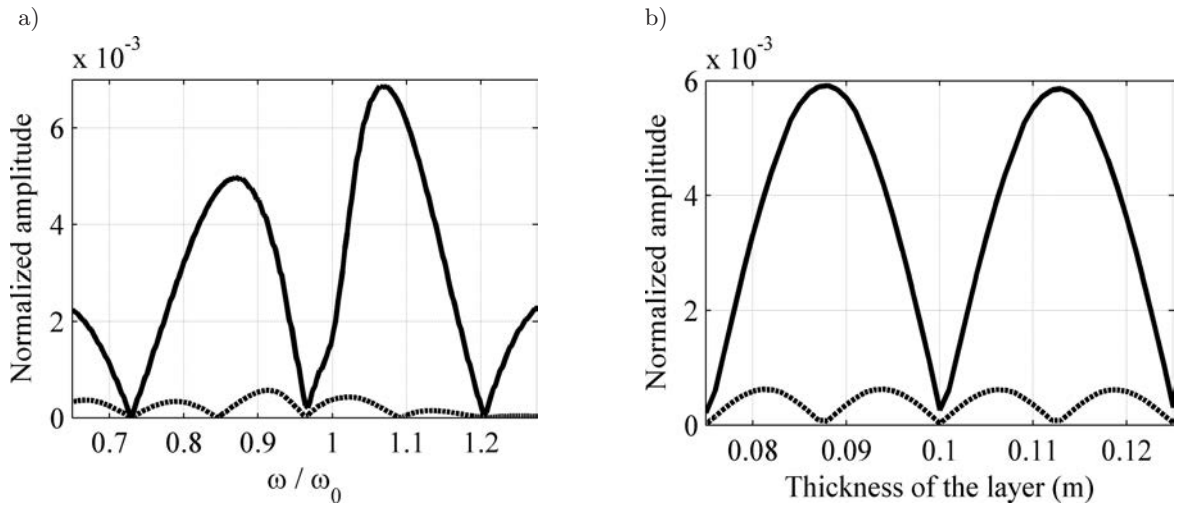

Fig. 4. The first (solid line) and second (dashed line) harmonic amplitudes of the reflected wave normalized by the pressure $P_A = 40$ kPa, $R_0 = 100$ μm, $\beta_0 = 10^{-7}$: a) $L = 0.1$ m, b) $f = 30$ kHz.

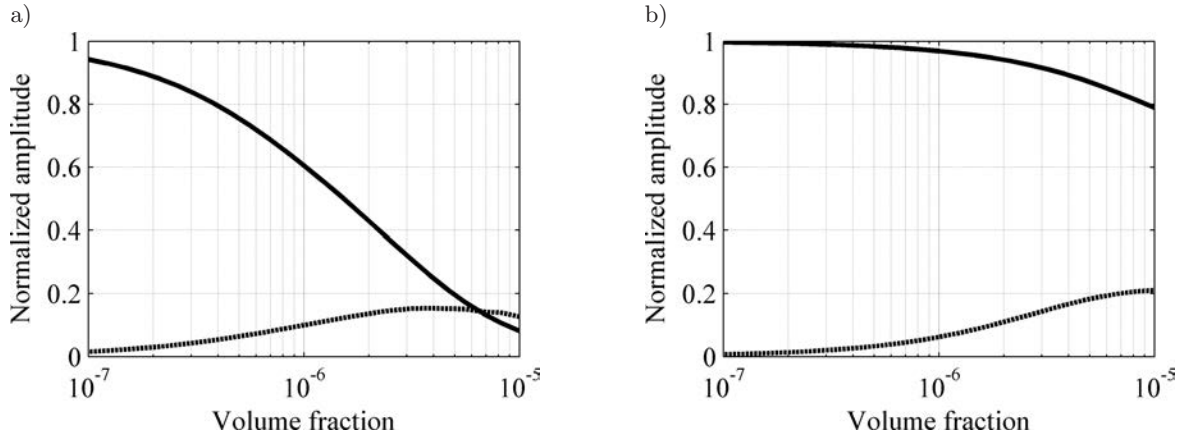

Fig. 5. The first harmonic amplitude (solid line) and the second one (dashed line) of the transmitted wave normalized by pressure P_A as functions of volume fraction for $f = 30$ kHz, $P_A = 40$ kPa and $L = 0.1$ m: a) $R_0 = 100$ μm, b) $R_0 = 40$ μm.

between the first and second harmonic amplitudes of the transmitted and reflected waves, respectively. Figure 9a presents the second harmonic amplitudes of the transmitted wave normalized by their first harmonic amplitudes as functions of volume fraction obtained for $f = 30$ kHz, different values of the incident wave amplitude and fixed values of the bubble radius. Similar results obtained for the reflected wave depicts Fig. 9b. Figure 10 shows an example of distribution of the second harmonic amplitude of the transmitted wave normalized by the first harmonic amplitude. The calculations were made for different layer thicknesses and different values of volume fractions at $f = 30$ kHz, $P_A = 20$ kPa and $R_0 = 40$ μm.

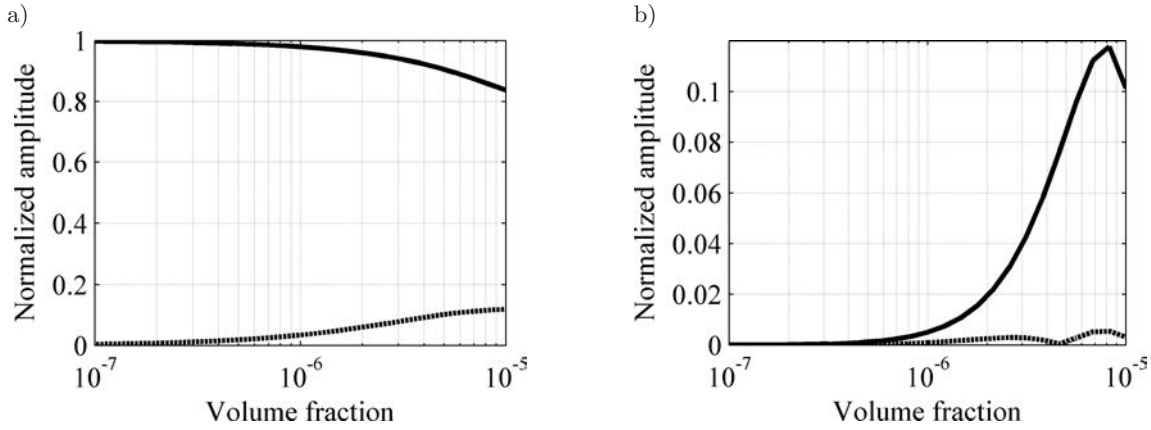

Fig. 6. The first harmonic amplitude (solid line) and the second one (dashed line) of the transmitted wave (a) and the reflected one (b) normalized by pressure P_A as functions of volume fraction; $f = 30$ kHz, $P_A = 20$ kPa, $L = 0.1$ m, $R_0 = 40$ μm.

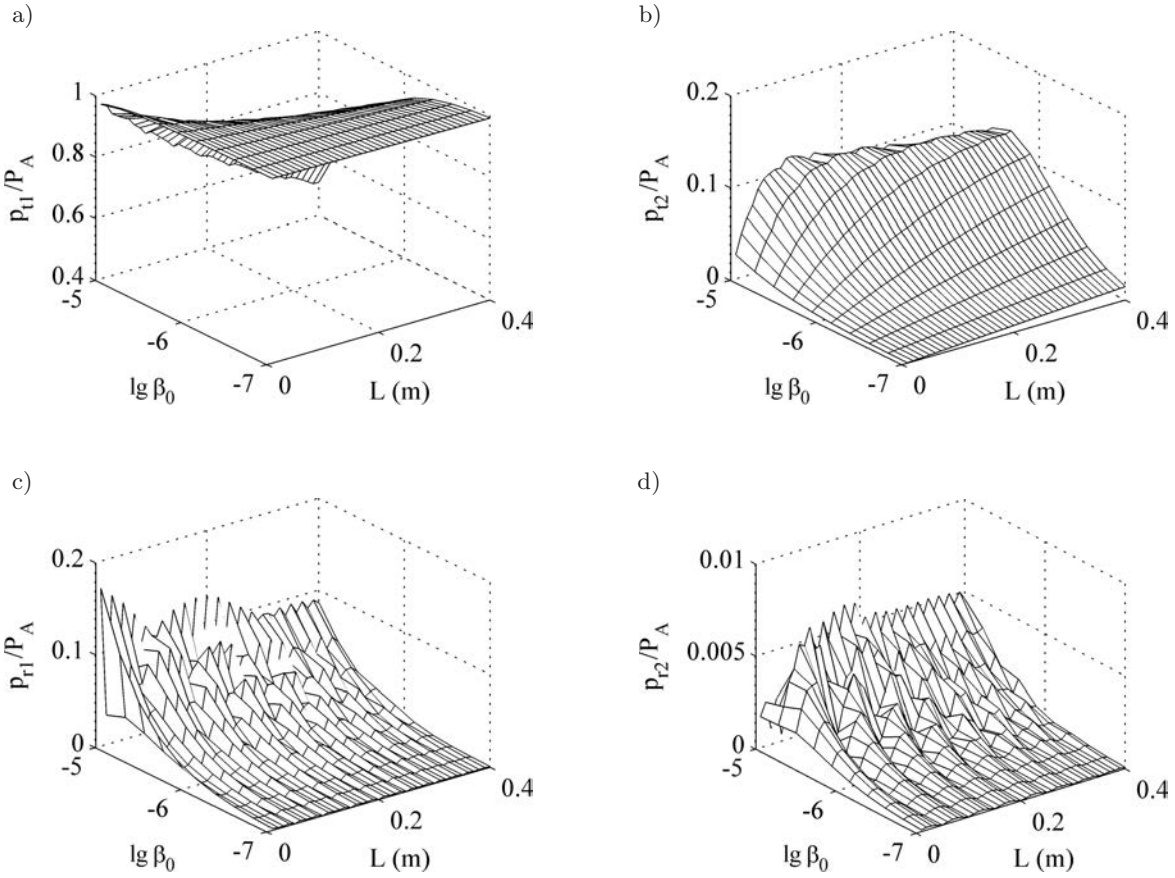

Fig. 7. The space distribution of the first and the second harmonic amplitude of the transmitted and reflected waves normalized by pressure P_A: $f = 30$ kHz, $P_A = 20$ kPa, $R_0 = 40$ μm.

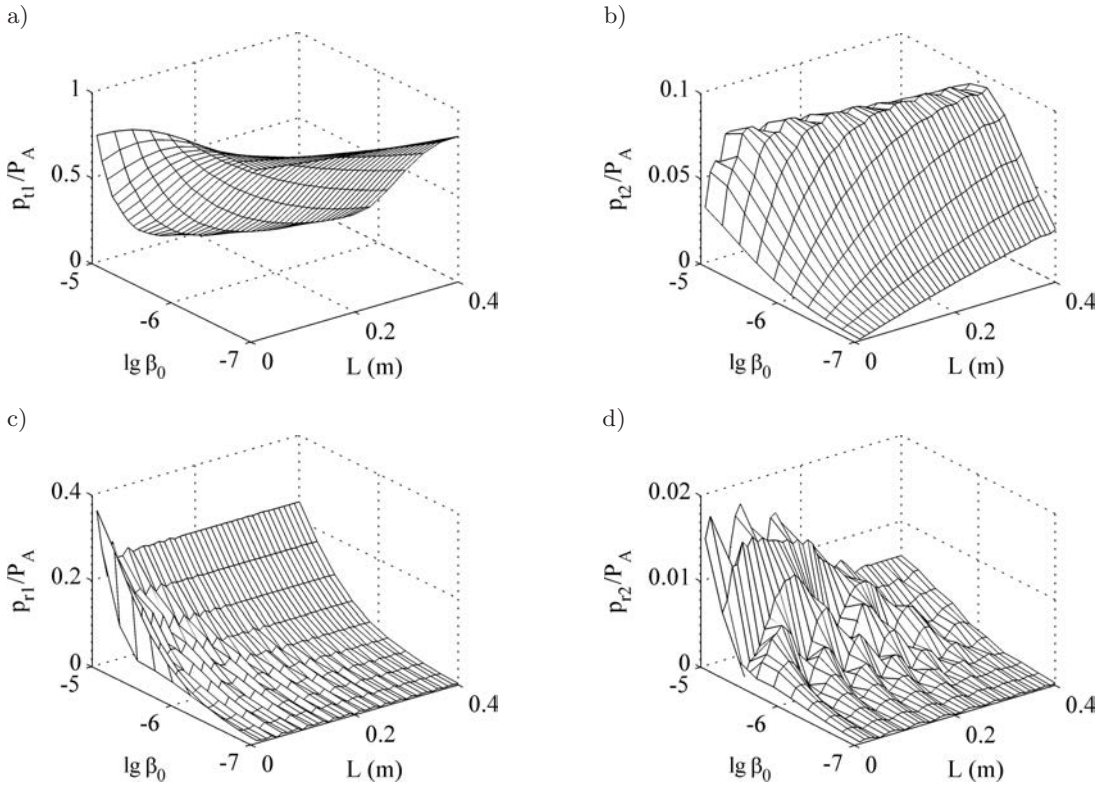

Fig. 8. The space distribution of the first and the second harmonic amplitudes of the transmitted and reflected waves normalized by pressure P_A; $f = 30$ kHz, $P_A = 20$ kPa, $R_0 = 100$ μm.

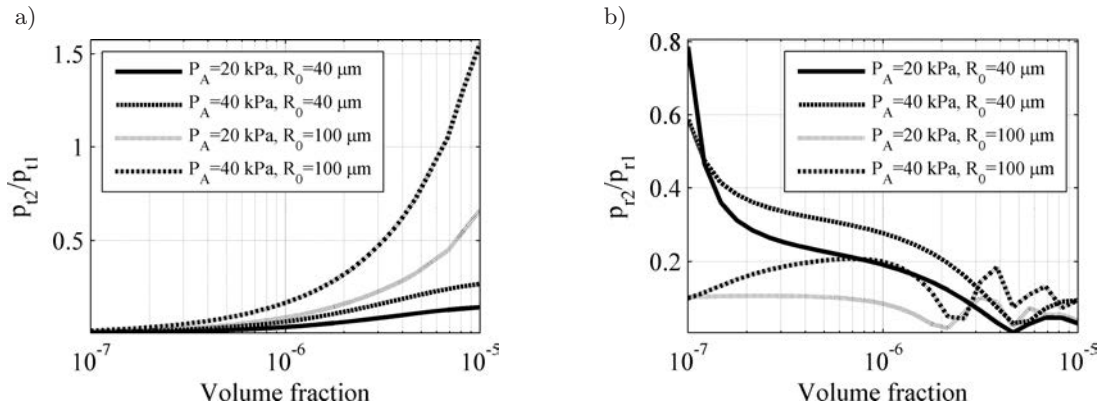

Fig. 9. The second harmonic amplitude of the transmitted (a) and reflected (b) waves normalized by their first harmonic amplitudes as functions of volume fraction; $f = 30$ kHz, $L = 0.1$ m.

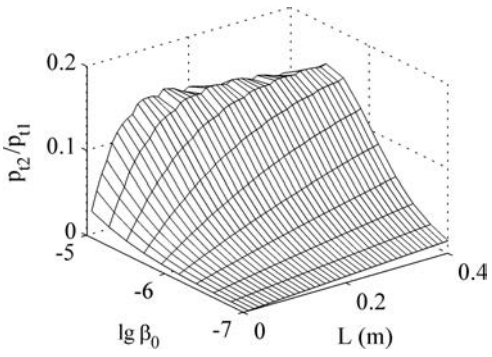

Fig. 10. The space distribution of the second harmonic amplitude of the transmitted wave normalized by the first harmonic amplitude; $f = 30$ kHz, $P_A = 20$ kPa, $R_0 = 40$ μm.

5. Conclusions

The problem of the efficiency of the higher harmonic generation in a bubbly liquid layer was considered and its mathematical model was constructed on the basis of two presented differential equations. Some results of the numerical investigations were discussed. The linear non-dissipative wave equation was solved numerically by employing the finite-difference method. The Rayleigh–Plesset equation describing the bubble oscillation was solved using the classical fourth order Runge–Kutta method. The changes of the transmitted and reflected waves were examined. Numerical cal-

culations were carried out using a computer program specially designed for this problem by the author.

The purpose of the paper was to conduct numerical investigations of the nonlinear generation by a bubble layer. Many different environmental and sounding signal parameters have an influence on the nonlinear waves propagation over the bubble layer. The influences of fixed environmental and sounding signal parameters on the second harmonic amplitudes of the transmitted and reflected waves were analyzed. First of all, the numerical calculations were made for different values of the layer thickness and volume fractions, as well as for different values of frequency and pressure amplitudes of the generated signals. A detailed analysis carried out for different sizes of bubbles shows how significant influence on the nonlinear generation efficiency has the gas void fraction. For example, when the frequency of sounding signal is fixed, we observe a larger attenuation of the first harmonic amplitude of the transmitted wave in case of resonant bubbles, than in that of bubbles with different radii. Near the resonance frequency of the bubbles, the acoustic impedance in the layer becomes significantly different from that obtained in case of a pure liquid and as a consequence the reflection coefficient increases. The results of numerical investigations show also that when the bubble population is not resonant, it is possible to find values of the layer thickness or the volume fraction for which the ratios of the second harmonic amplitudes of the transmitted wave to their first harmonic amplitudes are the greatest and, in consequence, the nonlinear generation efficiency is the best. It is much more difficult to find such values of these parameters when the bubbles frequency is resonant.

All the results presented in this paper were obtained assuming that the single bubble layer is surrounded by media with contrasting physical properties. Although this paper deals with the harmonic wave propagation only, it is not difficult to extend this model to the case of more than one layer having different features. It is also possible to develop computer programs for biharmonic waves as well as for continuous signals and impulse signals with different envelopes. This model can be useful in studying the wave propagation in a bubbly environment, for example, it can be employed in the simulation of the efficiency of parametric sonars operating in different forms of the nonlinear layer.

Acknowledgment

This article is an extended version of the paper "Numerical testing of nonlinear generation efficiency in a bubble layer" presented at the 58th Open Seminar on Acoustics, OSA 2011, September 13–16, 2011, Jurata, Poland.

References

1. Baranowska A. (2011), *Numerical modeling of the nonlinear wave propagation in a bubble layer*, Hydroacoustics, **14**, 9–16.
2. Commander W., Prosperetti A. (1989), *Linear pressure waves in bubbly liquids: Comparison between theory and experiments*, Journal of the Acoustical Society of America, **85**, 732–746.
3. Druzhinin O.A., Ostrovsky L.A., Prosperetti A. (1996), *Low-frequency acoustic wave generation in a resonant bubble layer*, Journal of the Acoustical Society of America, **100**, 6, 3570–3580.
4. Hamilton M.F., Blackstock D.T. [Eds.] (1998), *Nonlinear Acoustics*, Academy Press, San Diego.
5. Karpov S., Prosperetti A., Ostrovsky L. (2003), *Nonlinear wave interactions in bubble layers*, Journal of the Acoustical Society of America, **113**, 3, 1304–1316.
6. Leighton T.G. (2008), *The Rayleigh-Plesset equation in terms of volume with explicit shear losses*, Ultrasonics, **48**, 85–90.
7. Perelomova A., Wojda P. (2010), *Studies of nonlinear sound dynamics in fluids based on the caloric equation of state*, Archives of Acoustics, **35**, 4, 619–633.
8. Vanhille C., Campos–Pozuelo C. (2008), *Nonlinear ultrasonic propagation in bubbly liquids: a numerical model*, Ultrasounds in Medicine and Biology, **34**, 5, 792–808.
9. Ye Z., Ding L. (1995), *Acoustic dispersion and attenuation relations in bubbly mixture*, Journal of the Acoustical Society of America, **98**, 1629–1636.

PAN ARCHIVES OF ACOUSTICS
Vol. **37**, No. 3, pp. 295–300 (2012)

DOI: 10.2478/v10168-012-0038-z

Recognizing the Sequences of Code Manipulated Short LFM Signals

Tadeusz LESZCZYŃSKI

University of Technology and Life Sciences
Kaliskiego 7, 85-796 Bydgoszcz, Poland; e-mail: leszcz@utp.edu.pl

(*received June 1, 2011; accepted June 13, 2012*)

Noise-like binary sequences combined with signals with linear frequency modulation might be successfully used to increase the reliability of the recognition of both probe and communication signals in the presence of natural and artificial interference. To identify such formed sequences the usage of the two-step matched filtering was suggested and the probabilistic model of the recognition of noise-like code sequences transferred by LFM signals was developed.

Keywords: sonar, LFM signal, matched filtering.

1. Introduction

In this study the signals recognition is understood in terms of distinguishing them from the noise or detecting them in the presence of other signals. The recognition of a signal (e.g. the echo of a probe signal) incoming at the input of the receiver is based on finding the correlation between this signal and the model of the probe signal.

Noise-like binary sequences are widely used in telecommunication, measuring, echo location and navigation systems. The collection of these sequences includes: Barker's, Willard's Neuman–Hoffman's and Alexis codes, the sequences of maximum length, golden codes, Kasami sequences, etc. (Davies, 1971; Glover, Grant, 1998; Howard, 2002; Luke, 2001; Proakis, 2001). This study is devoted to the recognition of the pseudo-noise binary sequences formed on the basis of the signals with linear frequency modulation (LFM signals, chirp signals). In digital compression, the detection of broadband signals and the identification of binary codes one can successfully use matched filtering realized in the time domain. Zeros and ones in a noise-like code sequence might be represented by *up-chirp* signals (the instantaneous frequency changes from low to high) and *down-chirp* signals (the instantaneous frequency changes from high to low). To identify such formed sequences the two-step matched filtering has to be used. The first filtering is related to the recognition of every single chirp signal forming a sequence, which results in obtaining a binary sequence, which is subjected to the second matched filtering.

In order to implement digital matched filtering in the time domain a chirp signal is presented as time series $\{x_n\}$ with the sampling frequency $f_s = 1/T_s \geq 2f_2$, so the number of samples equals N, where $N = \mathrm{ENT}(Tf_s)$, ENT – the integer part of a number. Each sample value of a chirp signal is determined from the formula:

$$x_r{=}x(rT_s){=}A\cos\left[2\pi\left(\frac{\Delta f}{2N}r+f_1\right)rT_s+\varphi_0\right], \quad (1)$$

where $a = \Delta f/\tau_i$, $\Delta f = f_2 - f_1$ is the deviation of the frequency, f_1 is the initial frequency, f_2 is the final frequency, τ_i is the duration of the chirp signal, φ_0 is the initial phase, $r = \overline{0, N{-}1}$.

The coefficients of the impulse response of a matched filter *IR* without a smoothing window is defined as the mirror reflexion of the input signal $\{x_n\}$, $n = \overline{1, N}$. In this case the coefficients of the impulse characteristics are determined from the formula:

$$h_n = x_{N-n}, \quad (2)$$

where $n = \overline{1, N}$.

In order to decrease Gibb's oscillations, which occur during the matched filtering of chirp signals, the smoothing windows $\{w_n\}$ are used. In the time domain the application of windows on the impulse responses *IR* of the filter is done by the multiplication of the weight factors of a *IR* by corresponding weight factors of the

smoothing window $\{h_n\, w_n\}$. In that case the algorithm of matched filtering with the use of a window is:

$$y_n = \sum_{m=0}^{N-1} x_{n-m} h_m w_m, \tag{3}$$

where y_n – n-th convolution result, $\{w_n\}$ – the collection of smoothing window coefficients. For the implementation of a specialized processor it is advisable to present formula (3) in a matrix form.

$$y_n = \mathbf{X} \cdot \mathbf{H}_w, \tag{4}$$

where

$$\mathbf{X} = [x_n \ldots x_{n-N+1}],$$

$$\mathbf{H}_w = \begin{bmatrix} h_0 w_0 \\ : \\ : \\ h_{N-1} w_{N-1} \end{bmatrix}.$$

The research results presented in the studies (Leszczyński, 2010; Pogribny, Leszczyński, 2008) demonstrate that the initial phase and frequency, as well as the sampling rate of both short LFM signals and matched filter impulse response have an important influence upon the compression of these signals within the time domain. In matched filtering in the time domain convolutions form the main lobe as well as side lobes. The main lobe is formed by the result of central convolution, whereas side lobes are formed with the remaining ones. The ratio of *PSR* (Peak-to-Side lobe Ratio) of the main lobe value to the maximum value of a side lobe, expressed in dB, is the measure of the degree of signal compression and significantly affects its recognition:

$$PSR = 20 \log \frac{y_c}{|y_m|}, \tag{5}$$

where y_c – the central convolution value, $|y_m|$ – the maximum absolute value of the convolution chosen among all convolutions without those forming the main lobe.

The convolution results form the set on the basis of the formula (3) and some of them might have negative values. It can also be noticed that the convolutions adopting negative values become the biggest after setting their absolute values and are usually located near the central convolution, becoming a part of and extending the main lobe, which worsens time resolution and *PSR*. Performing nonlinear operations on the convolutions results (replacing negative convolution values with zeros) increases the *PSR* coefficient and decreases the width of the main lobe, which significantly affects the recognition of the chirp signal. The parallel matched filters systems presented in the studies (Leszczyński, 2010; Pogribny, Leszczyński, 2011) allow one to increase the resolution of recognition to the borderline – only one sample in the main lobe with the location of its position within the actual sampling period. Concurrently, such parallel systems allow one to obtain a result after N periods (where N is the number of all signal samples), which is $log_2 N$ faster than in systems using "fast convolutions".

2. Forming code sequences

Forming code sequences of *up-chirp* and *down-chirp* signals brings to the situation in which an *up-chirp* signal is sent to the filter detecting *down-chirp* signals, or inversely. It causes the occurrence of the increased noise level of an output signal at the matched filters output in comparison with the recognition of the proper signal, when the noise level is lower as compared to the main lobe. It results from a high correlation between an *up-chirp* and a *down-chirp* signal. When a *down-chirp* signal enters the input of a filter responding to *up-chirp* signals at this filter output there is the increase of the level of side lobes in the absence of the main lobe. The matched filters systems presented in the studies (Leszczyński, 2010) determine the value of the *PSR* coefficient identifying two consecutive maxima within the time interval determined by the number $N$of time steps (clocks), where N is the number of the coefficients of matched filter impulse characteristics. Such an approach allows one to increase the reliability of identification of a chirp signal by using simultaneously two criteria – reaching by an output signal the appropriate threshold δ_y and minimal *PSR* value. To avoid the misinterpretation of the increased level of a noise signal at the output of a filter responding to *up-chirp* signals when a *down-chirp* signal is sent at its input an interval between signals, at least equal to the duration of the signal, has to be introduced. This imposes appropriate limitations on the presented method of coding zeros and ones of code sequences by *up-chirp* and *down-chirp* signals. The results of the simulation of matched filtering of *up-chirp* and *down-chirp* signal pairs as well as *up-chirp* signal pairs are presented in Figs. 1 and 2. As shown in Fig. 2 chirp signals of one type coming directly one after another at the input of a filter designed for their detection slightly increase the level of side lobes in comparison with the case when the distance between them equals the pulse duration.

The presentation of ones and zeros of code sequences using appropriate chirp signals should take into account the presence of identical symbols of a code sequence coming directly one after another. This paper proposes two ways of forming code sequences. The first way uses *up-chirp* and *down-chirp* signals, whereas the other one uses only chirp signals of one type (*up-chirp* or *down-chirp*).

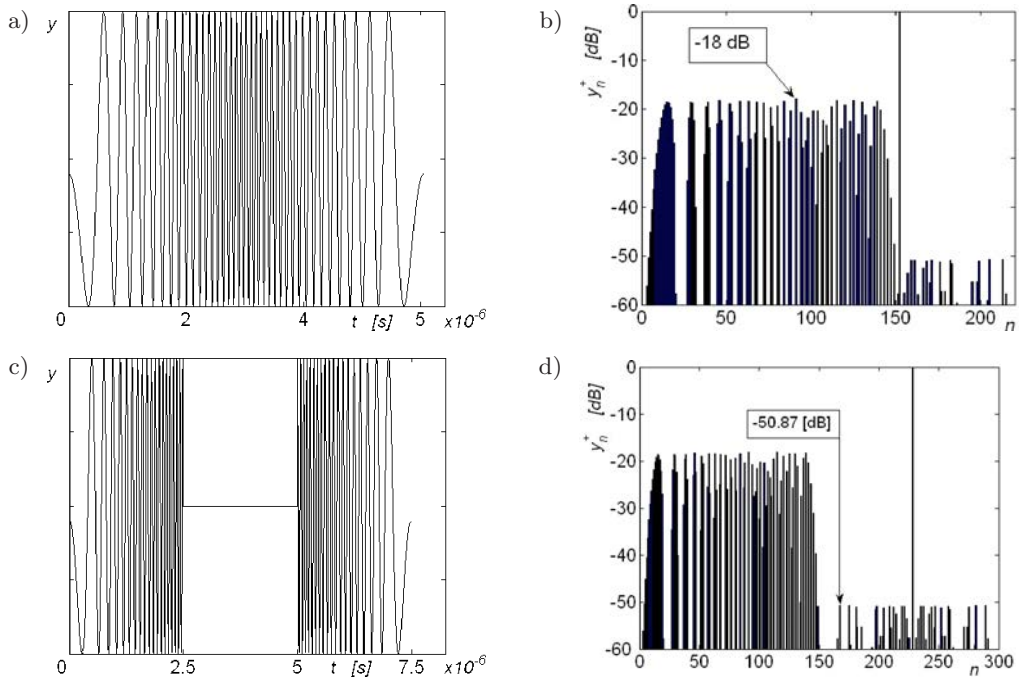

Fig. 1. The result of the matched filtering of a pair of *up-chirp* (0–15 MHz) and *down-chirp* (15 MHz – 0) signals coming at the input of a filter detecting *down-chirp*, the duration of both signals is identical and equals $T = 2.5$ µs. In the filtration process a rectangular window was used as well as non-linear operations. The signal initial phase and sampling frequency are optimal: a) the *up-chirp* signal and the *down-chirp* signal coming directly after it, b) the signal at the output of a matched filter detecting *down-chirp* signals at the input, which signal was provided (a), c) an *up-chirp* signal with an interval equal to the impulse duration and then a *down-chirp* signal, d) a signal at the output of a matched filter detecting a *down-chirp* signal at the input, which signal was provided (c).

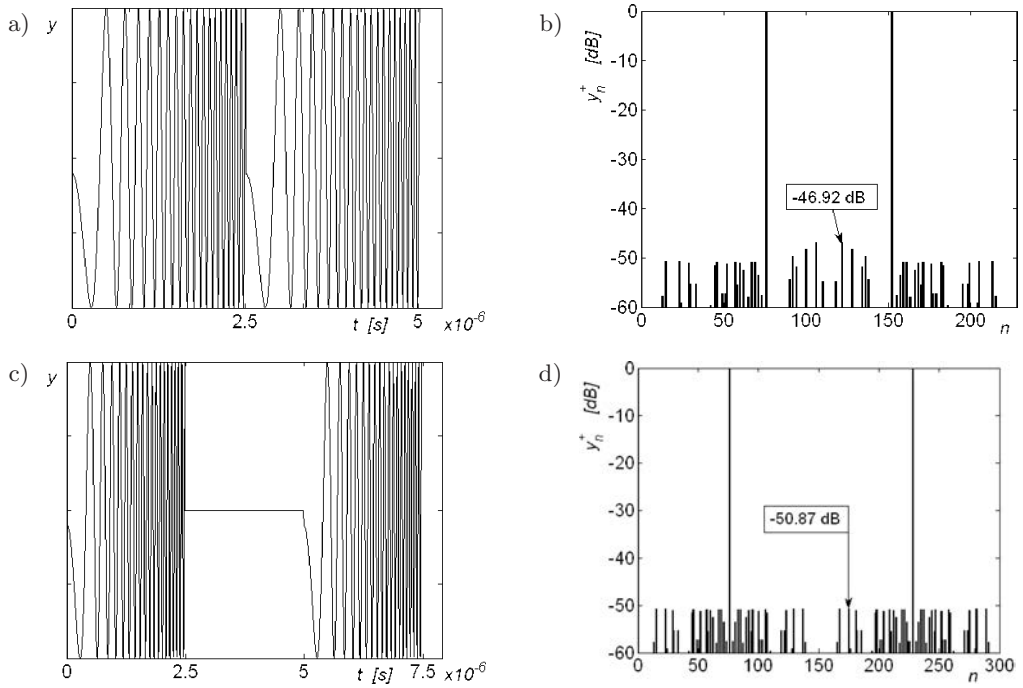

Fig. 2. The result of the matched filtering of a pair of *up-chirp* signals (0–15 MHz) sent at the input of a filter detecting *up-chirp* signals, the signal duration is $T = 2.5$ µs. In the filtration process a rectangular window was used as well as non-linear operations. The signal initial phase and sampling frequency are optimal: a) two *up-chirp* signals coming directly one after another, b) the signal at the output of a matched filter detecting *up-chirp* signals at the input, which signal was provided (a), c) two *up-chirp* signals with an interval equal to the impulse duration, d) a signal at the output of a matched filter detecting an *up-chirp* signal at the input, which signal was provided (c).

Let us consider the example of coding ones with *up-chirp* signals and zeros of a noise-like sequence 11010 with *down-chirp* signals.

Then the probing signal has the form of:

upup_down_up_down

where **up** is an up-chirp signal, **down** is a down-chirp signal, _ is an interval between the signals.

When using chirp signals of one type (e.g. *up-chirp*) the coding process is as follows:

- one is represented by two consecutive *up-chirp* signals (without an interval between the signals),
- zero is represented by a single *up-chirp* signal.

The probing signal formed on the basis of the same noise-like sequence, where only an *up-chirp* signal is used to code ones and zeros might be presented as follows:

upup_upup_up_upup_up

3. Identifying binary noise-like sequences

Using matched filtering to identify binary codes the replacement of 0 with -1 must be made. As a result of such a transformation the binary sequence $a_0, a_1, a_2, \ldots, a_i, \ldots, a_{n-1}$ converts to the sequence of $b_0, b_1, b_2, \ldots, b_i, \ldots, b_{n-1}$, where $a_i \in \{0, 1\}$ and $b_i \in \{-1, 1\}$ for $i = 1, 2, \ldots, n-1$. Such transformation can be performed using the formula:

$$b_i = 2a_i - 1 \qquad \text{for} \qquad i = 0, 1, \ldots, n-1. \tag{6}$$

The matched filtering algorithm for the input sequence $b_0, b_1, b_2, b_3, \ldots, b_i, \ldots, b_n$ can be written as:

$$y_j = \sum_{m=0}^{n-1} b_{j-m} h_m, \tag{7}$$

where $h_j = b_{n-j}$, $j = 1, 2, \ldots, n$.

The coefficients of the impulse response for this filter are defined by the terms of a searched noise-like code written in the reverse order. In the matched filtering of the input sequences $b_0, b_1, b_2, b_3, \ldots, b_i, \ldots, b_n$ non-linear operations are also used, which increases the probability of their recognition in the presence of incorrect symbols in a code sequence.

Figure 3 presents the structure of a system using two-step matched filtering to recognize code sequences transmitted by *up-chirp* and *down-chirp* signals (Fig. 3a) and transmitted by the signals of one type *up-chirp* or *down-chirp* (Fig. 3b).

The structure presented in Fig. 3a consists of two channels of strictly equalled delays depended on the transition process taking place in these channels. The upper channel with a $[f_1, f_2]$ band responds to a *down-chirp* signal, whereas the lower one with a $[f_2, f_1]$ band responds to a *up-chirp* signal. The compressed output

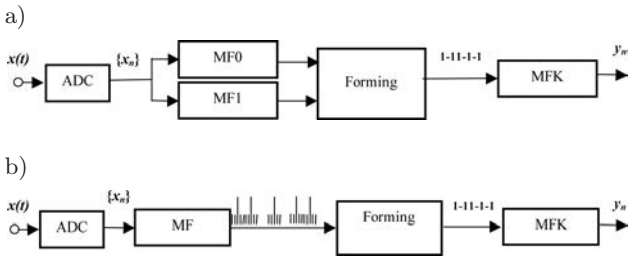

Fig. 3. The structures of the system identifying code sequences transmitted by chirp signals using two-step matched filtering: a) the structure using two matched filters MF0 and MF1, where one detects an *up-chirp* signal, whereas the other one detects a *down-chirp* signal, b) the structure using one matched filter detecting *up-chirp* signals.

signals of the MF0 and MF1 filters are used for creating a binary pulse train in a forming system. The zero-one sequence is transposed in a sequence consisting of $+1$, -1 elements, which goes to the input of an MFK matched filter responding to a specific code sequence.

The second method is illustrated in Fig. 3b. This structure consists of only one channel, and ones and zeros are represented by one type of a chirp signal (e.g. *up-chirp*). The forming system, on the basis of a signal level at the filter output and asked intervals, which should occur between the high levels, creates a zero-one sequence transposed in a sequence $\{+1, -1\}$, which goes to the input of an MFK matched filter responding to a specific code sequence. The systems identifying code sequences transmitted by chirp signals using two-step matched filtering were realized on the basis of the evaluation module X5-400M produced by Innovative Integration Company.

4. The influence of noises on the code sequences recognition

To examine the influence of noises on the recognition of code sequences transmitted by chirp signals the author suggested using a probabilistic model presented below.

The probability of the correct recognition of a noise-like code, in which zeros and ones are represented by chirp signals might be defined as follows.

Let us denote by:

- A – an event consisting in a correct recognition of a code sequence,
- B_k – an event consisting in the occurrence of k errors within a received code sequence,
- C_i – an event consisting in an incorrect recognition of a chirp signal representing the ith-position in a code sequence,
- $P(A/B_k)$ – the conditional probability of the correct recognition of a code sequence with the occurrence of k errors in it,

- $P(C_i) = p_i$ – the probability of an incorrect recognition of a chirp signal representing the ith-position in a code sequence,
- $P(B_k)$ – the probability of the occurrence of k errors within a received code sequence.

The collection $\{P(B_k)\colon k = \overline{0,n}\}$ forms a complete set of events, so:

$$\sum_{k=0}^{n} P(B_k) = 1. \tag{8}$$

Applying the formula for total probability and assuming that the distribution of the probability of events $\{C_i\,(i{=}\overline{1,n})\}$ is Bernoulli's distribution and conditional probabilities $P(A/B_k)$ are calculated using a computer simulation method, then the probability of the correct recognition of a code sequence might be calculated from the formula:

$$\begin{aligned} P(A) &= (1-p)^n + \sum_{k=1}^{n} \frac{m_k}{\binom{n}{k}} \binom{n}{k} p^k (1-p)^{n-k} \\ &= (1-p)^n + \sum_{k=1}^{n} m_k p^k (1-p)^{n-k}, \end{aligned} \tag{9}$$

where n is the length of a code sequence, m_k is the number of cases of the correct recognition of the code distorted on k positions (calculated using a computer simulation method, which involves conducting the matched filtering of the tested sequence for all possible distortions on k positions, and checking if the central convolution has the highest value among all possible convolutions), p is the probability of the incorrect recognition of a chirp signal.

If the probabilities of the incorrect recognition of the signals representing one (p_1) or zero (p_0) in a code sequence are different ($p_0 \neq p_1$), with the remaining invariable assumptions, then the probability $P(A)$ has to be calculated from the formula:

$$\begin{aligned} P(A) = \sum_{k_1=0}^{n_1} \sum_{k_0=0}^{n_0} & \frac{m_{k_1+k_0}}{\binom{n_0+n_1}{k_1+k_0}} \binom{n_1}{k_1} p_1^{k_1} \\ & \cdot (1-p_1)^{n_1-k_1} \binom{n_0}{k_0} p_0^{k_0} (1-p_0)^{n_0-k_0}, \end{aligned} \tag{10}$$

where n is the number of ones in a code sequence, n_0 is the number of zeros in a code sequence, $n_0 + n_1 = n$ is the length of a code sequence, p_1 is the probability of the incorrect recognition of one, p_0 is the probability of the incorrect recognition of zero.

The probabilities p, p_0, p_1 of the incorrect recognition of chirp signals representing ones and zeros in a code sequence might be calculated using Monte-Carlo method for the given level of interference. Knowing the probabilities of the incorrect recognition of chirp signals one can, using the developed approach, evaluate the probability of the correct recognition of a probing signal formed of the sequence of chirp signals created according to a chosen code sequence. Figure 4 shows the graphs of the probability changes $P(A)$ of the correct interpretation of sample code sequences according to the probability p of the incorrect recognition of a chirp signal.

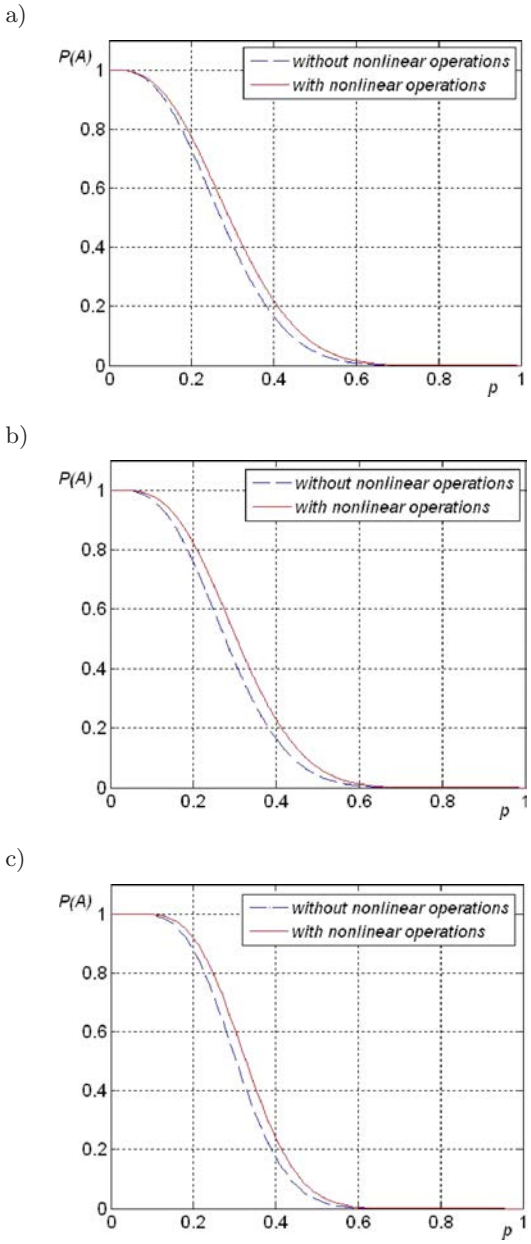

Fig. 4. The dependence of the probability of the recognition of a code sequence for a code word on the probability p of not recognizing a chirp signal: a) a sequence 1111100110101 type AB of length $n = 13$, b) 001111100110101 type N of length $n = 15$, c) a sequence 000001110011101010110110 type N of length $n = 24$.

The calculation results presented in Fig. 4 were obtained assuming that the probabilities of the distortion of zeros and ones in a code sequence are the same ($p_0 = p_1 = p$). The obtained results show that

the use of non-linear operations together with matched filtering of code sequences increases the probability $P(A/B_k)$ of their recognition with the occurrence of incorrect symbols in a code sequence. For every code sequence there is a maximum value of the probability $p_{\max}$ of the incorrect recognition of a chirp signal, for which a code sequence is still accurately recognized. The value $p_{\max}$ depends on the length and type of a code sequence. Using the proposed model of the recognition of code sequences transmitted by chirp signals one can evaluate the noise level SNR_{in} disturbing the reception of single chirp signals, which does not influence significantly the accuracy of the recognition of these sequences.

5. Conclusion

The forming methods and the systems of the recognition of code sequences transmitted by the signals with the linear frequency modulation presented in this work can be effectively used in relation to probe and communication signals. Moreover, these systems work in the real time. The developed probabilistic model of the recognition of noise-like code sequences transmitted by chirp signals allows one to choose the optimal code sequence providing its accurate recognition at a given probability of the incorrect recognition of a single chirp signal.

References

1. Davies A.C. (1971), *Properties of Waveforms Obtained by Nonrecursive Digital Filtering of Pseudorandom Binary Sequences*, IEEE Transaction on Computers, **20**, 3, 270–281.
2. Glover I., Grant P. (1998), *Digital Communications,* Prentice Hall, England.
3. Howard R.M. (2002), *Principles of Random Signal Analysis and Low Noise Design,* John Willey & Sons, New York.
4. Leszczyński T. (2010), *The methods of the identification resolution increase of short signals with linear frequency modulation* [in Polish: *Metody zwiększania rozdzielczości rozpoznawania krótkich sygnałów z liniową modulacją częstotliwości*], Rozprawy Nr 146, University of Technology and Life Sciences, Bydgoszcz.
5. Luke H.D. (2001) *Binary Alexis Sequences with Perfect Correlation*, IEEE Transaction on Communications, 6, 966–969.
6. Proakis J. (2001), *Digital Communications,* McGraw-Hill, New York.
7. Pogribny W., Leszczyński T. (2011), *Optimization of short Probe Linear Frequency Modulated Signal Parameters*, Archives of Acoustics, **36**, 4, 861–871.
8. Pogribny W., Leszczyński T. (2008), *Recognition Improvement of short chirp signals,* Electronics and Telecommunications Quarterly, **54**, 2, 113–125.

PAN ARCHIVES OF ACOUSTICS
Vol. **37**, No. 3, pp. 301–316 (2012)

DOI: 10.2478/v10168-012-0039-y

Beam Tracing with Refraction

Marjan SIKORA[(1)], Ivo MATELJAN[(1)], Nikola BOGUNOVIĆ[(2)]

[(1)] *Faculty of Electrical Engineering, Mechanical Engineering and Naval Architecture, University of Split*
Ruđera Boškovića 32, Split HR-21000, Croatia; e-mail: sikora@fesb.hr

[(2)] *Faculty of Electrical Engineering and Computing, University of Zagreb*
Unska 3, Zagreb, HR-10000, Croatia

(*received September 30, 2011; accepted June 22, 2012*)

This paper presents the beam tracing with refraction method, developed to examine the possibility of creating the beam tracing simulation of sound propagation in environments with piecewise non-homogenous media. The beam tracing with refraction method (BTR) is developed as an adaptive beam tracing method that simulates not only the reflection but also the refraction of sound. The scattering and the diffraction of sound are not simulated. The BTR employs 2D and 3D topology in order to efficiently simulate scenes containing non-convex media. After the beam tracing is done all beams are stored in a beam tree and kept in the computer memory. The level of sound intensity at the beginning of each beam is also memorized. This beam data structure enables fast recalculation of results for stationary source and geometry. The BTR was compared with two commercial ray tracing simulations, to check the speed of BTR algorithms. This comparison demonstrated that the BTR has a performance similar to state-of-the-art room-acoustics simulations. To check the ability to simulate refraction, the BTR was compared with a commercial Finite Elements Method (FEM) simulation. In this comparison the BTR simulated the focusing of the ultrasound with an acoustic lens, with good accuracy and excellent performance.

Keywords: simulation, beam tracing method, refraction.

1. Introduction

In acoustics, the beam tracing method has primarily been used to simulate architectural environments in which waves propagate in a single homogenous medium. Other geometric methods, such as the virtual image source method and the ray tracing method, have also been designed to analyze the propagation of sound in homogenous medium. Simulating the propagation of sound in a non-homogenous environment with more than one medium has typically been conducted with method like Finite Elements Method (FEM), which calculates the numerical wave equation solution. Although these methods are well developed and widely used, they have significant limitations (wavelength/dimension ratio, simulation in full 3D). That is why, in many applications numerical simulations are not a good or practical choice. The method presented in this paper – the beam tracing with refraction (BTR) method – was developed with the intent to fill the gap between geometrical and numerical wave equation solution simulations. The BTR aims to simulate environments containing more than one media (which until present time has not been simulated with the beam tracing method) that have large dimensions compared to the sound wavelength and that require simulation in 3D (which is a problem for numerical method of wave equation solution).

In the second section of the paper, a brief review of existing acoustic simulation methods and their characteristics is presented. In the third section, the BTR is fully explained. The fourth section presents results from simulations of several scenes with the BTR and compares them with results from two geometrical simulations and one FEM simulation. The fifth section presents the conclusions and ideas for future work.

2. Previous work

Simulation methods in acoustics can be divided into two groups: geometrical and numerical wave equation solutions. Geometrical methods are primarily used for room acoustic simulations.

The first geometrical methods that were developed were the virtual source method and the ray tracing method (Kleiner *et al.*, 1993). These methods are often combined to overcome their individual limitations. In these combinations, the virtual source method is used to simulate early reflections (because of its accuracy), and the ray tracing method is used to simulate later reflections (because of its efficiency). Along with specular reflections, which are the most important phenomena in room acoustics, the ray tracing method is used to simulate diffuse reflections and diffraction. There exist several modified versions of the ray-tracing method such as the ray tracing in time domain (Alpkocak, 2010) or the ray tracing with refraction (Fink, 1994). The ray tracing with refraction method was developed by Kevin Fink for the simulation of acoustic lenses. This ray tracing simulation calculates focusing of the sonar beam by tracing the propagation of rays through an acoustic lens made of rubber and through seawater, a medium in which sonar is used.

The beam tracing method was first reported by Heckbert and Hanrahan (1984) and by Walsh, Dadoun and Kirkpatrick (1985) as a visualization technique. This method was developed to overcome limitations of the ray tracing method while retaining its efficiency. Because it uses beams instead of rays and a point detector instead of a spherical detector, it ensures spatial coherence and avoids the problem of aliasing inherent to the ray tracing method.

Siltanen *et al.* (2007) presented the acoustic radiance transfer method based on the room acoustic rendering equation (RARE). The RARE is an integral equation which generalizes above mentioned geometrical room acoustics modeling algorithms. Its formulation is adopted from computer graphics. Similar to the BTR, it calculates intensities of sound instead of the pressure, and to get the intensity at any point it sums intensities transmitted through the direct path and the reflections reaching that point. Like the BTR the memory consumption of the RARE algorithm is high, in typical cases hundreds of megabytes, but this allows the recalculation of the intensity of sound for different receiver without repeating complete algorithm. As it is a room acoustics modeling algorithm, the RARE doesn't include effects of the refraction of the sound.

Since the BTR is based on the beam tracing method, its development would now be examined in more detail. The beam tracing method was first used for acoustic simulation by Maercke, Maercke and Martin (1993), who used cone tracing instead of ray tracing. They overlapped cones slightly to achieve spatial coherence, which became a potential source of aliasing. This problem was solved later by Lewers (1993), who used beams with triangular sections instead of cones. This enabled him to achieve full spatial coherence without overlapping the beams. He also introduced a method of radiant exchange for calculating diffuse reflections. The next step in the development of the beam tracing method was taken by Farina (1994; 2000) and by Drumm (2000). They introduced an adaptive beam division algorithm that divided a beam into several smaller beams when it encountered more than one reflective plane. Both authors incorporated simulation of diffuse reflections into their models, and Farina simulated edge scattering as well.

The development of the beam tracing method continued toward interactive applications with the introduction of advanced spatial data structures. Funkhouser *et al.* (1998) presented an implementation of the beam tracing method for interactive auralization of architectural environments. Using spatial data structures, they achieved the performance required for interactive simulation of a moving listener and a stationary source. Later, they added diffraction to their model (Tsingos, Funkhouser, 2001) to improve the quality of the auralization. Finally, Laine *et al.* (2009) presented their implementation of the interactive beam tracing method, which was (in scenes of moderate complexity) able to produce auralizations at interactive rates, not only with a moving listener but also with a moving source.

Until now, implementations of the beam tracing method that simulate refraction existed only in the field of visualization, in which the refraction of light is simulated to visualize the interaction of light with water or with curved objects made of glass (Shah, Pattanaik, 2007). As far as the authors are aware, there is no beam tracing simulation in acoustics that is able to calculate the refraction of sound. The FEM is currently the method of choice for simulating the refraction of sound. The FEM is used for simulation in fields such as medical ultrasound, sonar and geology (Shah, Pattanaik, 2007; Wojcik *et al.*, 1994; 1998), both to design ultrasound transducers and to analyze the propagation of sound. The FEM is suitable for simulation of environments with many different media. In the FEM, a scene is composed of a number of finite elements, each of which can have different acoustical parameters. This structure allows the FEM to be used not only to simulate scenes containing several media but also to simulate diffuse environments in which there are no clear boundaries between different media. The FEM simulates all relevant wave phenomena, including reflection, refraction and diffraction, as it is based on numerical integration of the wave equation.

Besides the FEM, several other numerical wave equation solutions methods have been developed such as the acoustics diffusion equation (ADE) modeling and the finite difference time domain (FDTD) method. The ADE modeling uses the analogy of the movement of a single particle in a gas to model the sound field (Picaut *et al.*, 1997). In the FDTD method sound pressures and particle velocities are estimated

at discrete grid locations for successive discrete times (Botteldoren, 1994).

The complexity of a FEM simulation is determined by the number of finite elements in the model. If the dimensions of the model are large compared with the wavelength of the sound, the model must be divided into a large number of finite elements. The complexity of simulating such a model can be a problem for a desktop computer. If the FEM simulation needs to be performed in full 3D, the computational complexity becomes even more problematic, and these simulations can often only be performed on computer clusters and grids.

Areas of application for beam tracing and the FEM in acoustics are shown in Fig. 1. Existing implementations of the beam tracing method in acoustics can efficiently simulate scenes where dimensions of model are larger than the wavelength of the simulated sound. The other limitation of the traditional beam tracing method is that the model contains only one medium. This makes the beam tracing method suitable for room acoustics simulations and virtual reality applications. FEM simulations can simulate models with any number of media, ranging from single-medium environments to diffuse environments, but when the size-to-wavelength ratio of the model increases beyond a certain limit, the computational complexity limits the utility of the FEM. The FEM is thus used in applications such as the medical ultrasound and the detection of faults in materials.

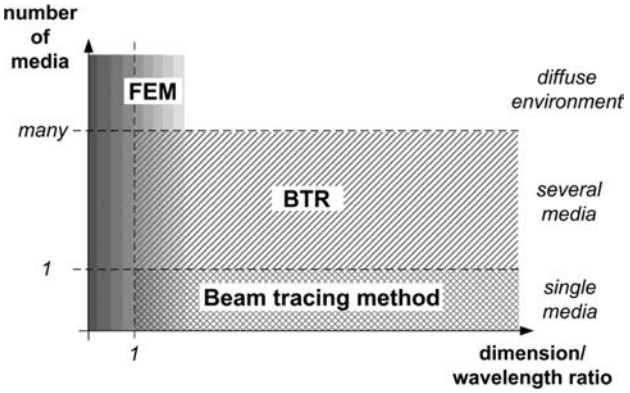

Fig. 1. Areas of application of simulation methods.

There is an area of simulation application that cannot be efficiently simulated with the beam tracing method or with the FEM. In these applications, the propagation space has dimensions that are large compared with the wavelength of the simulated sound, the space is composed of more than one media (or one medium with variable physical characteristics), and the simulation has to be done in full 3D. The BTR was developed with the intent to efficiently predict intensity of ultrasound in marine environments such as farmed fisheries and oyster farms, and for the simulation of the ultrasound propagation in the human head, where in medical applications the ultrasound propagates through several layers of soft tissue and bone.

3. Models and methods

The BTR is designed to simulate the propagation of sound in non-convex spaces composed of different media. The BTR simulates two wave phenomena: specular reflection and the refraction of sound. Diffuse reflection and diffraction of sound are not currently incorporated in the BTR. These phenomena are already solved with the beam tracing method, and published by several authors (Farina, 2000; Drumm, 2000; Funkhouser *et al.*, 1998; Tsingos, Funkhouser, 2001). The BTR has been specialized to include the refraction.

This section first explains the physical model of the BTR, then data structures and algorithms of the simulation, and finally the implementation of the simulation.

3.1. Physical model of simulation

The BTR traces beams with triangular cross-section. When beams hit the boundary surface between two media, they are divided into smaller beams, to adjust to individual triangles that make the boundary surface. After the division, each divided beam is reflected or refracted, and such beams are further traced in the same manner. The tracing stops when the level of the intensity on the end of the beam is smaller than predefined threshold, or when the volume of the beam is smaller than predefined volume threshold.

The result of BTR simulation is the level of sound intensity at a single point or at points in a rectangular raster. First, the physical model used for calculation of the intensity level will be explained, and after that the method for constructing the geometry of the reflected and the refracted beam.

3.1.1. The intensity of sound

Following the law of power averaging, the total sound intensity at the receiver is calculated by summing the individual intensities of each beam that contains the receiver. The reason the BTR employs this method rather than summing the pressures of each beam is because the phase of the reflected sound pressure wave can be treated as a random variable in the case of a highly reverberant environment. If this method of calculation was used in a scene that is not highly reverberant, then the results would not include sound interference. The individual beam that contains the receiver can be either the direct beam (coming directly from the source), or indirect beam (that has been already reflected or refracted on the boundary surface between two media). The sound intensity at

a point inside a direct beam is calculated using the following equation:

$$I = \frac{P_A}{4 \cdot \pi \cdot r^2} \cdot e^{-\gamma \cdot r}, \tag{1}$$

where P_A is the acoustical power of the source of the sound, r is the distance from the source and γ is the attenuation coefficient of the media within which the beam propagates. The first term in the equation describes the attenuation of the sound caused by the propagation of the spherical wave. The second term in the equation describes the attenuation caused by viscosity and other dissipative processes in the media (Pierce, 1981).

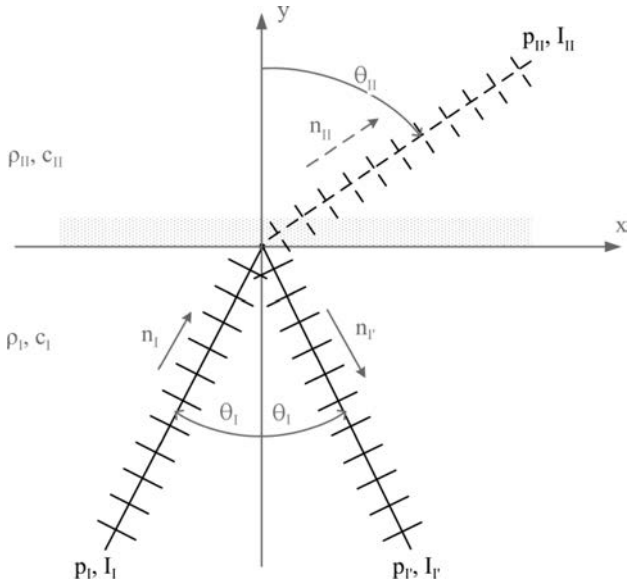

Fig. 2. The reflection and refraction of sound on a boundary surface.

When sound encounters a boundary surface that divides two media, the sound beam is reflected and refracted (Fig. 2). The sound intensity of such indirect beam is determined using the following equations:

$$I_{I'} = R^2 \cdot I_I, \tag{2}$$

$$I_{II} = \left(1 - R^2\right) \cdot I_I, \tag{3}$$

where I_I is the intensity of the incoming sound beam, $I_{I'}$ is the intensity of the reflected sound beam, I_{II} is the intensity of the refracted sound beam and R is the amplitude of sound reflection coefficient of the boundary (Pierce, 1981; Vorlander, 2008). The reflection coefficient $R$is calculated using the following expression:

$$R = \left| \frac{Z_{II} - Z_I}{Z_{II} + Z_I} \right|, \tag{4}$$

where Z_I and Z_{II} are the acoustic impedances of the two media. The acoustic impedance is function of the angle of incidence θ_I, as in (Pierce, 1981).

The traditional way to calculate the sound intensity of a point inside an indirect (reflected) beam is to generate path of the sound from the receiver to the source, in order to get the exact distance that the sound travelled. This path generation creates the exact path that sound traverses from the source to the receiver. It is computationally complex because one has to calculate all of the intersections of the sound path with the boundary surfaces using virtual sound sources.

In the BTR, to decrease the computational complexity of the path calculation, the intensity of the sound at a point inside an indirect beam is calculated in a different way (Fig. 3). The intensity is calculated relative to the sound intensity at the barycenter of the starting triangle of the beam (I_0) using the following equation:

$$I_{\mathrm{BTR}} = I_0 \frac{r_1^2}{r_2^2} \cdot e^{-\gamma \cdot (r_2 - r_1)}, \tag{5}$$

where I_0 is the intensity of the sound at the barycenter of the starting triangle of the indirect beam, r_1 is the distance from the virtual source of the beam to the barycenter of the starting triangle of the beam, r_2 is the distance from the virtual source of the beam to the receiver and γ is the attenuation coefficient determined by the entity in which the beam propagates.

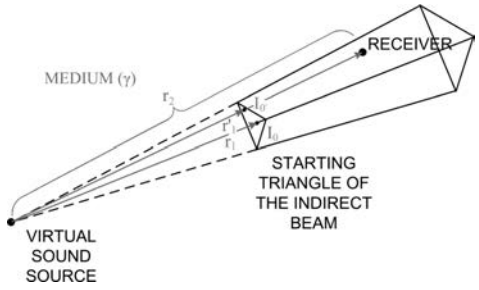

Fig. 3. Calculating the intensity of indirect sound in the BTR.

I_0 is calculated as the intensity of sound of original beam using Eq. (1), and then transformed with Eq. (2) for reflected, and with Eq. (3) for refracted beam. It is stored in the data structure of the indirect beam, so all data required to calculate the intensity of sound is stored with the beam.

The drawback of this method is that an error is introduced because the sound intensity should be calculated relative to the real intersection of the sound ray with the starting triangle of the indirect beam rather than the barycenter of the starting triangle. The equation for the exact sound intensity is:

$$I = I_0' \frac{r_1'^2}{r_2^2} \cdot e^{-\gamma \cdot (r_2 - r_1')}. \tag{6}$$

Let us examine the magnitude of this error. The error is largest for the first reflection/refraction of the

beam because the beam is at its widest. The angular width of such a beam is 26.5° and it is determined by the shape of the icosahedron. For the square room, the worst error is 2.54 dB. The detailed description of how the worst error is calculated is given in Appendix A. For subsequent reflections and refractions, the error gets smaller because beams get divided, so they have smaller angular widths.

BTR has the similar complexity of the first part of algorithm – the tracing of beams – as other splitting beam tracing algorithms. But in the second part – the calculation of sound intensity – BTR shows the advantage over the traditional beam tracing method. In the BTR, there is no path generation, which can be time-consuming in the case of multiple reflections/refractions. All information needed for the calculation of the sound intensity is already recorded within the beam data structure. Let us consider the gain in the computational complexity. If n is the number of beams that hit the receiver, and m is the order of reflection/refraction, the time complexity of re-computing all m^{th} reflections in the BTR is linear: $O(n)$. In the traditional method with path generation, the time complexity is exponential $O(n^m)$ because there have to be m intersection points for n beams. The complexity is clearly considerably lower in the BTR. This feature of BTR has the capability of acceleration of the beam tracing algorithm, similar to already published efficient methods for the reduction of computation time (Stephenson, 1996; Siltanen *et al.*, 2009).

3.1.2. The geometry of the beam

When a beam hits a boundary surface, the geometry of the beam is changed. The BTR generates one reflected and one refracted beam for each incoming beam. Edge rays of reflected beam have the angle opposite to the angle of edge rays of the incoming beam – θ_I (Fig. 2). Edge rays of the refracted beam are generated according to Snell's law:

$$\frac{\sin(\theta_I)}{\sin(\theta_{II})} = \frac{c_I}{c_{II}}. \tag{7}$$

If the incoming angle θ_I is greater than the critical angle $\theta_{I-\mathrm{crit}}$:

$$\theta_{I-\mathrm{crit}} = \arcsin\left(\frac{c_I}{c_{II}}\right) \tag{8}$$

then only the reflected beam is generated.

Because the Snell law (Eq. (7)) is not linear, the beam loses focus after refraction. This problem was detected and described in one of the first papers on beam tracing for visualization (Heckbert, Hanrahan, 1984). In the BTR, this problem is solved by refocusing the refracted beam. To do this, three pairs of beam edge rays are intersected, resulting in three intersection points. The new focus of the beam is calculated as the arithmetic average of these intersections. Figure 4 illustrates the problem of losing focus of the refracted beam (the reflected beam is not shown). Edge rays of incoming beam are displayed with solid black line. Edge rays of refracted beam are displayed with dotted black line. Intersections of edge rays of the refracted beam are marked with circles. One can see that edge rays lose focus – they do not intersect in single point (Fig. 4 – detail – right).

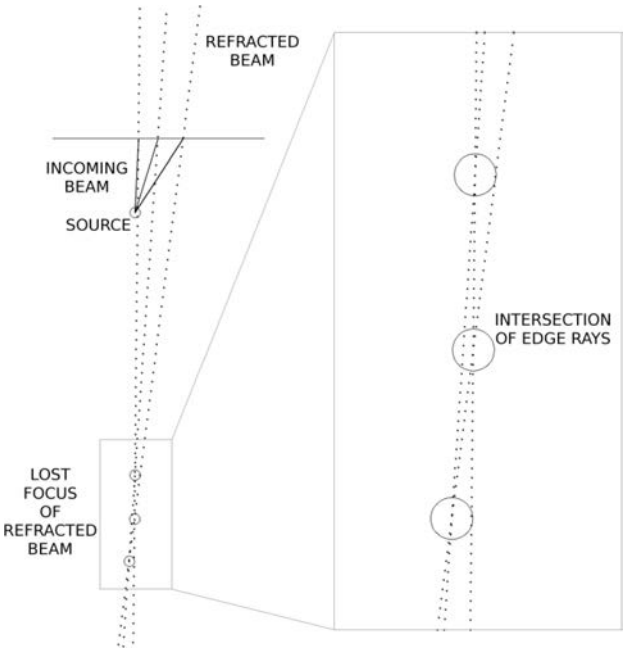

Fig. 4. The reflection and refraction of sound on a boundary surface.

This method of refocusing and its influence on the accuracy of the results have already been analyzed (Sikora *et al.*, 2010). It was shown that refocusing the initial beam causes the edge rays to have an average angular error of 0.13°. All subsequent beams are already divided and are thinner than the original beam. Thus, their edge rays are more parallel, which decreases this angular error. The influences of angular and intensity errors are tested using the example of refraction in an acoustic lens that is presented in Subsec. 4.2.

3.2. Data structures

3.2.1. Scene composition

The simulated propagation space in the BTR is called a scene, and its topology has three levels of hierarchy: entity, shell and boundary surface. An example scene is presented in Fig. 5.

An entity represents a volume containing a single medium and is defined by one or more shells. A simple entity is defined by a single shell. It can be convex (E1) or non-convex (E3). Entities that contain one or

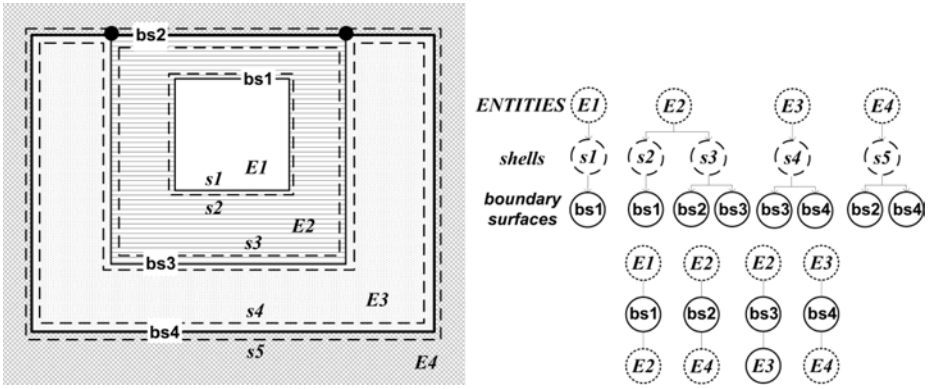

Fig. 5. The topology of a scene.

more islands are non-convex and have several shells (E2). A shell is a closed triangular mesh that defines the outer boundary of an entity (s2, s3, s4) or the inner boundary of an enclosing entity (s1, s5). A shell is two-dimensional object that is used to define the extent of an entity, which is a three-dimensional object. An entity doesn't have any geometry information, but only the list of shells that surround it. The orientation of triangles in the mesh of the shell defines the space that is inside of the entity.

A shell is composed of one or more boundary surfaces. A boundary surface is a triangular mesh that divides exactly two entities. Thus, a boundary surface is not always a closed mesh, but a set of boundary surfaces that compose one shell must be a closed mesh. A boundary surface has no orientation.

The scene topology is used during beam tracing to accelerate the geometric operations involving traversing beams between neighbor entities. When a beam hits a boundary surface, the topology determines in which entity it will continue to propagate, knowing that one boundary surface divides exactly two entities. In addition, as every beam "knows" inside which entity it is currently propagating, only local geometrical complexity affects the performance of the algorithm. This algorithm is explained in greater details in Subsec. 3.3.

Triangular meshes that compose boundary surfaces are topologically structured. They are composed of vertices, edges and triangles, and their spatial relationships are defined by a winged-edge structure. The mesh topology is used during beam division to speed up the process of finding which neighboring triangles are hit by the beam.

Boundary surfaces are based on triangular meshes instead of the polygons normally used in the beam tracing method. This choice was made because classical beam tracing is used in architectural environments, while the BTR is designed for man-made environments that are not necessary regular.

A binary space partitioning (BSP) tree is calculated for each entity in the scene. The BSP tree is used by the beam division algorithm to determine the correct order of visibility of illuminated triangles. The BSP tree is used to speed up the visualization process and to solve cases of cyclic hiding.

The mesh topology and the BSP tree are calculated automatically during the preprocessing phase of the simulation. The topology of the scene is not calculated by the simulation and has to be defined by the user when setting up the scene.

3.2.2. Beams

Beams in the BTR have triangular cross sections and are defined by three edge rays that intersect in the focus of the beam. Initial beams have the form of a triangular pyramid, with the focus of the beam at the position of the sound source. Transformed beams, which are created after reflection and refraction of the initial beams, take the form of clipped pyramids, with beam foci in the positions of the virtual sound sources (Fig. 6). The starting triangle of the beam is the place where the beam enters the entity through which it propagates. The ending triangle of the beam is the place where the beam leaves the entity, if it is refracted, or the place where the beam is returned back to the entity, if it is reflected.

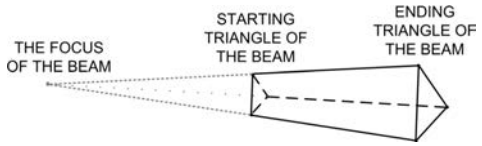

Fig. 6. A transformed beam in BTR.

In classical beam tracing, such as the method developed by Drumm (2000) and Funkhouser *et al.* (1998), beams have polygonal cross sections. The advantage of such an approach is that fewer beams are needed to trace a scene than are necessary with triangular beams. However, the performance gains that result from a lower number of beams are diminished by the complexity of polygon-polygon clipping operations that occur when such polygonal beams intersect with a geometry made of polygons. In the BTR, as all of

the beams have triangular cross sections and because shells are defined by triangle meshes, all geometric operations operate on two triangles. Special attention was paid to the design of the triangle-triangle clipping algorithm that is used in the BTR with the goal of maximizing performance. The BTR clipping algorithm differs from the classical Sutherland-Hodgman algorithm (Sutherland, Hodgman, 1974). Rather than using a unified algorithm for all combinations of two triangles, the BTR first detects the combination of triangles with a few simple geometric tests and then creates the resulting clipped triangles for that particular combination. As a result, the BTR clipping algorithm performs better than other approaches.

3.3. Algorithm of BTR

After the scene geometry is defined and the calculation of the topology is done, the algorithm of BTR begins. Its flow diagram is shown in Fig. 7.

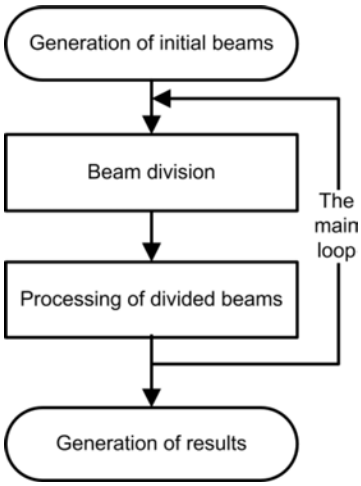

Fig. 7. The algorithm of BTR.

After the initial beams have been generated, the main loop of algorithm starts. In this loop, for every beam the beam division is performed, after which the divided beams are processed. After the main loop is finished, the results are generated in the form of raster with the distribution of sound intensity.

3.3.1. Initial beams

The process of beam tracing starts with the generation of initial beams. The foci of initial beams are at the position of the sound source. Beams are generated using the icosahedron in such a way that three edge rays of one beam pass through vertices of one triangle of an icosahedron. This process results in 20 initial beams. The cross section of each beam is an equilateral triangle. Initial beams propagate through the entity that contains the source of the sound. The information about the entity where the beam propagates is recorded with each beam and is updated whenever refraction occurs.

3.3.2. The main loop of the algorithm

After the initial beams are generated, they are pushed onto the raw beam stack, and the main loop of algorithm starts (Algorithm 1).

Algorithm 1. The main loop.

```
while the raw beam stack (RBS) is not empty
  pop one raw beam (rb) from RBS
  do the beam division of rb
  push beams produced by division of rb on
       the divided beams stack (DBS)
  process divided beams from DBS
repeat
```

In the main loop, one beam is popped from the raw beams stack and intersected with the shell(s) of the entity in which it propagates. This intersection triggers the beam division process. During the beam division process, the original raw beam is divided into several raw beams. The divided beams are then processed, resulting in several finished beams that are pushed onto the stack of finished beams and several new raw beams (from reflection and refraction) that are pushed onto the stack of raw beams. The loop repeats until the stack of raw beams is empty, which means that beam tracing is done.

3.3.3. Beam division

Each beam propagates inside of an entity and eventually encounters one of the entity shells that combine to represent the boundary of an entity. In the simplest case, the entire beam intersects only one triangle of the shell's mesh. In this case, it is not necessary to perform beam division. Generally, however, the beam intersects several triangles of the shell's mesh. In that case, the beam has to be divided into several smaller beams, one for each intersected triangle of the mesh. In addition, as entities in the BTR can be non-convex, some of the intersected triangles may obscure each other. In this case, the precise region that is not obscured has to be determined to generate an accurate beam division. The correct beam division is of the utmost importance because it ensures the spatial coherence of the beam tracing method and preserves the sound energy of the beam.

The beam division process implemented in the BTR is composed of these phases:

- finding intersected triangles and their transformation to the beam space (Subsec. 3.3.3.1)
- projecting and clipping triangles (Subsec. 3.3.3.2)
- hiding and dividing triangles (Subsec. 3.3.3.3)
- creating divided beams (Subsec. 3.3.3.4).

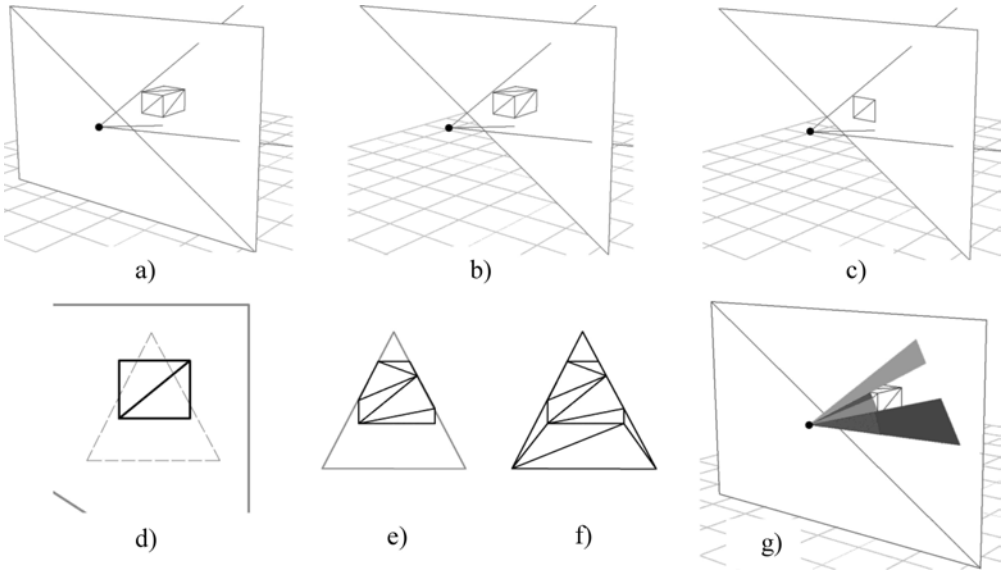

Fig. 8. Example of the process of beam division: a) the starting geometry, b) illuminated triangles, c) backface culling, d) perspective projection, e) clipping with the beam section, f) hiding and dividing triangles, g) divided beams.

The beam division process is illustrated in Fig. 8. This simple example shows the division of a beam, displayed with three edge rays, that propagates from the source displayed with small black circle. The beam first encounters a shell in the form of a box, positioned in front of another shell displayed with two large triangles (Fig. 8a).

3.3.3.1. Finding intersected triangles and their transformation to the beam space. The beam division process begins by determining the order of visibility of the triangles. This is done by traversing the previously calculated BSP tree from the position of the sound source. The next step is the phase of finding triangles that are completely or partially within the beam. These triangles are candidates for beam division. The backface culling process is performed to remove those triangles whose normal vector points in the direction opposite to the beam propagation. The triangles that remain are transformed from the world space to the beam space. The world space is the coordinate space of the scene as displayed in Fig. 8a. The beam space is the coordinate space that has z axis as the direction of beam propagation. After all triangles are transformed to the beam space, they are clipped with the plane $z = 0$. This is done to avoid geometry distortion due to parts of the triangles that are beyond the focal point.

This stage in the beam division process is illustrated in Figs. 8a–8c. Figure 8a displays the geometry on the start of the process. Figure 8b displays those triangles that are within the beam. In this stage the lower left triangle of the second shell is eliminated from further processing. Figure 8c displays the result of the backface culling process. After that stage only two front triangles of the first shell (box) and one triangle from the second shell remain for subsequent processing.

3.3.3.2. Projecting clipping triangles. Transformed triangles are then projected to 2D as preparation for the hidden surface algorithm. This algorithm is performed on the projected triangles in 2D rather than in 3D to increase performance. Triangles are projected using a perspective projection onto the projection plane orthogonal to the z-axis (the direction of beam propagation). Then, all projected triangles are clipped with the projected section of the beam to consider only the parts of the triangles that are within the beam volume. After this, the triangles are added to a binary sorted tree. The order in which the tree is sorted is determined by the order of visibility of the triangles.

This stage in the beam division process is illustrated in Figs. 8d and 8e. Figure 8d shows the perspective projection of triangles from Fig. 8c. Two triangles from the first shell (box) are displayed in black. They are positioned in front of the triangle from the second shell which is displayed in gray, and which is only partially visible. The projected section of the beam is displayed with thin dashed line. Figure 8e shows the triangles from Fig. 8d, clipped with the projected section of the beam. Two black triangles are divided into several smaller ones. The clipping of the gray triangle resulted with the single triangle. After clipping, black triangles still overlap the gray one. The reason is because the hiding of triangles is not jet performed.

3.3.3.3. Hiding and dividing triangles. The next phase is the application of the hidden surface algorithm. Algorithm traverses projected triangles, in the

order of visibility. Projected triangles are stored in a binary sorted tree named PT. Hidden triangles, after they are processed, are saved in a list named HT. In the first step all foremost triangles from PT with the same order of visibility are transferred to HT. This is done because they cannot possibly occlude each other, and further checking is not necessary. After that, every triangle t from PT is checked for the occlusion with triangles (already processed) from HT. If the triangle t is not occluded by any triangle hT from HT, it is moved from PT to HT. Otherwise, if the triangle hT occludes t, they are subtracted. Triangles resulting from this subtraction are added to PT and the loops are restarted.

In the case of occlusion, the loop is restarted several times. In order not to check triangle pairs twice, the information of already checked triangle pairs is recorded, and in further occlusion checks, they are skipped. To avoid overhead, two more tests are performed: if t and hT have the same order of visibility they cannot occlude each other, and the occlusion test is skipped. Also if they are neighbors, since we have already done the backface-culling, they also cannot occlude each other, and the occlusion test is skipped.

The results of the hidden surface algorithm are displayed in Fig. 8f. In this figure, triangles from the previous phase (Fig. 8e), are processed according to their order of visibility. In this case black triangles, which are closer to the source of the beam, are subtracted from the gray triangle. The process gives in 10 triangles, which do not overlap each other, while covering the whole area of the beam section.

3.3.3.4. Creating divided beams. The process of beam division in the BTR terminates with the creation of divided beams. The initial beam that has been divided is removed from the raw beams stack. Divided beams are created and pushed onto the divided beams stack. These beams are created from the 2D triangles that result from the hiding and dividing phase. These hidden 2D triangles are first projected back from the beam space to the world space. Divided beams are then constructed so that their three corner rays originate at the source of the original raw beam and pass through the three corners of hidden triangles.

Figure 8g displays divided beams generated from the triangles in Fig. 8f. Beams are displayed in different shades of gray. One can see only four beams, which occlude the other six beams.

3.3.4. Processing divided beams

The beam division results in several divided beams that reside in the divided beams stack. These beams are now adapted to the geometry of the entity. The next step is to process the interaction of these beams with the shell of the entity (Algorithm 2).

Algorithm 2. The algorithm for processing divided beams.

```
while the divided beams stack (DBS) is not empty
  pop one divided beam (db) from DBS
  close db with the plane of the
        intersecting triangle
  push closed beam on the finished beams
        stack (FBS)
  if termination criteria are not fulfilled
      create one reflected beam from db
      push reflected beam on RBS
      if incoming angle of db is less than
        critical
          create one refracted beam from db
          push reflected beam on RBS
      endif
  endif
repeat
```

The algorithm repeats until all divided beams are processed. In each pass, one divided beam is popped from the divided beams stack. The popped beam is then closed using the plane of the intersecting triangle. The sound intensity at the end of the beam is calculated, and the beam is then pushed on the finished beams stack. The finished beams stack contains beams that are completely processed and ready to be used to generate the results.

The finished beam is then checked to determine whether it meets the termination criteria. Further tracing of a finished beam is not performed if the sound intensity at the end of the finished beam is below a predefined level. The tracing also stops if the beam volume is lower than a predefined volume threshold.

If these criteria are not fulfilled, then tracing continues, and new reflected and refracted raw beams are generated. For each divided beam, one reflected and one refracted raw beam is created. If the incoming angle of the divided beam is greater than the critical angle (Eq. 8), only a reflected beam will be created.

Newly created reflected and refracted beams are put onto the raw beams stack and are subsequently processed. The beam tracing is finished when the raw beams stack is empty and all beams in it have been processed and transferred to the finished beams stack.

3.3.5. Generation of results

After the beam tracing is finished, the generation of results starts. The result of the BTR is the rectangular raster of points with the distribution of level of sound intensity. To calculate the level of sound intensity for each point, simulation has to determine which beams contain the point. The finished beams are organized into an octree to speed up the spatial search algorithm. By using the octree, only the leaf that contains the receiver has to be searched instead of the whole collection of finished beams. Because the number of beams in one leaf of the octree is approximately

two orders of magnitude smaller than the total number of beams, the computational complexity of this part of the algorithm is considerably decreased by using the octree structure.

The search of the leaf of the octree results with the list of all beams that contain the receiver. The level of the sound intensity of each beam is then calculated as presented in Subsec. 3.1.1 and summed to get the total level of sound intensity for the desired point in space.

3.4. Implementation

The simulation was coded in Microsoft Visual Studio C++ using Microsoft Foundation Classes for user interfaces and DirectX for displaying 3D graphics. The simulation code had 23 000 lines, including proprietary BSP and octree classes.

Special attention was paid to the numerical robustness of the code. All relational operators were replaced with relational functions that compare values using both absolute and relative margins (Goldberg, 1991). In addition, all geometrical relational functions in the BTR are designed to check boundary situations. For example, the function that checks whether a point is inside a triangle returns not only true or false, but also information about whether the point is collinear with the edge of the triangle and whether the point is collocated with a vertex of the triangle. In addition, these geometric relational functions use the above-mentioned relational functions instead of the usual relational operators of C++.

All arithmetic in the BTR is done in double precision. DirectX forces floating point math by default, but this property is overridden to enforce double precision arithmetic.

4. Results

In this section the performance and the accuracy of the BTR was tested. The BTR was first tested to check if it detects all reflection paths in a rectangular room. Then a comparison with room acoustics simulations was done to check the speed of the BTR. The BTR was compared to two commercial ray tracing simulations and one interactive beam tracing simulation.

Finally, the comparison with the FEM simulation of ultrasound propagation was done to check the ability of the BTR to simulate refraction. The BTR was compared to the FEM simulation, because there are no commercial beam tracing or ray tracing simulation that can simulate refraction.

4.1. Reflection detection test

First test of the BTR was check if it detects all reflection paths in a room. The test room was a simple rectangular room. The Eq. (9) gives the number of reflections for such a room:

$$N_r = \sum_{n=1}^{r} 4 \cdot n + 2 \sum_{m=r-1}^{0} \left(1 + \sum_{n=1}^{m} 4 \cdot n \right), \qquad (9)$$

where N_r is number of reflections, and r is the order of reflections. The tests were performed for reflections up to the fifth order. Table 1 and Fig. 9 show the number of reflections detected by the BTR compared to the exact number of reflections calculated with Eq. (9).

Table 1.

r	Nr (exact)	Nr (BTR)	
0	0	0	–
1	6	6	100%
2	24	24	100%
3	62	63	98.39%
4	128	126	98.44%
5	231	237	97.40%

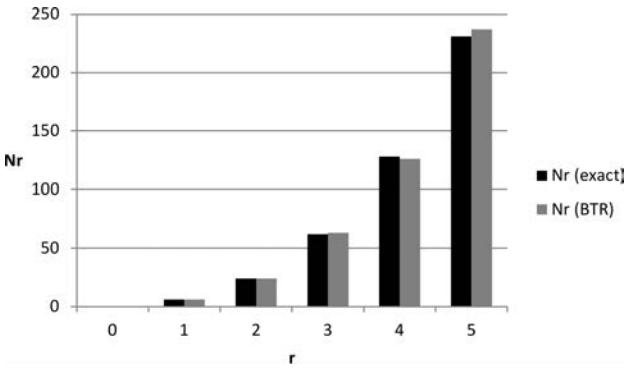

Fig. 9. Results of the reflection detection test.

The reflection detection ratio for the first two orders of reflection is 100%, for the third order is 98.39%, for the fourth order is 98.44%, and for the fifth order is 97.40%.

4.2. Comparison with two ray-tracing room acoustics simulations

BTR's performance and accuracy were compared with two commercial room acoustics simulation programs based on the ray tracing method. These two simulation programs were part of the 3rd round robin on room acoustical simulations (Bork, 2005). The tests were performed on a computer equipped with an Intel Core2 T5600 processor (1.83 GHz), 2 GB of RAM and Microsoft Windows XP operating system.

The tests were based on the three scenes shown in Fig. 10. In this figure, the room geometries are displayed with solid lines and the position of the source is indicated with a small black sphere. The source was unidirectional emitting sound at 1 kHz with a power of

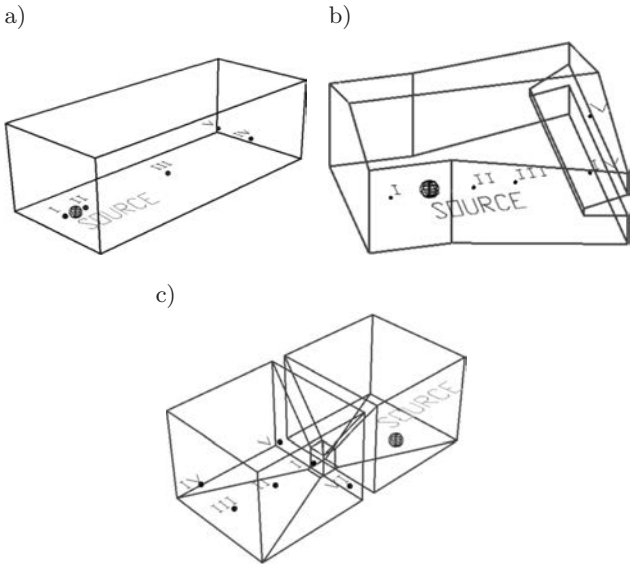

Fig. 10. Test scenes: a) Shoebox, b) Aura, c) Concave.

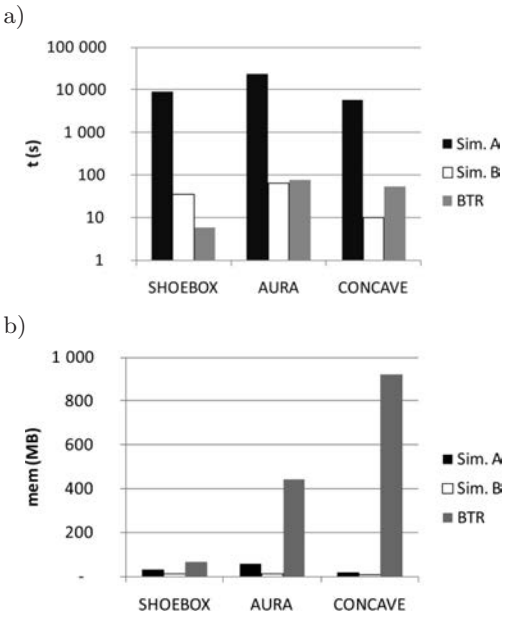

Fig. 11. Wall-clock time (a) and memory consumption (b) in three simulations of the tested scenes.

1 mW. The boundary surfaces had absorption coefficients of 10%. The scattering coefficient was set to zero.

Test scenes were traced with two commercial room acoustic simulations and the BTR. The first ray tracing simulation (Feistel *et al.*, 2007) was named *Simulation A*, and it required that the number of initial rays was set as a parameter before the simulation was executed. To determine the optimal number of initial rays, several simulations were performed with different number of initial rays. The number of initial rays was finally fixed to 10000 because for greater number of rays simulation gave practically the same results, and the calculation time significantly increased.

The second ray tracing simulation (James *et al.*, 2008) was named *Simulation B*, and the number of rays that this simulation traced was automatically determined by the simulation program. In the BTR, the beams were traced until the level of the sound intensity dropped below 40 dB. In all simulations, the tracing was performed for direct sound and three reflections.

The average difference of the level of the sound intensity in control points between the BTR and *Simulation A* was 3.87 dB, and between the BTR and *Simulation B* was 0.87 dB.

Simulation A was the slowest by two orders of magnitude for all three scenes (Fig. 11a). The speeds of the BTR and *Simulation B* were similar. The BTR was faster for the simplest scene (*Shoebox*), and *Simulation B* was faster for the other two scenes.

Simulation B had the lowest memory consumption for all three scenes (Fig. 11b). The BTR had by far the highest memory consumption because the BTR keeps all traced beams permanently in the memory. The other two simulations store the traced rays only while their contributions to the sound field are calculated. The advantage of the method that the BTR uses is that only part of the processing has to be redone when scanning a different part of the room or when scanning with a different resolution. In such situations, the BTR works significantly faster than the other two simulations.

The tests presented in this chapter show that although the BTR is not designed for room acoustics, it has good speed, compared to commercial ray-tracing simulations. The BTR was as fast as the fastest ray tracing simulation. The memory consumption of the BTR was higher than the ray tracing simulations but allowed faster recalculation of the results in cases with fixed scene geometries and fixed source positions. The drawback of the BTR is its exponential space complexity. The BTR has the space complexity $O(n^r)$, where n is the number of triangles in the model, and r is the order of reflections calculated in the simulation. Because of this the BTR cannot be used efficiently for the calculation of later reverberations.

4.3. Comparison with the beam tracing room acoustics simulation

The BTR was then compared to Evertims simulation (Noistering *et al.*, 2008). This is an interactive simulation, which is composed of three components: the graphical interface, the simulation engine and the auralization software. The simulation engine of Evertims simulation is based on the beam tracing method. It calculates the room impulse response, which is subsequently used for the auralization. For each reflection Evertims calculates the direction of arrival. Evertims calculates specular reflections and doesn't take into account the diffraction of sound.

The tests of the BTR and Evertims were performed on the computer equipped with an Intel Core2Duo E6550 processor (2 GHz), 4 GB of RAM and Microsoft Windows 7 operating system.

Evertims and the BTR were tested on the model of Sigyn hall in Turku, Finland (Fig. 12), which was composed of 561 triangles. Both simulations calculated the room impulse response, composed of direct sound and reflections up to the third order. Simulations were performed for the single source of sound. To get the fair comparison, Evertims simulation performed the calculation of the impulse response without the auralization of the sound. On the other hand the BTR didn't calculate the refraction.

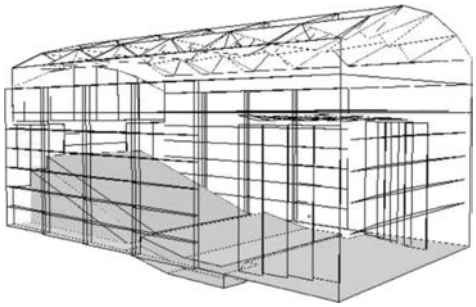

Fig. 12. The model of Sigyn hall in Turku, Finland.

The comparison of performance of BTR and Evertims is presented in Fig. 13. The speed of the BTR was similar to the speed of the Evertims simulation (Fig. 13a). The memory consumption of the BTR is much higher (Fig. 13b) than Evertims. The reason for this is probably the adaptive beam tracing used in the BTR, which results in greater number of beams, and consequently greater memory consumption.

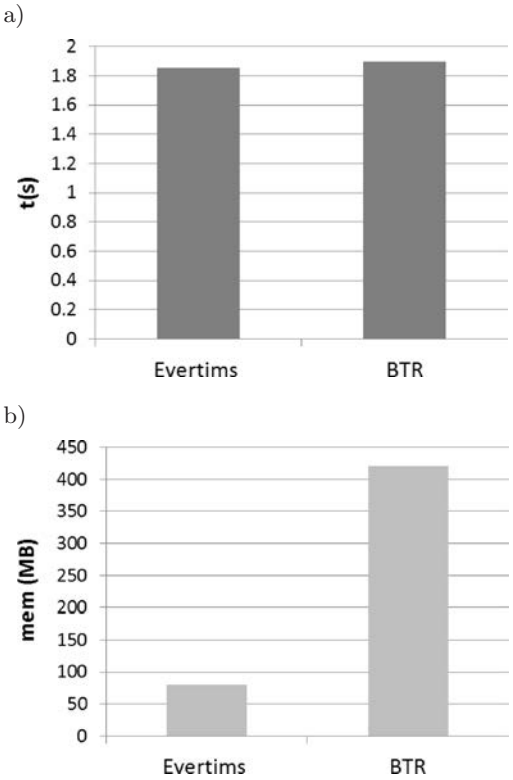

Fig. 13. The speed (a) and the memory consumption (b) of the simulation of Sigyn hall with Evertims and the BTR.

4.4. Comparison with the FEM simulation of ultrasound propagation

The tests presented in the previous chapter have checked the speed of the BTR algorithm. However, the main advantage of the BTR over other beam tracing methods is that it can trace not only reflections but refractions as well. To verify this property of the BTR, a simple scene with an acoustic lens was constructed (Fig. 14).

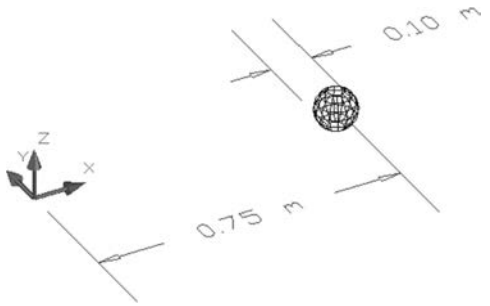

Fig. 14. The scene used to test refraction in the BTR.

The acoustic lens scene consisted of a unidirectional sound source ($f = 100$ kHz; $P = 100$ W) emitting ultrasound into a space filled with glycerol ($c = 1920$ m/s; $\rho = 1260$ kg/m^3; $\gamma = 3 \cdot 10^{-6}$ m^{-1}). In the glycerol, there was an entity made of rubber ($c = 900$ m/s; $\rho = 930$ kg/m^3; $\gamma = 43 \cdot 10^{-3}$ m^{-1}). The rubber entity was a sphere with a diameter of 0.1 m centered 0.75 m from the sound source (located at the origin of the coordinate system in Fig. 14 and Fig. 15).

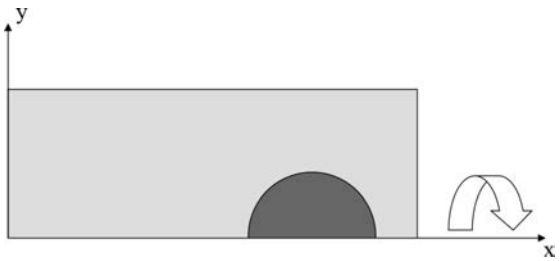

Fig. 15. 2.5D FEM simulation model-rotation around the x-axis.

The acoustic lens scene was first simulated with the BTR and compared with a ray tracing simulation (Sikora *et al.*, 2010). The results of these two methods agreed well. To gain further insight, the BTR was compared with a well-established FEM simulation

(Wojcik *et al.*, 1998). This simulation takes a finite-element and explicit time-domain approach to solve the propagation of ultrasound.

Because simulating this scene in full 3D with the FEM, would be too computationally complex to perform on a desktop computer, the simulation was performed in 2.5D by utilizing the rotational symmetry of the acoustic lens scene. The rotational axis is the line from the source of the sound (the origin of coordinate system) through the center of the rubber sphere (Fig. 15). In this 2.5D setup, one finite element had dimensions of 0.36×0.36 mm, for a total of $2\,222 \times 833 = 1\,850\,926$ elements.

The BTR scene structure had two entities: the outer, non-convex entity filled with glycerol, and the inner, convex entity filled with rubber. Both entities had only one shell, in the form of a sphere. The geometry of the sphere consisted of 224 equilateral triangles (Fig. 14). The BTR simulation traced direct sound and reflections/refractions up to 4th order.

The results of the FEM and the BTR simulations are shown in Fig. 16a and 16b, respectively. In the left part of figures one can see an area with the high intensity ultrasound surrounding the source. This area is shown in white. The sound intensity level decreases as the sound travels from the source towards the rubber sphere situated in the right part of the model. As sound decreases, the color in figures changes from white to gray. Inside the rubber sphere, the focusing of the ultrasound occurs, as shown in Fig. 16a for the BTR and 16b for the FEM. The areas where the sound focuses are shown as lighter gray areas inside the sphere. In both figures, one can see how the refraction on the boundary between the glycerol and the front of the rubber sphere bends the ultrasound toward the primary focus, which is situated in the back of the sphere. The position and maximum intensity of the primary focus is nearly the same in both simulations. The difference between the locations of the maximum is 0.7 mm, and the difference between the sound intensity levels is 1 dB.

a)

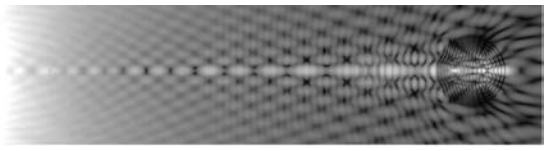

b)

Fig. 16. The simulation of the acoustic lens scene with the FEM (a) and the BTR (b).

In the left part of the sphere, there is also a secondary focus, which occurs because the refracted ultrasound that has entered the sphere reflects two more times inside the sphere. It first reflects from the back of the sphere, and then from the upper of lower boundary of the sphere. Because of multiple reflections/refractions and because of the longer path that the sound traverses after the first refraction, the secondary focus has lower intensity level.

Figures 16 and 17 show two differences between the FEM and the BTR. Since the FEM calculates the pressure of the sound taking the phase into account, its results exhibit the effects of the sound wave interference, which can be seen as the line patterns. Since the BTR calculates the intensity of sound, it doesn't take the phase into account, so results of the BTR don't show the interference lines. Also, the BTR creates a clear shadow region behind the lens, while the FEM simulation does not, because the FEM calculates the diffraction of the sound.

a) b)

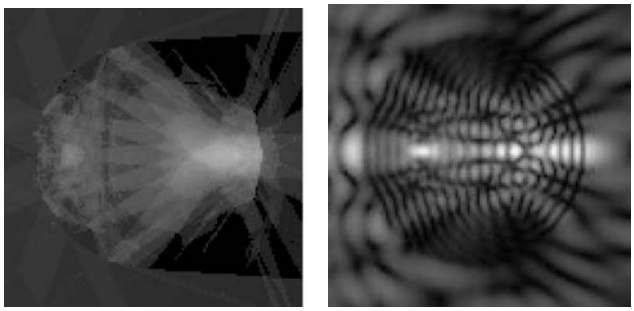

Fig. 17. The distribution of the level of sound intensity for the area of the rubber lens: the BTR (a) and the FEM (b).

Let us consider the performance of the FEM and the BTR simulations. Both simulations were executed on the same hardware platform, which consisted of an Intel Core2Duo processor with a frequency of 2.4 GHz and 4 GB RAM.

Figure 18a shows that the BTR simulation executed approximately 10 times faster than the FEM simulation. The BTR also used less than half of the memory that the FEM used (Fig. 18b). The price for this good performance from the BTR is that the FEM simulation modeled more wave phenomena than the BTR, and that the error in the beam refocusing in the BTR caused certain discrepancies. On the other hand, the FEM could not perform this simulation in full 3D, but only in 2.5D. In addition, given a higher sound frequency, the performance of the BTR would stay the same, while the performance of the FEM would decrease. Because of the required wavelength/finite element size ratio, the number of finite elements would have to be increased, and the performance of the FEM would decrease significantly.

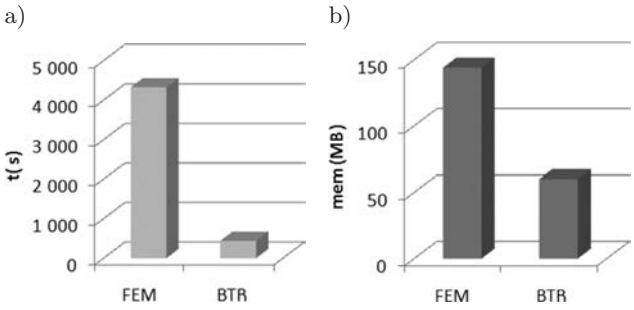

Fig. 18. The speed (a) and the memory consumption (b) of the simulation of acoustic lens with the FEM and the BTR.

This test showed that the BTR is a good choice for situations in which the dimensions of the scene are large compared with the wavelength of ultrasound and the interference and diffraction of sound do not have to be simulated. In such cases, the BTR provides excellent performance and good accuracy.

5. Conclusion and future work

This paper presents the beam tracing with refraction (BTR) method, which is designed for the simulation of sound propagation in environments with more than one media. The BTR method can simulate reflection and refraction of sound.

Although primarily designed for non-homogenous environments such as situations with temperature vertical gradients, the BTR can also be efficiently used for room acoustics. The BTR is suitable for the quick estimation of stationary sound field intensity distribution during the design of sound reinforcement systems. After the beam tracing is done all beams with the level of sound intensity at their beginning are stored as a beam tree structure in the computer memory. That enables the fast recalculation of results for the stationary source and geometry. The BTR is not suitable for the analysis of long delayed reflections of high order, but this limitation can be overcome by combining the BTR with other methods, which is a common practice today – most commercial simulation packages combine the virtual source method for early reflections, the ray tracing for higher order reflections and the statistical reverberation tail creation.

Three tests were performed to check the quality of BTR method: two to determine the speed of the BTR and one to check the ability to simulate the refraction of sound. The speed of BTR was checked against two commercial room acoustic ray-tracing simulations and against an interactive beam tracing simulation. The ability of the BTR to simulate the refraction of sound was checked by the comparison with the commercial FEM simulation. Tests showed that refraction can be simulated with the beam tracing method, and that it can be efficiently used for simple models made of few different media, bearing in mind that diffraction and interference are not simulated. On the other hand, the method of calculating the sound intensity used in the BTR shows to be useful in room acoustics, for quick estimation of stationary sound field distribution, where several recalculations have to be performed for stationary source.

In the future, it would be desirable to incorporate other wave phenomena such as diffraction, interference and diffuse reflections into the BTR to obtain more realistic results. In addition, both beam tracing and generation of the results should be parallelized to increase the performance on the multicore processors that are now common.

Appendix A.

The approximated sound intensity of the receiver I_{BTR} is calculated with Eq. (5), where I_0 is the intensity at the barycenter of the starting triangle of the beam, r_1 is the distance from the virtual source of the beam to the barycenter of the starting triangle, and r_2 is the distance from the virtual source to the receiver (Fig. 3). The exact sound intensity of the receiver I is calculated with Eq. (6), where I_0' is the intensity at the intersection of r_2 and the starting triangle of the beam, and r_1' is the distance from the virtual sound source to the intersection. The relative error of the BTR intensity ΔI is:

$$\Delta I = \frac{I_{\mathrm{BTR}}}{I}. \tag{10}$$

Using Eqs. (5) and (6) Eq. (I) is transformed to:

$$\Delta I = \frac{I_0}{I'} \cdot e^{-\gamma(r_1' - r_1)} \tag{11}$$

From Eqs. (1) and (3) one can get expressions for I_0 and I_0':

$$I_0 = (1 - R^2)\frac{P_A}{4 \cdot \pi \cdot r_1^2} \cdot e^{-\gamma \cdot r_1}, \tag{12}$$

$$I_0' = (1 - R^2)\frac{P_A}{4 \cdot \pi \cdot r_1'^2} \cdot e^{-\gamma \cdot r_1'}. \tag{13}$$

Using Eqs. (12) and (13) the ratio of I_0/I_0' is:

$$\frac{I_0}{I_0'} = \frac{r_1'^2}{r_1^2} e^{-\gamma(r_1 - r_1')}. \tag{14}$$

Entering Eq. (14) into Eq. (11) one gets the relative error of the BTR intensity ΔI:

$$\Delta I = \frac{r_1'^2}{r_1^2}. \tag{15}$$

The relative error expressed as the level of the intensity is:

$$\Delta L_I = 10 \cdot \log \frac{r_1'^2}{r_1^2}. \tag{16}$$

From Eq. (16) it is evident that error of the BTR sound intensity level depends only on the difference of the distance between the source and the barycenter and the distance between the source and the real intersection of the sound beam. In the worst case those two distances can be the distances between the source and the closest and the farthest point on the starting triangle of the beam.

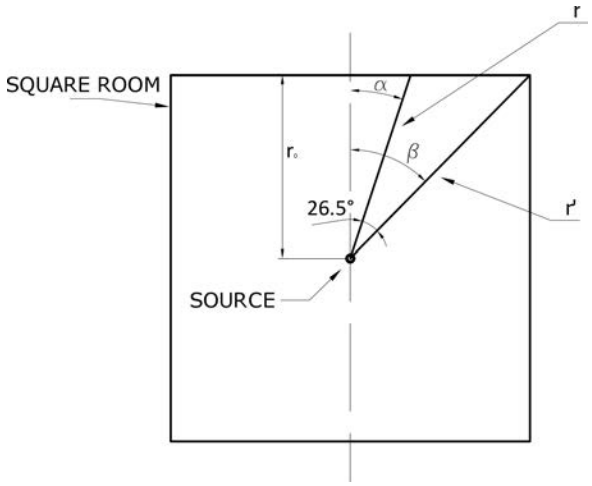

Fig. 19. A square room used to estimate the intensity error.

Let us examine a square room with an initial beam like one on the following Fig. 19. To calculate the maximum error it is enough to consider the 2D case.

The maximum error is for the beam that stretches to the corner of the room. For such beam r and r' can be expressed as:

$$r = \frac{r_0}{\cos(\alpha)}, \tag{17}$$

$$r' = \frac{r_0}{\cos(\beta)}, \tag{18}$$

$$\alpha = \beta - 26.5^\circ, \tag{19}$$

$$\beta = 45^\circ. \tag{20}$$

When Eqs. (17) and (20) are entered in Eq. (16) we get that the maximum error of the BTR sound intensity level is $\Delta L_I = 2.54$ dB.

However we have to stress here that this is the worst case scenario. This error is the maximum error for the initial beam, and the initial beam is the widest possible beam in the BTR. The subsequent beams, because of the beam division, have the smaller angular difference and consequently the error is smaller.

References

1. Alpkocak A., Sis M.K. (2010), *Computing impulse response of room acoustics using the ray-tracing method in time domain*, Archives of Acoustics, **35**, 4, 505–519.
2. Bork I. (2005), *Report on the 3rd Round Robin on Room Acoustical Computer Simulation – Part II: Calculations*, Acta Acustica united with Acustica, **91**, 753–763.
3. Botteldooren D. (1994), *Acoustical ?nite-difference time-domain simulations in a quasi-Cartesian grid*, Journal of Acoustical Society of America, **95**, 2313–2319.
4. James A., Dalenback B.I., Naqvi A. (2008), *Computer Modelling With CATT Acoustics – Theory and Practise of Diffuse Reflection and Array Modeling*, Proceedings of 24th Reproduced Sound Conference, 20–21.11, Brighton, UK.
5. Drumm I. (2000), *The adaptive beam tracing algorithm*, Journal of Acoustical Society of America, **107**, 3, 1405–1412.
6. Farina A. (1994), R*amsete un nuovo software per la previsione del campo sonoro in teatri, ambienti industriali ed ambiente esterno*, Atti del XXII Congresso Nazionale AIA, 13–15 April, Lecce.
7. Farina A. (2000), *Validation of the pyramid tracing algorithm for sound propagation outdoors: comparison with experimental measurements and with the ISO/DIS 9613 standards*, Advances in Engineering Software, **31**, 4, 241–250.
8. Feistel S., Ahnert W., Miron A., Schmitz O. (2007), *Improved methods for calculating room impulse response with EASE 4.2 AURA*, Proceedings of 19th International congress on Acoustics, 2–7 September, Madrid.
9. Fink K. (1994), *Computer Simulation of Pressure Fields Generated by Acoustic Lens Beamformers*, M.Sc. Thesis, University of Washington.
10. Funkhouser T., Carlbom I., Elko G., Pingali G., Sondhi M., West J.A. (1998), *Beam Tracing Approach to Acoustic Modeling for Interactive Virtual Environments*, Proceedings SIGGRAPH 98, pp. 21–32, Orlando.
11. Goldberg D. (1991), *What every computer scientist should know about floating-point arithmetic*, ACM Computing Surveys, **21**, 1, 5–48.
12. Heckbert P.S., Hanrahan P. (1984), *Beam Tracing Polygonal Objects*, Proceedings of the 11th annual conference on Computer graphics and interactive techniques, pp. 119–127, New York.
13. Kleiner M., Dalenback B.I., Svensson P. (1993), *Auralization – An Overview*, Journal of Audio Engineering Society, **41**, 11, 861–875.
14. Laine S., Siltanen S., Lokki T., Savioja L. (2009), *Accelerated beam tracing algorithm*, Applied Acoustics (Elsevier), **70**, 1, 172–181.
15. Lewers T. (1993), *A combined beam tracing and radiant exchange computer model of room acoustics*, Applied Acoustics (Elsevier), **38**, 2, 161–178.
16. Maercke D., Maercke D., Martin J. (1993), *The prediction of echograms and impulse responses within the Epidaure software*, Applied Acoustics (Elsevier), **38**, 2, 93–114.

17. Noisternig M., Katz B.F.G, Siltanen S., Savioja L. (2008), *Framework for Real-Time Auralization in Architectural Acoustics*, Acta Acustica united with Acustica, **94**, 1000–1015.

18. Picaut J., Polack J.-D., Simon L. (1997), *A Mathematical Model of Diffuse Sound Field Based on a Diffusion Equation*, Acta Acustica united with Acustica, **83**, 614–621.

19. Pierce A.D. (1981), *Acoustics – An Introduction to its Physical Principles and Applications*, McGraw-Hill.

20. Shah M., Pattanaik S. (2007), *Caustic Mapping: An Image-space Technique for Real-time Caustics*, IEEE Transactions on Visualization and Computer Graphics, **13**, 272–280.

21. Sikora M., Mateljan I., Bogunović N. (2010), *The effect of refraction as a non-linear transformation on beam tracing simulation of sound propagation*, Proceedings of 1st EAA EUROREGIO Congress on Sound and Vibration – Acta Acustica united with Acustica, **96**, Supp. 1, 62.

22. Siltanen S., Lokki T., Kiminki S., Savioja L. (2007), *The room acoustic rendering equation*, Journal of Acoustical Society of America, **95**, 2313–2319, **122**, 3, 1624–1635.

23. Siltanen S., Lokki T., Savioja L. (2009), *Frequency Domain Acoustic Radiance Transfer for Real-Time Auralization*, Acta Acustica united with Acustica, **95**, 106–117.

24. Sutherland I.E., Hodgman G.W. (1974), *Reentrant polygon clipping*, Communications of the ACM, **17**, 1, pp. 32–42.

25. Stephenson U. (1996), *Quantized Pyramidal Beam Tracing – a new algorithm for room acoustics and noise immission prognosis*, Acta Acustica united with Acustica, **82**, 517–525.

26. Tsingos N., Funkhouser T. (2001), *Modeling Acoustics in Virtual Environments Using 1the Uniform Theory of Diffraction*, Proceedings of ACM SIGGRAPH 2001, pp. 545–552, Los Angeles.

27. Vorlander M. (2008), *Auralization*, Springer.

28. Walsh J.P., Dadoun N., Kirkpatrick D.G. (1985), *The geometry of beam tracing*, Proceedings of the first annual symposium on Computational geometry, pp. 55–61, Toronto.

29. Wojcik G.L., Vaughan D.K., Murray V., Mould J. Jr. (1994), *Time-domain Modeling of Composite Arrays for Underground Imaging*, Proceedings of the IEEE Ultrasonics Symposium, pp. 1027–1032, Cannes.

30. Wojcik G.L., Vaughan D.K., Abboud N., Mould J. Jr. (1998), *Finite Element Modeling for Ultrasonic Transducers*, Proceedings of Ultrasonic transducer engineering Conference, pp. 19–42, San Diego.

PAN ARCHIVES OF ACOUSTICS
Vol. **37**, No. 3, pp. 317–322 (2012)

DOI: 10.2478/v10168-012-0040-5

Sound Diffusers with Fabric Covering

Tadeusz KAMISIŃSKI, Krzysztof BRAWATA, Adam PILCH,
Jarosław RUBACHA, Marcin ZASTAWNIK

AGH University of Science and Technology
al. A. Mickiewicza 30, 30-059 Kraków, Poland; e-mail: kamisins@agh.edu.pl

(*received October 11, 2011; accepted June 28, 2012*)

Fabric covering is often used by designers, as it can easily mask acoustic structures that do not match an interior. However, in the case of sound diffusers based on change in the phase of the reflected wave, the use of fabric covering is not without its effect on acoustics. It reduces the effectiveness of these structures and raises acoustic absorption. In the paper, the authors analyzed the acoustical properties of a selected fabric used to cover sound diffusers. Sound absorption and scattering coefficients for a system composed of sound diffusers and a fabric situated at different distances d were measured. The results were compared to the sound absorption predicted on the basis of Kuttruff's and Mechel's theoretical models. Analysis of the results indicates that the fabric has a significant influence on the system's acoustic parameters. It is also observed, that fabric applied directly on a phase grating diffuser, produces higher absorption than when it is at some distance from it.

Keywords: fabric covering, Schroeder diffusers, absorption, scattering.

1. Introduction

In room acoustics, the most important property of the material is the absorption coefficient introduced by Sabine (1922). Despite the many corrections that have been introduced to the reverberation time formula, Sabine's basic equation, which is based only on geometry and the absorption coefficient, is still widely used, not only by non-professionals. However, the Sabine's formula does not always give precise results. Initially, the method of sound absorption coefficient averaging was investigated (Eyring, 1930). How materials are distributed was then accounted for a theoretical model (Fitzroy, 1959). No new acoustic parameter describing the reflection from walls was proposed until 1976 (Kuttruff, 1976), when Kuttruff reckoned with the fact, that reflections from walls are not purely specular, a fact which influences the reverberation time. Three years later, Schroeder (1979) found that diffuse reflections are desirable, especially those from the ceiling in low concert halls. In that paper, Schroeder showed that reflection from a structure will be diffuse, if phase shifts of the waves reflected from small parts of the structure are random. On the basis of the number theory, he proposed a quadratic-residue sequence to shape the depth of the structure. Being easy to apply and giving high diffusion over a wide frequency band, quadratic-residue diffusers (QRD) became very popular.

Nowadays, many interiors of cinemas, television studios, home theatres, and philharmonic halls are equipped with some kind of diffusers. Sometimes they are in harmony with the room's design, while in historical rooms, specialist acoustics structures do not match the interior. In such cases, they are often concealed behind an acoustically transparent fabric, to mask the acoustic structure without changing its properties. However, as might be expected, transparency applies only to a covering used on highly absorptive materials. A different approach is needed in masking structures with low absorption coefficients and special care should be taken especially where QRDs are concerned. This type of diffuser was designed to reflect evenly in every direction as much sound as possible. Fujiwara and Miyajima (1992) were the first to measured the absorption of diffusers which greatly exceeded the expected value. The first attempt to explain this phenomenon was made by Kuttruff (1994). In his calculation Kuttruff assumed a constant sound pressure on the plane of the diffuser. His theoretical model results in a too low absorption. A year later, Mechel (1995) developed a much more complex model and showed

that absorption is caused not only by viscous and thermal losses, but also by the flow of air between adjacent wells of the diffuser. He was also the first to calculate and measure the influence of resistive layers situated on the entrances of the wells on the absorption coefficient. Based on his approach, Wu *et al.* (2000) pointed out the possibility of creating a highly absorptive structure that would combine the QRD and a resistive covering.

The goal of this study is to show the influence of resistive layers on acoustic parameters (absorption and scattering coefficient) of diffusers. Ways of minimizing the additional absorption from a textile covering are also investigated.

2. Prediction of sound absorption

2.1. Absorption of a resistive layer above a rigid plate

Let us consider the absorption of a resistive layer above a rigid plate. The equivalent interaction impedance of a flexible single screen with cavity backing z_e can be expressed as a parallel combination of the interaction impedance z and the structural impedance z_s (Ingard, 1994):

$$z_e = zz_s/(z+z_s). \tag{1}$$

For a limp sheet, there is $z_s = -i\omega m$, where m is the mass per unit area of the sheet. If $z = r + ix$, then

$$z_e = \frac{r(\omega m)^2}{r^2+(\omega m - x)^2} - i\omega m \frac{r^2 - x(\omega m - x)}{r^2+(\omega m - x)^2}. \tag{2}$$

According to Wu's assumption (Wu, 2000), textile cover is purely resistive, so the reactance part of z is $x = 0$. For the textile cover used in the measurements, $m = 0.15$ kg/m^2.

The input impedance for a resistive screen over an air layer of thickness d is expressed by

$$Z(\phi) = z_e - \frac{i\cot(k_z d)}{\cos(\phi)}, \tag{3}$$

where $k_z = k_0\cos(\phi)$ is the normal component of the wave vector $\mathbf{k}_0$ for angle of incidence ϕ. With the input impedance $Z(\phi)$ known, the absorption coefficient $\alpha(\phi)$ is expressed according to (Ingard, 1994) by

$$\alpha(\phi) = \frac{4\mathrm{Re}(Z)\cos\phi}{(1+\mathrm{Re}(Z)\cos\phi)^2 + (\mathrm{Im}(Z)\cos\phi)^2}. \tag{4}$$

The impedance of textile cover located at different distances d from the rigid plate was measured using an impedance tube. By comparing it with the absorption coefficient for normal incidence $\alpha(0)$ calculated according to (4), the resistance of textile cover was found to be equal $r\rho_0 c = 40$ rayl, where $\rho_0 c$ is the impedance of air.

In order to compare the absorption coefficient of a resistive screen situated over a rigid plane measured in diffuse field and calculated using (4), integration over hemisphere should be done

$$\alpha_{\mathrm{diff}} = 2\int_0^{\pi/2} \alpha(\phi)\cos\phi\sin\phi\ \mathrm{d}\phi. \tag{5}$$

2.2. Absorption of quadratic residue diffusers

In both Kuttruff's and Mechel's models of sound absorption, the calculation of admittance of a single well is carried out in the same way. In Kuttruff's approach, the absorption of a QRD is calculated by averaging the admittance of each well, while in the Mechel model, mutual interaction between wells is taken into account. The geometry of the analyzed system, composed of diffuser and textile cover, is presented in Fig. 1.

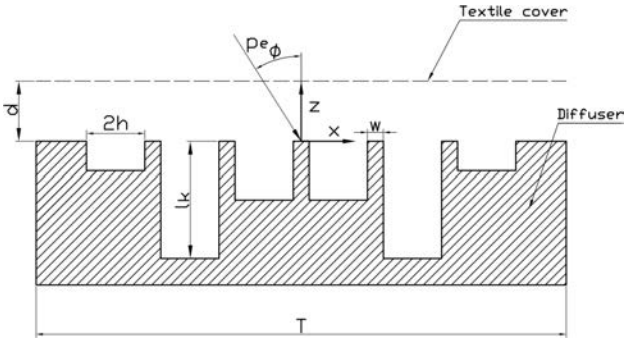

Fig. 1. Geometry of the system composed of a quadratic residue diffuser and textile cover at the distance d.

Normalized input admittance of one well is equal to

$$G(x_k) = \frac{\tanh(\Gamma_w k_0 l_k)}{Z_w}, \tag{6}$$

where $k_0 l_k$ is the Helmholtz number. For a QRD it is calculated according to (Mechel, 1995)

$$k_0 l_k = \frac{f}{f_0}\frac{\pi}{N}\mathrm{mod}(k^2, N); \quad k = 0, 1, \ldots, N-1. \tag{7}$$

Propagation constant Γ_w and wave impedance Z_w in wells (Mechel, 2008) are:

$$\Gamma_w = k_0 j\sqrt{\frac{1+(\kappa-1)\dfrac{\tan(k_{\alpha 0}h)}{k_{\alpha 0}h}}{1-\dfrac{\tan(k_\nu h)}{k_\nu h}}}, \tag{8}$$

$$Z_w = \frac{Z_0}{\sqrt{\left[1+(\kappa-1)\dfrac{\tan(k_{\alpha 0}h)}{k_{\alpha 0}h}\right]\left[1-\dfrac{\tan(k_\nu h)}{k_\nu h}\right]}}, \tag{9}$$

where

$$k_0 = \frac{\omega}{c}, \qquad k_\nu^2 = -j\frac{\omega}{\nu}, \qquad k_{Pr}^2 = \kappa \mathrm{Pr} k_\nu^2, \tag{10}$$

where $\nu = 15 \cdot 10^{-6}$ m^2/s is the kinematic viscosity of air, $\kappa = 1.401$ is the adiabatic exponent and Pr = 0.6977 is the Prandtl number.

With $T = N(2h+w)$, being the width of one period, its average admittance is given by

$$\langle G \rangle = \frac{2h}{T} \sum_{k=0}^{N-1} G(x_k). \tag{11}$$

With the normalized impedance of $Z = 1/\langle G \rangle$, the absorption coefficient can be calculated according to (4).

In Mechel's model (Mechel, 1995), the sound field in front of the diffuser is decomposed into the incident plane wave $p_e(x,y)$ and the scattered field $p_s(x,y)$, which itself is made up of plane waves and higher spatial harmonics:

$$\begin{aligned} p(x,z) &= p_e(x,z) + p_s(x,z), \\ p_e(x,z) &= P_e \exp[j(-xk_x + zk_z)], \\ p_s(x,z) &= \sum_{n=-\infty}^{+\infty} A_n \exp(-\gamma_n z) \exp(-j\beta_n x), \end{aligned} \tag{12}$$

where the wave numbers are

$$\begin{aligned} k_x &= k_0 \sin\phi_e = \beta_0, \\ k_z &= k_0 \cos\phi_e, \\ \beta_n &= \beta_0 + n\frac{2\pi}{T}, \\ \gamma_n &= k_0 \sqrt{(\sin\phi_e + n\lambda_0/T)^2 - 1}. \end{aligned} \tag{13}$$

The wells' admittance is first transformed by Fourier analysis

$$g_n = \frac{1}{T} \int_0^T G(x) \exp\left(jn\frac{2\pi}{T}\right) \mathrm{d}x \tag{14}$$

and the amplitudes A_n of the spatial harmonics are then calculated

$$\sum_{n=-N}^{+N} A_n \left[g_{-m-n} - j\delta_{m,-n}\frac{\gamma_n}{k_0} \right] = P_e(\delta_{m,0}\cos\phi_e - g_{-m}), \qquad m = -N, \ldots, +N, \tag{15}$$

where $\delta_{m,n}$ is the Kronecker symbol.

The absorption coefficient including higher spatial harmonics is

$$\alpha(\phi_e) = 1 - \left|\frac{A_0}{P_e}\right|^2 - \frac{1}{\cos\phi_e} \sum_{n_s \neq 0} \left|\frac{A_{ns}}{P_e}\right|^2 \cdot \sqrt{1 - (\sin\phi_e + n_s\lambda_0/T)^2}, \tag{16}$$

where $P_e = 1$ is the amplitude of the incident wave and n_s, as indices of spatial harmonics, are determined by the condition

$$-\frac{T}{\lambda_0}(1 + \sin\phi_e) \leq n_s \leq \frac{T}{\lambda_0}(1 - \sin\phi_e). \tag{17}$$

Only theoretical models for calculating the absorption coefficient are presented – there is no reliable model to calculate the scattering coefficient. The diffusion coefficient obtained in free field can be accurately predicted, because its definition and the method of measurement are in agreement with the physical phenomenon. On the other hand, measuring the scattering coefficient involves determining the difference between the absorption of a rotating and a stationary sample. Physically, absorption is the same, but due to the integrated impulse response method used in the measurement, the results are different because of non-specular reflection from the sample.

3. Measurement system

The measurements were conducted in Laboratory of Technical Acoustics' reverberation chamber at the Department of Mechanics and Vibroacoustics, AGH in Krakow. The chamber volume is $V = 180.4$ m^3, the total area of the walls is $S = 193.7$ m^2.

To measure the sound absorption coefficient, two omni-directional sound sources were used, powered by the CREST CPX 2600 amplifier, which received the input signal from an NI PXI-4461 card output. Signals were recorded using six GRAS 46AQ microphones connected to an NI PXIe-4496 card. An application was developed in the LabVIEW environment to generate the measurement signal, record the response of the room and determine the impulse responses. A wideband modulated test signal (sine sweep) was used. Temperature and humidity were measured using an LB-701H thermohygrometer controlled directly by the LabVIEW module.

When measuring the scattering coefficient in accordance with the ISO 17491-1 standard, a sample with a diameter of 2.75 m was positioned on a turntable placed on the floor of the reverberation chamber (Fig. 2). The turntable was operated by an NI PXIe-

Fig. 2. The QRD covered with fabric used in the scattering coefficient measurement.

8180 controller. The test signal was generated and the response was recorded using B&K Dirac 4.1 software. A Waveterminal U2A card was used as the I/O interface. An amplifier and an omni-directional sound source were used in the measurements as described above. As a test signal, an MLS was used with a 48000 Hz sampling frequency and a sequence composed of $2^{19}-1$ samples. In both cases the chamber was equipped with five fixed diffusers, selected in accordance with Annex A to ISO 354. The positions of the microphones and sound sources remained unchanged throughout the measurements. The impulse responses of the chamber were determined using signals with a length of 10.9 seconds. On the basis of preliminary measurements, the possibility of using a shorter signal than the maximum length of the reverberation time for some frequencies was verified. Doing so would shorten the measurements during which the ambient conditions should have remained unchanged.

As a diffuser, a one-dimensional pseudo-stochastic periodic surface structure based on the first number $N = 7$ was used with a well width of $2h = 22$ mm, $w = 6$ mm and a maximum depth of $l_{\max} = 44$ mm. A circular sample with a diameter of 2.75 m contained 13.5 periods of sequences. The diffuser was covered with a thin 100% polyester fabric commonly used to cover diffusers, with a surface weight of $m = 0.15$ kg/m^2. The fabric was stretched on a steel rim with a diameter equal to that of the diffuser. Side surfaces were screened by the cover fitted to the total height of the sample.

4. Results

4.1. Sound absorption coefficient

The sound absorption coefficient was measured in accordance with the ISO 354 standard for the following configurations:

a) fabric + sound reflecting surface at a distance of 0, 5, 10 and 14 cm

b) fabric + sound diffuser at a distance of 0, 5 and 10 cm

The results for a) are shown in Fig. 3. In order to improve the readability of the graph, sound absorption values for selected distances d are presented. The results show, that the maximum value of absorption does not change for different distances d, but only shifts along the frequency axis. Good agreement between the theoretical model and measurements was obtained. For all distances, absorption at low frequency is higher than predicted. The maxima occur at similar frequencies, but in the case of measurements, the resonance has smaller $Q = f_r/\Delta f$, where f_r is the resonant frequency, and Δf is the bandwidth. For antiresonance, where the width of the air layer is equal to the half-

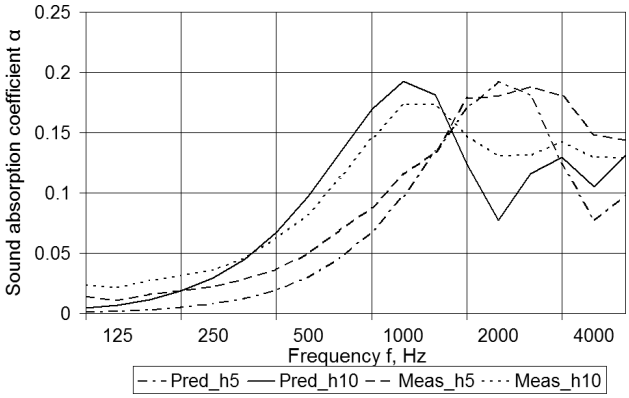

Fig. 3. The sound absorption coefficient for the fabric stretched over the reflecting surface. The number in the legend indicates the distance (in cm) between the fabric and the surface, Pred – prediction, Meas – measurement.

length of the incident wave, it is almost impossible to observe a minimum in the measured curve.

The absorption coefficient of the diffuser with and without fabric stretched over it is shown in Fig. 4. The measurements indicate significant absorption in the 100–1000 Hz range, while prediction based on both models provides values near 0. For higher frequencies both Mechel's and Kuttruff's models predict for the diffuser with fabric covering an increase in absorption for the frequency range (1600–2500 Hz), which is consistent with the measurements. The calculated values of the sound absorption coefficient α are underestimated when calculated according to the Kuttruff model. In the case of the Mechel model, the maximal predicted value is larger than that measured, but the peak has a much bigger Q-factor.

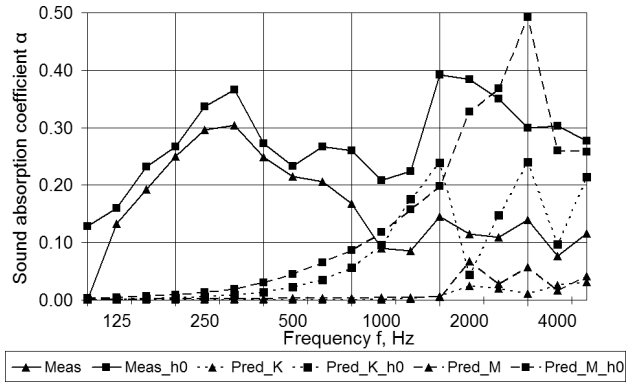

Fig. 4. The sound absorption coefficient for the QRD with and without fabric cover. Prediction based on Kuttruff's and Mechel's model is included. The letter K stands for the Kuttruff model and M for the Mechel model, the line without given height, represents absorption of the diffuser without a fabric covering.

Note the significant increase over the entire frequency range in the absorption of the diffuser with the fabric as compared to that without it (Fig. 5). When

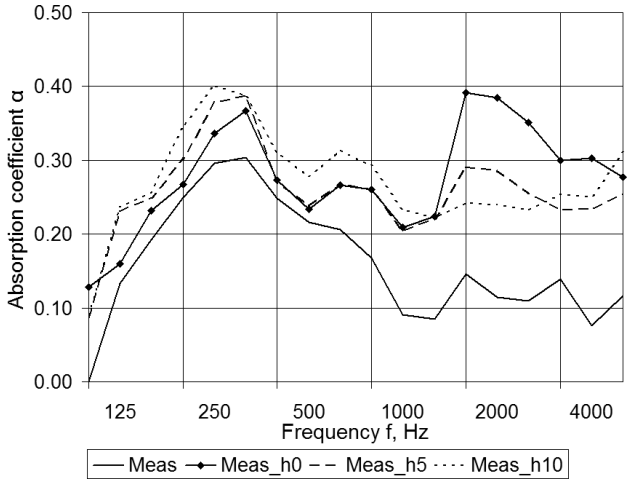

Fig. 5. The sound absorption coefficient for the fabric stretched over the QRD. The number in the legend indicates the distance (in cm) between the fabric and the diffuser. The line without a given height represents the absorption of a diffuser without a fabric covering.

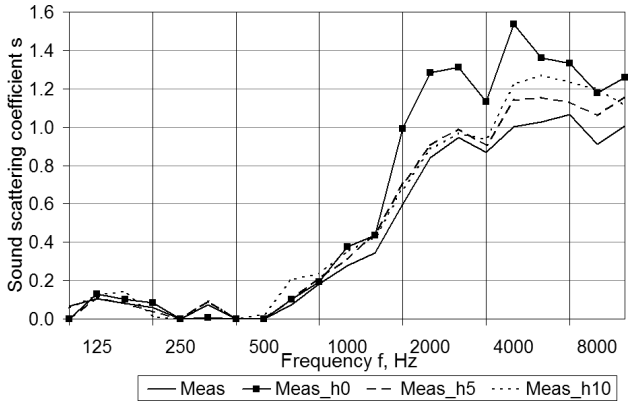

Fig. 6. The sound scattering coefficient for the fabric stretched over the QRD. The number in the legend indicates the distance (in cm) between the fabric and the diffuser. The line without a given height represents the scattering of the diffuser without fabric covering.

the fabric is placed directly on the diffuser, a noteworthy increase in absorption occurs as compared to distances $d = 5$ cm and $d = 10$ cm, mainly in the 1600–2500 Hz frequency range, where the structure scatters sound the most effectively. For $f = 1600$ Hz the phase shifts between adjacent wells are an integer multiple of $\lambda_0/4 = c/(4f)$, which causes significant airflow between them and gives the highest absorption when resistive material is put on the entrance to the wells.

Among the measured distances between the fabric and diffuser, the smallest absorption occurs at $d = 5$ cm. At $d = 10$ cm, the absorption for frequencies 1600–2500 Hz is the lowest (the fabric cover does not influence the near field of the diffuser), but there is an increase in absorption for the 400–1000 Hz frequency range.

4.2. Sound scattering coefficient

Measurements were conducted to determine the effect of fabric on sound scattering by the fabric-covered diffuser (the results are shown in Fig. 6). ISO standard 17497-1 recommends, that the measurement of the scattering coefficient should be restricted to structures with the sound absorption coefficient α below 0.5. Note that systems composed of the diffuser and the fabric show a greater than or close to 0.5 absorption coefficients in the 250–400 Hz range, and that the authors are aware that the results are characterized by a greater error.

The results show that the fabric has a small effect on sound scattering at low and medium frequencies. In contrast, at higher frequencies the scattering coefficient increases, especially when the fabric is placed directly on the diffuser. In the characteristics shown in Fig. 6, the values of the scattering coefficient exceed 1 for some frequencies. This is acceptable and might be caused by diffraction at the sample edges. The difference in the scattering coefficient for the diffuser with fabric placed directly on its surface may be due to several concurrent factors. The fabric causes additional scattering of reflected sound and interacts with the wells of the diffuser. The error of the measurement method due to the sample's excessive sound absorption in this frequency range may also be significant.

5. Conclusion

The paper presents results of studies on the absorption and scattering of a system composed of a fabric covering placed at some distance from diffuser done in remodeling of interiors to improve room acoustics. It was shown that when the reflecting surface is masked, the sound absorption coefficient α is strongly dependent on the properties of the covering fabric (especially its resistance) and the thickness of the air layer between the fabric and reflective surface. While the properties of the fabric determine the maximum value of sound absorption, the air layer affects the frequency, at which the maximum occurs. For QRDs, the most significant change in absorption occurred when the fabric was placed directly on the diffuser's surface. Particularly large differences were observed at frequencies above 1600 Hz. As in the case of the reflecting surface, absorption depends on the resistance of the fabric, but the thickness of the air layer influences not only the position of the maximum, but also its value, especially where the covering is placed close to the diffuser. The results of the measurements showed a significant increase in the sound scattering coefficient for frequencies above 1250 Hz, with much higher results when the fabric was placed directly on the surface of the diffuser surface. This may be attributable to an error in the

method, which requires structures with a sound absorption coefficient $\alpha \leq 0.5$. No significant differences were observed at lower frequencies.

The results lead to the conclusion that stretching the fabric directly on the surface of the diffuser, significantly affects its acoustic performance, mainly sound absorption. This conclusion is of particular importance for the interior equipment of music halls (Kamisiński, 2010), where sound diffusers are important elements and where fabric covering may adversely reduce the acoustic energy of the first reflection. When the reflective plane is covered, the lowest absorption is obtained when fabric is laid directly on the plane. For QRDs, the lowest absorption was observed for air layer of thickness $d = 5$ cm. To further reduce of the absorption coefficient of diffusers, stiffening the construction and reducing the height/width ratio should be considered (Pilch, Kamisiński, 2011). It can be concluded that even a very light fabric covering can affect the absorption and scattering characteristics of sound diffusers and caution is advised in using fabric covering intuitively.

Acknowledgment

This study was conducted as a part of the development project No. N R03 0036 06 "A measurement system and procedures for studying sound diffusers" (2009–2012).

References

1. Eyring C.F. (1930), *Reverberation time in dead rooms*, J. Acoust. Soc. Am., **1**, 217–241.
2. Fitzroy D. (1959), *Reverberation formulae which seems to be more accurate with non-uniform distribution of absorption*, J. Acoust. Soc. Am., **31**, 893–897.
3. Fujiwara K., Miyajima T. (1992), *Absorption characteristics of a practically constructed Schroeder diffuser of quadratic-residue type*, Appl. Acoust., **35**, 149–152.
4. Ingard U. (1994), *Notes on sound absorption technology*, Noise Control Foundation, New York.
5. Kamisiński T. (2010), *Acoustic Simulation and Experimental Studies of Theaters and Concert Halls*, Acta Physica Polonica A, **118**, 78–82.
6. Kuttruff H. (1994), *Sound absorption by pseudostochastic diffusers Schroeder diffusers*, Appl. Acoust., **42**, 215–231.
7. Kuttruff H. (1976), *Nachhall und effektive Absorption in Räumen mit diffuser Wandreflexion*, Acustica, **35**, 3, 141–153.
8. Mechel F.P. (2008), *Formulas of Acoustics*, Springer, Berlin.
9. Mechel F.P. (1995), *The wide-angle diffuser-A wide-angle absorber?*, Acustica, **81**, 379–401.
10. Pilch A., Kamisiński T. (2011), *The Effect of Geometrical and Material Modification of Sound Diffusers on Their Acoustic Parameters*, Archives of Acoustics, **36**, 4, 955–966.
11. Sabine W.C. (1922), *Collected papers on acoustics*, Harvard University Press, London.
12. Schroeder M. (1979), *Binaural dissimilarity and optimum ceilings for concert halls: More lateral sound diffusion*, J. Acoust. Soc. Am., **65**, 4, 958–963.
13. Wu T., Cox T.J., Lam Y.W. (2000), *From a profiled diffuser to an optimized absorber*, J. Acoust. Soc. Am., **108**, 2, 643–650.

PAN ARCHIVES OF ACOUSTICS
Vol. **37**, No. 3, pp. 323–329 (2012)

DOI: 10.2478/v10168-012-0041-4

Multi-Channel System for Sound Creation in Open Areas

Andrzej GOŁAŚ, Katarzyna SUDER-DĘBSKA

AGH University of Science and Technology
al. A. Mickiewicza 30, 30-059 Kraków, Poland; e-mail: suder@agh.edu.pl

(*received March 31, 2011; accepted July 2, 2012*)

There are typically two systems in use for sound reinforcement in open areas: the central, "wall of sound" system with speakers localized at the sides of the stage, and the zone system, in which additional speakers are introduced to obtain a uniform sound pressure level throughout the area of listening. In the past two decades the line array systems gained great popularity. The main purpose of their use is to obtain a uniformly distributed sound level throughout the listening area in order to achieve good speech intelligibility. The present paper aims to present an alternative and original method of sound reinforcement in open areas which is in contrast to the above solutions. This new method allows achieving a uniformly distributed sound pressure and good speech intelligibility in the area of interest, and also allows to gain spatial sound impression that accompanies sound reproduction in concert halls. Another advantage of the proposed system is the reduction of the sound level outside the area of interest, i.e. reduction of the noise level outside the area of listening.

Keywords: sound creation system, open area, spatial impression, noise, geometrical method, inverse image source method.

1. Introduction

During the sound reinforcement in open areas with so called "wall of sound", there are two ways to create the acoustic field: in small areas, by using high power loudspeaker sets localized centrally (on the stage) and, for large areas, by using the zone sound system (Hojan, 2003; Ishizawa *et al.*, 1998; Toole, 2008]. An alternative method is the use of line array systems which, compared to the "wall of sound", provide a more uniform distribution of the acoustic field across the entire area of listening (Ureda, 2001). The main purpose of their use is to obtain a uniformly distributed sound level throughout the listening area in order to achieve good speech intelligibility but other parameters describing the properties of the acoustic field in the object are ignored.

In the case of listening in concert halls and opera houses, many authors (Ando, 1985; Beranek, 1996; Bradley, 1991; Bradley *et al.*, 2000; Hidaka *et al.*, 2000; Kulowski, 2007; Kuttruff, 2009; Long, 2006; Marshall, Barron, 2001) draw attention to a number of parameters, such as the "Clarity" group parameters, the parameters relating to speech intelligibility on the analysed object, or the "Lateral Sound" group parameters, very important when listening to music. Unfortunately, in the case of outdoor concerts, because of the dominance of the direct sound from the sound sources, particularly the spatial sound impressions are considerably limited (Meyer, 2009). It is this factor that has led the authors to propose a sound system for open areas that would allow obtaining simultaneously a uniform sound reinforcement in the area of interest, good speech intelligibility, and spatial sound impression similar to that achieved in concert halls.

It should also be noted that in the case of sound reinforcement in open areas, a high noise level is emitted outside the area of listening. It is usually very inconvenient to the outsiders. The proposed system for sound reinforcement in open areas allows a considerable reduce of that noise.

Formulating the objective of the research

The objectives of the present paper were (Fig. 1):

1) to build a multi-channel sound creation system in open area;
2) to reduce noise level emitted outside the open area of sound reinforcement.

The object of interest are squares and market places in cities (limited slightly by thes urrounding buildings)

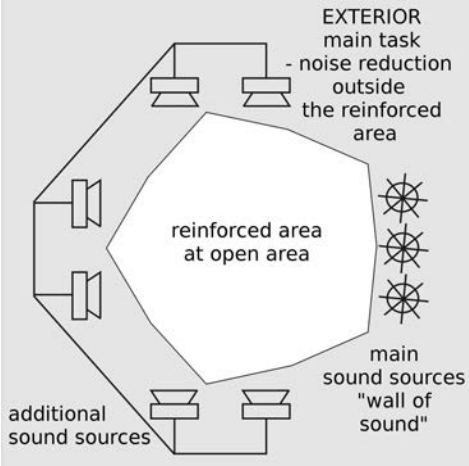

Fig. 1. Schematic diagram of a multi-channel sound creation system in an open area.

in which various artistic events are organised, concert shells in parks, etc., further referred to as open areas. The idea behind the concept was to create, in an open area, the acoustic field with properties similar to the ones of the acoustic field in a good concert hall. The created acoustic field was supposed to meet the following quality criteria (Mechel, 2008):

1. SPL (Sound Pressure Level) [dB];
2. D Definition [%] – parameter characterizing speech intelligibility;
3. C_{50} Clarity [dB] – parameter characterizing speech intelligibility;
4. C_{80} Clarity [dB] – parameter characterizing music reproduction clarity;
5. LF Lateral Energy Fraction [%] – parameter characterizing spatial sound impression;
6. LFC Lateral Energy Fraction Coefficient [%] – parameter characterizing spatial sound impression;
7. STI Speech Transmission Index – parameter characterizing speech intelligibility;
8. AL_{Cons} Articulation Loss of Consonats [%] – parameter characterizing speech intelligibility, referring to the loss of consonant intelligibility.

The above-mentioned quality criteria on the analysed object should have the following values (based on e.g. (Kulowski, 2007):

1. SPL – assuming that for the open area, the background noise level may reach ca. 50 [dB], whereas the sound pressure level in the area of listening should be at least 75 [dB], and distribution of this parameter should be even enough for the difference between the highest and lowest SPL value not exceed 6 [dB];
2. Definition – above 70 [%], C_{50} – $\geq +3$ [dB], STI – at least 0.6, AL_{Cons} – maximum 10 [%], for the speech reception to be at least good;
3. C_{80} from the range -5 [dB] $\div +9$ [dB], or slightly above $+9$ [dB], for the clarity of music to be at least of a medium quality;
4. LF and LFC – in the range 10 [%] $\div$ 25 [%].

Sound system description

To generate an acoustic field with the properties described above, a multi-channel sound system was utilised. This system consists of the main and additional sound sources. The sound emitted by instruments without any amplification, as well as loudspeaker sets on the stage as the main and central sound sources can be used. Additional sound sources are extra loudspeakers which simulate the sound reflected from walls, as it occurs indoors.

The system should ensure in the examined area the sound quality equivalent to that achieved in closed rooms with good acoustic properties. It should ensure values of the sound parameters equally good to ones in good concert halls, and minimise the noise outside the area of listening. The image source method was used in an inverse order (Gołaś, Suder–Dębska, 2010) to synthesise the structure of the sound sources distribution in the open area, further referred to as the inverse image source method. In general, the method is to assume the desired properties of the acoustic field on the object, and the distribution and parameters of the sound sources ensuring the effect which is as close to the expectation as possible.

Inverse Image Source Method

The image source method is one of the geometrical methods which, for a specific area with determined geometry and acoustic parameters, and for a predefined localization of the sound sources, allows to determine the parameters of the acoustic field. The idea of the Inverse Image Source Method is presented in Fig. 2. The Inverse Image Source Method involves an innovative use of the conventional image source method to solve the inverse problem. It means that, on the examined object (open area), the type of the desired

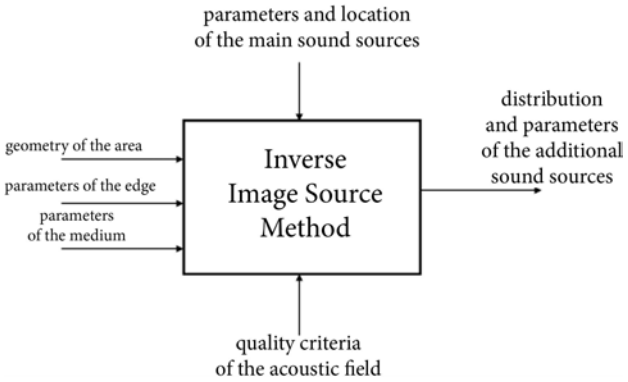

Fig. 2. Idea of the Inverse Image Source Method.

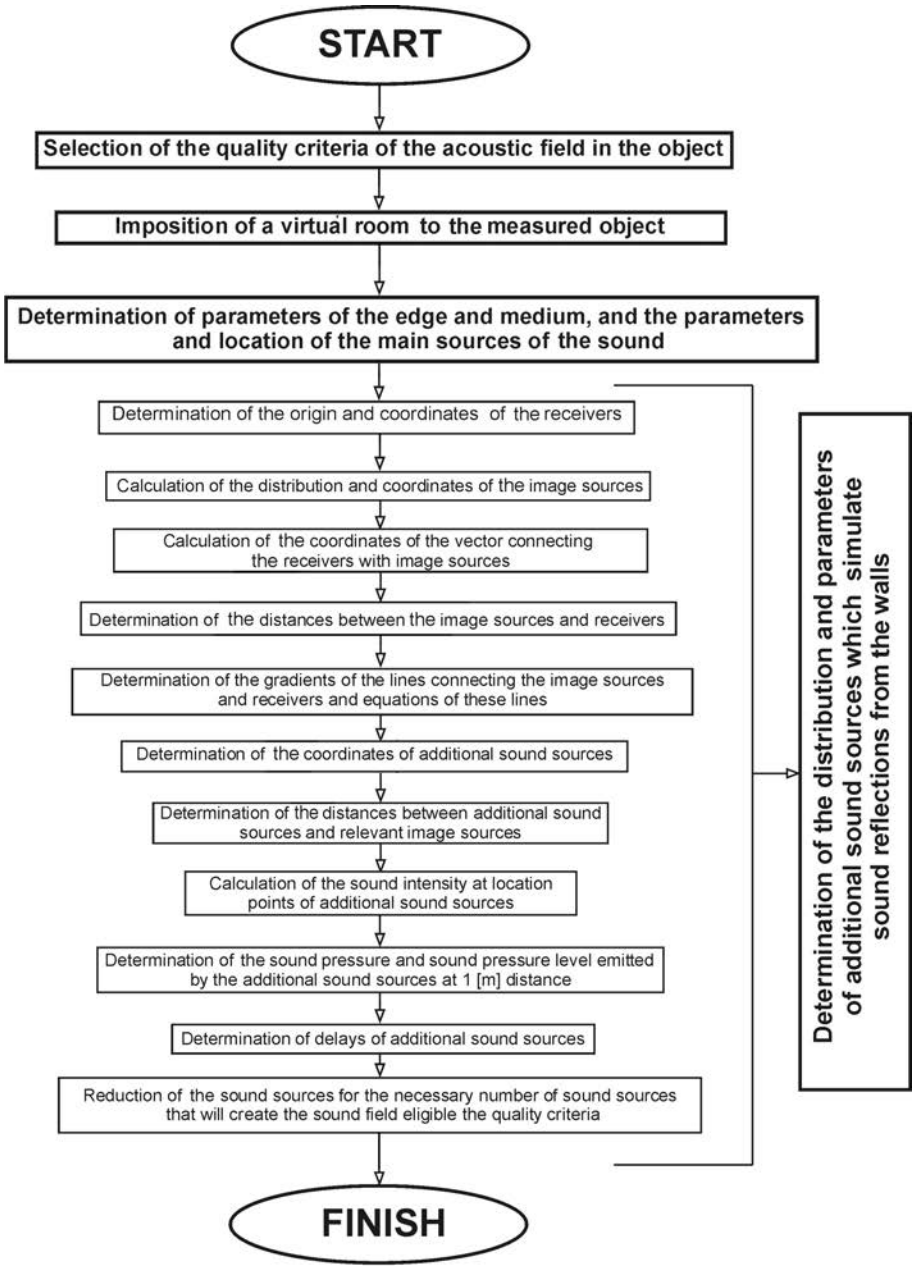

Fig. 3. Algorithm of the Inverse Image Source Method.

acoustic field, its acoustic parameters, is initially assumed, and then, based on the inverse image source method, the distribution of additional sound sources which surround the reinforced area, their power, and delays are determined in such a way that the acoustic field with the assumed properties is created. These additional sound sources imitate sound reflections from the wall. The algorithm of the inverse image source method (Fig. 3) can be briefly described as follows:

1) determining the desired values of acoustic parameters;
2) determining acoustic parameter distribution on the examined object for a conventional sound system type;
3) determining, based on the inverse image source method, the distribution and parameters of additional sound sources creating the acoustic field on the object with the properties as close to the predefined quality criteria as possible.

2. Analysing the central system

Numerical simulations of various types of the central sound system were performed based on the EASE software.

An open area dimensioned 24 [m] × 32 [m] was assumed as the analysed object. For the examined area, asphalt surface, air temperature 20 [°C], and humidity

60 [%] were assumed. Simulation tests were performed for the conventional central system with loudspeakers localized at the sides of the stage. Figure 4 shows the model of the analysed object.

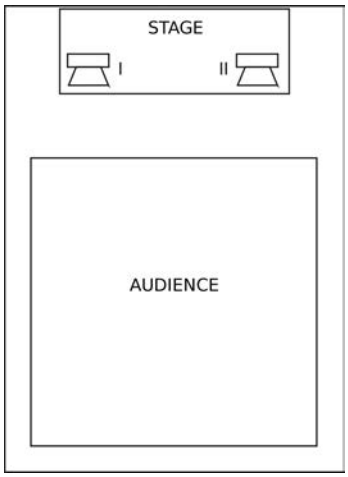

Fig. 4. Numerical model of the open area for the central sound system

The conventional central sound system was analysed in 15 configurations: 12 times for various types of loudspeakers placed individually at the sides of the stage, and 3 times for 4 loudspeakers of various types placed at the sides of the stage, with the speakers operating at the sound power of the level which can generate the sound pressure level at the level about 100 [dB] ÷ 115 [dB] in all the cases (there are mean SPL values obtained during concerts and events). Simulation results, such as mean values of the acoustic parameters are given in Table 1.

Figure 5 shows the distribution of the SPL parameter for two Community WET315–94 speaker sets localized at the sides of the stage. Figure 6 shows the distribution of the LF parameter for the system as above.

Fig. 5. SPL parameter distribution for the Community central sound system.

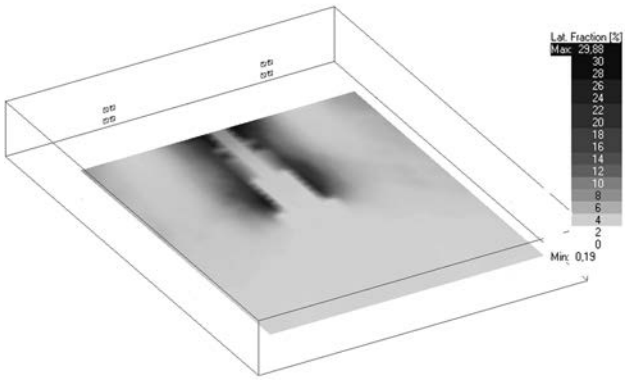

Fig. 6. LF parameter distribution for the Community central sound system.

Table 1. Simulation results for the reinforced area.

System	SPL [dB]	Definition [%]	C_{50} [dB]	C_{80} [dB]	LF [%]	LFC [%]	AL_{Cons} [%]	STI
2 x EAW KF750F	115.4	99.9	40.4	50.1	2.3	3.2	1.0	0.99
2 x Community WET315–94	98.8	99.9	40.9	51.9	2.9	4.1	1.0	0.99
2 x Dynacord VariLine VL262	98.6	99.9	40.2	51.9	5.6	8.0	1.0	0.98
2 x HK Audio VT115X	100.6	99.9	40.4	52.6	3.8	5.5	1.0	0.99
2 x JBL PRO AM4215/64P	103.0	99.9	40.9	56.8	3.5	5.1	1.0	0.99
2 x MERIDIAN DSP5500	94.9	99.9	40.4	51.9	7.7	10.8	1.0	0.98
2 x Meyer Sound UPA-2P	111.2	99.9	40.2	53.3	4.2	5.8	1.0	0.99
2 x Peavey IMP652S	94.4	99.9	40.6	47.0	7.1	10.0	1.0	0.98
2 x Proel NEXT15HP	104.9	99.9	40.9	50.2	4.1	5.9	1.0	0.99
2 x Renkus – Heinz STX4–94	109.4	99.9	40.6	52.5	4.4	6.5	1.0	0.99
2 x Tannoy T300	105.3	99.9	40.7	54.7	4.4	6.4	1.0	0.99
2 x Yamaha F15	99.0	99.9	40.5	54.2	4.1	6.0	1.0	0.98
8 x Community WET315-94	104.8	99.9	40.0	56.0	3.2	4.6	1.0	0.99
8 x JBL PRO AM4215/64P	108.9	99.9	39.5	51.5	3.8	5.7	1.0	0.99
8 x Renkus – Heinz STX4–94	115.3	99.9	39.4	50.9	4.8	7.2	1.0	0.99

According to the simulation results, in all configuration cases the speech intelligibility is excellent, which is not surprising with the direct sound from the main sources at the sides of the stage dominating on the object. Yet, the clarity parameter in music perception is exceeded (high C_{80} values). Spatial impressions are very poor as well, as indicated by the LF and LFC values of the order of a few percent. The difference is noticeable only in the case of the SPL parameters, it is, however, dependent on the parameters of individual loudspeakers. Consequently, from the analysed configurations, the highest SPL values can be achieved using EAW loudspeakers, and the lowest from Peavey loudspeakers.

3. Multi-channel sound creation system in the open area

Numerical simulations of a multi-channel sound creation system were performed based on the EASE software.

An open area dimensioned 24 [m]×32 [m] was assumed as the analysed object. For the examined area, asphalt surface, air temperature 20 [°C], and humidity 60 [%] were assumed. So, it was an object identical to that analysed for the central sound systems. The difference is that the new sound system was used in the case of the multi-channel sound creation system, composed of the main sources on the stage and additional, delayed, sources of sound surrounding the auditorium, and their sound power levels reduced adequately in relation to the sound power levels of the main sound sources. The main sound sources are two loudspeakers placed at the sides of the stage, with 102 [dB] sound power level each, and the parameters of the additional sound sources are given in Table 2. A schematic distribution of the sound sources is given in Fig. 7, where I and II are the main sound sources. The multi-channel sound creation system described was built based on the inverse image source method.

Table 2. Additional sound sources parameters which simulate the sound reflected from the walls.

source number	coordinates [m]	sound power level [dB]	delay [ms]
1	(32.00; 5.20; 1.55)	84.5	88
2	(32.00; 9.05; 1.55)	83.5	104
3	(32.00; 14.95; 1.55)	83.5	104
4	(32.00; 18.80; 1.55)	84.5	88
5	(9.05; 0.00; 1.55)	91.3	40
6	(13.05; 0.00; 1.65)	82.5	110
7	(17.00; 0.00; 1.55)	88.5	55
8	(21.10; 0.00; 1.55)	82.0	118
9	(23.00; 0.00; 1.50)	86.5	70
10	(9.05; 24.00; 1.55)	91.3	40
11	(13.05; 24.00; 1.65)	82.5	110
12	(17.00; 24.00; 1.55)	88.5	55
13	(21.10; 24.00; 1.55)	82.0	118
14	(23.00; 24.00; 1.5)	86.5	70

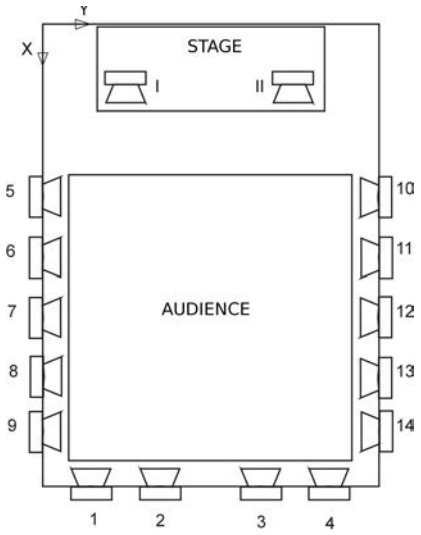

Fig. 7. Schematic diagram of the sound sources distribution for the multi-channel system for sound creation in open areas (based on the Inverse Image Source Method).

For the object described above in the EASE 4.3 software, the acoustic field was simulated using geometrical methods with taking into account the interference between individual loudspeakers ("All source contributions are added first in a complex manner and then the resulting complex sum squared. This retains all the phase effects such as cancellations and additions" (EASE, 2009)).

Mean values of the acoustic parameters described in the introduction obtained in the area of interest with the proposed multi-channel sound creation system are given in Table 3.

Table 3. Mean values of the acoustic parameters achieved in the reinforced area with the multi-channel sound creation system (with Visaton BG17 speakers).

system	SPL [dB]	D [%]	C_{50} [dB]	C_{80} [dB]	LF [%]	LFC [%]	AL_{Cons} [%]	STI
multi-channel sound creation system	76.9	88.3	10.5	15.9	13.1	17.8	1.9	0.83

Figure 8 and Fig. 9 present, respectively, the distribution of SPL and LF parameters in the reinforced area for the multi-channel system for sound creation in open areas.

According to the performed simulations, the sound pressure level in the area of interest is relatively uniform – in almost 90 [%] of the area, the SPL differences are below 6 [dB], speech intelligibility is at a very good/excellent level, as indicated by the values of Def-

Fig. 8. Distribution of the SPL parameter in the reinforced area for the multi-channel system for sound creation in open areas.

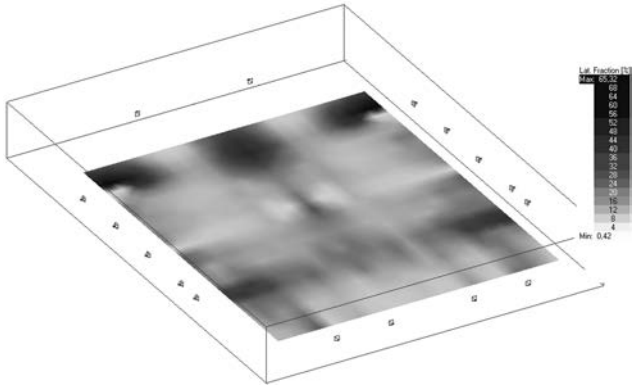

Fig. 9. Distribution of the LF parameter in the reinforced area for the multi-channel system for sound creation in open areas.

inition – over 85 [%], C_{50} – over 10 [dB], STI – over 0.8, AL_{Cons} – less than 2 [%]. Clarity in music perception is also at a satisfactory level, as indicated by the C_{80} parameter, and much better than that in the case of the central sound system. The proposed solution allowed to achieve spatial impression as in rooms, which is indicated by the LF and LFC values, where over 80 [%] of the area exhibits values of the desired range.

4. Noise outside the reinforced area

As already mentioned, in the case of concerts taking place in market places, squares etc., the problem of sound emitted outside the reinforced area emerges. Particularly, in the case of events lasting several days, the noise may be very strenuous to persons staying nearby. Therefore, according to the authors, it is essential to reinforce the sound in open areas in such a manner so that the sound emitted outside was as quiet as possible. Therefore, the area dimensioned 84 [m] × 92 [m] in the centre of which the open area of interest is located (the sound level was analysed in the area surrounding the object, in the radius exceeding 40 metres) was also analysed. The analysis was performed for two sound reinforcement configurations, the central sound system for EAW KF750F loudspeakers, due to the fact that they emitted the highest noise level within the reinforced area, and for Peavey IMP652S loudspeakers, since they emitted the lowest noise level, and the third configuration was the proposed multi-channel system for sound creation in open areas. Table 4 presents the simulation results.

Table 4. Differences between the mean values of SPL parameter inside and outside the reinforced area for the three analysed configurations of sound system.

system	ΔSPL [dB]
2 x EAW KF750F	11
2 x Peavey IMP652S	10
multi-channel sound creation system	14

Figure 10 presents the distribution of the SPL parameter outside the reinforced area for the multi-channel system for sound creation in open areas.

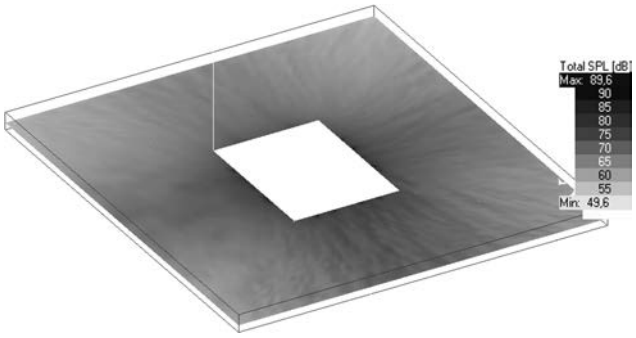

Fig. 10. Distribution of the SPL parameter outside the reinforced area for the multi-channel system for sound creation in open areas.

Noticeably, the highest differences between the mean values of the SPL parameter inside and outside the reinforced area can be achieved while using the multi-channel system for sound creation in open areas. While using the central loudspeakers configuration, the noise level outside the area is very high and clearly depends on the power output of the installed speakers. The differences between the values of noise level from the multi-channel system for sound creation in open areas and the noise level from the central systems are of the order of some over twenty decibels with the advantage of the multi-channel system. Furthermore, it has to be stressed that for the multi-channel system for sound creation in open areas the noise level emitted in the distance of around 40 metres from the reinforced area is close to the background noise, whereas for the central system the noise level is from 69 [dB] to even above 80 [dB].

5. Summary and conclusions

As the analysis carried out indicates, the proposed multi-channel system for sound creation in open areas allows to achieve a relatively uniform sound pressure level across the area of interest and good/satisfactory clarity of sound for both music and speech with a good/very good mark. A considerable improvement of spatial impressions is noticeable after utilising the multi-channel sound system – when used, the LF and LFC parameters are within the range recommended for concert halls. Without the system, the LF and LFC parameters are of several percent values, which means they are too low. As it could have been expected, after introducing additional loudspeaker sets surrounding the listener, the intelligibility of speech decreased, but the STI and AL_{Cons} parameters prove that it still remains at a good/very good level.

As a result of analysis performed outside the area, it can be stated that the use of the proposed multi-channel system for sound creation in open areas may allow reduction of the noise emitted outside the area. In the least favourable case, the reduction is around 20 [dB], whereas in the best case, the reduction may be even above 35 [dB]. It is of essential importance, especially considering the fact that for the proposed system, only within 40 metres from the reinforced area, the noise level achieved is below 50 [dB], so its value is close to the background noise level.

To sum up, it should be concluded that the multi-channel system for sound creation in open areas may fulfil the objectives assumed, namely, it can create, within the area of interest, an acoustic field with the properties close to that of rooms (closed spaces) and, at the same time, allow to reduce the noise outside the reinforced area.

The proposed system exists only as a computer model at the moment. Using some components of the multi-channel system (Ciesielka, 2009) (e.g. loudspeakers, amplifiers, signal processors), an attempt was made to build a true multi-channel system for sound creation in open areas based on the inverse image source method. First preliminary studies of this system in a measured object and results of the measurements confirm the results obtained through the simulations (Gołaś *et al.*, 2011).

References

1. Ando Y. (1985), *Concert Hall Acoustics*, Springer-Verlag.
2. Beranek L. L. (1996), *Acoustics and musical qualities*, The Journal of the Acoustical Society of America, **99**, 5, 2647–2652.
3. Bradley J. S. (1991), *A comparison of three classical concert halls*, The Journal of the Acoustical Society of America, **89**, 3, 1176–1192.
4. Bradley J. S., Reich R. D., Norcross S. G. (2000), *On the combined effect of early– and late-arriving sound on spatial impression in concert halls*, The Journal of the Acoustical Society of America, **108**, 2, 651–661.
5. Ciesielka W. (2009), *A multi-channel system for sound control in the open space*, Archives of Acoustics, **34**, 4, 559–577.
6. EASE 4.3 User's Guide and Tutorial (2009), Acoustic Design Ahnert, Germany.
7. Gołaś A., Suder–Dębska K. (2010) *Acoustic field synthesis based on inverse image source method*, Proceedings of The 17th International Congress on Sound and Vibration, Cairo, Egypt.
8. Gołaś A., Suder–Dębska K., Ciesielka W., Filipek R. (2011), *Verification of inverse image source method applied for acoustic field creation in open area*, Acta Physica Polonica A, **119**, 6-A, 966–971.
9. Hidaka T., Beranek L. L., Masuda S., Nishihara N., Okano T. (2000), *Acoustical design of the Tokyo Opera City (TOC) concert hall, Japan*, The Journal of the Acoustical Society of America, **107**, 1, 340–354.
10. Hojan E. (2003), *Principles of amplify the room and open area*, [in Polish: *Zasady nagłaśniania pomieszczeń i przestrzeni otwartej*], Wydawnictwo Naukowe UAM.
11. Ishizawa M., Mafune Y., Endo H., Riko Y. (1998), *A manufacturer's review of the progress of large scale electro-acoustic systems in auditoria*, Acta Acustica united with Acustica, **84**, 311–319.
12. Kulowski A. (2007), *Room Acoustics*, [in Polish: *Akustyka sal*], Wydawnictwo Politechniki Gdańskiej.
13. Kuttruff H. (2009), *Room Acoustics*, Spon Press.
14. Long M. (2006), *Architectural Acoustics*, Elsevier.
15. Marshall A. H., Barron M. (2001), *Spatial responsiveness in concert halls and the origins of spatial impression*, Applied Acoustics, **62**, 91–108.
16. Mechel F. P. (2008), *Formulas of Acoustics*, Springer-Verlag.
17. Meyer J. (2009), *Acoustics and the Performance of Music*, Springer Science+Business Media, LCC.
18. Toole F. E. (2008), *Sound Reproduction. Loudspeakers and rooms*, Focal Press.
19. Ureda M. S. (2001), *Line arrays: Theory and applications*, The 110th Convention of Audio Engineering Society.

PAN ARCHIVES OF ACOUSTICS
Vol. **37**, No. 3, pp. 331–340 (2012)

DOI: 10.2478/v10168-012-0042-3

Subjective Assessment of Concert Halls: a Common Vocabulary for Music Lovers and Acousticians

Alicia GIMÉNEZ[(1)], Rosa María CIBRIÁN[(2)], Salvador CERDÁ[(3)]

[(1)] *Departamento de Física Aplicada, Universitat Politècnica de València*
Camino de Vera s/n, 46022 Valencia, Spain; e-mail: agimenez@fis.upv.es
[(2)] *Departamento de Fisiología, Universitat de València*
Blasco Ibañez 15, València, Spain; e-mail: Rosa.M.Cibrian@uv.es
[(3)] *Departamento de Matemática Aplicada, Universitat Politècnica de València*
Camino de Vera s/n, 46022 Valencia, Spain; e-mail: salcerjo@mat.upv.es

(*received July 7, 2011; accepted July 17, 2012*)

In recent years we have interviewed members of the audience after musical performances and asked them to evaluate the acoustics of the concert halls. A group of 'music lovers' (with a high level of musical training and experience) and 'acousticians' (with a wide knowledge of the physical characteristics of sound transmission) also attended each performance and answered the same questions as the general public. This group thereby served as a control group when evaluating surveys of the general public. In this paper, the results obtained when analyzing these control group surveys are presented. This analysis shows that a common vocabulary exists between music lovers and acousticians when rating a hall, although the grouping of the questions for each factor depends on the training of the respondents.

Keywords: room acoustics, subjective evaluation.

1. Introduction

The main objective of room acoustics is to study the behavior of sound within a room. The study of room acoustics involves finding relationships between the geometric and acoustic characteristics of a room or hall using various acoustic parameters. The aim is to achieve the audition desired by the listener according to the purpose of the sound. An analysis of this specialized research requires an understanding the different 'techniques' that each researcher employs in an attempt to systematize the two approaches (objective and subjective) used in the study. In recent years we have interviewed members of the audience after musical performances and asked them to evaluate the acoustics of the concert halls. A group of 'music lovers' (with a high level of musical training and experience) and 'acousticians' (with a wide knowledge of the physical characteristics of sound transmission) also attended each performance and answered the same questions as the general public. This group thereby served as a control group when evaluating surveys of the general public.

In this paper, we focus on the analysis of the opinion of this control group composed of 'music lovers' and 'acoustic specialists'. Both groups have the capacity to evaluate the acoustics of the halls but they make their evaluations from two different perspectives: from a musical perspective or technical training. This is revealed in the differing evaluations of some of the items in the survey of subjective assessment of the halls that we used (Gimenez *et al.*, 2011). And, especially in the relative importance that each group ('music lovers' and 'acoustic specialists') gives to some items over others. This differing evaluation of some aspects of the musical quality of the halls will be highlighted in this work.

Each author in the literature uses different methods to assess subjective perception. In 1952, Parkin, Schoeles, and Derbyshire (1952) presented a study on reverberation times in British halls and included results of a survey of critics, music teachers, and composers. Blankenship, Fitzgerald, and Lane (1955) made in 1955 a subjective assessment of halls at the University of Texas by collecting the responses of architects, acousticians, and musicians. Beranek published a book entitled *Music, Acoustics and Architecture* in 1962 (Beranek, 1962) which provided results from a large study conducted by the author in the late 1950s on the quality of acoustics in 54 concert halls throughout the world using the subjective assessments of mu-

sicians, directors, and music critics. A list of 18 subjective effects was presented by Beranek in the conclusion of his study. Following this work, two major studies were carried out in which subjects attended a series of concerts in various halls. Hawkes and Douglas in a 1971 study (Hawkes *et al.*, 1971) asked music students and professional musicians attending live concerts to complete questionnaires with a set of 16 bipolar scales. The main result of this study was the definition of a subset of orthogonal subjective parameters for factor analysis: reverberance; balance and blend; intimacy; definition and brilliance. In a 1988 study by Barron (1988) expert listeners (acoustic consultants) attended live performances in 11 British concert halls and completed a survey after each concert. This questionnaire was shorter than previous studies, but was designed in the light of findings from earlier studies. The study concluded that subjects made subjective assessments from two perspectives: those who prefer reverberation, and those who prefer intimacy. Barron compared these results with those obtained in laboratory tests by the Berlin group (summarized in Cremer *et al.*, 1982). These results and the absence of musical experts in their study, led Barron to describe a third preferred type of subjective assessment that is linked to clarity. Gade used questionnaires in his research on the acoustics of musicians performing on stage (Gade, 1989a; 1989b). He asked a large number of musicians to indicate the items they regard as most important and the subjective responses were: reverberance; support; timbre; dynamics; hearing each other; and time delay. Gade grouped these subjective aspects into 'soloist' and 'ensemble' concerns. A study by Sotiropoulou, Hawkes, and Fleming in 1995 (Sotiropoulou *et al.*, 1995) examined evaluations made by general concert-goers and used factor analysis to obtain four independent subjective factors: body, clarity, tone quality, and proximity. Cox and Shield made a notable study of the acoustics of the Royal Festival Hall in 1999 (Cox *et al.*, 1999) and included a survey of the general public, comparisons between musicians playing instruments, as well as comparisons between non-musicians and experts (after attending many concerts). Unfortunately, the results only examined one hall.

To conclude this review of research conducted on subjective assessment using surveys over the last decade, we find that the most recent works of Beranek and colleagues (Beranek, 2003; 2008; Hidaka *et al.*, 2000) are used as the main reference. The main objective of this study was to obtain a quality ranking for opera and concert halls.

Many researchers have been making subjective assessments using laboratory tests (Ando, 1977; Choi *et al.*, 2005; Gilbert *et al.*, 1995; Marmellota, 2010; Okano, 2002; Schroeder *et al.*, 1974; Yamaguchi, 1972; Zahorik, 2009). These results corroborate and complement those obtained with questionnaires and surveys. Published results are more accurate and closer to reality if they have been verified by various investigators using several experimental approaches (Gade, 2007). These results suggest that the functional efficiency of music halls can be examined from various points of view: the acoustician, musician, and the general public. It may be believed that these views should match as the joint efforts of architects and acousticians are intended to effectively satisfy the needs of the musician and concert-goer (regardless of their knowledge of acoustics and music). However, this is not necessarily true because psychological factors that exert a strong influence on musicians cannot be felt or understood by acousticians nor general listeners – and *vice versa*.

Our paper proposes to achieve the following:

- Define the terminology that enables music lovers to express their assessment of music halls.
- Define the terminology that enables acoustic specialists to express their assessment of music halls.
- Integrate the contribution of music lovers and acousticians in a common vocabulary.

For this purpose we assembled a group of experts composed of 'music lovers' from the Conservatory of Music of Valencia and 'acoustics' from the Universitat Politècnica de València. Assessments of halls through a survey were compared with those made by concert-goers attending the performances. The evaluation of the results of the survey to obtain the ranking of halls showed that the valuations of the public were similar to those of the experts but a little less rigorous, which was perfectly acceptable, and revealed that expert opinion was consistent with the general public and *vice versa*.

However, we also noticed a slight variation in the evaluation of the items in the survey between the two subgroups that made up the panel. So we decided to specifically address this issue and investigate these slight differences in appreciation of the musical quality between 'music lovers' and 'acousticians'.

2. Methodology

2.1. Subjects

The group of experts was formed of 26 individuals: 14 experienced acousticians (architectural acousticians, technical acousticians, consultants, university lecturers and researchers); and 12 music-lovers who although not experts in acoustics, nevertheless have considerable experience in music and were trained at the Valencia Music Conservatory.

2.2. Halls

In the Table 1 we show the main typological characteristics of the nine halls in which the expert group made evaluations.

Table 1. Main typological characteristics of halls studied.

Hall	Year built	Shape	Use	Seating capacity	V [m^3]	Vol./seat [m^3/per.]	RT(s)
Auditorio de Ribarroja (Valencia)	1994	rectangular	theatre, opera, dance and concerts	783	7830	10	1.79
Auditorio de Benaguacil (Valencia)	1960	rectangular, fan shaped on two levels	music band concerts	509	3480	6.9	2.25
L'Auditori de Torrent (Valencia)	1997	irregular hexagonal	conferences, congresses, concerts of all types, opera and dance	606	6430	10.6	1.87
Palau de la Música de Valencia	1987	central stage with upper amphitheater, side and front boxes (shoulders)	conferences, congresses, concerts of all types, opera and dance	1817	14700	8.1	2.42
Paraninfo Universitat Politècnica de València	1978	retangular	conferences, congresses and soloist musician concerts; chamber orchestra and chorus	385	2700	7	1.3
Teatro La Unión Musical de Lliria (Valencia)	1951 (1992)	fan-shaped on two levels	orchestra and music band concerts	967	6287	7.3	1.43
Teatro Principal de Alicante	1905–1915	italian theatre, horseshoe shape and boxes on different floors	theatrical representations, orchestra and soloist concerts, opera, chorus and dance	1102	4539	4.1	1.21
Auditorio de Castellón	2004	irregular trapezoidal shape	conferences, congresses, concerts of all types, opera and dance	1200	14850	12.4	2.43
Basilica de Sant Jaume Algemesi (Valencia)	1500–1580 (1985)	rectangular apsidal nave, semi-cylindrical ceiling, side corridors with square chapels and rectangular hemispheric ceilings	religious events and organ, orchestra, chamber orchestra and chorus concerts	640	12144	19	5.07

2.3. Questionnaires

We have verified that the questionnaire is a valid instrument for evaluating the subjective perception of listeners in concert halls, and we have found a good correlation between experts and the public in general; although there is a slight tendency by the public to overvalue the acoustic quality of the halls (Hidaka *et al.*, 2000). Partial results have been discussed in various forums (Gimenez *et al.*, 2006a; 2006b). In these conferences, we have presented evaluations of some concert halls and an initial analysis of the data using factor analysis. The small number of surveys made in previous works has obliged us to use all the results without distinguishing the three types of listener mentioned above. As a result, we have a sufficient database of responses from 'music lovers' and 'acousticians' to present a partial result for these two groups. The questionnaire for validating the subjective assessment of the concert halls (Gimenez *et al.*, 2006a; 2006b), contained 58 questions divided into six sections:

Section A: 'General aspects of the hall'. Background noise, visibility of the orchestra, comfort of the seating, architecture and decor, etc.

Section B: 'Detailed acoustic perception'. Characteristics of the psychoacoustic quality are assessed in this section.

Section C: 'Global acoustic perception' includes items about the global perception of the orchestra, global orchestral balance, and an evaluation of global acoustic perception in the hall.

Sections D, E and F: 'Sociological data', 'Musical preferences' and 'Commentaries' include a total of six questions.

Table 2. Sections B and C of the questionnaire, adapted to the journal.

HALL ..... DATE ..... CONCERT/OPERA .....

	AREA	ROW	SEAT	DK/NA[1]

Section B: DETAILED ACOUSTIC PERCEPTION[2]

	VG	G	F	P	VP	DK/NA
B01 Can you clearly distinguish the sounds of the different instruments?						
B11 Can you clearly distinguish the soloist (if there is one)?						
B21 How do you perceive the orchestra overall?						
DO YOU CONSIDER THAT IN THIS HALL:	VM[2]	M	F	S	VS	DK/NA
B41 High sounds predominate (high frequencies)						
B42 Low sounds predominate (low frequencies)						
B43 Sound is perceived equally from all directions						
HAVING HEARD THE MUSIC, THE SENSATION IT PRODUCES WITH RESPECT TO PROXIMITY OR DISTANCE FROM THE MUSICIANS IS THAT OF A HALL THAT IS:						
B51 Large						
B52 Open						
B53 Wide						
YOU FIND THE SOUND OF THE HALL:						
B61 Reverberating (persistence of the sound, the different sounds are superimposed)						
B62 Dry (the sounds are not prolonged sufficiently)						
B63 Intimate (the music gives the impression of being played in a small enclosure)						
B64 Lively, rich, brilliant (richness of high tones that disappear slowly)						
B65 Warm (rich in low sounds that are perceived and distinguished clearly)						
B66 Clear (details of the musical execution are distinguished separately)						
B67 Blurred (individualized sounds of the musical execution are confused and mixed)						
THE CONCERT HEARD IN THIS HALL PRODUCES THE SENSATION THAT THE MUSIC IS:						
B71 Smooth, the opposite of rough						
B72 Exciting (predominance of high sounds and a loud level), the opposite is calm						
B73 Balanced, the opposite is distorted						
B74 Loud (loud sound), the opposite is weak						
B75 Pleasant, the opposite is unpleasant						
B76 Light, the opposite is dense						
B81 Do you feel enveloped by the sound?						
B82 If you do NOT feel enveloped, indicate the direction from which you hear the sound:	FRONT	LEFT	RIGHT	FLOOR	CEILING	DK/NA

Section C: OVERALL ACOUSTIC PERCEPTION

	VM	C	F	S	VS	DK/NA
C01 Do you perceive the orchestra to be loud overall?						
C02 How balanced do you perceive the orchestra overall?						
INDICATE YOUR PERCEPTION OF THE DIFFERENT ELEMENTS OF THE ORCHESTRA:						
C11 The string section dominates						
C12 The double bass section dominates						
C13 The woodwind section dominates						
C14 The brass section dominates						
C15 The percussion section dominates						
C16 The piano dominates						
C17 The soloist dominates						
C18 The chorus dominates						
	VG	G	F	P	VP	DK/NA
C21 How do you classify the acoustics of this hall overall?						

C31 How do the acoustics of this hall compare to another/others that you visit regularly?	MUCH BETTER	BETTER	SIMILAR	WORSE	MUCH WORSE	DK/NA

C41 What other halls do you know whose acoustical quality is comparable with that of this hall?	
A	
B	
C	

(1) DK/NA: don't know/no answer or not applicable; VG: very good; G: good; F: fair; P: poor; VP: very poor. (2) VM: very much; C: considerably; F: fairly; S: slightly; VS: very slightly.

Each item can be rated from 1 to 5 points (corresponding to more or less agreement with the question) and the value 0 indicates a non-response. This work has not taken into account the questions in sections A, D, E and F as these questions are not specifically about a musical evaluation of the hall and include other collateral aspects such as comfort and decor. In this study, we have used the 23 questions in section B, as well as questions c01 and c02 that cover specific aspects of sound quality assessment (see Table 2).

2.4. Procedure

The group of experts was given set positions throughout the audience seating area of the halls and changed positions between acts. In this way, responses from the two groups corresponded to the same positions. The surveys were made during the following 14 musical performances (see Table 3).

2.5. Statistical analysis

The main applications of factor analysis are for reducing the number of variables and detecting structures in the relationship between the variables. The factor analysis we carried out consists of extracting the principal components by analyzing the correlations matrix for eigenvalues over one. We completed the process by rotating the factors using the varimax procedure. The questions are considered to be included within a factor when they have the highest rate of correlation in this factor (in absolute value) that exceeds 30%. In this paper we have processed 246 surveys.

3. Results and discussion

Below are the results obtained by data reduction using factor analysis through the determination of the main components.

Table 3. List of concerts. Distribution of experts in the halls.

HALL	CONCERT	Acousticians	Music Lovers
Auditorio de Ribarrroja (Valencia)	Mozart (*The Marriage of Figaro*)	5	6
	C.M. von Weber (*Der Freischütz*); Strauss (*Don Juan*); Brahms (*Symphony No. 2 in D Major*)	6	6
Auditorio de Benaguacil (Valencia)	Bernstein (*Divertimento for Orchestra*); R. Miller (*The Forest of Tears*); Rimsky-Korsakov (*Scheherazade*)	6	7
	M. Galvez-Taroncher (*Night of Sobs*); M. Ohana (*Concert for Piano and Orchestra*); Stravinsky (*The Firebird*)	7	6
L'Auditori de Torrent (Valencia)	G. Verdi (*Rigoletto*)	14	12
	E. Bermell (*Dolores Tormo*); Bernstein (*Divertimento for Orchestra*); Gershwin (*Rhapsody in Blue*); F.A. Comos (*Carmina Gueguel Massmanian Estelles*); J.G. Gomez-Deval (*O Camino de Santiago*); M. Gould (*Jericho*)	8	10
Palau de la Música de Valencia	Haydn (*Symphony "The Miracle", Symphony "Drumroll"*)	10	7
	Strauss (*Parergon zur Symphonia Domestica for Piano and Orchestra, Op. 73*); X. Montsalvatge (*Short Concert for Piano and Orchestra*); Ravel (*Le tombeau de Couperin*); M. de Falla (*El Amor Brujo*)	8	6
Paraninfo de la Universitat Politècnica de València	Chopin (*Cello Sonata in G minor, Op.* 65); C. Bersgen (*Sonata for Flute and Piano*); J. Francaix (*Trio for Flute, Cello and Piano*); K. Weill (*Five Songs for Voice and Piano*)	14	12
Teatro de la Unión Musical de Lliria, (Valencia)	Beethoven (*Symphony No. 1*); J.A. Valls-Subirats (*Concert for Piano and Orchestra*); E. Chabrier (*Rhapsody for Orchestra*)	13	12
	I. Albéniz (*Almera*); M. Bautista (*Suite Generis for Tuba and Piano*); G. Faure (*Dolly Suite Op 56*); A.von Zemlinsky (*Trio*); J. Matitia (*The Devil's Rag*)	5	10
Teatro Principal de Alicante	Beethoven (*Overture 'Egmont'*); P. de Sarasate (*Bohemian Airs*), (*Carmen Fantasy*); Tchaikovsky (*The Nutcracker Ballet Suite*)	13	10
Auditorio de Castellón	Ravel (*Alborada del Gracioso*), (*Tzigane*); C. Saint-Sans (*Havanera Op 83*); I. Albéniz (*Five Pieces of Iberia*)	8	10
Baslica de Sant Jaume de Algemesí (Valencia)	Handel (*"The Messiah"*)	9	6

3.1. Acousticians

We have obtained seven factors that explain 71% of the total variance. Each factor explains 14%, 12%, 11%, 10%, 9%, 8% and 7%, respectively. We can observe that some consecutive questions are grouped in the results from acousticians. This could be a consequence of the fact that the survey was designed by acousticians, and the nature of the authorship may also explain why the obtained factors are quite balanced. However, the groupings of non-consecutive questions are interesting. Interpretation is always perilous, but we suggest the following:

Factor 1: (14%). This factor contains questions b72–b76. It includes the adjectives: exciting, balanced, strong, pleasant and light. Therefore, we can consider it as a factor of pleasantness. The correlation factors are between 0.86 and 0.65.

Factor 2: (12%). Questions b51 to b53 evaluate the subjective dimension of the room, and question b71 relates to sensations of softness. The correlation factors are between 0.89 and 0.52. This sensation may depend on the subjective perception of the 'size' of the room, because both impressions are related with early reflections.

Factor 3: (11%). Questions b43, b64, c01 and c02 are listed in this factor. The correlation factors are between 0.90 and 0.52. These are questions related to the perception of the orchestra, the directionality of the sound, and the presence of high frequencies. We can interpret this factor as relating to the perception of sound.

Factor 4: (10%). Questions of clarity and the global perception of the orchestra are included in this factor (b01, b11, b21). It can be argued that acousticians analyze an orchestra's global perception from the point of view of **clarity**.

Factor 5: (9%). Questions b41, b42 and b67. The correlation factors are between 0.86 and 0.46. An unbalanced perception (high or low frequencies prevail) is listed together with the adjective 'cloudy'. We can say that imbalance is a masking effect or caused by a mixture of sounds (**lack of balance**).

Factor 6: (8%). Questions b61, b65 and b81. The correlation factors are between 0.77 and 0.55. The determination of an objective parameter that describes the perception of being **enveloped** by sound is a matter that is being researched at the moment. The grouping of reverberation, warmth, and the perception of envelopment may assist researchers interested in this topic (see factor 5 for music lovers).

Factor 7: (7%). Questions b62, b63 and b66. The correlation factors are between 0.75 and 0.52. This question corresponds to **dry**. Intimate (small room) and clear (separate details of the musical execution are distinguishable) are grouped in this final factor. These perceptions can be explained by a reduced level of sound reverberation.

3.2. Music lovers

We have also obtained seven factors that explain 62% of the total variance. Each factor explains 18%, 8%, 8%, 8%, 7%, 7% and 6%, respectively. In this case, factor 1 includes ten questions. The following three factors include three questions, and the last three factors only include two questions. A possible interpretation of each factor is:

Factor 1: (18%) This **pleasantness** factor is similar to factor 1 for the acousticians (it includes almost all the questions in that factor), including: b43, b63–b66 and b71, b73–b76 (correlation factors between 0.44 to 0.78). The questions correspond to rating: intimate, live (brilliant), warmth, clearness, sensation of soft music, balance, high sonority, pleasantness, and lightness. More characteristics are included for this factor than in the case of the acoustic survey.

Factor 2: (8%) Questions b11, b67, b72 and c02 (correlation factors between 0.76 to −0.59). A term appears with negative correlation in this factor. Next to the cloudy term is the prevalence of high frequencies and the ease with which the soloist can be distinguished (negative correlation). Question c02 enquires as to the perception of a balanced orchestra. We named this factor 'precision of sound'.

Factor 3: (8%) Questions b01, b21, c01 (correlation factors between 0.73 to 0.57). This factor regards perception of the orchestra: the ease with which the orchestra and instruments can be perceived and the orchestra's overall force.

Factor 4: (8%) Questions b41, b42, b61 (correlation factors between 0.81 to 0.57). This factor is similar to factor five for the acousticians; namely, the unbalanced perception of high or low frequencies, and is grouped with 'reverberance'.

Factor 5: (7%) Questions b52, b81 (correlation factors of 0.55). The music lovers group feel enveloped by the sound. This fact, together with the observations made for acousticians in factor 6, are interesting when designing an objective parameter for envelopment.

Factor 6: (7%) Questions b51, b53 (correlation factors between 0.77 and 0.67). This factor includes the perceived **'size'** of the room for music lovers.

Factor 7: (6%) Questions b43 and b62 (correlation factor 0.43 and 0.88). The observation that the sound is equally perceived in all directions is grouped with dry. It could be argued that **isodirectionality** can be valued negatively by music lovers.

3.3. The common vocabulary

It can be observed that the same questions appear in the seven factors found in both groups. However, the explanation of the variance in the case of acousticians is higher than that of the music lovers and the distribution of the questions differs. This shows that differences between acousticians and music lovers are very significant in the obtained factors. Even if we force the analysis to obtain just four factors, the differences between the groups remain the same. However, it is possible to see that there are factors supporting a similar explanation for both groups of subjects. Factors 1 which has been interpreted as a factor of 'pleasantness' is common in both cases, as well as being the main factor (18% for music lovers and 14% for acousticians). The 'size' factor also appears in both groups – but is more important for acousticians (12%) than for music lovers (7%). There is also a factor of being enveloped by sound that has similar percentages (8% and 7%). Finally, the 'lack of balance' factor of the acousticians corresponds to an 'unbalanced perception' by the music lovers. However, the perception of the acousticians includes a group we call sound perception (11%), that compares with the corresponding factor for the music lovers of the perception of the orchestra (8%). Given these similarities, we performed a factor analysis with the least number of factors that explain about 50% of the variance and obtained four factors. Table 4 shows the components obtained in accordance with the questions studied and their correlations. Each factor explains 19%, 11%, 9%, and 9%, respectively. We can observe in this case that the contiguous questions are generally grouped together. We can consider the factors below as a common vocabulary:

Factor 1 (19%): Quality factor about **pleasantness**. This factor incorporates the main factor of the group of acousticians and the music lovers group. The only question that is not included is b43 that appeared in F1 for music lovers (low correlation).

Factor 2 (11%): Quality factor about **global sound perception**. This factor groups factors 3 and 4 of the acousticians (sound perception and clarity) and factors 2 and 3 of the music lovers (cloudy and perception of the orchestra). It also includes the question b81 about feeling enveloped by the sound that previously appeared in other factors (F6 for the acousticians and F5 for the music lovers).

Factor 3 (9%): Factor about room 'size' perception or **subjective room size**. This factor includes factor 2 for the acousticians, for which it is the second most important factor, and includes factors 5 and 6 for the music lovers (a less important factor for this group).

Factor 4 (9%): This factor is about **balance in frequencies** from the musical point of view (reverberation included) that corresponds to factor 4 for the music lovers. It also groups factors 5 and 6 for the acousticians.

We have used the results obtained to propose a new grouping of factors for the subjective evaluation of concert halls. These new factors constitute a common view of the acoustic quality of concert halls by the two groups that represent the artistic and technical traditions of music listening.

Table 4. Questions at each factor in *The Common Vocabulary*.

Factor 1	Factor 2	Factor 3	Factor 4
b63. (0.69)	b01 (0.67)	b51 (0.68)	b41 (0.66)
b64. (0.58)	b11 (0.67)	b52 (0.66)	b42 (0.73)
b65. (0.58)	b21 (0.66)	b53 (0.77)	b61 (0.62)
b66. (0.71)	b67 (−0.48)		
b71. (0.53)	b81 (0.45)		
b72. (0.56)	c01 (0.39)		
b73. (0.70)	c02 (0.48)		
b74. (0.68)			
b75. (0.71)			
b76. (0.63)			

The common language shared between musicians and acousticians is more similar to the language of musicians given that factor 1 of the musicians is practically identical to the common factor 1 for both acousticians and musicians; factor 4 of musicians is identical to the common factor 4; while the factors 2–3 and 5–6 of the musicians only differ in one question with respect to the common factors 2 and 3, respectively, for both acousticians and musicians.

For concert halls and opera houses, Beranek (1996) said that in recent years a common language of acoustics has been developed that emerges from the dialogue between musicians and acousticians.

In the literature, field studies into the multidimensional evaluation of auditorium acoustics by means of subjective surveys were performed with expert listeners (Hawkes *et al.*, 1971, Barron, 1998; Beranek, 2003; 2008; Hidaka *et al.*, 2000) and general audiences (Sotiropoulou *et al.*, 1995; Cox *et al.*, 1999). As far as we know, there is no specific work comparing surveys between music lovers and acousticians. Our results show that differences and similarities exist between these groups of experts – their general evaluations of the hall being similar but with each type of expert focusing on differing aspects.

The order of importance that we have found for acousticians is: pleasantness, subjective dimension, perception of the orchestra, clarity, lack of balance,

envelopment and dry-intimate factor. The order of importance for music lovers is: pleasantness, precision of sound, perception of orchestra, lack of balance, openness of the hall, perceived size and iso-directionality. Although the terms that appear are common for subjective evaluations or halls it is worthwhile emphasizing the inclusion of the subjective dimension (acousticians) and perceived size (music lovers). A similar result was given by Lokki *et al.*, (2011) in which individually elicited attributes include factors such as openness and the width of sound.

However, the results provided by the experts are more consistent than the results of the general public (Cox *et al.*, 1999). On further comparing the results of our two groups of experts (acousticians and music lovers) it can be seen that the acousticians are the more consistent of the two groups when consistency is evaluated with the percentage of explained variance in the factoral analysis (71% compared to 62%).

All of these differences indicate that the acousticians value the technical aspects by grouping them into balanced factors; while the music lovers make a grouping that includes nearly all of the items in one group (which therefore has greater weight).

Nevertheless, when a common language is considered and a set of four factors with 50% of the explained variance is established, we find that the first two factors can be considered as factors of overall perception – while the other two factors, refer to a more detailed analysis of sound. This twin point of view is apparent in early works on subjective evaluation (Fischetti *et al.*, 1992). Moreover, our results agree with the view presented by Gade, in which the subjective characteristics are assembled into two groups: 'soloist' and 'ensemble' (Gade, 1989a; 1989b). Our results also coincide with the general view of Barron (1988) who considers as important factors: reverberation, intimacy, and clarity.

Our results can also be compared with those of Lokki (Lokki *et al.*, 2011). Although Lokki obtains nine groups of characteristics, given the nearness of the resulting groups it is possible to make a grouping of just four: reverberance_1 (size of space); reverberance_2 (envelopment); definition; and a group that includes size of sound, loudness, separation, distance and openness (main dimension). These four factors can be related with the four factors that we have obtained as below:

- Factor 1. . . . . Reverberance_2.
- Factor 2. . . . . Main dimension.
- Factor 3. . . . . Reverberance_1.
- Factor 4. . . . . Definition.

4. Conclusions

In this paper we present, using a subjective assessment survey, the qualities of sound perception most relevant for each group (musicians and acousticians) where their ratings are similar.

During the past five years we have surveyed a group of experts listening to performances in various concert halls in the region of Valencia in Spain. This group consists of musical and acoustic experts. We present the results of a factor analysis of the surveys.

The analysis of these surveys reveals varying results for 'music lovers' and 'acousticians'. While all the questions can be grouped into seven factors for both groups – the groupings are nevertheless distinct.

These results imply that educational training is an important factor in the evaluation of concert halls, even for expert groups:

- The number of factors – seven – is the same in both groups, but the group of acoustic experts shows more variance than the group of music lovers (71% compared to 62%).
- For the acousticians the first four factors have percentages of between 14% and 10%; while for the music lovers, the first factor with a factor of 18% is the only one with a value greater than 10%.
- Factor 1 of the acousticians (14%) includes five questions and factor 1 of the music lovers includes ten questions. However, there are questions in common.
- The questions are distributed almost equally (four or five) between all the factors for the acousticians; while for the music lovers the questions are encompassed in the first factor.

All of these differences indicate that the acousticians differentiate the technical aspects by grouping them into factors that contain contiguous questions, while the music lovers group almost all of the items into one factor (which therefore acquires greater weight). This may be caused by the fact that the survey was mostly designed by acoustic experts.

By analyzing all of the surveys together we have obtained a common vocabulary for musical and acoustic experts. We have found that contiguous questions are generally grouped together and that four factors are found and can be interpreted as follows:

- Factor 1: (19%) – quality factor about sound perception.
- Factor 2: (11%) – quality factor about perception of orchestra.
- Factor 3: (9%) – factor regarding room 'size' perception (subjective room size or acoustical intimacy).
- Factor 4: (9%) – factor regarding balance in frequencies from the musical point of view (reverberation included).

The first two factors can be considered as factors of overall perception; while the other two factors refer to a more detailed analysis of sound. This common language between acousticians and music lovers is more similar to that of the musicians.

Acknowledgments

This study has been supported with FEDER funds. The Spanish Ministry of Science and Innovation also supported the present study in a coordinated investigation project framework (references BIA2003-09306-C04 and BIA2008-05485). The translation of this paper was funded by the Universitat Politècnica de Valencia, Spain.

References

1. Ando Y. (1977), *Subjective preference in relation to objective parameters of music sound fields with a single echo*, J. Acoust. Soc. Am. **62**, 6, December, 1436–1441.

2. Barron M. (1988), *Subjective study of British symphony concert halls*, Acustica, **66**, 1–14.

3. Beranek L. (1962), *Music acoustics & architecture*, John Wiley & Sons, New York, NY.

4. Beranek L. (1996), *Concert halls and opera houses*, Springer-Verlag, New York, NY.

5. Beranek L. (2003), *Subjective rank-orderings and acoustical measurements for fifty-eight concert halls*, Acta Acustica united with Acustica, **89**, 3, May/June, 494–508.

6. Beranek L. (2008), *Concert Hall Acoustics*, J. Audio Eng. Soc., **56**, 7/8.

7. Blankenship J., Fitzgerald R. B., Lane R. (1955), *Comparison of objective and subjective observations on music rooms*, J. Acoust. Soc. Am., **27**. 774–780.

8. Choi Y-J., Fricke F. R. (2005), *Evaluation of the relative acoustic performance of two auditoria using measurements and auralization*, Acta Acustica United with Acustica, **91**, 1051–1062.

9. Cremer L., Müller H. A. (1982), *Principles and applications of room acoustics*, Vol. I, II, Applied Science Publishers, London.

10. Cox T. J., Shiels B. M. (1999), *Audience questionnaire survey of the acoustics of the Royal Festival Hall, London, England*, Acustica united with Acta acustica, **85**, 547–559.

11. Fischetti A., Hemin Y., Jouhaneau J. (1992), *Relations between Subjective Spatialisation, Geometrical Parameters and Acoustical Criteria in Concert Halls*, Applied Acoustics, **37**, 233–247.

12. Gade A. C. (1989a), *Investigations of musician's room acoustic conditions in concert halls. Part I. Methods and laboratory experiments*, Acustica, **69**, 193–203.

13. Gade A. C. (1989b), *Investigations of musician's room acoustic conditions in concert hall. Part II. Field experiments and synthesis of results*, Acustica, **69**, 249–262.

14. Gade A. C. (2007), *Acoustics in halls for speech and music*. Chapter 9, [in:] *Handbook on Acoustics*, J. Rossing [Ed.], Springer.

15. Gimenez A., Sendra J. J., Vela A., Daumal F., Cibrian R., Zamarreño T., Arana M., Romero J., Giron S., San Martin M. L., Cerda S., Galindo M., Aramendia E., Lacatis R., Bustamante R., San Martin R., Segura J., Muñoz M. S., Miralles J. L. (2006a), *Process of developing a test of subjective response of listeners in general and musical experts, as an assessment tool of music perception in concert halls, auditoriums and theaters* [in Spanish], Tecni-Acustica 2006, Gandia, ISBN 84-87985.

16. Gimenez A, Sendra J. J., Vela A., Daumal F., Cibrian R., Zamarreño T., Arana M., Romero J., Giron S., San Martin M. L., Cerda S., Galindo M., Aramendia E., Lacatis R., Bustamante P., San Martin R., Segura J., Muñoz M. S., Miralles J. L. (2006b), *Responses from listeners and music experts to a survey to assess the perception of music in concert halls, auditoriums and theaters* [in Spanish], Tecni-Acustica 2006, Gandia, ISBN 84-87985.

17. Giménez A., Cibrián R. M., Girón S., Zamarreño T., Sendra J. J., Vela A., Daumal F. (2011), *Questionnaire survey to qualify the acoustics of Spanish concert halls*, Acta Acustica united with Acustica, **97**, 6, November/December, 949–965.

18. Hawkes R. J., Douglas H. (1971), *Subjective acoustic experience in concert auditoria*, Acustica, **24**, 235–250.

19. Hidaka T., Beranek L. (2000), *Objective and subjective evaluations of twenty-three opera houses in Europe, Japan, and the Americas*, J. Acoust. Soc. Am., **107**, 1, January, 368–383.

20. Lokki T., Pätynen J., Kuusinen A., Vertanen H., Tervo S. (2011), *Concert hall acoustics assessment with individually elicited attributes*, J. Acoust. Soc. Am., **130**, 2, 834–849.

21. Martellotta F. (2010), *The just noticeable difference of center time and clarity index in large reverberant spaces*, J. Acoust. Soc. Am., **128**, 2, 654–663.

22. Okano T. (2002), *Judgments of noticeable differences in sound fields of concert halls caused by intensity variations in early reflections*, J. Acoust. Soc. Am., **111**, 1, 217–229.

23. Parkin P. H., Scholes W. E., Derbyshire A. G. (1952), *The reverberation times of ten British Concert Halls*, Acustica, **2**, 97–100.

24. Schroeder M. R., Gottlob D., Siebrasse K. F. (1974), *Comparative study of European concert halls: correlation of subjective preference with geometric and acoustic parameters*, J. Acoust. Soc. Am., **56**, 4, 1195–1201.

25. Sotiropoulou A. G., Hawkes R. J., Fleming D. B. (1995), *Concert hall acoustic evaluations by ordinary concert-goers: I, multidimensional description of the evaluatios*, Acustica, **81**, 1–19.

26. Soulodre G. A., Bradley J. S. (1995), *Subjective evaluation of new room acoustic measures*, J. Acoust. Soc. Am., **98**, 1, 294–301.

27. Yamaguchi K. (1972), *Multivariate analysis of subjective and physical measures of hall acoustics*, J. Acoust. Soc. Am., **52**, 1271–1279.

28. Zahorik P. (2009), *Perceptually relevant parameters for virtual listening simulation of small room acoustics*, J. Acoust. Soc. Am., **126**, 2, 776–791.

PAN ARCHIVES OF ACOUSTICS
Vol. **37**, No. 3, pp. 341–347 (2012)

DOI: 10.2478/v10168-012-0043-2

Influence of MoO_3 on the Structure of Lithium Aluminum Phosphate Glasses

Yasser B. SADDEEK[(1)], S. M. ABO-NAF[(2)]

[(1)] *Physics Department, Faculty of Science, Al-Azhar University*
Assiut 71524, Egypt; e-mail: ysaddeek@gmail.com

[(2)] *Glass Research Department, National Research Centre (NRC)*
El-Behoos Str., Dokki, 12622 Cairo, Egypt

(*received November 30, 2011; accepted July 17, 2012*)

IR spectroscopy, density and ultrasonic velocity measurements have been carried out for aluminum lithium phosphate glasses with and without MoO_3. The observed changes in the FTIR spectra of the glasses were related to the modifier/former role of molybdenum ions. The results revealed that the density increases with increasing MoO_3 content, which was attributed to the increase in the compactness and packing of the glass network. The ultrasonic data were analyzed in terms of creation of new bonds of MoO_3 attached to phosphate units. The new bonds increased the average crosslink density and the number of network bonds per unit volume along with a strengthening of the different modes of vibrations which in its turn increased the ultrasonic velocity, the rigidity and hence the elastic moduli of the glasses.

Keywords: phosphate glasses, IR, density, elastic properties.
PACS: 43.35.Ae, 61.43.Fs, 62.20.Dc, 62.80.f, 78.30.Ly, S10.15.

1. Introduction

Lithium phosphate glasses have been gained great attention during the last decades due to their wide range of compositional and structural possibilities. The low melting and glass transition temperatures, high electrical conductivity, high thermal expansion coefficient of these glasses enable their use in laser host matrices, lithium micro-batteries or in electro-optical systems (Chowdari, 1988; Selvaraj, 1988; Chowdari, 1991; Donald, 1993; Proulx, 1994; Jiang, 1998; Hudgens, 1998; Brow, 2000; Campbell, 2000; Dai, 2002; Sharaf El-Deen, 2008; Cozar *et al.*, 2008). The physical properties of phosphate glasses can be improved by introducing alumina, which provides higher chemical durability, alkali and transition metal oxides like MoO_3 (Bridge *et al.*, 1986; 1987; Chen, 1999; Reis *et al.*, 2002).

It was reported that the network of lithium phosphate glasses is a polymeric arrangement of phosphate groups with variable lengths, and is dominated by linkages between PO_4 tetrahedra. Addition of Li_2O to P_2O_5 converts the three-dimensional phosphate network into linear phosphate chains, and changes the phosphate structural groups from PO_4 to PO_3 to PO_2 to PO as the molar ratio of Li_2O/P_2O_5 passes from 0 to 1, to 2 and to 3. The linear chain structure results in a cleavage of P–O–P linkages and a creation of non-bridging oxygens (NBO's) in the glass (Wells, 1975; Rao, 2002; Prasad, 2005; ElBatal *et al.*, 2008; Šubčik *et al.*, 2009). On the other hand, the structure of MoO_3-P_2O_5 glasses were stated to belong to a group of glasses, which incorporate distorted octahedral structural units [MoO_6] or tetrahedral structural units [MoO_4] within the glass network. MoO_3 plays a modifier role upon the addition of MoO_3 to P_2O_5 glasses with ratio <50 mol% by forming non-bridging oxygens, and a former role when MoO_3 > 50 mol% throughout the complete Mo-P-O range by increasing the crosslink density of P_2O_5 (Bridge *et al.*, 1986; 1987; Moustafa *et al.*, 1998).

Introducing molybdenum ions in lithium phosphate glasses produces some variable interesting electrical properties which are related to the ability of molybdenum ions to exist in glasses in three possible valences, namely Mo^{3+}, Mo^{5+} and Mo^{6+} (Bih *et al.*, 2008; ElBatal *et al.*, 2008; Chowdari *et al.*, 1991). Recently, it was found that substitution of PbO by MoO_3 in MoO_3–PbO-La_2O_3–P_2O_5 glasses leads to a polymerization of the phosphate chains by increasing the packing and the cross link density of the phosphate network (Saddeek, 2011). Accordingly, this work aims

to extend the available informations of MoO_3 in the environment of the Al_2O_3-P_2O_5-Li_2O glass system by using FTIR and ultrasonics to study its availability for the use in opto-electronic devices in a further work.

2. Experimental procedures

Glass samples with the formula x MoO_3-$2Al_2O_3$-$68P_2O_5$- $30Li_2O$ with $0 \leq x < 40$ wt% were prepared by the melt-quenching technique. The starting materials to obtain these glasses are $(NH_4)_2HPO_4$, Li_2O, Al_2O_3 and MoO_3 of reagent grade purity. The starting materials were mixed together by grinding the mixture repeatedly to obtain a fine powder. The mixture was melted in a porcelain crucible in an electrically heated furnace under ordinary atmospheric conditions at a temperature of about 1273 K for 2 h to homogenize the melt. The obtained glass samples from the melt quenching into preheated stainless-steel mould were heat treated at a temperature of about 20K below their calorimetric glass transition temperature for 2 h to remove any internal stresses. The obtained glasses were lapped and two opposite sides were polished to be suitable for use in the ultrasonic velocity measurements. Non-parallelism of the two opposite side faces was less than 0.01°. The composition given in table 1 refers to the nominal composition (the starting mixture). The glass samples were kept in desiccators to prevent possible attack by moisture. X-ray diffraction patterns were recorded to check the amorphous nature of the glass samples using a Philips X-ray diffractometer PW/1710 with Ni-filtered Cu-K_α radiation ($\lambda = 1.542$ Å) powered at 40 kV and 30 mA. The patterns (not shown) revealed broad humps characteristic of the amorphous materials and did not reveal discrete or any sharp peaks.

Infrared (IR) spectra for the glass powder (after crushing them into powder form) were obtained using an IR Fourier spectrophotometer type JASCO, FT/IR–430 (Japan). For this purpose, each sample was mixed with KBr in the proportion of 1 : 100 (by weight) for 20 min and pressed into a pellet using a hand press. At least two spectra for each sample were recorded in the wavenumber range of 400–2000 cm^{-1} with a resolution of 4 cm^{-1}, corrected for dark-current noise and normalized. The resulted spectra were curving fitted (Proulx *et al.*, 1994) to get quantitative values for the band areas of heavily overlapped bands. The curve-fitting procedure is based on a least-squares minimization which in its turn involves entering the values of the wavenumber of the component bands (determined by using the deconvolution technique) and then a program determines the best estimate of the parameters of the component curves. The deconvolution process involves several steps: computation of an interferogram of the sample by computing the inverse Fourier-transform of the spectrum, multiplication of the interferogram by a smoothing function and by a function consisting of a Gaussian–Lorentzian band shape and Fourier transformation of the modified interferogram. The deconvolution procedure is typically repeated iteratively for best results. At iteration, the line shape is adjusted in an attempt to provide narrower bands without excessive distortion. Therefore, each IR spectrum has its characteristic peak positions.

The density ρ of the glass samples was determined using the Archimedes technique by applying toluene as an immersion fluid. At least, three samples of each glass were used to determine the density. A random error in the density values was found as ±1%. The molar volume V_m has been determined as M/D, where M is the molar weight of the glass. The values of the packing density (V_t) were calculated as $V_t = (1/V_m)\sum_i V_i x_i$, where $V_i = (4\pi/3)N_A[mR_A^3 + nR_O^3]$, R_A and R_O are the Pauling radii (Å) of ions in the oxide A_mO_n.

The ultrasonic velocities, longitudinal (ν_L) and shear ones (ν_T), at room temperature (∼300 K) were obtained using the pulse-echo method. In this method, x-cut and y-cut transducers (KARL DEUTSCH) operated at the fundamental frequency of 4 MHz along with a digital ultrasonic flaw detector (KARL DEUTSCH Echograph model 1085) were used. The uncertainty in the measurement of the ultrasonic velocity is ±10 m/s. Besides the density, two velocities were utilized to determine two independent second-order elastic constants (SOECs): C_{11} and C_{44}. For the pure longitudinal waves $C_{11} = \rho v_L^2$, and for the pure transverse ones $C_{44} = \rho v_T^2$. The bulk modulus (K_e), Young's modulus (Y), the Debye temperature (θ_D) and the Poisson's ratio (σ) may be determined using the standard relations (Rao, 2002):

$$\sigma = 1/2 - C_{44}/2(C_{11} - C_{44}), \tag{1}$$

$$Y = 2(1+\sigma)C_{44}, \tag{2}$$

$$K_e = C_{11} - 4/3C_{44}\,, \tag{3}$$

$$\theta_D = (h/k)v_D\left[\frac{3q\,\rho\,N_A}{4\pi\,M}\right]^{1/3}, \tag{4}$$

where v_D is the mean ultrasonic velocity given by $\left[\frac{1}{3}\left(\frac{1}{v_L^3} + \frac{2}{v_T^3}\right)\right]^{-1/3}$, h is the Planck's constant, N_A is the Avogadro's number, and k is the Boltzmann's constant. The uncertainty in the measurement of the elastic moduli is ±0.15 GPa.

3. Results and discussion

3.1. Structural analysis

Figure 1 shows the IR spectra of the Al_2O–Li_2O-P_2O_5 glass system with and without MoO_3 Figures 2 a–c show the deconvolution of the IR spectrum of the glasses containing different ratios of MoO_3 wt% as an

example. The main features of the IR spectra of the studied glasses are four bands at ∼525, ∼745, ∼1088 and ∼1645 cm^{-1}. The presence of MoO_3 creates two additional bands at ∼1268 and ∼1430 cm^{-1}. The common IR features of these glasses are that the absorption bands for glasses containing MoO_3 become wider, and their broadening increases with the increasing MoO_3 content. Moreover, the absorption bands are strongly overlapped especially at ∼525 and ∼1000 cm^{-1}. The position of the absorption band at ∼745 cm^{-1} was shifted to a lower wavenumber and its area became decreased. Moreover, the absorption band at 1000 cm^{-1} was shifted to a higher wavenumber.

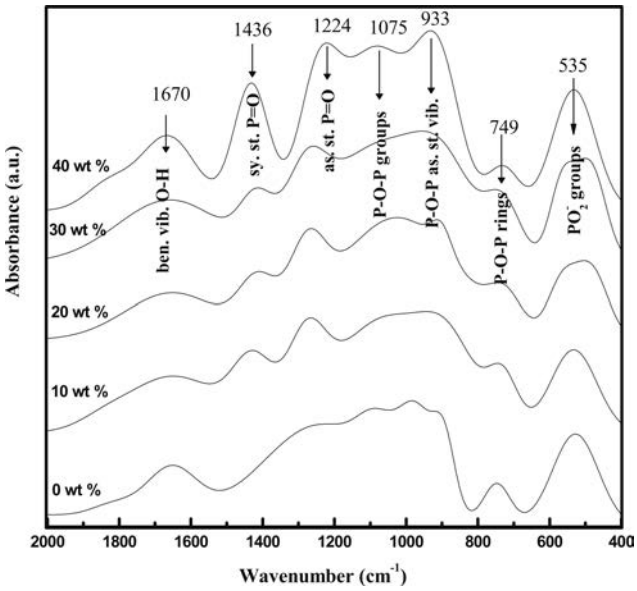

Fig. 1. Infrared absorption spectra of the glass system $2Al_2O_3$-$30Li_2O$-$68P_2O_5$-$xMoO_3$ ($0 \le x \le 40$ wt%).

The IR absorption at around 520 cm^{-1} is attributed to the bending vibrations of the O=P–O linkages (Ciceo Lucacel *et al.*, 2009). This band may be superimposed with the vibrations of the MoO_6 structural units that play a modifier role (Little Flower *et al.*, 2007). The bands at around 745 cm^{-1} are assigned to asymmetric stretching vibrations of the P–O–P rings (Moustafa *et al.*, 1998) The bands at around 910 cm^{-1} are related to P–O–P symmetric stretching vibrations of bridging oxygen atoms in the P–O–P bonds (Sudarsan *et al.*, 2004). The band at around 995 cm^{-1} can be ascribed to symmetric stretching vibration of the PO_4^{3-} tetrahedra (P–O^- ionic group) (Jastrzebski *et al.*, 2011; Lazarev, 1968; Ciceo Lucacel *et al.*, 2009) This band may be overlapped with another one ascribed to the Mo-O stretching vibration in the $[MoO_4]^{2-}$ units that play a former role (Šubčik *et al.*, 2009). The vibrational bands at around 1275 and 1410 cm^{-1} have been attributed to the asymmetric stretching of the double bonded oxygen vibrations and to the symmetric stretching mode of P=O (Sudarsan,

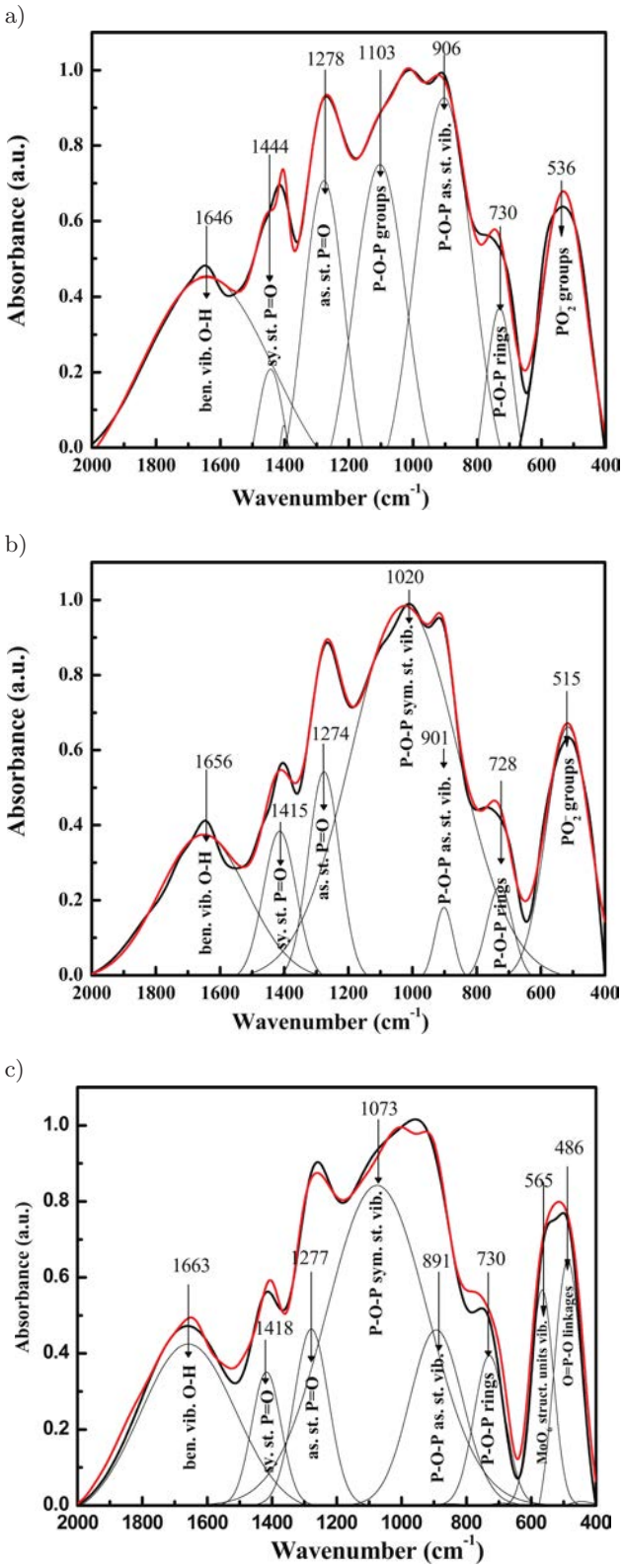

Fig. 2. Band deconvolution of the IR spectrum for $2Al_2O_3$-$30Li_2O$-$68P_2O_5$-$xMoO_3$ glass ($0 \le x \le 40$ wt%; a) $x = 10$, b) $x = 20$, c) $x = 30$

2004; Magdas *et al.*, 2008) In addition to the above features, there is a small absorption band in the spectra of all glasses at around 1660 cm^{-1}. Such a band

was attributed to the bending vibrations of O-H bonds brought by air moisture during the preparation of the KBr pellets for the infrared measurements (Khafagy, 2001; Boudlich *et al.*, 2002).

Recently, it was reported that in Li_2O-P_2O_5 glasses, the increase of the Li_2O content causes the formation of terminal phosphate groups $PO_3^{2-}$and an increase in the average length of the P=O bond (Ivascu *et al.*, 2011). An addition of Al_2O_3 to lithium phosphate glasses causes a shift of the main absorption bands of the PO_4 units to higher wavenumbers. This shift was attributed to two reasons; the first one is the formation of P–O–Al bridging bonds connected to phosphate groups instead of P–O–Li bonds where Al–O has a higher bond strength than P-O; the second one is the formation of charge compensation pairs between Li^+ and the aluminum (VI) polyhedra (Brow, 2000; Manupriya, 2009; Lide, 2004). Therefore, as represented in the studied glass system, as the MoO_3 content is increased, for $0 \leq x \leq 20$ and $20 \leq x \leq 40$ (wt%) two regions can be formed in the IR spectra as shown in Fig. 1. The features of the first region are,

a) the intensity of the vibrational bands related to the phosphate glasses is decreased,
b) the bands due to symmetric stretching vibrations of P–O–P rings are shifted to a lower wavenumber,
c) the bands due to P–O–P asymmetric stretching vibrations of the bridging oxygen atoms in the P–O–P bonds are rapidly shifted to a higher wavenumber.

These features suggest the modifier role of MoO_3 by breaking up the P–O–P linkages and occupying the positions between P–O–P layers creating NBOs to form MoO_6 without a change of the number of P=O bonds the features of the second regions are:

a) the intensity of the illustrated vibrational bands related to phosphate glasses is increased,
b) the whole of the latter bands are shifted to a higher wavenumber.

The shift of the bands can be explained by taking into account the strength of the bands and the effect of the bond energy of Mo-O. The strength of the vibrational bands can be attributed to the decrease in the phosphate chains length, the increasing ratio of the oxygen atoms to the phosphorus ones (O/P), and to the bridging of Mo with oxygen atoms to form $[MoO_4]^{2-}$ units which have a former role. In this region, MoO_3 enters the glass network by breaking up the P–O–P linkages and forming P–O–Mo bonds. Accordingly, the P=O bond will be converted into bridging oxygen and the phosphate bonds will be shortened (Higazy, 1985; Cozar *et al.*, 2006). The overlapping of the absorption bands in this region confirmed the formation of shorter bonds, and the value of O/P larger than 3 confirmed the rupture of P=O bonds. A similar behavior in tungsten lead phosphate glasses has been observed (Abid *et al.*, 2002).

3.2. Analysis of the elastic moduli

Table 1 shows the values of the density of MoO_3-Li_2O-Al_2O_3-P_2O_5 glasses with the different additions of MoO_3. The values of the density of the studied glasses agree well with that reported elsewhere (Abid, 2002; Montenero, 2004; Cozar et al., 2006). In general, both the packing of the glass network and the molecular weight of each contributed oxide affect the density in the glass system. It is generally accepted that the density increases when the concentration of the third component (MoO_3) is increased while the ratio of the other concentrations remain always constant.

On the other hand, the packing density of Li_2O, Al_2O_3, P_2O_5 and MoO_3 are considered to be 8, 21.5, 34.8 and 21.3 $m^3\,mol^{-1}$, respectively (Wells, 1975; Saddeek, 2011). Accordingly, the Mo^{3+} ions can occupy an interstitial position in the interstices of the lithium phosphate network increasing the connectivity of the structure with further addition of the MoO_3 content. Thus, the increase in the density can be related to the constitution of the glasses rather than to the type of the structural unit.

As reported earlier, the ultrasonic velocity into a glassy material depends on the rigidity, cross-link density and the number of bonds per unit volume of the structure of the glasses, i.e. a harder material will produce a higher velocity, whereas a softer material will produce lower velocity, irrespective of their densities (Bridge, 1986; Saddeek, 2007; Eraiah *et al.*, 2010). The variation of the values of the longitudinal and shear ultrasonic wave velocities with the MoO_3 content is listed in Table 1. The ultrasonic velocities, Debye temperature (θ_D), and the elastic moduli, i.e. the Young's modulus (Y) and bulk modulus (K_e) of the studied glasses, increase while the Poisson's ratio decreases with the increase of the MoO_3 content.

According to the IR analysis, there is some type of modification of the chemical bonds linked to the phosphate structural units with the addition of MoO_3 in the interstices of the lithium phosphate network This addition creates $[MoO_4]^{2-}$ structural units bridging oxygens and smaller rings of the phosphate groups. This creation is associated with an increase of O/P and bridging bonds P-O-Mo that has high bond energy. These factors contribute to the increase of the average crosslink density (n_c) and to the number of network bonds per unit volume (n_b) of the glass system. The average crosslink density and the number of network bonds per unit volume can be estimated according to an earlier work (Higazy et al., 1985). Thus, the observed increase in the ultrasonic velocity can be explained by assuming that, Mo^{3+} enter interstitially and as a result some type of modification of the P–O–P, and Li–O–P linkages, which already exist in the glass, into Mo–O–P, and Li–O–P bonds will occur. The conversion of these linkages results in an increase in

Table 1. The density (ρ), packing density (V_t), longitudinal (v_L) and shear (v_T) ultrasonic velocities, Debye temperature (θ_D), Poisson's ratio (σ), average cross link density (n_c), number of network bonds per unit formula unit (n_b), Young's modulus (Y), and the bulk modulus (K_e) of the glass system $2Al_2O_3$-$30Li_2O$-$68P_2O_5$-$xMoO_3$ glass (where $x = 0$, 10, 20, 30 and 40 wt%).

Composition of glass wt%				ρ	V_t	v_L	v_T	θ_D	σ	n_c	$n_b \times 10^{28}$	Y	K_e
Li_2O	Al_2O_3	P_2O_5	MoO_3	[kg/m^3]	–	[m/s]	[m/s]	[K]	–	–	[m^3]	[GPa]	[GPa]
30	2	68	0	3566	0.60	4103	2210	332.2	0.217	2.84	7.11	68.6	35.44
30	2	68	10	3644	0.62	4155.8	2245	341	0.215	2.90	7.31	69.7	35.98
30	2	68	20	3717	0.64	4202	2278	348.7	0.212	2.97	7.54	70.7	36.60
30	2	68	30	3758	0.66	4251.5	2313	358.6	0.209	3.03	7.78	71.9	37.22
30	2	68	40	3805	0.67	4324.1	2355	367.4	0.208	3.10	7.96	73.1	38.26

the packing density, which contract the glass network. Therefore, the structure of the glass will be strengthened and hence the increase of the rigidity will contribute to the increase in the ultrasonic velocity.

In solid materials, the Debye temperature (θ_D) plays an important role in the determination of elastic moduli and atomic vibrations. θ_D represents the temperature at which all the low frequency 'lattice' vibrational modes are excited (Rao, 2002). As a consequence, the Debye temperature, θ_D, which depends directly on the mean ultrasonic velocity and on the atomic vibrations of the lighter structural groups like phosphates will increase as the MoO_3 content increases. The increase in θ_D can be explained by taking into account two factors. Firstly, the clear shift of the vibrational modes in the IR absorption spectra towards higher frequencies as the MoO_3 content increases and the change in the relative strength of bonds in the glass network. The bond strength of Li_2O, Al_2O_3, P_2O_5 and MoO_3 are 77.9, 119.2, 28.2 and 69.8×10^9 J m^{-3} (Lide, 2004). The increase of the bond strength, the rigidity and the average cross-link density of the studied glasses decrease the Poisson's ratio.

The values of the bulk modulus (K_e) and Young's modulus (Y) are listed in Table 1. As discussed before, addition of MoO_3 to the Li_2O-Al_2O_3-P_2O_5 glass creates new linkages attached to the phosphate structural units. These linkages have a high bond energy and increase both the number of bonds per unit glass formula unit and the packing density of the glass structure. On the other hand, the bulk modulus of a covalent network is determined by the bond density (number of bonds in a unit volume), and by the stretching force constant. The stretching force constant is related to the cation field strength of the modifier, i.e. high field strength cations polarize their environment strongly and enhance the ion-dipole interaction. Thus, the increase in the packing density can be attributed to two factors, firstly, the change in the coordination polyhedra of MoO_3 from MoO_6 to MoO_4, which in its turn change the type of bonding of the investigated glasses and secondly, the local contraction of the network around the Mo and Li cations that have a high-field-strength which polarizes their environment strongly and enhances the ion-dipole interactions. However, the elastic moduli are sensitive in a greater extent to the density of covalent bonds in the structure, which resist deformation. Therefore, it can be concluded that the elastic moduli will increase and these conclusions are in agreement with that reported earlier (Damodaran, 1989; Sidkey, 2002; Muńoz *et al.*, 2004; Saddeek *et al.*, 2009).

4. Conclusion

The analysis of IR spectra indicates that the Mo^{3+} ions are preferentially incorporated into the phosphate network as former forming the $[MoO_4]^{2-}$ units. New bonds have a high bond strength and bridging oxygens were created. The sound velocities, Debye temperature, and the elastic properties show an increasing trend with the increase in the MoO_3 content. This behavior was attributed to the increase of the cross link density; the number of network bonds per unit volume, the rigidity as well as the high-field-strength of Mo^{3+} polarizes their environment strongly.

Further work is required to study the electrical and optical properties of these materials with and without the radiation effect to improve the use in optoelectronic devices.

Acknowledgments

The authors wish to thank Al-Azhar University-Egypt for the financial support. Also, Prof. Dr. Moenis Azzoz, Glass department, National research center, Dokki, Cairo – Egypt is acknowledged for his help and fruitful discussions. The authors also wish to express their gratitude to Mr. Khamis Shaaban, Physics department, Faculty of science, Al-Azhar University-Egypt for his kind helps in preparation of glass samples.

References

1. Abid M., Elmoudane M., Et-tabirou M. (2002), *Spectroscopic studies of the structure of sodium lead oligophosphate glasses*, Phys. Chem. Glasses, **43**, 267–270.
2. Bih L., Abbas L., Nadiri A., Khemakhem H., Elouadi B. (2008), *Investigations of molybdenum redox phenomenon in Li_2O–MoO_3–P_2O_5 phosphate glasses*, J. Mol. Struct. **872**, 1–9.
3. Boudlich D., Bih L., El Hassane Archidi M., Haddad M., Yacoubi A., Nadiri A., Elouadi B. (2002), *Infrared, Raman, and Electron Spin Resonance Studies of Vitreous Alkaline Tungsten Phosphates and Related Glasses*, J. Am. Ceram. Soc., **85**, 623–630.
4. Bridge B., Patel N. (1986), *The elastic constants and structure of the vitreous system Mo-P-O*, J. Mater. Sci., **21**, 1187–1205.
5. Bridge B., Patel N. (1987), *Composition dependence of the infra-red absorption spectra of molybdenum phosphate glasses and some crystalline analogues*, J. Non-Cryst. Solids, **91**, 27–42.
6. Brow R., Click C., Alam T. (2000), *Modifier coordination and phosphate glass networks*, J. Non-Cryst. Solids, **274**, 9–16.
7. Brow R. (2000), *Review: the structure of simple phosphate glasses*, J. Non-Cryst. Solids, **263**, 1–28.
8. Campbell J., Suratwala T. (2000), *Nd-doped phosphate glasses for high-energy/high-peak-power lasers*, J. Non-Cryst. Solids, **263**, 318–341.
9. Chowdari B., Gopalakrishnan R., Tang S., Kuok M. (1988), *Characterization of Ag_2O:MoO_3:P_2O_5 glasses*, Solid State Ion., **28**, 704–709.
10. Chowdari B., Tan K., Chia W., Gopalakrishnan R. (1991), *Thermal, physical, electrical and XPS studies of the Li_2O: P_2O_5: MoO glass system*, J. Non-Cryst. Solids, **128**, 18–29.
11. Ciceo Lucacel R., Hulpus A., Simon V., Ardelean I. (2009), *Structural characterization of phosphate glasses doped with silver*, J. Non-Cryst. Solids, **355**, 425–429.
12. Cozar O., Magdas D., Ardelean I. (2008), *EPR study of molybdenum-lead-phosphate glasses*, J. Non-Cryst. Solids, **354**, 1032–1035.
13. Cozar O., Magdas D., Nasdala L., Ardelean I., Damian G. (2006), *Raman spectroscopic study of some lead phosphate glasses with tungsten ions*, J. Non-Cryst. Solids, **352**, 3121–3125.
14. Dai S., Sugiyama A., Hu L., Liu Z., Huang G., Jiang Z. (2002), *The spectrum and laser properties of ytterbium doped phosphate glass at low temperature*, J. Non-Cryst. Solids, **311**, 138–144.
15. Damodaran K., Rao K. (1989), *Elastic Properties of Alkali Phosphomolybdate Glasses*, J. Am. Ceram. Soc., **72**, 533–539.
16. Donald I. (1989), *Methods for improving the mechanical properties of oxide glasses*, J. Mater. Sci., **24**, 4177–4208.
17. ElBatal H., Hamdy Y., Marzouk S. (2008), *Gamma ray interactions with V_2O_5-doped sodium phosphate glasses*, Mater. Chem. Phys., **112**, 991–1000.
18. Eraiah B., Smitha M., Anavekar R. (2010), *Elastic properties of lead-phosphate glasses doped with samarium trioxide*, J. Phys. Chem. Solids, **71**, 153–155.
19. Higazy A., Bridge B. (1985), *Elastic constants and structure of the vitreous system Co_3O_4-P_2O_5*, J. Non-Cryst. Solids, **72**, 81-108.
20. Hudgens J., Brow R., Tallant D., Martin S. (1998), *Raman spectroscopy study of the structure of lithium and sodium ultraphosphate glasses*, J. Non-Cryst. Solids, **223**, 21-31.
21. Ivascu C., Timar Gabor A., Cozar O., Daraban L., Ardelean I. (2011), *FT-IR, Raman and thermoluminescence investigation of P_2O_5–BaO–Li_2O glass system*, J. Molec. Struct., **993**, 249–253.
22. Jastrzebski W., Sitarz M., Bułat K. (2011), *Infrared spectroscopy of different phosphates structures Spectrochim*, Acta A, **79**, 722–727.
23. Jiang S., Myers M., Peyghambarian N. (1998), *Er^{3+} doped phosphate glasses and lasers*, J. Non-Cryst. Solids, **239**, 143–148.
24. Khafagy A. (2001), *Infrared and Ultrasonic Investigations of Some $[(MnO_2)_x$–$(P_2O_5)_{100-x}]$.1 wt% Nd_2O_3 Glasses*, Phys. Stat. Sol. (a), **186**, 105–114.
25. Lazarev A. (1968), *Kolebatielnyje spektry i strojenije silikatov* [in Russian], Nauka, Leningrad.
26. Lide D. (2004), *CRC Handbook of Chemistry and Physics*, 84th edition, CRC Press, Boca Raton, Fl.
27. Little Flower G., Sahaya Baskaran G., Srinivasa Reddy M., Veeraiah N. (2007), *The structural investigations of PbO–P_2O_5–Sb_2O_3 glasses with MoO_3 as additive by means of dielectric, spectroscopic and magnetic studies*, Physica B, **393**, 61–72.
28. Magdas D., Cozar O., Chis V., Ardelean I., Vedeanu N. (2008), *The structural dual role of Fe_2O_3 in some lead-phosphate glasses*, Vib. Spectrosc., **48**, 251–254.
29. Manupriya K., Thind K., Singh G., Sharma, Rajendran V. (2009), *Influence of addition of Al_2O_3 on physical, structural, acoustical and in-vitro bioactive properties of phosphate glasses*, Phys. Status Solidi A, **206**, 1447–1455.
30. Montenero A., Aielli M., Gnappi G., Lorenzi A., Sglavo V., Royer Carfagni G. (2004), *Mechanical properties of PbO–ZnO–P_2O_5 glasses*, Phys. Chem. Glasses, **46**, 538–543.
31. Moustafa Y., El-Egili K. (1998), *Infrared spectra of sodium phosphate glasses*, J. Non-Cryst. Solids, **240**, 144–153.
32. Muñoz F., Agulló-Rueda F., Montagne L., Marchand R., Durán A., Pascual L. (2004), *Structure and properties of $(25\text{-}x/2)Li_2O.(25\text{-}x/2)Na_2O.xPbO.50P_2O_5$ metaphosphate glasses*, J. Non-Cryst. Solids, **347**, 153–158.

33. Prasad S., Sahaya Baskaran G., Veeraiah N. (2005), *Spectroscopic, magnetic and dielectric investigations of $BaO–Ga_2O_3–P_2O_5$ glasses doped by Cu ions*, Phys. Stat. Sol.(a), **202**, 2812–2828.

34. Proulx P., Cormier G., Capobianco J., Champagnon B., Bettinelli M. (1994), *Raman and low frequency Raman spectroscopy of lead, zinc and barium metaphosphate glasses doped with Eu^{3+} ions*, J. Phys. Condens. Matter, **6**, 275–283.

35. Rao K. (2002), *Structural Chemistry of Glasses*, Elsevier, North Holland.

36. Reis S., Faria D., Martinelli J., Pontuschka W., Day D., Partiti C. (2002), *Structural features of lead iron phosphate glasses*, J. Non-Cryst. Solids, **304**, 188–194.

37. Saddeek Y. (2011), *Network structure of molybdenum lead phosphate glasses: Infrared spectra and constants of elasticity*, Physica B, **406**, 562–566.

38. Saddeek Y., Afifi H., Abd El-Aal N. (2007), *Interpretation of mechanical properties and structure of $TeO_2–Li_2O–B_2O_3$ glasses*, Physica B, **398**, 1–7.

39. Saddeek Y., Gaafar M., Bashier S. (2010), *Structural influence of PbO by means of FTIR and acoustics on calcium alumino-borosilicate glass system*, J. Non-Cryst. Solids, **356**, 1089–1095.

40. Saddeek Y., Shaaban E., Aly A., Sayed I. (2009), *Characterization of some lead vanadate glasses*, J. Alloys and Compounds, **478**, 447–452.

41. Selvaraj U., Rao K. (1985), *Characterization Studies of Molybdophosphate Glasses and a Model of Structural Defects*, J. Non-Cryst. Solids, **72**, 315–334.

42. Sharaf El-Deen L., Al Salhi M., Elkholy M. (2008), *Spectral properties of PbO–P2O5 glasses*, J. Non-Cryst. Solids, **354**, 3762–3766.

43. Sidkey M., El Mallawany R., Abousehly A., Saddeek Y. (2002), *Relaxation of longitudinal ultrasonic waves in some tellurite glasses*, Mater. Chem. Phys., **74**, 222–229.

44. Šubčik J., Koudelka L., Mošner P., Montagne L., Revel B., Gregora I. (2009), *Structure and properties of MoO_3-containing zinc borophosphate glasses*, J. Non-Cryst. Solids, **355**, 970–975.

45. Sudarsan V., Mishra R., Kulshreshth S. (2004), *Thermal and structural studies on TeO_2 substituted $(PbO)_{0.5}(P_2O_5)_{0.5}$ glasses*, J. Non-Cryst. Solids, **342**, 160–165.

46. Wells A. (1975), *Structural Inorganic Chemistry*, 4th edition, Clarendon Press, Oxford.

PAN ARCHIVES OF ACOUSTICS
Vol. **37**, No. 3, pp. 349–354 (2012)

DOI: 10.2478/v10168-012-0044-1

Correction of Acoustics in Historic Opera Theatres with the Use of Schroeder Diffuser

Tadeusz KAMISIŃSKI

AGH University of Science and Technology
al. A. Mickiewicza 30, 30-059 Kraków, Poland; e-mail: kamisins@agh.edu.pl

(*received July 16, 2012; accepted July 24, 2012*)

The paper deals with the problem of acoustic correction in historic opera theatres with the auditorium layout in the form of a horseshoe with deep underbalcony cavities limited with a semicircular wall surface. Both geometry of the cavities and excessive sound absorption determine acoustic phenomena registered in this area of the hall. The problem has been observed in the Theatre of Opera and Ballet in Lviv, Ukraine, where acoustic tests were carried out, simulation calculations performed, and finally a diffusion panel worked out designed for the rear wall of the underbalcony space. Acoustic measurements carried out after installation of the diffusers revealed favourable changes in the sound strength factor G within the range of medium and high frequencies in the underbalcony and auditorium centre area. By replacing textile tapestry with diffusion panels, a significant reduction of sound absorption was achieved for the frequency range above 1 kHz and an increase of uniformity of acoustic parameters registered in the hall. The method presented in the paper can be applied in historic halls of the similar type as well as contemporary rooms where there is a need for correction of acoustic flaws related to sound focusing or the echo effect.

Keywords: opera house, Schroeder diffuser, Lviv, underbalcony, horseshoe plan, focusing, scattering.

1. Introduction

Period opera theatre houses on a horseshoe plan also contemporarily maintain their special position as outstandingly fine interiors. Such halls offer the sense of closeness of the sound source and good eye contact among the audience. Large number of boxes and sumptuous decor contribute to better sound diffusion on one hand, but increase acoustic absorption on the other resulting frequently in excessive reduction of the reverberation time. Another problem encountered in halls of that type consists in transferring the first reflection of the sound from walls, that in many cases are fully occupied by boxes. Other elements difficult for both an architect and an acoustician are underbalcony cavities situated by the hall's rear wall with concave geometry. Unfavourable dimensions of the cavity, acoustic absorption of the wall tapestry and chair upholstery as well as sound focusing effect of the rear wall result in deterioration of subjective reception of both music and speech.

A complex of unfavourable acoustic phenomena occurring in underbalcony areas of theatres with layout in the form of a horseshoe induced the present author to undertake studies on possible ways to overcome the difficulty. The issues reported in this paper are based on acoustic simulation and experimental studies carried out in connection with rehabilitation of the Lviv Theatre of Opera and Ballet started in 2008 (Kamisiński *et al.*, 2009) (Fig. 1). Installation of Schroeder diffusers on the rear semicircular underbalcony wall of the house in May 2012 constituted

Fig. 1. An overall view of the Opera House in Lviv.

a crowning of the planned acoustic correction of the interior.

The Salomea Kruszelnicka Lviv State Academic Theatre of Opera and Ballet designed by Zygmunt Gorgolewski has been erected in the year 1900. The Opera's auditorium has the volume of 5,500 m^3 and 998 seats (of which 404 in stalls and 576 in boxes), resulting in the space volume of 4.69 m^3 per person with the stage volume of 10,700 m^3 and orchestra pit volume of about 100 m^3. The research work on and analysis of the Opera House's acoustic parameters and materials carried out by the present author revealed that in the underbalcony space there was excessive sound attenuation in the range of higher frequencies. In order to improve audition conditions it has been decided that the quantity of sound-absorbing element would be reduced by a change of finish of the rear wall under the balcony.

Reduction of sound absorption introduced by the rear wall results in more acoustic energy being reflected and directed back to spectators. In theatres constructed on a horseshoe plan, the rear wall is concave in most cases with the focal point located in the region of the hall centre (Iannace, Ianniello, 2008). Therefore application of a reflective material would result in intensified focusing of sound reflected from the rear wall and consequently, arising of acoustic faults such as coloration in the auditory centre or an echo on the stage and in the front portion of the auditorium area (Gołaś, Suder–Dębska, 2008).

An example of the use of Schroeder diffuser in a concert interior of historic interest is the Carnegie Hall in New York (Fig. 2). On the rear flat wall, the diffuser was installed in order to reduce echo heard on the stage (Cox, D'Antonio, 2003).

Fig. 2. Schroeder diffusers (QRDs) applied to the rear wall of Carnegie Hall to prevent echoes.

Figure 3 shows a view of the underbalcony space in the Lviv Opera House hall before installation of diffusion panels. In this case, it has been decided that the diffuser would be installed on a semicircular wall which would allow to test the function of the structure in different geometrical situations.

Fig. 3. A view of semicircular underbalcony space in Lviv Opera House before installation of diffusion panels.

2. Numerical simulations

In order to evaluate the effect of the diffusing structure planned to be installed on the hall's rear wall, computer simulations were carried out for distributions of acoustic parameters in this area. The numerical model was implemented in CATT-Acoustic program with the use of geometrical data characterising the hall and results obtained from laboratory tests of decor materials (upholstery, tapestries, lambrequins) (Kamisiński *et al.*, 2010b). Validation of the model was based on the measured acoustic parameters of the interior before installation of the diffusion panels. The numerical simulations were carried out for situations without the diffuser and for the conditions taking into account the sound absorption and diffusion parameters of the diffuser's prototype measured by means of the laboratory method.

Results of both simulations are presented in Figs. 4a and 4b. To illustrate the effect of the planned adaptation, the parameter known as the sound strength G was selected, defined by means of formula (Kulowski, 2011):

$$G = 10 \log \frac{\int_0^\infty p^2(t)\,\mathrm{d}t}{\int_0^\infty p_{10}^2(t)\,\mathrm{d}t} \tag{1}$$

where $p(t)$ is the impulse response (acoustic pressure as a function of time) and p_{10} – the impulse response in free field at distance of 10 m from a sound source with the same acoustic power as the source used in the measurements.

Parameters G_{mid} and $G_{4\,\mathrm{kHz}}$ used further in this paper refer to the octave frequency bands for which the calculations were carried out, 0.5–1 kHz and 4 kHz, respectively.

The performed analyses of distribution of the sound strength G revealed that in the area close to the

a)

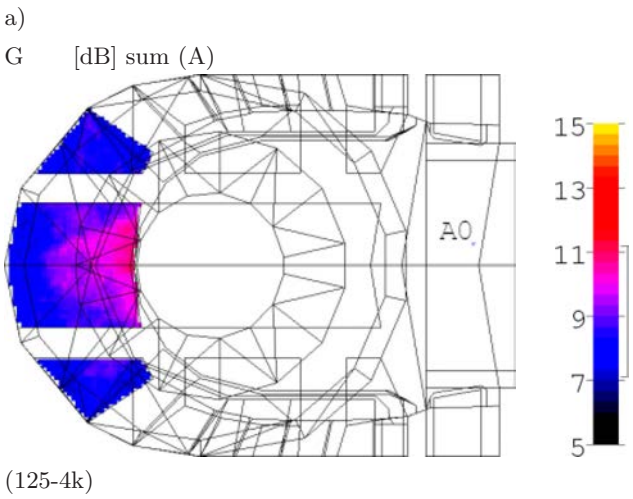

b)

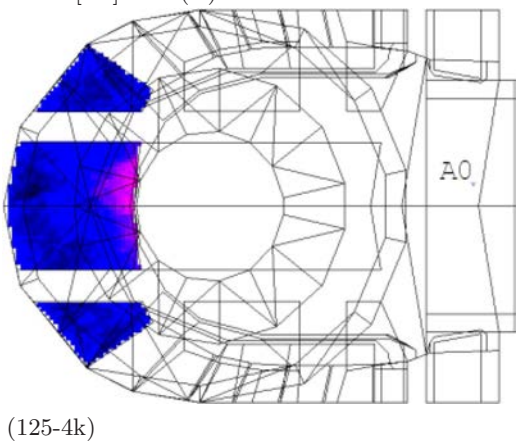

Fig. 4. The forecasted distribution of G values under the balcony in the hall's stalls: a) wall with tapestry; b) wall with the diffuser.

hall centre a decrease of value of the indicator occurred after installation of the diffuser in the underbalcony cavity, but distribution of the parameter has clearly gained in evenness as a result of occurrence of diffused reflections. Based on the observation one can conclude that introduction of sound diffusing element onto the rear wall will cause reduction of the sound focusing phenomena in this area and have a positive effect on audition qualities. Much better results should be expected when observing the simulated parameters for frequencies above 1 kHz, as in this very range the sound absorption is being reduced, and diffusion increased (Fig. 4). When interpreting the plots, one should also bear in mind the limitations of the ray method used by CATT-Acoustic program.

Figure 5 shows the forecasted distribution of C_{80} parameter under the balcony on the hall's stalls for: (a) the back wall with textile tapestry; (b) the same wall with Schroeder diffuser. The parameter, known as the clarity and expressed in dB, is defined as (Miśkiewicz *et al.*, 2012):

$$C_{80} = 10 \log \frac{\int_0^T p^2(t)\,\mathrm{d}t}{\int_T^\infty p^2(t)\,\mathrm{d}t}, \tag{2}$$

where T (80 ms) is the time elapsed after arrival of the direct sound.

Analysis of simulation shows (Fig. 5) that the use of the diffuser will result in an increase of the sound clarity C_{80} in last rows of the stalls.

Figure 6 shows the comparison of sound absorption coefficient values for textile tapestry and the diffusion panel.

According to the adopted assumptions, a solution that will allow to avoid the effect consists in application

a)

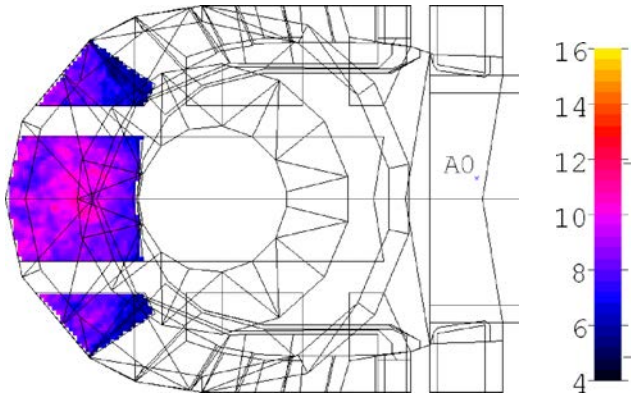

b)

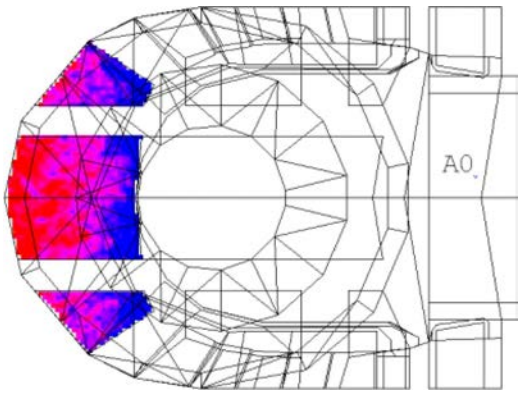

Fig. 5. Forecasted distribution of C_{80} values under the balcony in the hall's stalls: a) wall with tapestry; b) wall with the diffuser.

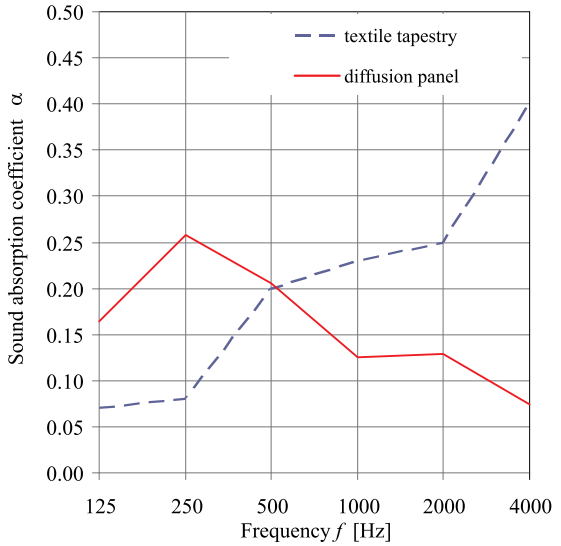

Fig. 6. Comparison of sound absorption coefficient values for textile tapestry and the diffusion panel.

of sound diffusing structures (Figs. 7 and 8) thanks to which the sound wave incident onto the wall will be diffused uniformly in all directions (Kamisiński *et al.*, 2010a).

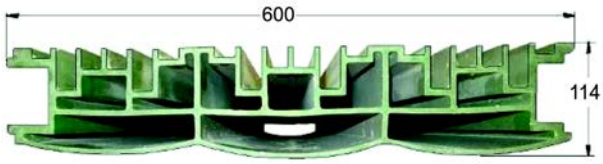

Fig. 7. Cross-section of the diffusion panel.

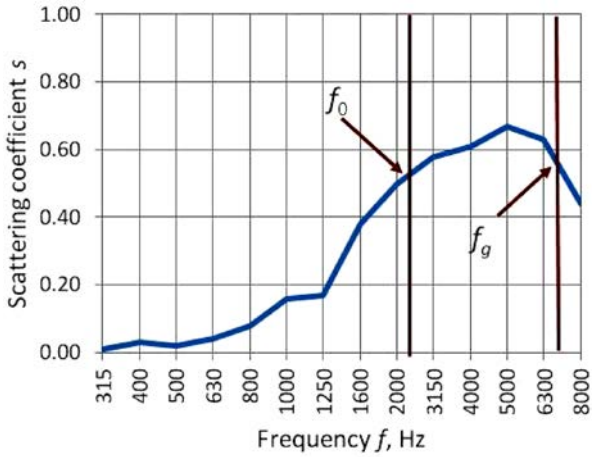

Fig. 8. The sound scattering coefficient s of the diffusion panel determined according to ISO 17497-1 (2004).

In Fig. 8, the lower f_0 and the upper f_g limit frequencies for sound diffusing effect of the examined structure are marked. It is assumed that the structure has the capacity to redirect the sound starting from frequency equalling 0.5 f_0 (Cox, D'Antonio, 2004). The design frequency f_0 is determined by the maximum depth of the diffuser. In the Opera House there was a very limited space designed for the diffuser, therefore it was very difficult to lower f_0. What is more, as indicated by (Pilch, Kamisiński, 2011), the higher deep-to-width ratio of one well of diffuser, the bigger sound absorption of the entire structure in low and mid frequency range. Consequently it was impossible to increase the range of effective diffusion of panels without interference with the reverberation time of the hall.

3. The follow-up tests in the Opera House

Repeated examination of the Opera House hall's acoustic parameters carried out, according to the predetermined methodology, before and after installation of the structure on the rear wall, was used for verification of the implemented system. To increase precision of the analysis of acoustic phenomena occurring in locations where main changes were forecasted, the grid of measurement points has been condensed in the area under the balcony in the centre of the Opera's stalls (Fig. 9).

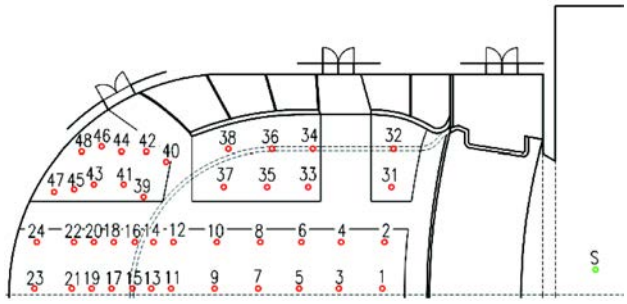

Fig. 9. Distribution of measurement points in the hall's stalls.

Figure 10 shows a view of semicircular back wall of the underbalcony space in the Lviv Opera House after installation of diffusion panels in the course of verification measurements.

Fig. 10. A view of the semicircular back wall behind the underbalcony space in the Lviv Opera House after installation of diffusion panels.

A comprehensive review of the measured acoustic parameters of the hall revealed that the parameters showing the highest sensitivity to introduction of the structure were the sound strength factors G_{mid} and $G_{4\,\mathrm{kHz}}$. The following Figs. 11 and 12 show distribution of the parameters on the auditorium's stalls surface.

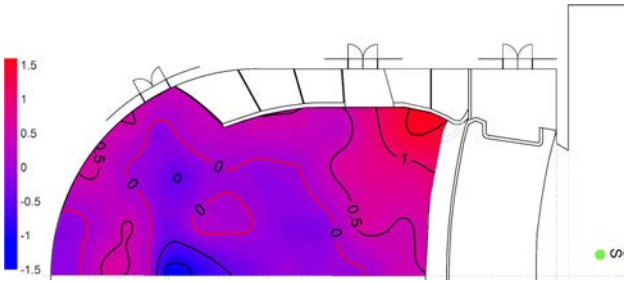

Fig. 11. Distribution of the sound strength G_{mid} increase after installation of the diffuser.

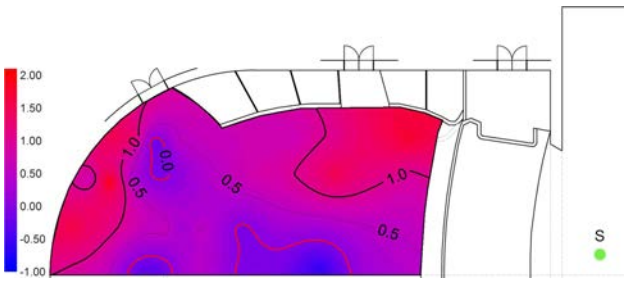

Fig. 12. Distribution of the sound strength factor $G_{4\,\mathrm{kHz}}$ increase after installation of the diffuser.

After application of the diffuser on the rear wall, one can observe a slight increase of value of the sound strength factor G_{mid} in the underbalcony area, while in the central part of the hall, values of the parameter have been reduced.

Values of the $G_{4\,\mathrm{kHz}}$ parameter, as shown in the figure above, are subject to distinct decrease in the central part of the hall, and locally increased as a result of providing the semicircular wall with the diffuser.

Analysis of the sound clarity index C_{80} for the 4 kHz has revealed (Fig. 13) that as a result of installation of the diffuser, values of the parameter significantly decreased on the hall's axis.

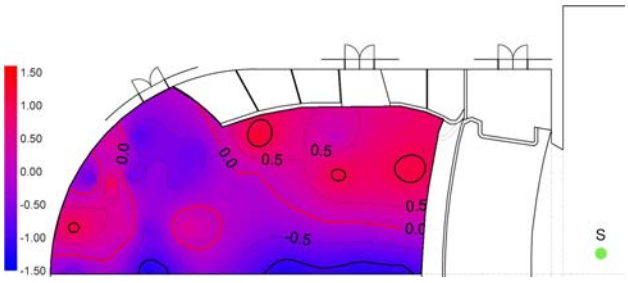

Fig. 13. Distribution of the sound clarity index $C_{80\,4\,\mathrm{kHz}}$ increase after installation of the diffuser.

$G_{80\,4\,\mathrm{kHz}}$ (the early sound strength) and $G_{\mathrm{L}\,4\,\mathrm{kHz}}$ (the late sound strength) for 4 kHz were also investigated. On the basis of measurement before and after installation of the diffuser (Fig. 14), it can be said that the sound strength is changed mainly in the early part, as $G_{80\,4\,\mathrm{kHz}}$ is very similar to $G_{4\,\mathrm{kHz}}$. $G_{\mathrm{L}\,4\,\mathrm{kHz}}$ distribution is very regular and reveals an about 0.7 dB increase for the whole stalls surface.

a)

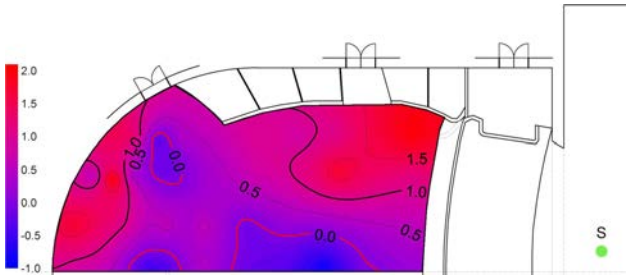

b)

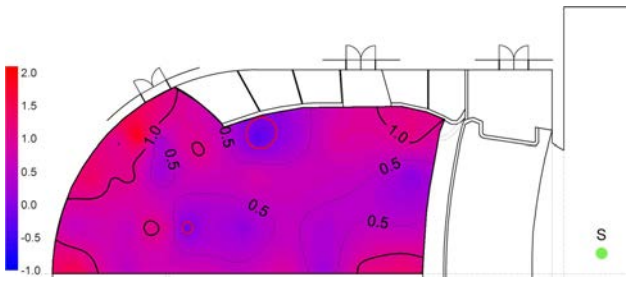

Fig. 14. Distribution of differences of sound strength factors: a) $G_{80\,4\,\mathrm{kHz}}$ and b) $G_{\mathrm{L}\,4\,\mathrm{kHz}}$.

4. Summary

The analysis of acoustic parameters of the Lviv Opera House hall measured before and after installation of the diffuser has shown that the best parameters allowing for observation of the discussed structure's effect were the sound strength values G_{mid} and $G_{4\,\mathrm{kHz}}$. To this end, interpolated distributions of measured values of the parameters over the stalls area were worked out. Parameters G_{mid} and $G_{4\,\mathrm{kHz}}$ are presented in the form of difference of values observed before and after installation of the diffuser (Figs. 11 and 12).

According to the generally observed regularity, value of the sound strength factor G_{mid} decreases with increasing distance to the sound source. On the other hand, in the central part of the hall, some increase of the parameter values can be observed caused by sound focusing effect of the back wall's concave surface. After installation of the diffusing structure, the effect has been reduced, as confirmed by the measured values of the sound strength factor and the distribution of increase in G_{mid} (Fig. 11). The observed change occurs for frequencies 500 and 1 kHz, i.e. below the frequency for which the designed diffusion panel effec-

tively diffuses the sound. Analysing absorption characteristics of the textile tapestry and the diffusing structure (Fig. 6) it can be found that below the frequency of 1 kHz, the diffuser is characterised with the sound absorption coefficient higher than this of the tapestry. As a result, after installation of the diffuser, a portion of energy is absorbed and does not come back to the auditorium. Above 1 kHz, sound diffusion starts to manifest itself with low absorption, giving the acoustic energy back to the hall in a way ensuring its uniform distribution. The phenomenon has been confirmed by means of analogous observation of the parameter $G_{4\,\mathrm{kHz}}$ that more clearly depicts the effect of the diffuser on the hall's acoustic field.

The performed research work revealed that significant changes in acoustic parameters occur for early reflections of waves incoming within the time interval of 80 ms, as can be seen from distribution of parameters G_{80} and C_{80} (Fig. 13). Its effect in later instants of time is not noticeable, as can be found based on analysis of the factor G_{L} (Fig. 14b).

Considering the function that the applied diffuser has accomplished in the hall's space one can claim on the grounds of the obtained results of the study that the range of its effect encompasses the seats under the balcony situated in front of the diffuser and the seats in the centre of the stalls. These are the regions of old opera houses constructed typically on a horseshoe plan where significant unevenness in distribution of acoustic parameters is observed as a result of concave shape of the rear wall. The use of the Schroeder diffuser allows to eliminate at least some of the related flaws.

It is worth mentioning that despite some earlier fears, the technocratic design of the Schroeder diffuser, after careful selection of the colour scheme, has ultimately won the acceptance of both the artistic milieu and the heritage conservation supervising authorities.

References

1. Cox T.J., D'Antonio P. (2004), *Acoustic Absorbers and Diffusers*, Taylor & Francis Ltd, 2nd Ed., London.
2. Cox T.J., D'Antonio P. (2003), *Engineering art: the science of concert hall acoustics*, Interdisciplinary Science Reviews, **28**, 2, 1119–1129.
3. Gołaś A., Suder–Dębska K. (2008), *Analysis of Dome Home Hall Theatre Acoustic Field*, Archives of Acoustics, **34**, 3, 273–293.
4. Iannace G., Ianniello E. (2008), *Sound-focusing effects in the plan of horse-shoe shaped opera theatres*, Proceedings of Acoustics' 08, pp. 2151–2156, Paris.
5. Kamisiński T., Kinasz R., Pilch A., Rubacha J. (2009), *Experimental study of acoustic parameters of the Lviv opera house concert hall* [in Polish], Proceedings of 16th Conference on Acoustic and Biomedical Engineering, pp. 16–17, Kraków–Zakopane.
6. Kamisiński T., Rubacha J., Pilch A. (2010a), *The Study of Sound Scattering Structures for the Purposes of Room Acoustics Enhancement*, Acta Physica Polonica A, **118**, 1, 83–86.
7. Kamisiński T., Kinasz R., Pilch A., Rubacha J. (2010b), *Acoustical correction of underbalcony cavities in Lviv Opera Hall* [in Polish], Technical Transactions, **107**, 8, 7–14.
8. Kulowski A. (2011), *Acoustics of Halls,* [in Polish: *Akustyka Sal*], Wydawnictwo PG, Gdańsk.
9. Miśkiewicz A., Rogala T., Rościszowska T., Rudzki T., Fidecki T. (2012), *Concert Hall Sound Clarity: A Comparison of Auditory Judgments and Objective Measures*, Archives of Acoustics, **37**, 1, 41–46.
10. Pilch A., Kamisiński T. (2011), *The Effect of Geometrical and Material Modification of Sound Diffusers on Their Acoustic Parameters*, Archives of Acoustics, **36**, 4, 955–966.
11. Standard ISO 17497-1 (2004), Sound scattering properties of surfaces. Part 1: Measurement of the random-incidence scattering coefficient in a reverberation room.

PAN ARCHIVES OF ACOUSTICS
Vol. **37**, No. 3, pp. 355–363 (2012)

DOI: 10.2478/v10168-012-0045-0

Perception of Mixture of Musical Instruments with Spectral Overlap Removed

Piotr KLECZKOWSKI

AGH University of Science and Technology
al. A. Mickiewicza 30, 30-059 Kraków, Poland; e-mail: kleczkow@agh.edu.pl

(*received June 27, 2011; accepted July 24, 2012*)

The issue of auditory segregation of simultaneous sound sources has been addressed in speech research but was given less attention in musical acoustics. In perception of concurrent speech, or speech with noise, the operation of time-frequency masking was often used as a research tool. In this work, an extension of time-frequency masking, leading to the removal of spectro-temporal overlap between sound sources, was applied to musical instruments playing together. The perception of the original mixture was compared with the perception of the same mixture with all spectral overlap electronically removed. Experiments differed in the method of listening (headphones or a loudspeaker), sets of instruments mixed, and populations of participants. The main findings were: (i) in one of the experimental conditions the removal of spectro-temporal overlap was imperceptible, (ii) perception of the effect increased when removal of spectro-temporal overlap was performed in larger time-frequency regions rather than in small ones, (iii) perception of the effect decreased in loudspeaker listening. The results support both the multiple looks hypothesis and the "glimpsing" hypothesis known from speech perception.

Keywords: sound segregation, spectral overlap, spectrogram, auditory scene analysis, time-frequency mask, multiple looks, glimpses.

1. Introduction

The auditory system's mechanisms for extracting sounds from separate sources rely on spatial, time and spectral parameters. It is well known that the segregation task becomes more difficult when spectro-temporal patterns of sounds overlap. Investigation on how the ear copes with overlapping sounds is a difficult task, as it involves: non-linear addition of masking, a sort of central masking called informational masking, illusion of continuity, binaural hearing and mechanisms collectively referred to as Auditory Scene Analysis (ASA) (Bregman, 1990). The segregation of overlapping sounds, besides ASA, has been investigated within research on speech perception. In ASA an analysis-synthesis process is assumed, where the acoustic scene is first decomposed into a set of segments, which are then grouped to form coherent and independent streams in a synthesis process.

Attempts have been made towards segregation of sounds by computational means. They are collectively referred to as Computational Auditory Stream Analysis (CASA, for a review, see Wang and Brown, 2006). An often used computational paradigm in CASA is to estimate time-frequency (t-f) mask, where "mask" denotes the operation of applying a mask. Masks are applied to spectrograms of mixed sounds. If the value of 1 is applied for a t-f unit in which the target energy is stronger than the total interference energy, and the value of 0 otherwise, the mask is called ideal binary mask (Wang, Brown, 2006; Brungart *et al.*, 2009).

Auditory segregation of overlapping sounds when the sources are musical instruments was given less attention, and concentrated on analysing sequences of pitches (Bregman, 1990). Kelly and Tew (2002, 2003) applied the operation of masking with coefficients varying from 0 to 1 to two musical instruments in a binaural recording. Their main finding was that it was possible to remove the weaker signal in a particular t-f location only if its level was lower by at least 15 dB, and no perceptible degradation of the signal should occur. In research on speech perception, including the applications of CASA, the speaker is a target and the background (typically noise) is a masker. In the case of the cocktail party effect one voice is a target and the others are a collective masker. Investigation on

segregation of musical instruments requires a different approach: contributions of individual instruments (or at least their groups) are all targets. Another problem in approaching segregation in musical acoustics is that it is difficult to construct stimuli so that perception is quantifiable.

This author has developed an appropriate modification of binary t-f masking, where all spectro-temporal overlapping between all individual sound sources is removed. This processing algorithm removes most of the energetic masking between individual sound sources. That property of signals changes conditions of segregation for the ear so it may have perceptual implications and is worth investigation. It has been applied both to musical instruments playing together (Kleczkowski, 2005, 2008) and to monaural mixes of multiple talkers (Kleczkowski, Pluta, 2012). The earlier works reported qualitative perceptual properties of this operation, while the latter showed that it did not change the rate of understanding of concurrent speech. The aim of this paper is to find basic quantifiable properties of this operation when performed on musical instruments playing together.

The removal of spectro-temporal overlap (RSO) is substantially different from removal of elements of sounds resulting from algorithms of lossy compression of audio signals. The RSO algorithm operates on separate sound sources, while compression techniques operate on the mixed signal. It can also be easily shown, that considerably more energy is removed from sounds with RSO than with lossy compression.

There were four objectives of this work: (i) to measure the perceptual difference between the natural and the spectrally non-overlapping presentations of musical instruments playing together, (ii) to evaluate the effect of the average size of t-f regions where overlapping is eliminated on this difference, (iii) to evaluate the relation between the perceived difference and the ratio of retained sound to removed sound, in terms of both energy and t-f surface, and (iv) to investigate whether the multiple looks and glimpses hypotheses also hold for perception of musical instruments and if so, to obtain any assessment of the size of "glimpses". The multiple-looks hypothesis (Viemeister, Wakefield, 1991) postulates that the ear is capable of integrating auditory percepts from small elements scattered in time. This hypothesis was confirmed within research on speech perception, and extended to the time-frequency domain, where the ear is supposed to analyse scattered spectro-temporal components of sounds (referred to as "glimpses") to perform segregation (Howard–Jones, Rosen, 1993a, 1993b; Cooke, 2006; Barker, Cooke, 2007; Lu, Cooke, 2008).

In experiment 1, listeners compared original mixes of musical instruments with their RSO versions in a psychophysical experiment over the headphones. The aim of experiment 2 was to test how the stimuli of experiment 1 were perceived in loudspeaker presentation, i.e. in settings typically encountered when listening to music.

2. Processing and stimuli

2.1. Implementation of the removal of spectro-temporal overlap

In the rest of this paper, a single and smallest possible element of a t-f distribution will be referred to as a "cell", while a group of neighbouring cells is referred to as a "region".

To remove spectro-temporal overlap between sound sources their separate acoustic signals are needed. After the t-f distributions (spectrograms) of all input signals are obtained, the spectrograms are compared cell by cell, and in each cell the signal characterised by the highest value of amplitude is chosen

$$|F|_{k,n,\mathrm{out}} = \max\left\{|F|_{k,n,1}, |F|_{k,n,2}, \ldots |F|_{k,n,p}\right\}, \quad (1)$$

where F is a t-f coefficient, k is the index of a frequency bin, n is the index of a time frame, p is the number of acoustic sources, and "out" denotes an output t-f signal. The argument of the modulus function on the left is passed to the output t-f signal. The operation in (1) was performed by a simple algorithm for finding the maximum element in a set. Cells belonging to other sounds in that t-f location were not passed to the output signal.

The operation in (1) is a "winner takes all" competition that takes place in each t-f cell, i.e. between contributions from all sound sources. An example of the occupancy map in the t-f plane resulting from RSO processing of two musical signals is presented in Fig. 1. As can be seen in this figure, the RSO results in a partition of the spectrogram of the mixed signal: some cells or regions contain only the contribution of one instrument, while the others only the contribution of the other one. There is no cell containing both contributions, thus there is no t-f overlap of sound sources.

The t-f analysis/synthesis method used was based on the Modified Discrete Cosine Transform (Malvar, 1992; Kleczkowski, 2002) – a perfectly invertible block t-f transform. A custom software for the entire procedure was written by the author in C.

Due to the properties of block transforms, the sizes of t-f cells had to follow a fixed grid. The duration of the individual t-f cell and its related bandwidth was chosen at 11.6 ms/43.06 Hz, with reasonable alternatives of 5.8 ms/86.12 Hz or 23.2 ms/21.53 Hz. The chosen size was a compromise between the duration of the auditory "time window", estimated by Moore *et al.* (1988) at around 8.3 ms at 500 Hz and 8 ms at 2000 Hz, and the frequency width of a t-f cell. The latter should be substantially narrower than a local

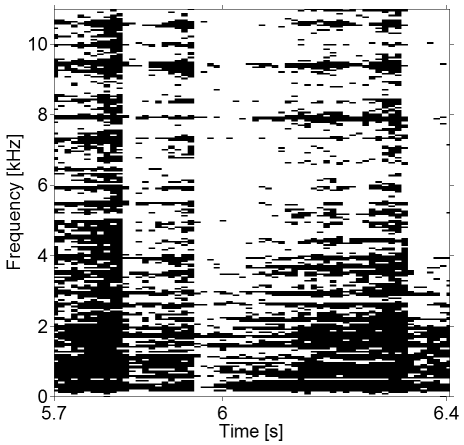

Fig. 1. The map of occupation of t-f cells after performing RSO operation according to (1) on spectrograms of two simultaneously playing instruments: drums and a synthesizer ("dr-sn" set in Table 1) . Black indicates all t-f cells where the synthesizer "won the competition", i.e. its amplitude was bigger that that of the drums. In the re-synthesized RSO mix, all t-f cells marked black in this figure contain only the contribution of the synthesizer. White indicates the opposite situation (amplitude of drums was bigger of the two). The map shows a 1.7 s long excerpt used in experiment 1. The frequency axis is limited to 11 kHz in order to increase the vertical resolution of the plot.

critical band (CB), even for lowest frequencies. With the first alternative, the bandwidth in low frequencies (86.12 Hz) would be close to one CB.

As can be seen in Fig. 1, a considerable part of the t-f occupancy map is covered by small scattered t-f regions, often consisting of a single t-f cell. By smoothing operations the average size of the t-f region can be made bigger. One of the objectives of this work (ii) was to investigate the relation between this size and perception of RSO. Therefore two modes of processing were used. The first will be referred to as individual cells mode: t-f regions are identical to t-f cells. The other mode, referred to as clustered cells mode, involved clustering of individual t-f cells into larger regions. Clustering was performed on individual spectrograms, prior to operation (1). It was based on local concentration of t-f energy. Clusters were formed as the result of two-dimensional averaging over the dimensions of time and frequency. Due to stochastic nature of this process clusters had no fixed dimensions nor did they always form compact shapes in the plane, but the number of small scattered regions or individual cells was considerably reduced. After clustering the RSO algorithm worked the same way as in individual cells mode using (1), just rendering occupancy maps that were smoother. More details on clustering are given in (Kleczkowski, 2008). Figure 1 shows an example of RSO mix in individual cells mode, while Fig. 2 shows the same mix in clustered cells mode. Two modes of RSO processing presented above also serve objective (iv) of this paper, i.e. the assessment of the size of "glimpses" in time and frequency.

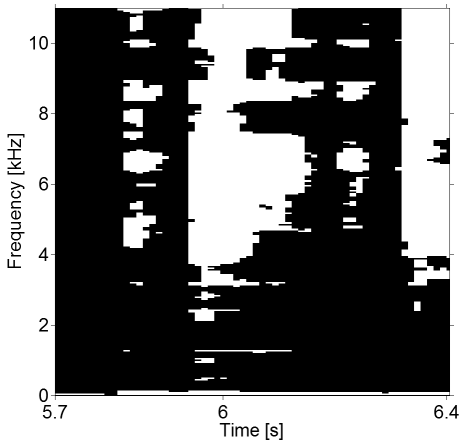

Fig. 2. The map of occupation of t-f regions by the same instruments as in Fig. 1 (the synthesizer – black, drums – white), after RSO in clustered cells mode.

2.2. Stimuli

The sound sources chosen for experiments were professional recordings of musical instruments: bass, two guitars (recorded in one track), drums, synthesizer and saxophone playing the same fragment of a pop-jazz piece. An excerpt lasting 7 s was chosen. Monophonic tracks (16 bits, 44.1 kHz) containing individual instruments were mixed in 12 combinations. The bass was included only in the mix of all five instruments, as it occupied the low end of the spectrum, with little spectral overlap with other instruments. Mixes included all possible combinations of two and three instruments, bass being excluded. Prior to mixing, the relative levels of all instruments were adjusted by a professional audio engineer, so that an appropriate balance of instruments was obtained. Figure 3 presents the t-f oc-

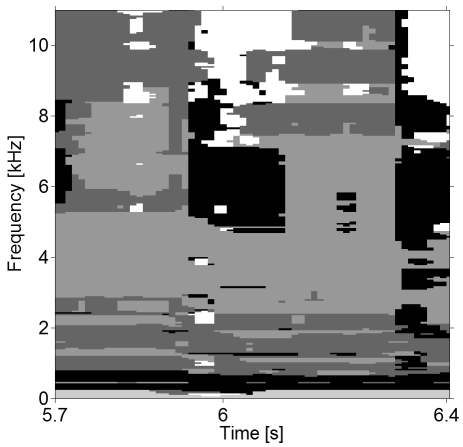

Fig. 3. The map of occupation of t-f regions by the sounds of drums – white, bass – light grey, the saxophone – grey, the synthesizer – dark grey, and guitars – black, i.e. the complete band ("all_5" set), after RSO in clustered cells mode.

cupancy map of the RSO mix of all five instruments, further referred to as "all_5", used in the experiment in the clustered cells mode.

For each of 12 sets of instruments, three stimuli were prepared: (I) the original mix, obtained by converting the original tracks to the t-f domain and mixing them in that domain to control for possible effects introduced by t-f processing, (II) RSO mix in the individual cells mode, (III) RSO mix in the clustered cells mode. Since RSO processing reduces the energy of all sound sources, stimuli (II) and (III) were normalised to have an RMS value equal to that of (I). The stimuli were also normalized across all sets.

Table 1 lists all stimuli used with their percentage of energy and t-f area retained after RSO. All stimuli were monaural. Examples of maps of occupation of the t-f plane are presented in Figs. 1 to 3. These figures show a 1.7 s long excerpt used in experiment 1. The frequency axis is limited to 11 kHz in order to increase the vertical resolution of the plot.

Table 1. Sets of instruments used as stimuli and their respective percentages of energy and efficient area retained in the mix after RSO. Energy and area values are averaged over instruments in the set. Symbols: b – bass, g – guitars, dr – drums, sn – synthesizer, sx – saxophone, IC – individual cells, CC – clustered cells.

Set of instruments	% energy retained		% area retained	
	IC	CC	IC	CC
dr-g	86.9	78.4	63.8	70.3
g-sx	87.7	82.5	70.5	64.2
dr-sx	88.8	83.6	60.3	65.5
dr-g-sx	79.3	70.5	46.1	49.7
sn-sx	83.8	79.1	65.9	61.2
dr-sn	85.8	82.2	62.9	67.9
dr-g-sn-sx	67.3	58.8	36.8	38.6
dr-sn-sx	76.7	70.5	45.1	46.8
dr-g-sn	71.5	63.9	46.8	50.3
g-sn	76.1	70.7	66.7	61.7
all_5	68.3	61.7	31.9	33.5
g-sn-sx	71.2	64.3	51.9	45.5

The percentage of energy retained was computed separately for each of the instruments in each of the stimuli. The values presented are means over all instruments in a given stimulus. The percentages of area retained were computed according to a similar rule. In the calculation of energy retained, all coefficients of the t-f distribution of a given instrument contributed to the calculation of the proportion's denominator. This method was considered improper for the calculation of area, since a considerable number of t-f coefficients of each instrument contained only background noise. Their effect was negligible in the calculation of energy, but would introduce a bias in the calculation of area. Therefore a threshold was set for a t-f coefficient to be included in the denominator: $|F| \geq 0.0003 \cdot \max\{|F|\}$. This threshold corresponded to -70 dB relative to the coefficient with the highest value, an approximation of the signal-to-noise ratio in the recording process. The coefficients thus selected contained about 99% of the energy of an instrument, and the corresponding area will be referred to as the effective area. The percentage of t-f area computed in this study is similar to the "visibility" parameter used by Barker and Cooke (2007), except that in the latter no correction for background noise was included.

It can be noticed in Table 1, that the least area retained is for the "all_5" set, and "dr-g-sn-sx" (four instruments) comes next. This can be easily explained: the effect of RSO is that the t-f plane has to be divided between competing sound sources. The more sources, the less average area remains available for each of them. This is less noticeable for energy, as each instrument has its own energy.

All stimuli were generated offline on a PC. They were stored as audio files at 16 bits, 44.1 kHz resolution.

3. Experiment 1

3.1. Choice of stimuli

A pilot test for this experiment participated by expert listeners showed that the perceptual difference between original mixes and RSO mixes increased substantially in the clustered cells mode. It also tended to increase with the number of instruments mixed i.e. with the reduction of energy and t-f area retained in RSO mixes (cf. Table 1, that has been ordered according to results of the pilot test). Two sets were chosen for experiment 1: "all_5" for its lowest values of energy and area retained in RSO mix, and "sn-sx", as its overall RSO detectability was medium while the discrepancy between its results for the individual and clustered cells modes was high. Out of the original 7 s long excerpt, a shorter 1.7 s long excerpt was used in experiment 1, as a compromise between eliminating memory-related aspects of the experiment and the length required to assess a musical material.

3.2. Subjects

Nineteen subjects aged 20-22, all of them students of the Acoustic Engineering course at the AGH University of Science and Technology, participated in this experiment. All listeners had normal hearing defined as thresholds within 20 dB of nominal at octave frequencies from 250 through 8000 Hz. The thresholds were measured by Békésy audiometry using headphones. All had at least some experience in psychoacoustics tests.

3.3. Experimental setup

Stimuli were played out from a PC netbook through a M-Audio Fast Track Pro USB audio interface. They were presented to the subject through Beyerdynamic DT 770 Pro closed headphones. Stimuli were monophonic but the presentation was diotic, as the listeners found monaural presentation tiring. An attempt to set a common level failed as some listeners found it too low or too high. The presentation level was set individually to a level that was comfortable for each listener during a practice session. The starting level was 75 dB SPL and the adjustment range allowed did not exceed ±6 dB. The listeners were seated in a sound isolated room fitted with sound absorbing material. The screen of a notebook PC contained control buttons to play/stop stimuli and to give answers. The software was developed by dr Marek Pluta of AGH University.

3.4. Experimental procedure

The same–different task was used, in 1AFC (One Alternative, Forced Choice) mode (Kingdom, Prins, 2010). Each trial consisted of a pair of stimuli: the original mix and the RSO mix, in random order, or two identical stimuli. They were separated by a pause of 200 ms. The subjects' task was to press one of two keys on a PC screen: "same" or "different". Feedback was given after each trial, i.e. the subject was informed in the computer screen whether his response was correct or false. This is recommended in experiments measuring sensitivity. The subject activated a next trial by pressing the "next" key. Tests for both sets: "all_5" and "sn-sx" were held separately, with a short break. Each of two tests consisted of 240 trials. 120 trials contained pairs of identical stimuli (original mixes and RSO mixes in both modes). The other trials contained an original mix and an RSO mix, with half of these pairs containing the individual cells mode and the other half containing the clustered cells mode. The sequence of different stimuli within the entire lot of 240 was random, but was held fixed for all subjects. Prior to the main experiment, each subject took a practice session of 30 trials.

3.5. Results and discussion

For each of the four experimental conditions and for each subject, the index of stimulus detectability d' was calculated according to (Gescheider, 1997):

$$d' = z(H) - z(F), \tag{2}$$

where H is hit rate i.e. the rate of detection of differences, and F is false alarms rate i.e. the rate of identical stimuli incorrectly classified as different, z denotes H or F rate converted to the location along the abscissa of standarized normal distributions, where $z(F)$ is a location along the noise distribution and $z(H)$ along the signal-plus-noise distribution. The main application of the d' index is to compare detectabilities of different stimuli, but it is usually assumed that $d' = 1$ is a threshold value, as this value corresponds to 76% correct recognitions in 2AFC (Two Alternatives, Forced Choice) tasks (Moore, 2003). Hence, a value below 1 indicates that the stimulus was not detectable.

Table 2 presents mean d' values for investigated stimuli, averaged over all subjects. The results in four experimental conditions can be summarised as follows. In individual cells mode the RSO effect was imperceptible with "sn-sx" stimulus (this condition will be further referred to as "imperceptible condition"). In the same mode with "all_5" stimulus perception was close to the threshold. In clustered cells mode the effect was perceptible with "sn-sx" stimulus and easily perceptible with "all_5"stimulus. There was a considerable spread in the results among listeners.

Table 2. Results of experiment 1: mean values of detectability index d' for investigated stimuli, averaged over all subjects; IC – individual cells mode, CC – clustered cells mode, σ – standard deviation.

Set of instruments	IC		CC	
	mean d'	σ	mean d'	σ
sn-sx	0.46	0.43	1.35	0.72
all_5	0.95	0.65	2.46	1.19

The comparison of data in Table 1 with data in Table 2 indicates that the decrease of energies retained in sounds after RSO processing increases the rate of recognitions of such processed mixes. This is the case in all four possible paired comparisons: the sn-sx set versus the all_5 set in both modes, and the individual cells mode versus the clustered cells mode for both mixes. When t-f areas are compared, three out of four comparisons support the statement that the decrease of t-f area retained increases the rate of recognition. The only exception is the all_5 set, where the increase in the rate of recognition is associated with a relatively slight increase of t-f area. This can be accounted for by random factors in the proportions of areas. The rule observed can be simply accounted for: the removal of energy and t-f area distorts sounds.

The condition of individual cells mode applied to "sn-sx" set, where RSO is imperceptible, can be used to demonstrate that the ear is able to perform the fusion of the auditory scene from the mixture of sounds altered by RSO processing. The term "fusion" is used here in the meaning of building a consistent percept out of some distinct parts.

It is doubtful that the continuity illusion is the basis for fusion, as the interrupting sound must exceed the interrupted sound at least by an amount causing complete masking (Bregman, 1990). In RSO, all sound components are removed when they fall just below 0 dB related to the masker. However, continuity illusion can support fusion.

Informational Masking (IM) seems to have an important contribution. The hypothetical role of IM can be the following. If RSO removes some spectro-temporal parts of sounds which would not be masked energetically by other sound sources in the mixture, then the difference brought by RSO should be perceptible. This removal takes place in the imperceptible condition. Therefore there must be some other factor or factors that make RSO in this condition imperceptible. The supposition that it is IM is supported by a known property of informational masking: it is stronger when both the target and masker are presented to the same ear. It is also supported by investigation on informational masking within a sound of one instrument (Kleczkowski *et al.*, 2010).

Another important conclusion from the existence of an imperceptible condition is that the multiple looks/glimpses hypotheses can hold for perception of musical instruments. However, as can be seen in Table 2, the ear is not completely successful in applying glimpses. In the remaining paragraphs of this section an attempt is made towards quantitative analysis of the frequency widths of "glimpses" in the imperceptible condition ("sn-sx", individual cells).

The number of contiguous cells (i.e. belonging to one sound source) along the frequency axis was assumed the width of a "glimpse". The t-f decomposition used the linear frequency scale, while a measure of bandwidth should use a perceptually justified frequency scale. The critical band was used as a unit of measure of widths of "glimpses". Thus, each counted number of contiguous cells n was converted to linear frequency bandwidth: $n \cdot 43.06$ [Hz], and that bandwidth was converted to a fraction of a local CB: $n \cdot 43.06 \,/\mathrm{CB}_l$ [Hz], where CB_l denotes frequency width of a local CB, according to the table by Zwicker (Fastl, Zwicker, 2007).

In order to present the results as a histogram, all resulting values were grouped into eight ranges: from 0 to 15% of CB_l, from 15% to 30% of CB_l, ..., from 90% to 105% of CB_l. All values greater than 105% of CB_l were included in one common group. The histogram of the results is shown in Fig. 4. More details on computation are included in the Appendix.

In individual cells mode 64% of values fell into the 0–15% of CB_l range, in clustered cells mode that proportion was 16%. The median of the results in individual cells mode was 10.2% of CB_l and the median in clustered cells mode was 43.9% of CB_l.

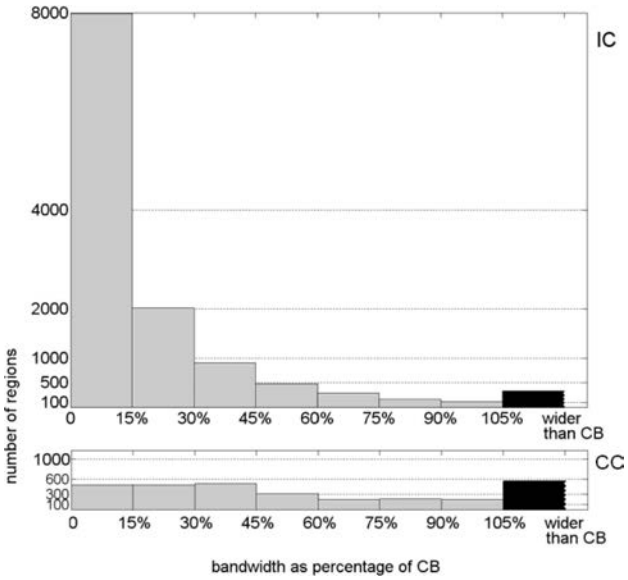

Fig. 4. Upper: the histogram of numbers of t-f regions in a particular range of frequency widths expressed as a percentage of a local CB, in individual cells mode. Lower: the analogous histogram in clustered cells mode. IC – individual cells mode, CC – clustered cells mode.

These results indicate that the hypothesis of "glimpses" holds better with narrow frequency widths of "glimpses". It has been demonstrated that with this particular stimulus (i.e. in the imperceptible condition), when 64% of "glimpses" have widths below 15% of CB_l the multiple looks/glimpses hypothesis holds perfectly. However, this statement must be accompanied by other conditions of experiment 1: 83.8% of the original energy and 65.9% of original t-f area were preserved in the "glimpses".

4. Experiment 2

4.1. Subjects and experimental setup

The subjects in this experiment were 111 students; 101 attended courses in engineering, of which 16 declared musical experience of at least two years, like playing a musical instrument or an involvement in some audio engineering task; 10 attended a musical degree course. None of the students had previous experience with psychoacoustics tests. For technical reasons the experiment was held in two different rooms, I and II, in nine groups of 6–14 listeners. Engineering students used room I, while musical degree students used room II. Both rooms were of similar size (45 and 55 m^2 respectively) and similar acoustical characteristics. In room II the reverberation time (RT20) was: 0.9 s at 128 Hz, 0.75 s at 1 kHz and 0.45 s at 4 kHz. The stimuli were played through one loudspeaker. The test setup in Room I: PC computer with Prodif 88 digital audio interface, Swissonic DA96 D/A converter,

Soundcraft Spirit 16/8 mixer and Genelec 1038A studio monitor; in Room II: PC computer, Digi 002 audio interface and Mackie 626 monitor. The listening level was set at about 80 dB according to the preference of listeners in each of the groups. All sound samples were normalised to the same RMS value. To minimize the effect of the place of listening, the subjects in large (8 and more) groups were asked to change their places randomly after having heard half of the samples.

4.2. Experimental procedure

Pilot experiments with a loudspeaker indicated that the proportion of correct recognitions did not exceed chance performance for all 12 sets in individual cells versions, in contrary to clustered cells versions, where significant differences were met. Therefore all clustered cells versions of Table 1 plus the individual cells version of the "all_5" set were chosen for the main experiment. This choice was supported by the results of experiment 1, where individual cells mode produced substantially lower detectability than clustered cells mode. Full 7 s long excerpts were used. The paradigm of a trial followed the ITU BS.1116-1 recommendation (ITU, 1997) for the evaluation of subtle differences in the quality of audio signals or equipment. An AXY test was used. The trial consisted of three observation intervals (A, X and Y), where A was a reference and was repeated in either X or Y. The other component of the X, Y pair was a stimulus different than a reference, i.e. it was a triple stimulus, hidden reference test. The subject's task was to indicate whether the interval X or Y contained the different signal. The original mix was used as a reference and assigned to the interval A. The listeners were given score sheets with the instructions. To make the task easier for subjects the sequences in intervals in a test trial were named AAB and ABA. The experiment started with a training run of all sets, then the main test with 13 test sequences followed. The sequence of presentation was as follows: double alert signal – AAB sequence with 500 ms breaks between intervals – single alert signal – AAB sequence (repeated) – 5 s for giving the answer. The reason for repeating was to help the listener in case he/she was not sure after just one hearing. In half of the trials the sequence was ABA. As listeners auditioned the test sequences in groups, all members of a group heard the same sequence. The sequence of sound sets (13 sets) between groups was randomised, and so were the sequences for a particular set (for a given set ABA sequence was used for half of the groups and AAB for the other half). For each of the 13 sets the score sheet contained a field to be filled with the recognised sequence. The correct sequence (either AAB or ABA) indicated that a listener recognised correctly the stimuli, i.e. recognised the difference between A and B.

4.3. Results and discussion

The results have been evaluated by two methods. One is used in some listening tests of audio equipment. The results were treated as categorical data (2 categories) and their significance level was determined from a binomial distribution. The other is used in psychophysics. A percentage of listeners who correctly recognised was treated as the percentage of answers for one listener. The decision audible/inaudible was then based upon the threshold of 75%.

In only four out of 13 sets was the difference recognized correctly by a significant ($p < 0.05$) proportion of listeners. In other sets, the results were far below significance. The results for the four significantly recognised stimuli are presented in Table 3. The p – value has been determined from a one-tailed binomial distribution.

Table 3. Statistically significant correct recognitions in experiment 2, all listeners. Alternative evaluation based on the psychophysical threshold of 75% is given in the right column.

Set of instruments	Percent correct recognitions	p – value	Effect audible according to 75% rule
dr-g-sn-sx	61	< 0.01	no
dr-sn-sx	63	< 0.01	no
dr-g-sn	73	< 0.001	no
g-sn	73	< 0.001	no

No common property was found in these four sets. Informally, listeners commented that they recognised differences on the basis of small artifacts, different in each of the sets.

The results for 26 musically experienced listeners (16 from engineering courses declaring at least two years of musical experience, and 10 from music courses) are given in Table 4. The paired-data t test was performed (using four sets occurring in both Tables 3

Table 4. Statistically significant correct recognitions in experiment 2, musically experienced listeners only. Alternative evaluation based on the psychophysical threshold of 75% is given in the right column.

Set of instruments	Percent correct recognitions	p – value	Effect audible according to 75% rule
dr-sn-sx	69	< 0.05	no
dr-g-sn-sx	77	< 0.01	yes
dr-g	77	< 0.01	yes
dr-g-sn	77	< 0.01	yes
g-sn	85	< 0.001	yes

and 4) to find whether musically experienced listeners were more sensitive to differences between versions of sound mixes. The result was positive at $p < 0.025$ (t-value = 3.45, df = 3). Although the difference in listening rooms and equipment were unlikely to affect the results, the results of students of music courses were not treated separately, to avoid the effect of this theoretically confounding factor. Creating a group for "musically experienced" listeners instead, of which 10 listened in room I and 16 in room II was meant to average out possible room effects.

The relation between percentages of the energy and area retained and the rate of recognition of RSO processing in this experiment is less pronounced than in experiment 1, but the same rule can be observed. The average energy retained in the clustered cells mode computed from to Table 1 is 72.2%, while the average energy in significantly recognised sets in Table 3 is 68.5%, and in Table 4 (musically experienced listeners): 66%. In the case of the area retained, the analogous percentages are: 54.6%, 53.5% and 49.3%.

Neither of the two stimuli assessed in experiment 1 as detectable (mean $d' > 1$) were detected in experiment 2, even by musically experienced listeners, indicating that the perceptual effect of RSO is substantially weaker when auditioned over the loudspeaker.

5. Conclusions

The following conclusions can be drawn from this work:

1. The perceptual effect of the operation of artificial removal of spectro-temporal overlap was imperceptible in one of four experimental conditions in experiment 1. This condition was easy to meet: a mix of two sound sources and individual cells processing, which can be considered a natural option for RSO. Therefore, the general conclusion is that the effect of RSO can be imperceptible.
2. Clustering of cells made the effect perceptible in both of the stimuli investigated in experiment 1.
3. In loudspeaker listening (experiment 2), the range of conditions in which the effect of RSO was imperceptible was considerably wider than in headphone listening. The effect was not perceived in 9 out of 13 stimuli investigated (69%), although most of them were of "clustered cells" type, found as perceptible in headphone listening.
4. The detectability of RSO processing increases with removing more energy and effective t-f area.
5. The effect of RSO in its imperceptible condition as found in this work indicates that the multiple looks/glimpses hypotheses hold in the perception of musical instruments. The results also indicate that "glimpses" are quite narrow in frequency, in the order of a fraction of the CB.

Appendix. The computation of relative width of t-f regions

In order to concentrate the analysis on the frequency widths of t-f components, the regions were assumed as one-cell wide vertical strips of cells in the t-f plane, consisting of contiguous cells belonging to one instrument (any strange cell broke the strip). Individual time frames were analysed, therefore it did not matter whether a strip was isolated in time, or was attached to any cells of the same instrument on either side of the strip. This approach was different from the assumption in (Cooke, 2006) that a glimpse (i.e. a region) contained all cells connected by being a part of the four-neighbourhood of any other element in the t-f region.

The aim was to count t-f regions of a similar logarithmic bandwidth. The computation was carried out in the range from 1270 to 9500 Hz. The lower frequency was chosen so that the relative bandwidth analysed was not wider than about 15% of a CB. Higher frequencies were not included because of considerable share of background noise in that band. The number of contiguous cells was counted separately in each of 12 CBs in the analysed range. The appropriate margin was included in the algorithm, so that wide regions exceeding limits of CBs were not broken and their whole width was counted. The results are approximate because no perfect alignment between fractions of CBs, limits of CBs and multiples of the cell's width could be obtained. The counting was carried out for both instruments in the pair and the results were averaged.

Acknowledgment

This study was partly supported by grant number R02 0030/2009 from the National Centre for Research and Development (Polish).

References

1. Barker J., Cooke M. 2007, *Modelling speaker intelligibility in noise*, Speech Communication, **49**, 402–417.
2. Bregman A.S. (1990), *Auditory Scene Analysis*, MIT Press, Cambridge.
3. Brungart D.S., Chang P.S., Simpson B.D., Wang D.L. (2009), *Multitalker speech perception with ideal time-frequency segregation: Effects of voice characteristics and number of talkers*, J. Acoust. Soc. Am., **125**, 4006–4022.
4. Cooke M.P. (2006), *A glimpsing model of speech perception in noise*, J.Acoust. Soc. Am., **119**, 1562–1573.
5. Fastl H., Zwicker E. (2007), *Psychoacoustics – facts and models*, Springer – Verlag, Berlin Heidelberg.
6. Gescheider G.A. (1997), *Psychophysics: The Fundamentals*, Lawrence Erlbaum Associates.

7. Howard–Jones P.A., Rosen S. (1993a), *The perception of speech in fluctuating noise*, Acustica, **78**, 258–272.

8. Howard–Jones, P.A., Rosen S. (1993b), *Uncomodulated glimpsing in 'checkerboard' noise*, J. Acoust. Soc. Am., **93**, 2915–2922.

9. ITU (International Telecommunication Union) (1997), *Methods for the subjective assessment of small impairments in audio systems including multichannel sound systems*, Recommendation BS.1116-1.

10. Kelly M.C., Tew A.I. (2002), *The continuity illusion in virtual auditory space*, Proc. 112th AES Conv. Preprint 5548.

11. Kelly M.C., Tew A.I. (2003), *The significance of spectral overlap in multiple-source localization*, Proc. 114th AES Conv. Preprint 5725.

12. Kingdom F.A.A., Prins N. (2010), *Psychophysics: A Practical Introduction*, Academic Press, London.

13. Kleczkowski P. (2002), *Acoustic Signal Expansion in Multiple Trigonometric Bases*, Acta Acustica united with Acustica, **88**, 526–535.

14. Kleczkowski P. (2005), *Selective Mixing of Sounds*, 119th AES Conv., New York, Preprint 6552, October 2005.

15. Kleczkowski P. (2008), *Selective mixing of a symphony orchestra recording*, Archives of Acoustics, **31**, 4 (Supplement), 91–99.

16. Kleczkowski P., Plewa M., Pluta M. (2010), *Masking a frequency band in a musical fragment played by a single instrument*, Acta Physica Polonica A, **119**, 991–995.

17. Kleczkowski P., Pluta M. (2012), *Understanding concurrent speech is not impaired by removal of spectro-temporal overlap*, Acoustics 2012 Conference, Hong Kong.

18. Lu Y., Cooke M. (2008), *Speech production modifications produced by competing talkers, babble, and stationary noise*, J. Acoust. Soc. Am., **124**, 3261–3275.

19. Malvar H.S. (1992), *Signal Processing with Lapped Transforms*, Artech House, London.

20. Moore B.C.J. (2003), *An Introduction to the Psychology of Hearing*, Academic Press, London.

21. Moore B.C.J., Glasberg B.R., Plack C.J., Biswas A.K. (1988), *The shape of the ear's temporal window*, J. Acoust. Soc. Am., **83**, 1102–1117.

22. Viemeister N.F., Wakefield G.H. (1991), *Temporal integration and multiple looks*, J. Acoust. Soc., **90**, 858–865.

23. Wang D.L., Brown G.J. (2006), *Fundamentals of computational auditory scene analysis* [in:] Wang D.L., Brown G.J. [Eds.], *Computational auditory scene analysis: Principles, Algorithms, and Applications*, IEEE Press/Wiley-Interscience., Hoboken NJ, pp. 1–44.

PAN ARCHIVES OF ACOUSTICS
Vol. **37**, No. 3, pp. 365–371 (2012)

DOI: 10.2478/v10168-012-0046-z

A Perceptionist's View on Psychoacoustics

Jens BLAUERT

Institute of Communication Acoustics
Ruhr-University Bochum
44780 Bochum, Germany; e-mail: jens.blauert@rub.de

(*received July 2, 2012; accepted August 2, 2012*)

Psychoacoustics is traditionally based on a world model that assumes a physical world existing independently of any observer – the so-called *objective* world. Being exposed to this world, an observer is impinged upon by a variety of *stimuli* reaching his/her sensory organs. These stimuli, if physiologically adequate, may cause biological transduction and signal processing in the sensory organs and its afferent pathways in such a way that finally a specific excitation of the cortex takes place, which results in *sensations* to appear in the observer's perceptual world. The sensations are understood as being *subjective*, since they require an observer to exist. This world model – also known as (objectivistic) *realism* – reaches its limits when it comes to explaining more complex phenomena of perception. Thereupon, in this paper, an alternative world model is emphasized and applied to psychoacoustics, namely the perceptionist's model. Like realism, *perceptionism* has a long tradition in epistemology. It appears to be suitable to improve our understanding of perceptual organization.

Keywords: psychoacoustics, perception, perceptionism, response, reality, stimulus.

1. Introduction

Acousticians usually refer to a world view which is strongly influenced by classical (*Newton*'s) mechanics. This is not surprising, because the physical section of acoustics is a branch of mechanics. This world model, known as (objectivistic) *realism* in epistemology, has a long philosophical tradition – e.g., (Descartes, 1641). It is assumed that there exists a world beyond perception which represents essential reality. This world is assumed to "*cause*" the perceptual world, but it is, by definition, never directly accessible. Whatever is perceived is, consequently, only an "*image*" of this (transcendent) real world, mediated by the sensory organs and limited by their imperfection. Taking this idea seriously, all percepts, consequently, lack essential reality. They are only a kind of illusion – in other words, subjective and shadowy. But, nevertheless, they provide a connection to the assumed real world such that we conclude by rational thinking that this transcendent real world must actually exist. The logic of the proof goes like this: If the transcendent world did not exist, also the perceived world would not exist. Yet, this conclusion is obviously logically questionable, as it recurs to an assumption that cannot be proven (a so-called "irrealis").

Nevertheless, isn't the assumption of a real world behind the perceived one justified by the fact that instrumental measurements methods are available that render results which are independent from specific observers and thus, assumingly, must exist independently of any observers? Aren't these instrumentally collected data free of any perceptual distortion and can thus be used to build a valid model of a "real" world?

This is indeed the world view of *realism* and, actually, it carries a long way, particularly in applied physics and engineering. Yet, unfortunately, it leads to substantial conceptual inconsistencies when applied to research into perceptual phenomena, because, along these lines of thinking, perceptual phenomena are conceived as subjective and illusionary in essence – and, hence, an ill-defined item to investigate scientifically.

The basic inconsistencies appear clearly when analyzing a philosophical problem known as the *retinal-image problem* (Becker, 1978; Blauert, Guski, 2009). Although taken from vision, we shall use this epistemological problem as an example here because of its very illustrative nature. The results of the analysis can easily be extrapolated to any other modality, such as audition, touch or proprioception.

1.1. The retinal-image problem

Visual perception – heavily simplified – is usually explained as follows: From the outside world, light rays enter the eyeball and, with the eye acting like a CAMERA OBSCURA, a "photographic" picture of the outside world is projected onto the retina, the *retinal image*. The retinal image (in physical terms, a pattern of electromagnetic waves) is the adequate stimulus for the visual system, that is, it stimulates sensory cells in the retina to send biologic signals upward the afferent neural pathways. These signals, after various processing steps, finally reach the visual cortex, where an adequate excitation pattern is somehow generated. This pattern triggers a conscious visual percept to appear in the observer's world. The details of this process are still considered enigmatic – and may stay so forever.

The problem within this model is best illustrated by an experiment of thought: Ophthalmologists, as is well known, can visually inspect the retina with special optical equipment. In doing so, they are able to see the retinal image. Now consider an optical equipment (realized, e.g., by mirrors, lenses and/or fiber optics) that allows persons to inspect their own retinas themselves. Wouldn't they then see retinal images which cause themselves, that is, are stimulus and sensation simultaneously and in one?

Since it is unacceptable from a logical point of view that an item "causes" itself (causa sui), there must be something wrong, and speculation may go as follows: The retinal images that the test persons see, are not the ones that actually cause them. There must have been earlier ones that did so. But when we would have tried to observe those earlier ones, they would have been images as well. Can images cause images? No, one could say, it is the electromagnetic wave pattern behind them. But haven't these wave pattern been detected with instruments that are also part of the perceptual world and, therefore, are "images" as well?

Obviously, the realist's world model raises fundamental epistemological doubts regarding its validity. Furthermore, from the point of view of psychoacoustics as a science, it has the disadvantage of classifying the research items of psychoacoustics, namely, auditory percepts, as suffering from a lack of essential reality and thus being principally inaccessible by exact sciences. It is therefore surely in the good interest of psychoacoustics to watch out for world models which do not have these disadvantage. Thus, *perceptionism* will now be considered and discussed as an alternative.

2. The perceptionist's world model

Perceptionism is a world model that, like realism, has a long philosophical tradition – compare, e.g., (HUME, 1740; KANT, 1781). Perceptionism puts to the fore what is consciously perceived, that is, the percept itself. In view of this model, the totality of percepts is the essentially real world. The conceptual foundation of perceptionism is expressed by a famous statement of BERKELEY (1710): "*esse est percipi*" (to exist is to be perceived). Accordingly, "to exist" and "to be perceived" are synonyms. In perceptionism, the world is understood as being completely describable and interpretable within the perceived world. Any (epistemologically questionable) assumption of transcendent worlds is thus considered superfluous[1]. From the point of view of psychoacoustics (and psychophysics at large) auditory events and acoustic events are both percepts and, ergo, basically represent the same amount of essential reality. As one percept obviously cannot "cause" another one (how should this be accomplished without witchcraft?). Thus, the perceptionist's view requires a reconsideration of the traditional stimulus/response paradigm.

Modern perceptionism has a strict biological foundation by recognizing the brain as the sole organ of consciousness (e.g., LUNGWITZ, 1947; MATURANA, 1978). This implies that each and every percept corresponds with a specific physiologic state of the brain. This holds as a one-to-one mapping, because brains as everything else in the world are in a state of steady transition and will never be exactly the same again (compare *Herodot's* $\pi\alpha\nu\tau\alpha' \rho\tilde{\varepsilon}\iota$

2.1. Perceptual organization

To apply a perceptionist's view to problems and tasks in psychoacoustics, a model of the perceptual organization of the world is needed. To this end, the totality of percepts may be grouped into different categories. Following a concept of LUNGWITZ (1947), suitable categories are *feelings, things* and *concepts*.

Feelings normally occur when sensors inside the body are activated, and they are usually perceived at or close to the positions of the sensors (e.g., stomach pain, fear in the heart). In special cases, feeling can also be located outside the limits of the body, for instance, phantom pain after amputation of limbs.

Things (sensory percepts, sensory events) for example, auditory, visual, or tactile or proprioceptive ones (LUNGWITZ, 1947; BLAUERT, DOMINICUS, 2013; BLAUERT, JEKOSCH, 2012) usually appear while sensory organs are active. They are mostly located outside the body, but in special cases they may also be inside – like tinnitus in the ear or light speckles in the eye

[1] Perception implies both a perceiver (observer) and what is perceived (percept). KANT (1781) has therefore introduced a conceptual observer as counterpart of the percept. It has been clarified (see LUNGWITZ, 1947; DOMINICUS, 2009) that this conceptual observer cannot be further analysed, since the polar opposition to any existence is non-existence. Something that exists, always exists as a polar counterpart to non-existence. This conjunction-in-opposition cannot be broken up.

due to a sick headache. Further, coordinative percepts (position, direction and strength) may be subsumed under sensory perception (see proprioception). Sensory percepts are modality-specific, that is, they are either auditory, visual, tactile, gustatory, olfactory, or coordinative.

Concepts (ideas, notions, thoughts) are associated with feeling or things, but do not directly originate from signals sent by body-internal sensors or sensory organs. In essence, concepts are more or less abstract remembrances of feelings, things or other concepts. On the one hand, they are certainly percepts themselves, on the other hand, they are pointers to other percepts[2].

3. The paradigm of psychoacoustics

In the following, the relationships between acoustic stimuli and auditory events will be discussed, since these are the primary item of psychoacoustic research.

In this paper, we shall argue solely on the basis of things and concepts, leaving out the feelings at the time being for the sake of simplification, although feelings, to be sure, are a very important category of percepts.

The commonly used experimental paradigm in psychoacoustics is shown in Fig. 1, which schematically represents a listener in a hearing experiment (Blauert, Guski, 2009). The input is given by a "stimulus" (acoustic event), S, in our case a sinusoidal acoustic wave. If this wave is in the range of hearing and the listener has a functioning auditory system, he/she will hear something, that is, in his/her world appears an auditory thing (auditory event), T. Yet, as this thing exists in the world of the listener, an outside observer can only get to know of it through an observable response, R, of the listener.

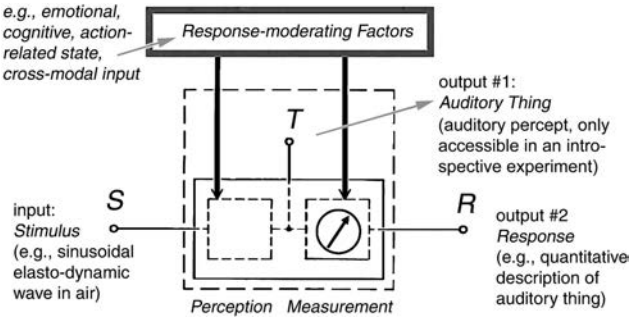

Fig. 1. The paradigm of psychoacoustical experiments.

[2]Perceptual categories are confluent, i.e. the borders between them are not strict. This is also reflected by the terminology used to describe them. For instance, the term "sensations" is used for sensory percepts (things) in psychology, while in colloquial language it is also used for feelings. Yet, the term feelings, used here in the sense of emotional responses, can in colloquial terms also mean the sense of tactility, i.e. what is felt at the skin when touched.

In psychoacoustics, the listeners are instructed and trained to respond by way of quantitative judgment upon perceptual attributes of their auditory events. Specifically, they are requested to assign numbers to attributes of what they hear. If the assignment of numbers to the perceptual attributes of auditory events actually reflects these attributes in a valid way, then this procedure can be taken as a measurement. In fact, the listener, who now assumes the role of an assessor, has two roles in the game: First, his/her auditory perceptual system is the item to be measured, secondly, the assessor him/herself is the measuring instruments to actually perform this measurement.

Since both, perception and measurement, are dependent on the assessors' individuality, the actual experimental situation and the mental state that the assessor is in, some models assume "modifying factors" to take account of these effects (e.g., Guski, 1999). In the following, the psychoacoustical paradigm of Fig. 1 will be evaluated from a perceptionist's point of view.

3.1. The "stimuli"

In psychoacoustics, the stimuli concerned are acoustic ones – "acoustic" meant in its physical sense, that is, vibrations and waves of elastic media. Vibration and waves are coordinative variation of matter. If very slow, we may see them or sense them by touch, if faster, we detect and measure them instrumentally. Note that *audition is not at all involved so far* (Blauert, 2006; Blauert, Jekosch, 2012).

From thinking about such visual and tactile perceptions and other relevant observations, a physical theory of mechanics has evolved – in its classical form – *Newton*'s mechanics. For instance, physical concepts like mass and force have been developed, leading to even more abstract concepts like, for instance, the wave theories of sound propagation in fluids and solids. Nevertheless, to be sure, the physics of mechanics is originally based on visual and tactile observation and successive thinking. In other words, it is a conglomeration built from visual/tactile things and concepts – surely percepts all together. Consequently, physical objects like *elasto-dynamic waves and vibrations are concepts and not things* (!), but nevertheless percepts. This obviously holds also for the acoustic stimuli in psychoacoustic experiments.

How come then that in terms of the world model of realism, physical objects are assumed to exist outside perception and thus being "absolutely objective". To discuss this, the meaning of objectivity has to be recollected first. In empirical sciences, the results of an experiment are considered objective if the results do not depend on specific observers. This actually means that you may bring your experiment to a different laboratory with different experimenters, and they would still get the same results.

To get as close as possible to the goal of objectivity, physics has "cultivated" instrumental measuring equipment to render result where the influence of the individual experimenter is minimized[3]. Further, physical theories are based on mathematics, that is, the results of physical experimentation are interpreted and described in mathematical terms. If experimental results differ from what is theoretically (mathematically) predicted, the differences are classified as "errors" and often disregarded. But note that mathematical thinking is governed by standardized logic rules. If two mathematicians come to different results with regard to a mathematical problem, at least one of them has violated the rules. In this way, mathematical thinking is certainly signified by a high amount of objectivity, but when experimental results are forced into a mathematical, that is, a conceptual framework, the achieved objectivity is conceptual as well – and certainly not "absolute" in any way.

All this can be dealt with within perception. An extrapolation to a transcendent world is not necessary. We do not need the notion of absolute objectivity at all. The amount of objectivity of an experimental result can be marked on a polar scale reaching from utmost objective to utmost subjective. Utmost subjectivity means that no two assessors agree on a result, utmost objectivity that all potential assessors would agree.

3.2. The auditory "things"

What listeners sensorily perceive in the course of listening experiment *exists* in their world *as being heard*. This is what we call the auditory things. Like any other things, they exist at specific times at specific locations, attributed with specific (auditory) features.

Classical psychoacoustics aims at assessing the relationship between features of the (physical) stimuli and features of the auditory things in a quantitative way. To this end, so-called "psychometric" methods have been developed that enable assessors to assign numbers to auditory features in such a way that relations between numbers reflect relations between the features under observation. These methods enable measurements of thresholds of perception, difference limens, points of perceptual equality, further, they allow for direct estimation of intervals, ratios and magnitudes.

In the attempt to measure auditory features in their "pure form", the according listening experiments are designed in such a way that the measurements are, hopefully, not biased by any conceptual context. For instance, signals are used that do not carry explicit meaning (sinusoids, complex tones impulses, noises, etc.). Further, the assessors are not provided with any contextual information (e.g., the nature of the sound source, the scenario and its history). Auditory features that have been investigated in this way are, for instance, loudness, pitch, sharpness, roughness and spatial extension. Yet, to be sure, context free perception does not really exist (Blauert, Guski, 2009). Already a "context-free" experiment is a context. Also, mind that auditory features are attributes of auditory things and not things themselves.

In any case, when assessing auditory features, the listeners have to be in an analytic (discretic) listening mode, concentrating on just the feature under observation and disregarding auditory things as a whole. However, humans are usually in a holistic (syncretic) listening mode, that is, attending to larger perceptual entities than auditory features or even auditory things. Cognitive psychology argues that the human brain, as a rule, does not think in sensory percepts (things) but in "objects". Objects are perceptual entities that represent an agglomeration of direct sensory input and conceptual reflection. Hence, to understand auditory perception in a more comprehensive way, the processes of object building need to be considered and understood. In this context, the well known *Gestalt* rules are, for instance, relevant. Numerous further "schemata" have been identified by psychologists to be involved in the neural processes of object forming.

From the point of view of a perceptionist, these processes do not pose any epistemological problem. Both sensory percepts (things) and concept are "brainchilds", that is, are bound to physiological processes in brains. Objects can be understood as conceptual constructs that result from agglomerating intercurrent series of things and related thoughts. Objects, thus, are perceptual entities of their own, but represent the underlying sensory percepts and the related reflections in a more abstract way. The same processes, by the way, also hold for "physical" objects (see Sect. 2.1), they are also conceptual constructs, that is, a particular kind of percepts.

Consequently, when analyzing and interpreting auditory things, it is necessary to see them in their perceptual context. Things have attributes that can be assessed separately, but even more so, things are elements of the formation process of objects – the actual building bricks of the world in perceptual terms.

This means that classical psychoacoustics can only render limited insight into the correlation between physical and auditory aspects of our world. In other words, its prognostic power when predicting auditory events from their physical correlates is limited. The common excuse is that the prediction errors are due to the subjective nature of auditory things in contrast to the objective nature of physical objects. This excuse will only be accepted by a perceptionist when phrased as follows: Physical objects are perceptual constructs

[3]In modern theoretical physic it has been realized that the item of observation may change with the actual kind of observation – another case against "absolute objectivity", that is, existence indepent from the observer.

that have been derived from results of measurements that are largely independent of specific observers, that is, which are rather abstract concepts. In contrast, auditory things have a much lower level of abstraction and are, consequently, more individual. Hence, physically measured data may certainly provide rough, general estimates of auditory attributes in specific, well defined situations. However, they show a severe deficit in terms of validity when it comes to the prediction of auditory things or even auditory object in specific situational contexts.

To increase the validity of the prognosis, processes have to be taken into account which classic psychoacoustics cannot unravel. Here knowledge from sensory psychology has to be taken into account, verified or at least supported by neurological findings to maintain the link to the biology of the brain and thus, to ensure the scientific foundation of the model. The "modifying factors" as introduced in Fig. 1, are really only a very rough approach to deal with this problem.

This means, among other things, that the classical psychometric methods have to be amended. Two different aims of measurement can be distinguished in this context, (i) analysis of auditory objects and scenes to identify and scale their different perceptual attributes individually, (ii) assessment of holistic features of auditory objects and scenes, for instance, the sound quality assigned to them by listeners. For measurements of type (i), method like the semantic differential or multidimensional scaling are applied, for type (ii), paired comparison or direct magnitude scaling on one-dimensional interval or ratio scales are in use.

Note however, that for the perceptionist all these measurements take place within the world of percepts. An extrapolation to a transcendent world beyond the perceived one is not obligatory to understand the latter.

3.3. The "responses"

Auditory things are directly experienced by the listener whose percepts they are. For an observer of this listener, these auditory things are not directly accessible, but only indirectly via the response of the listener – which can, for instance, be a spoken verbal description of what he/she hears. The observer then concludes that there exists a perceptual world for the listener and that there are auditory things and/or objects in it.

A realist could now argue with the perceptionist as follows: On the basis of the response of the listener, you conclude that there exists a perceptual world of this listener to which you principally do not have direct access. Isn't the listener's world just such a transcendent world as you otherwise try to deny? The perceptionist's answer is as follows: My directly experienced percept is, of course, the response of the listener and not the listeners' auditory thing. So, the item which is a *fact of direct experience* for the listener, is only a *fact of description* for me, the observer (Lungwitz, 1947). The listeners' auditory things are thus concepts for me and not things – yet, without doubts, percepts in any case. These concepts arise as a conclusion from what I hear as a spoken message, that is, from auditory objects in my world. An extrapolation to the existence of a world beyond perception and, thus, beyond the biologic capabilities of the brain, is logically not imperative.

After having introduced a distinction between facts of experience and facts of description, it is interesting to have a closer look at the attributes of those auditory things that relay facts of description, and on the subsequent concepts which represent them. This concerns the scientific fields of communication sciences and, particularly, of semiotics (the theory of signs).

It is a generic task of the auditory system to act as a kind of antenna with a subsequent processing stage to provide the brain with input for the formation of its perceptual world. In this way, for example, the identification of sound sources in the environment regarding their temporal and spatial position can be explained. Further, the auditory system is of paramount importance for inter-individual communication – in human beings mainly via speech (spoken language).

Generally, it can be stated that all auditory things and, thus, also the acoustic stimuli as being correlated with them, can be conceived as sign carriers that relay information about the world. As a consequence, meaning may be assigned to the relayed signs. It is the specific schemata that underlie these processes of thinking which are investigated by semiotics.

Semiotic teaches that three requisites are indispensable for the assignment of meaning to happen, namely, an auditory thing, a listener and a conceptual reference. Only when these three components are present, signs can be understood, that is, a meaning may become apparent. By the way, audio engineers, sound designers, and also composers and musicians, etc., can be seen as engineers of aural communication. They provide sound signals which lead to auditory things that carry meanings, which are, hopefully, understood by the listener as intended.

The processes of meaning assignment are complex. For instance, when spoken language is understood, the auditory things have been identified as speech sounds (phones) and as belonging to a certain language (allophones), and these have then been interpreted on the word and sentence levels. Thereby phonetic, syntactic and grammatical rules have been observed and prosodic characteristics have been considered. Of course, as a further condition of successful meaning assignment, the vocabulary used must be known to the listener.

In any case, the interpretation of acoustic and auditory "cues" requires cognitive processes at a higher level of abstraction. It is thus not surprising that in

semiotics a notion is put forward as to which the conceptual interpretation of the world is primarily based on signs, their recognition, interpretation and a subsequent assignment of meaning. Thereby the interpretation of known signs may well become a routine operation after a while, and the assignment of meaning is then conceived as a schematic process in these cases.

The semiotic way of interpreting the world is highly important for the predictions of actions (and reactions) of people, since people usually do not act and judge upon what they hear and where they hear something, but rather on what they hear actually means to them in their individual situation.

Signs can have the character on an *index*, an *icon*, or a *symbol* (Jekosch, 2005). An index is a copy or slightly modified copy of a sound as originating from a particular event, for example, the breaking of a drinking glass when falling from a table. An icon represents an abstraction from of the original sound in such a way that a simplification has taken place, but the relevant features have been preserved or even enhanced. A symbol has not necessarily any direct relationship with the event that it symbolizes. Therefore, the relationship between symbols and what they symbolize has to be learned, as, for instance, the relationship of *Morse*-code units and the letters that they symbolize. Indices, icons and symbols are concepts, and thus percepts from the perceptionist's point of view. They differ in the amount of abstraction from their underlying sensory percepts, namely, the auditory things which they represent. While indices relate to individual events, icons do so for a class of events in a more abstract way. Symbols, finally, abstract completely from their perceptual roots. Their meaning is originally arbitrary and must therefore be deliberately assigned, and then be learned.

When it comes to measurement of the meaning that auditory things communicate, the traditional methods of psychoacoustics and sensory and cognitive psychology are rarely helpful. If methods like the semantic differential or multidimensional scaling are applied at all, the scenarios in which they are applied must represent real communication scenarios. More adequate are questionnaires and behavioral tests in representative situations as, for instance, applied in cognitive psychology and the social sciences.

4. Discussion and conclusion

In this contribution we promote a world view that is different from the objectivistic *realism* which is usually favored by engineers. This alternative is *perceptionism*. The basic ideas of both, objectivistic realism (also discussed as, e.g., scientific realism or positivism) and perceptionism (also discussed as constructivism or concientialism), have a long tradition in epistemology.

Perceptionism is based on the notion that to be perceived and to exist are synonyms (Berkeley, 1710). Any assumption of existence beyond perception, that is, existence independent from observers, is discarded as a game of thoughts without any empirical evidence. Thus, in the perceptionist's view, "absolute objectivity" does not exist. Even physical objects are unmasked as perceptual items, namely, as a conglomerate of visual and tactile percepts plus successive theoretical thinking.

To develop logical consistence of the perceptionist's model, two issues have to be realized:

- Concepts (thought, ideas, concepts, notions) are real percepts and not in any way enigmatic, shadowy items. In particularr, concepts are percepts that point to other percepts. They essentially are remembrances, although more or less abstract ones [7, 15, 16].
- It is necessary to distinguish between facts of experience and facts of description. While auditory things in my own world are facts of experience, auditory things in the world of somebody else are (only) facts of description in my world – but nevertheless percepts.

A driving reason to look closer into the perceptionist's world view is the following: Since perceptionism puts physical objects at the same epistemological level with auditory things and concepts – actually unmasks them as being concepts (constructs), any discrimination against psychoacoustic as an assumingly absolutely subjective science looses its substance. In fact, physics itself is recognized as being basically perception-based. *Objectivity is thus identified as being relative in essence, so is subjectivity.*

Acknowledgments

The author gratefully acknowledges ideas and constructive criticism offered by Prof. Dr. U. Jekosch, Dresden and Dr. R.-D. Dominicus, Ratingen. The material of this article has been orally presented at the 59th International Conference of the Polish Acoustical Society, OSA 2012, in PL-Boszkowo.

References

1. Becker R. (1978), *The problem with the retina image*, [in German: *Das Problem mit dem Netzhautbild*], Huber, Bern–Stuttgart–Wien.
2. Berkeley B.G. (1710), *Treatise on the principles of human knowledge*, Jeremy Peypat, Dublin.
3. Blauert J. (2006), *Reality, virtual reality –and the roots of psychoacoustics*, [in German: *Scheinwelten, Wirkwelten –und die Wurzeln der Psychoakustik*, Fortschr. Akustik, DAGA'06, 303–304, Dtsch. Ges. Akustik, Berlin.

4. Blauert J. (2011), *Epistemologic bases of binaural listening – a perceptionist's approach*, Proc. Forum Acusticum 2011, pp. 2149–2154, European Acoust. Ass., Madrid.
5. Blauert J., Dominicus R.-D. (2013), *The things, feeling and thoughts of the aural world – an epsistemolic analysis regarding quality judgment*, [in German: *Die Dinge und Gefühle der auralen Welt – Eine epistomologische Analyse mit Hinblick auf Qualitätbeurteilung*], [in:] *Faszinosum "Klang": Anthropologie – Medialität – kulturelle Praxis*, Schmidt W.G. [Ed.], De Gruyter, Berlin (in press).
6. Blauert J., Guski R. (2009), *Critique of "pure" psychoacoustics*, Fortschr. Akustik—-NAG/DAGA'09, 1550–1551, Dtsch. Ges. f. Akustik, Berlin.
7. Blauert J., Jekosch U. (2007), *Auditory quality of concert halls – the problem of references*, Proc. 19-th Int. Congr. Acoust., ICA 2007, Revista de Acústica, **38**, paper RBA 06–004.
8. Blauert J., Jekosch U. (2012), *A layer model of sound quality*, J. Audio-Engr. Soc., **60**, 4–12.
9. Descartes R. (1641), *Meditationes de prima philosophia*, (German ed.: *Meditationen über die Erste Philosophie*, Reclam, Stuttgart, 1986).
10. Dominicus R.-D. (2009), *The subject theory of radical constructivism*, [in German: *Die Subjekttheorie des radikalen Konstruktivismus*, Diplomica-Verlag, Hamburg.
11. Guski R. (1999), *Personal and social variables as co-determinants of noise annoyance*, Noise and Health, **3**, 45–56.
12. Hume D. (1740), *A treatise of human nature*, German ed., vol. 1 & 2, *Ein Traktat über die menschliche Natur*, Meiner, Hamburg, 1978/1989).
13. Jekosch U. (2005), *Assigning meaning to sounds – Semiotics in the context of product-sound design*, [in:] Communication acoustics, Blauert J. [Ed.], Springer, Berlin–Heidelberg–New York NY.
14. Kant I. (1781), *Critique of pure reason*, [in German: *Critik der reinen Vernunft*], Johann-Friedrich Hartknoch, Riga.
15. Lungwitz H. (1947), *The discovery of the psyche*, [in German: *Die Entdeckung der Seele*], 5-th ed., De Gruyter, Berlin.
16. Maturana H.U. (1978), *Biology of language: The epistemology of reality*, [in:] *Psychology and Biology of Language and Thought: Essays in Honor of Eric Lenneberg*, Miller G.A., Lenneberg E. [Eds.], pp. 27–63, Academic Press, New York.

PAN ARCHIVES OF ACOUSTICS
Vol. **37**, No. 3, pp. 373–393 (2012)

DOI: 10.2478/v10168-012-0047-y

Chronicle

59th Open Seminar on Acoustics
Boszkowo, Poland, September 10 – 14, 2012

The Scientific and Organizing Committees of 59th Open Seminar on Acoustics would like to present the abstracts of papers submitted for this conference. The Open Seminar on Acoustics (OSA) is an annual conference, the largest in the country which has been bringing Polish acousticians together for nearly sixty years. It is organized sequentially by different departments of Polish Acoustical Society (PTA) – in 2012 by the Poznań Division. The conference presents all sections of acoustics, such as: physical acoustics, technical acoustics, environmental acoustics, speech acoustics, hearing acoustics, musical acoustics, architectural acoustics, etc. The aim of the conference is to exchange scientific experience in the field of acoustics, promote science and integrate specialists from various fields. The integration of Polish acousticians is extremely important because of the interdisciplinary nature of acoustics as a science. This allows the exchange of ideas, research methods and possibilities of application used by researchers and practitioners the many branches of acoustics.

Arkadiusz Józefczak
Organizing Committee Chairman

Abstracts

Computer simulations for testing the acoustic field using intensive sound method

Augustyn Aneta

KOMAG Institute of Mining Technology
Pszczyńska 37, 44-101 Gliwice, Poland

The paper is an attempt of presentation of multivariant analyses of acoustic field on the basis of tests made with use of intensive sound method. The scope of tests refers especially to the impact of existing objects on acoustic field in open spaces (environment). Computer simulations in the scope of tests of acoustic field with use of intensive sound method were the subject of the analyses. The simulations were possible after a series of acoustic measurements made at the previous stage of the project. The measurements were made in a closed space and in the environment surrounding the tested object. The scope of applied tests covered the measurements of sound intensity with use of intensive sound method inside industrial object as well as the measurements of sound level in the environment taken by the pressure method at points, which were under assessment. A series of computer simulations, which aimed at validation of intensive sound method, as well as at proving the superiority of this method in testing of acoustic field in the environment were the project objectives. Scope of the project includes the tests carried out in anechoic chamber at the Institute of Thermal Technology in Lodz as well as the tests realized on industrial object.

⋆ ⋆ ⋆

Statistical analysis of the equivalent noise level

Batko Wojciech[1], batko@uci.agh.edu.pl
Przysucha Bartosz[2], b.przysucha@pollub.pl

[1] AGH University of Science and Technology
Faculty of Mechanical Engineering and Robotics
Department of Mechanics and Vibroacoustics
al. A. Mickiewicza 30, 30-059 Kraków, Poland
[2] Lublin University of Technology
Faculty of Management
Department of Quantitative Methods
in Management of Economy
Nadbystrzycka 38, 20-618 Lublin, Poland

In the article, the authors focus their attention on the analysis of the probability density function of the equiva-

lent noise level in the context of the problems of the analysis of the uncertainty results present in the control of environmental noise hazards. They examine the issues of accuracy and applicability of the classical normal distribution for the interval estimation of the expected values of the equivalent sound level. What is more, they provide procedures for its derivation, with the assumption of a given distribution of the results produced by sample results of measurements. The results obtained give grounds for the correct calculation of the uncertainty of the controlled rate of acoustic environmental hazards.

⋆ ⋆ ⋆

A perceptionist's view on psychoacoustics

Blauert Jens

Ruhr-University Bochum
Institute of Communication Acoustics
44780 Bochum, Germany

Psychoacoustics is traditionally based on a world model that assumes a physical world existing independently of any observer – the so-called objective world. Being exposed to this world, an observer is impinged upon by a variety of stimuli reaching his/her sensory organs. These stimuli, if physiologically adequate, may cause biological transduction and signal processing in the sensory organs and its afferent pathways in such a way that finally a specific excitation of the cortex takes place, which results in sensations to appear in the observer's perceptual world. The sensations are understood as being subjective, since they require an observer to exist. This world model – also known as (objectivistic) realism – reaches its limits when it comes to explaining more complex phenomena of perception. Thereupon, in this paper, an alternative world model is emphasized and applied to psychoacoustics, namely the perceptionist's model. Like realism, perceptionism has a long tradition in epistemology. It appears to be suitable to improve our understanding of perceptual organization.

⋆ ⋆ ⋆

Investigation of relative vibratory detection thresholds on wrist

Bogusz Edyta
Skrodzka Ewa

Adam Mickiewicz University
Institute of Acoustics
Umultowska 85, 61-614 Poznań, Poland

In the paper relative values of vibration detection thresholds on two points on a wrist and index, middle and ring fingertips are presented. Measurements on fingertips were done to calibrate measurement setup and to find relative differences in thresholds for the wrist and fingertips. Palestesiometer P8 (Emson-Mat) was used as a measuring device. Measurements were performed in frequencies of 4, 16, 25, 63, 125, 250, 400 and 500 Hz. Two measuring probes were used: with diameter of 5 and 12 mm, working with the force 0.1 and 1.2 N, respectively. Both hands of women and men were investigated. Results show that hand and measuring probe size were not significant factors for fingertips thresholds. For the wrist not significant factors were gender and the place on the wrist. Thresholds found for the wrist were significantly higher than those for fingertips. Differences in threshold values were up to 20 dB in frequencies below 125 Hz. No statistically significant differences were found in results for sighted, blind and visually handicapped subjects.

⋆ ⋆ ⋆

The problem of determining the orchestra pit acoustic parameters

Brawata Krzysztof
Kamisinski Tadeusz

AGH University of Science and Technology
al. A. Mickiewicza 30, 30-059 Kraków, Poland

The paper presents results of acoustic measures performed in selected opera houses orchestra pit for the analysis of stage parameters (ST) and the sound strength (G). Analysis of collected data has allowed the development of research capabilities with the parameter G, while there were significant limitations on the applicability of ST. The article presents significant limitations of current methodologies used in acoustic research in orchestra pit and proposes opportunities for other research methods to enable a better assessment of the interior.

⋆ ⋆ ⋆

The use of the idea of smart acoustics to acoustic climate management

Czajka Ireneusz
Suder–Dębska Katarzyna
Gołaś Andrzej

AGH University of Science and Technology
Faculty of Mechanical Engineering and Robotics
Department of Power Engineering
and Environmental Protection
al. A. Mickiewicza 30, 30-059 Kraków, Polska

The implementing the climate-energy package is one of the most important factors determining the future of energy in the European Union, linked to the idea of Smart Cities. Taking into consideration the current projections, it can be assumed that by 2030 the urban population will double and will be around 2.64 billion. Hence, increase the residents' needs and requirements of these cities. It is therefore necessary to undertake intensive, integrated actions to the effective production and use of energy in each sector, while protecting the environment and improving quality of life. As a result of the idea of Smart Cities, cities will become more efficient and sustainable in areas such as transport, energy, information and communication technologies. The idea of Smart Acoustics allows such a broad of acoustic climate of agglomeration to reduce the adverse impact of noise on people staying in it. In the paper there has been briefly discussed some aspects of the two areas of noise and vibration threats occurring in the cities, that are mass events, and more commonly used of air conditioning equipment.

⋆ ⋆ ⋆

Propagation of acoustic wave in polyatomic gases in high temperatures

Czyż Henryka, hczyz@prz.edu.pl

Rzeszow University of Technology
Department of Physics
Powstańców Warszawy 6, 35-959 Rzeszów, Poland

Presented work concerns the phenomena occurring during the propagation of acoustic waves in polyatomic gases at high temperature. The formula expressing acoustic waves velocity depends on the specific heat ratio at constant pressures c_p to a specific heat at constant volume c_v. In normal temperature κ is constant and is determined by the internal structure of the gas molecules. In high temperature vibrations of molecules begin to play an important role and the dependence of the specific heat at constant pressure and specific heat at constant volume on the temperature is obtained. In theses cases the dependence of acoustic wave velocity on the temperature is complicated. This subject contains important aspects of the development of modern aviation and rocketry technology.

⋆ ⋆ ⋆

The effect of musical activity of listeners on their tuning ability

Dziedzic Tomasz, Kleczkowski Piotr

AGH University of Science and Technology
Department of Mechanics and Vibroacoustics
al. A. Mickiewicza 30, 30-059 Kraków, Poland

In this work the effect of musical activity of listeners on their ability of tuning sounds was investigated. This ability is directly tied with the perception of pitch. The research on a large group of seventy listeners with variable degree of musical activity led to separate conclusions on the effects of musical education and musical activity. The effect of acoustic disturbances typically met during musicians' work on the quality of tuning was also examined.

⋆ ⋆ ⋆

Experimental verification of computational simulation destined for received directional characteristics of panel sound source

Flach Artur, Frączek Jacek
Gorazd Łukasz, Kamisiński Tadeusz
Szeląg Agata, Wiciak Jerzy

AGH University of Science and Technology
al. A. Mickiewicza 30, 30-059 Kraków, Poland

The paper describes an experiment carried out on the set of sound panels designed for generating high sound pressure level. The influence of arrangement of two sound panels on directional characteristic of the set was studied. Measured characteristics were compared with results received from model computation. This analysis showed compatibility of both received characteristics. Thus, one may say that proposed computer model makes it possible to predict the sound field of source in the form of various configuration of loudspeaker panels what facilitates the control of sound spread.

⋆ ⋆ ⋆

Localization of amplitude-panned stereophonic phantom sources in the horizontal plane

Frank Matthias

University of Music and Performing Arts Graz
Institute of Electronic Music and Acoustics
Leonhardstraße 15, 8010 Graz, Austria

The localization of stereophonic phantom sources has been studied for decades. However, most studies were limited to the standard ±30 degree loudspeaker setup. This article reviews some experimental results and models for phantom source localization using amplitude panning on the standard loudspeaker setup, as well as on non-standard setups. By incorporating the directivity of human hearing, a model is developed that predicts the localization of broadband phantom sources for loudspeaker pairs at arbitrary directions on the horizontal plane. Moreover, the article investigates subjective differences in the localization of phantom sources and presents a way to predict these differences.

⋆ ⋆ ⋆

Source width of frontal phantom sources: perception, measurement, and modeling

Frank Matthias

University of Music and Performing Arts Graz
Institute of Electronic Music and Acoustics
Leonhardstraße 15, 8010 Graz, Austria

Phantom sources are known to evoke perceptual differences compared to real sound sources. One of these differences is an increase of the perceived source width. This article discusses the perception, measurement, and modeling of the perceived source width for frontal phantom sources with different symmetrical loudspeaker arrangements. First, the perceived source width is evaluated by a listening test. The test results are compared to technical measures that are applied in room acoustics: the interaural cross correlation coefficient (IACC) and the lateral energy fraction (LF). Furthermore, an adaptation of the latter measure is developed to extend its application to simultaneous sound incidence. Finally, a geometrical model is presented for the prediction of the perceived source width.

⋆ ⋆ ⋆

Statistical distributions of levels and energy of aircraft noise

Gałuszka Michał

Adam Mickiewicz University
Institute of Acoustics
Umultowska 85, 61-614 Poznań, Poland

In many cases statistical distribution of random variable is nearly normal. The sound exposure level LAE measures the noise of sound events, such as aircraft operations or train pass-bys. The empirical mean estimates the central tendency of LAE distribution. Due to random nature of noise generation and propagation, this estimation is uncertain. If the statistical distribution of SEL is normal, then the standard deviation of LAE yields the exact measure of this uncertainty. Furthermore, in such a case one can define this uncertainty with the assumed confidence level. It

is shown in this study that both, the statistical distributions of sound energy e and the sound exposure level SEL of an aircraft noise, are not normally distributed. Since the classical method of uncertainty estimation is difficult to be applied in this case, we propose a new method based on the kernel density estimator (KDE). The paper presents an analysis of the distributions data, as well as elucidates the observed deviation from the normal distribution.

⋆ ⋆ ⋆

Wavelet approach to RF signal analysis for structural characterization of soft tissue phantom

Gambin Barbara[1], bgambin@ippt.gov.pl
Doubrovina Olga[2]

[1] Institute of Fundamental Technological Research
Polish Academy of Sciences
Pawińskiego 5B, 02-106 Warszawa, Poland
[2] Byelorussian State University
Faculty of Humanities
Department of Information Technology
4, Nezavisimosti avenue, 220030 Minsk, Republic of Belarus

To develop the theoretical and experimental basis for temperature measurement during heating of internal regions of soft tissues we would like at first to find an answer to the question what parameters characterizing the ultrasonic acoustic signal, being recorded during the heating, are significantly associated with the local temperature increase. First step is to study acoustic properties of self fabricated soft tissue phantoms by different approaches to proof efficiency of methods used in the future analysis, which will be more complicated in the case of heating. The paper contains the wavelet approach of registered RF signal transmitted by soft tissue phantom samples in the constant room temperature. Three phantoms with different structures have been measured. We claim that there is qualitative differences in the wavelets forms between phantom without scatterers and with seldom number of strong scatterers, while the large number of scatterers demonstrates qualitatively similar wavelet characteristics as phantom without scatterers.

⋆ ⋆ ⋆

Pitch representation in the frequency following response (FFR)?

Gockel Hedwig E.

MRC-Cognition and Brain Sciences Unit
15 Chaucer Road, Cambridge CB2 7EF, UK

In recent years, there has been increased interest in the scalp-recorded frequency following response (FFR), which is an electrical recording that reflects sustained phase-locking of a population of neurones in the upper brainstem to stimulus-related periodicities. It provides a non-invasive measure of neural processing in humans, which can be compared to behavioural responses concerning the listener's perception. It has been argued (e.g. Russo *et al.*, 2008) that the FFR reflects processes important for the perception of pitch and that changes in the FFR with experience and/or training provide a measure of neural plasticity at the level of the brainstem.

Several experiments will be presented, aimed at elucidating the origin and the specifics of the information present in the FFR. It will be argued that the neural responses measured by the FFR preserve temporal information important for pitch, but do not necessarily represent pitch-related processing over and abo ve that already present in the auditory periphery [Supported by Wellcome Trust Grant 088263].

Reference

1. Russo N.M., Skoe E., Trommer B., Nicol T., Zecker S., Bradlow A., Kraus N. (2008), *Deficient brainstem encoding of pitch in children with autism spectrum disorders*, Clin. Neurophysiol. 119, 1720–1731.

⋆ ⋆ ⋆

The risk of noises environmental pollution in the shale gas harvesting

Gołaś Andrzej
Czajka Ireneusz
Suder–Dębska Katarzyna

AGH University of Science and Technology
Faculty of Mechanical Engineering and Robotics
Department of Power Engineering
and Environmental Protection
al. A. Mickiewicza 30, 30-059 Kraków, Poland

The problem of fuel extraction in recent years is more and more acute. The discovery of large layers of shale gas in Poland caused the emergence of giant hopes to become independent of imported gas. It places great emphasis on exploration and exploitation of deposits of this fuel. At the same time it is said a lot about the impact of the technology used to extraction of this gas on the environment. Therefore, the authors decided to present an outline of environmental pollution and noise in the search and exploration of shale gas based on the technology of hydraulic fracturing. It has been also presented the proposed system of visualization of the environment.

⋆ ⋆ ⋆

Modification of the measurement set-up to study the acoustic field of structures with cylindrical symmetry

Gorazd Łukasz[1]
Snakowska Anna[1]
Jurkiewicz Jerzy[2]

AGH University of Science and Technology
[1] Faculty of Mechanical Engineering and Robotics
Departament of Mechanics and Vibroacoustics
[2] Faculty of Electrical Engineering, Automatics, Computer Science and Electronics
Department of Metrology
al. A. Mickiewicza 30, 30-059 Kraków, Poland

The paper points out certain difficulties one comes across when attempting to obtaining reliable measurement results in experimental studies on the cylindrical waveguide acoustic field, especially for some specific configuration of sources located inside the system. An appropriate modification of the measurement set-up is proposed allowing to avoid, to a considerable degree, the above-mentioned diffi-

culties and ambiguities. Theoretical considerations pertaining to acoustic field distribution inside a cylindrical "unechoic" duct and phenomena occurring at the duct outlet, based on mathematical models of infinite and semi-infinite waveguide, respectively, reveal that, for certain configurations of sources, acoustic pressure may vary rapidly along the duct axis. In the measurement practice this can result in significant errors and ending up with result contrary to expectations, e.g. absence of the anticipated axial symmetry of the field in case of axisymmetric excitation.

⋆ ⋆ ⋆

Signatures and acoustic images of objects moving in water

Grelowska Grażyna[1]
Kozaczka Eugeniusz[1,2], kozaczka@pg.gda.pl
Kozaczka Sławomir[1]
Szymczak Wojciech[1], w.szymczak@amw.gdynia.pl

[1] Polish Naval Academy
Institute of Hydroacoustics
Śmidowicza 69, 81-103 Gdynia
[2] Gdansk University of Technology
Faculty of Ocean Engineering and Ship Technology
Narutowicza 11/12, 80-233 Gdańsk, Poland

Observation of underwater space is part of a general trend, which primary purpose is to protect and increase safety in the selected area. The basic aim of the paper is presentation of designated acoustic characteristics typical for objects moving on the water surface and under water, which represent some knowledge about detection of these objects. Create a catalog of acoustic signature and not only acoustic, as well as acoustic images of objects, mainly objects moving under water, may be an important contribution to efforts to increase the security of water areas and the public facilities located in nearby vicinity. This is a part of general security policy with regard mainly to the type of threats of terrorism and sabotage, but not only.

⋆ ⋆ ⋆

Ultrasonic studies of magnetic fluids: theoretical models and experimental results

Hornowski Tomasz

Adam Mickiewicz University
Institute of Acoustics
Umultowska 85, 61-614 Poznań, Poland

Magnetic fluids belong to a new class of magnetic materials that apart from properties typical to liquid, exhibit also week rigidity characteristic to solidlike media. Due to the possibility of remote controlling fluid's parameters using magnetic field, magnetic fluids have attracted considerable interest in their potential application in technological, biological and medical fields, such as seals, bearings, sensors, drug delivery, or magnetic hyperthermia. Recently, ultrasonic methods have been successfully applied to study different properties of magnetic fluids such as the particle (or aggregate) size distribution (PSD), level of anisotropy in external magnetic field or magnetic field-induced microstructure. The usefulness of the ultrasonic methods lies in their relative simplicity, non-invasive nature and thus in the possibility of performing the measurements in an intact, concentrated, dispersed system. In order to gain information on magnetic fluid properties from ultrasonic measurements the results of the ultrasonic studies have to be analyzed using appropriate theoretical model. One of such theory is based on the assumption that magnetic fluid can be treated as consisting of two phases: solid skeleton made of interacting clusters and fluid composed of carrier liquid with free magnetic particles.

⋆ ⋆ ⋆

Ultrasonic and thermal measurements of magnetic nanofluid stabilized with dextran biocompatible layer

Hornowski Tomasz, Józefczak Arkadiusz
Skumiel Andrzej, Dąbek Leszek
Leszczyński Błażej, Mikołajczak Jakub

Adam Mickiewicz University
Faculty of Physics
Institute of Acoustics
Umultowska 85, 61-614 Poznań, Poland

Magnetic nanofluids consist of nano-sized iron oxide particles suspended in carrier liquid. Magnetic nanoparticles used in this study are coated by a dextran biocompatible polymer that shields them from the surrounding environment and can be functionalized by attaching carboxyl groups, biotin, avidin and other molecules. Magnetic nanoparticles have proven its use as cell magnetic separators, transport of antitumor molecules, for hyperthermal treatment and as contrast agent for nuclear magnetic resonance (NMR), among other biomedical applications. A method based on propagation of ultrasonic waves is used to measure the particle (or aggregate) size distribution (PSD). The ultrasonic results are analyzed using Winogradow theory. Also the heating rate of the magnetic fluids in the alternate magnetic field is measured. It is found that the heating effect is associated with a lag between the field and magnetization due to the relaxation nature of the magnetization process in magnetic fluids This make possible to describe the results of thermal measurements within the framework of Rosensweig theory.

⋆ ⋆ ⋆

Structural noise reduction of a fluid-loaded smart structure

Iwański Dariusz, iwanski@agh.edu.pl
Wiciak Jerzy, wiciak@agh.edu.pl

AGH University of Science and Technology
Faculty of Mechanical Engineering and Robotics
Department of Mechanics and Vibroacoustics
al. A. Mickiewicza 30, 30-059 Kraków, Poland

In the present paper results of reduction of structural noise in fluid are presented. Resonant frequencies of circular fluid loaded plate were measured using swept sine technique on laboratory stand. The other side of the plate contains piezo elements used both as sensors and actuators. Actuators were used to generate vibrations of the plate and other to reduce sound pressure level in fluid, i.e. water and air. Results were compared with numerical calculations. Final

results reveal reduction of sound pressure level in fluid by more than 25 dB using only one piezo element.

⋆ ⋆ ⋆

Special-purpose windows airborne sound insulation measurements

Jakubowski Piotr
Kuśmirek Magdalena
Weryk Mateusz

Ship Design and Research Centre
Wały Piastowskie 1, 80-958 Gdańsk, Poland

Due to constantly increasing environmental noise levels, there is a need to build external walls with a relatively high sound insulation. If the building is located in the city center or near the large arteries, the required resultant external wall sound insulation is determined individually (based on the results of noise measurements in the vicinity of the building, then the calculations), and usually exceed the value of $R'_{A2} = 40$ dB. In case of marine windows or windows for the purpose of drilling platforms, sound insulation, required by shipowners, determined in the laboratory should be at least $R_w = 52$ dB. Obtaining a proper sound insulation of outside wall (or bulkhead) is associated primarily with the proper selection of materials from which wall (or bulkhead) is made of, but also its components, such as windows, and the technique and accuracy of installation is extremely important. Please note that the wall sound insulation is affected by insulation of all its elements.

⋆ ⋆ ⋆

Complexation in aqueous systems of α-D-glucose and DMSO in the ultrasonic study

Kaczmarek–Klinowska Milena
Kubiak Aleksandra
Hornowski Tomasz
Skumiel Andrzej

Adam Mickiewicz University
Faculty of Physics
Institute of Acoustics
Umultowska 85, 61-614 Poznań, Poland

Our investigations were concerned with the complexation processes in aqueous solutions of α-D-glucose and DMSO. The speed and absorption of ultrasonic waves were measured by a resonance method using the Resoscan TM System apparatus. Additionally, the density and the capacity in the investigated systems were measured, too. On the base of these data, thermodynamical parameters – such as molar volume, molar adiabatic compressibility and their excess functions, have been calculated. To be able to express the concentration of the ternary solution in mole fraction, the initial solutions of the water/α-D-glucose (water/ 6× α-D-glucose) ratio of 550/1 and of the water/DMSO at the same ratio, have been prepared. The composition of molecular complexes formed in the solution was determined on the basis of the correlation between the extremes of excess functions, ultrasonic absorption and the compositions of the mixtures.

⋆ ⋆ ⋆

Correction of acoustics in historic theatrical halls with the use of schroeder diffuser

Kamisiński Tadeusz, kamisins@agh.edu.pl

AGH University of Science and Technology
Faculty of Mechanical Engineering and Robotics
Department of Mechanics and Vibroacoustics
al. A. Mickiewicza 30, 30-059 Kraków, Poland

The paper deals with the problem of acoustic correction in historic theatrical halls with the auditorium layout in the form of a horseshoe with deep sub-balcony cavities limited with vaulted wall surfaces. Both geometry of the cavities and excessive sound absorption determine acoustic phenomena registered in this area of the hall. The problem has been observed in the Opera Hall in Lviv, Ukraine, where acoustic tests were carried out, simulation calculations performed, and finally a diffusion panel worked out designed for the rear wall of the sub-balcony cavity. Acoustic measurements carried out after installation of the system of diffusers revealed favourable changes in the sound strength parameter G within the range of medium and high frequencies in the sub-balcony and auditorium centre area. By replacing textile tapestry with diffusion panels, a significant reduction of sound absorption was achieved for the frequency range above 1 kHz and increase of uniformity of acoustic parameters registered in the hall. It is worth mentioning that despite some earlier fears, the technocratic design of the Schroeder diffuser, after careful selection of the colour scheme, has ultimately won the acceptance of the artistic milieu.

⋆ ⋆ ⋆

Noninvasive tissue temperature imaging by means of ultrasounds echo strain estimation

Karwat Piotr, Litniewski Jerzy
Secomski Wojciech, Kujawska Tamara
Krawczyk Kazimierz, Kruglenko Eleonora
Gambin Barbara, Nowicki Andrzej

Institute of Fundamental Technological Research
Polish Academy of Sciences
Pawińskiego 5B, 02-106 Warszawa, Poland

Therapeutic and surgical applications of ultrasound require monitoring of temperature changes. For these purposes ultrasonic techniques would be the most preferred from an utility and economic point of view. In this paper an attempt to apply the estimation of echo-signals displacement for monitoring of temperature changes during ultrasonic heating of tissues in vitro is presented. The data obtained by ultrasonic measurements have been processed to determine a map of echoes displacements and compared with the temperature distributions measured by thermocouples. The obtained results enable evaluation of temperature fields and give a promising prognosis for combining the ultrasonic tissue heating techniques with tissues temperature estimation.

⋆ ⋆ ⋆

How to listen professionally

Kawahara Kazuhiko

Kyushu University
Faculty of Design
6-10-1 Hakozaki, Higashi-ku, Fukuoka, 812-8581, Japan

What is the professional listening? Sound/Acoustic Professionals listening categorized into three phases. The ability to discriminate between different sounds. The ability to correlate the auditory difference with the physical properties of sounds. And the ability to imagine the proper sounds when given the acoustic properties of the sounds. The ability could be trained through listening training. In this paper, as a listening training, Technical Listening Training in Kyushu University was described. Through trainings, trainees can share their experience. The shared experience reinforces trainees to express their auditory impression with coherent words. And the use of coherent words supports smooth communication in their group. This word co-herency is also the professional listening ability.

⋆ ⋆ ⋆

Application of frequency and spatial compounding techniques for attenuation estimation in soft tissue

Klimonda Ziemowit, Litniewski Jerzy, Nowicki Andrzej

Institute of Fundamental Technological Research
Polish Academy of Sciences
Pawińskiego 5B, 02-106 Warszawa, Poland

The attenuation of the ultrasound within the soft tissue is often associated with pathological states which involve changes of tissue structure, like tumors. We are currently developing a technique for parametric imaging of attenuation and we intend to apply it for *in vivo* characterization of tissue. The method bases on tracking the spectral mean frequency shift resulting from the frequency dependence of the attenuation coefficient. The mean frequency lines are determined for each Radio Frequency (RF) line of the image data and next the attenuation profiles are estimated from the mean frequency shift. The high variance of the amplitude of backscattered echoes results in the variation of the attenuation estimates. In order to reduce the variation the spatial compounding and frequency compounding techniques were applied. These techniques effectively reduced the variation of the attenuation estimation, what was verified processing the simulated data and the echoes from the tissue mimicking phantom with uniform echogenicity but varying attenuation coefficient.

⋆ ⋆ ⋆

Detection of selected emotion in speech signal

Kłaczyński Maciej, Wszołek Wiesław

AGH University of Science and Technology
Department of Mechanics and Vibroacoustics
al. A. Mickiewicza 30, 30-059 Kraków, Poland

The goal of the present study is to examine use of speech acoustic signal and eletroglottographic signal (EGG) for purpose of automatic emotion recognition. The authors focuses on examining the impact of speaker's emotional state on the course of laryngeal tone. An experiment was to simultaneously record both acoustic and EGG signal of speech without emotional features and speech signal with features of happiness, sadness and anger. For all recorded signals following parameters were estimated: fundamental frequency (f0), jitter, shimmer and additionally for EGG signals open quotient (OQ) and speed quotient (SQ). And also for the spoken words of test was calculated the time courses of the root mean square (RMS) and the dynamic spectrums from recorded signals. Statistical analysis of calculated results led to conclusions: both acoustic and EGG signal of speech are suitable for the identification of emotion in voice; it is possible to develop models of vocal expression of emotion characteristics for different states; not all emotional states combined with a strong vocal expression.

⋆ ⋆ ⋆

A statistical approach in detection of noise events to aircraft noise assessment

Kłaczyński Maciej
Wszołek Tadeusz
Batko Wojciech

AGH University of Science and Technology
Department of Mechanics and Vibroacoustics
al. A. Mickiewicza 30, 30-059 Kraków, Poland

Long-term acoustical climate monitoring of the environment raises several problems related to large quantities of recorded data, which often represents information unrelated to the studied noise source. Manual verification of such data is time-consuming and costly. Therefore, to develop effective methods for automatic identification of transport noise sources (especially aircraft noise) becomes an important task for the proper determination of noise levels. In earlier authors' research to identification of noise sources and identify the type of airplane operations were used automated pattern recognition methods such as: artificial neural networks (Multi-Layer Perceptron, Adaptive Resonance Theory, Self Organizing Maps), minimum distance classifiers (Nearest Neighbor, k-Nearest Neighbor, Nearest Mean). In current research the probabilistic algorithm (statistical decision based on a threshold of discrimination) of classification was used. Acoustic pattern recognition method b ased on statistical decision has a 92% of correctness.

⋆ ⋆ ⋆

Transmission properties of underwater acoustic channel

Kochańska Iwona

Gdansk University of Technology
Faculty of Electronics Engineering, Telecommunications, and Computer Science
Department of Marine Electronic Systems
Narutowicza 11/12, 80-233 Gdańsk, Poland

Transmission properties of underwater acoustic channel are strongly conditioned by specific geographic location, and vary over time. In reliable communication systems, there is a need for adaptive matching of physical layer parameters of the data transmission signaling protocol. to instantaneous, often strongly varying, channel conditions. To achieve this goal, parameterized description of

the underwater communication channel is necessary. The paper presents results of impulse response measurements performed in a shallow-water, nonstationary channel, being then a basis for statistical characteristics of the WSSUS model of the time-varying, multipath channel. Transmission parameters were calculated, determining a design specification of physical layer of the communication protocol for a system based on the OFDM technique.

⋆ ⋆ ⋆

Loudness scaling for normal and hearing-impaired listeners: from measurements in the past to present models and future applications

Kollmeier Birger

University of Oldenburg
Medical Physics & Centre of Excellence "Hearing4all"
D-26111 Oldenburg, Germany

Categorical loudness scaling can be used to assess the "recruitment" phenomenon in patients with a "compression loss" in inner ear function which is usually connected to a dysfunction of the outer hair cells. A pure inner hair cell loss, on the other hand, will cause a shift of the loudness function comparable to a pure "attenuation" loss. In order to make these characteristic changes in loudness function accessible to clinical usage, the following developments were performed that will be reviewed and discussed:

- A fast and reliable Adaptive Categorical Scaling procedure (ACALOS, Brand and Hohmann, 2002) was introduced which is available on a clinical audiometry workstation,
- Fitting functions and a connection to "classical" loudness models (such as, e.g., recent variations of the Zwicker loudness model using a transformation between sone and CU,
- In comparison to other psychoacoustical methods for estimating the compression loss in hearing-impair ed listeners, ACALOS appears to be very time-efficient and easy to use. It thus qualifies as valuable clinical & research tool to be used in audiology.

⋆ ⋆ ⋆

Low-frequency rail noise risk in the environment

Kompała Janusz

Central Mining Institute
Plac Gwarków 1, 40-166 Katowice, Poland

In recent years in many countries, low-frequency noise – up to 200 Hz, has been regarded as one of the major environmental problems of human protection against excessive noise. For example, in accordance with the recommendations of the European Commission to be implemented in the near future, the ideas have been established among which there has also been the necessity to create a basis for assessment and mitigation of low-frequency noise in the environment. The research that has been carried out proved also that low-frequency noise emitted by the rail sources would not cause health problems but might be the source of many nuisances.

⋆ ⋆ ⋆

Lightweight curtain walls with high sound insulation

Koprowska Hanna M., akustyka@itb.pl
Szudrowicz Barbara

Building Research Institute (ITB)
Departments of Acoustics
Ksawerów 21, 02-656 Warszawa, Poland

Fully glazed lightweight curtain walls are used both in public buildings with qualified acoustics, as well as housing, because of theirs aesthetic and constructions qualities. A major issue in the design of the building is to provide a sufficiently low sound levels in rooms, highly influenced by the sound insulation of the facade. The measurements of acoustic insulation of the three types of light curtain walls were made in the Acoustic Laboratory of the Building Research Institute (ITB). The results of laboratory tests have been discussed divided into single and double structures. Influence of construction of insulated glass has been described for the solutions with single glazing. The impact of an aluminum frame, ventilation shutters and way of glazing on the sound insulation of lightweight curtain walls has been discussed.

⋆ ⋆ ⋆

Soft tissue in vitro heating by ultrasound beam and acoustical properties of soft tissue phantoms

Kruglenko Eleonora, Mizera Andrzej
Gambin Barbara, Tymkiewicz Ryszard
Zienkiewicz Bogusław, Litniewski Jerzy

Institute of Fundamental Technological Research
Polish Academy of Sciences
Pawińskiego 5B, 02-106 Warszawa, Poland

The paper presents preliminary results of measuring the temperature inside the tissue in vitro during the process of heating by the ultrasound beam with low power and measuring the acoustic properties of soft tissue phantoms. These models were built to further research into the link between the temperature of the acoustic properties, because in vitro tissue samples proved to be unique and unstable. The three tissue phantoms answer to pulse excitation were measured and pulse propagation velocity, attenuation and statistics of signal envelope have been examined. The influence of the number of scattering elements on the obtained parameters is discussed.

⋆ ⋆ ⋆

Influence of material used for regenerator on properties of a thermoacoustic heat pump with traveling wave

Kruk Bartłomiej

Wrocław University of Technology
Wybrzeże Wyspiańskiego 27, 50-370 Wrocław, Poland

Acoustic wave propagating in a gas is described by changing the pressure and the oscillating motion of the particles, but there is another important factor – the oscillating heat. Research in the thermoacoustics began with the observation of the heat transfer between gas and solids. These interactions are too small to have been seen in the sound

wafting in the air-rated through which we communicate every day. The term thermo-acoustics was defined by Nikolaus Rott, who explained it as a combination of two thermal and acoustic phenomena. The intense sound wave and the pressure in the thermoacoustics can be used to create: powerful engines, heat pumps and thermoacoustic refrigerators.

⋆ ⋆ ⋆

Recognition of musical instruments in polyphonic recordings for mean, mode, and median-based sound parameters

Kubera Elżbieta[1], elzbieta.kubera@up.lublin.pl
Wieczorkowska Alicja A.[2], alicja@poljap.edu.pl

[1]University of Life Sciences in Lublin
Akademicka 13, 20-950 Lublin, Poland
[2] Polish-Japanese Institute of Information Technology
Koszykowa 86, 02-008 Warszawa, Poland

In this paper we describe experiments on the recognition of musical instruments in polyphonic recordings using random forests as classifiers. The feature vectors applied to parameterize the analysed sound segments are based on means, modes, and medians of short-time sound features, calculated through the entire segment. The results of these experiments are presented and discussed in this paper.

⋆ ⋆ ⋆

Resonance model of the human tissue used in surgery simulator

Leniowska Lucyna[1], lleniow@univ.rzeszow.pl
Leniowski Ryszard[2]

[1] University of Rzeszów, Institute of Technology
Al. Rejtana 16C, 35-959 Rzeszów, Poland
[2] Rzeszów University of Technology
Department of Computer and Control Engineering
Al. Powstańców Warszawy 12, 35-959 Rzeszów, Poland

During the real robotic surgery, there is a wide range of contacts of surgical instruments with live tissue. The behavior of biological tissues as volumetric objects differs substantially from the physical materials, i.e. those where the degree of deformation is small. The development of reliable mathematical models of soft tissue enables to create virtual training tools used in minimally invasive surgery, where the key role is played by a simulation of phenomena occurring in real surgery. In this paper the properties of the model tissue with a reduced dynamic, which was subjected to simple and complex deformations. Built on the base of the model virtual organs are part of a training system developed for conducting virtual operations (training) using the surgical robot ROCH-1.

⋆ ⋆ ⋆

Comparison of numerically calculated pressure drop for selected helicoidal resonators

Łapka Wojciech

Poznań University of Technology
Institute of Applied Mechanics
Jana Pawła II 24, 60-965 Poznań, Poland

This paper presents the comparison between numerically obtained pressure drops for helicoidal resonators with the same ratio $s/d = 1.976$ and other dimensional relationships, but different number of helicoidal turn $n = 0.671$ and $n = 0.695$, as well as $n = 1.0$. Acoustic system of straight cylindrical duct with helicoidal resonator inside is considered. Two modules of Comsol Multiphysics numerical environment were used to solve air flow problem: aeroacoustics with flow and CFD Turbulent Flow. Air flow velocities between 1 m/s and 20 m/s with the step of 1 m/s were applied. Observed difference between aeroacoustical and CFD results tend to conclusion that experimental measurements of pressure drops should be done for all cases.

⋆ ⋆ ⋆

Demands on measurement models for the perceptual qualities of virtual acoustic environments

Maempel Hans-Joachim, Weinzierl Stefan

TU Berlin, Audio Communication Group
Straße des 17. Juni 135, 10623 Berlin, Germany

Virtual acoustic environments (VAEs) are frequently intended for the reproduction of and the interaction with acoustic scenes. While different technical approaches such as sound field synthesis and binaural synthesis vary in their capability of accurately reproducing certain features of the physical sound field, there is no agreement as to the perceptual criteria for the evaluation of VAEs. Frequently suggested global attributes such as presence, authenticity, plausibility and naturalness are reviewed. We propose a systematization of different properties, discuss the suitability for different research objectives, and consider demands for their measurement. In this context, methodological issues regarding operationalization, experimental references, and criterion-free test procedures are discussed.

⋆ ⋆ ⋆

Auralisation quality estimation

Małecki Paweł, pawel.malecki@agh.edu.pl

AGH University of Science and Technology
Department of Mechanics and Vibroacoustics
al. A. Mickiewicza 30, 30-059 Kraków, Poland

This paper shows the set of parameters meant to establish "how good" the auralisation is. The basic concept is to compare actual reverberant room acoustic with its auralisation. The measurement of first-order ambisonic impulse response is provided both for the actual room and its auralisation. The article shows the results of comparison and analysis of significant factors that influence quality of auralisation.

⋆ ⋆ ⋆

Nonlinear active noise control of sound transmitted through a plate

Mazur Krzysztof, Pawełczyk Marek

Silesian University of Technology
Institute of Automatic Control
Akademicka 16, 44-100 Gliwice, Poland

Active Noise Control (ANC) of noise transmitted through a vibrating plate causes many problems not observed in classical ANC using loudspeakers. One of the

problems is related to nonlinearities existing in systems using vibrating plates. Those nonlinearities are due to nonlinear vibrations and use of nonlinear actuators, like MFC patches. In case of noise transmission though a plate, nonlinearities exist in both primary and secondary paths. Existence of nonlinearities in the system may degrade performance of linear feedforward control systems usually used for ANC. The performance degradation is especially visible for simple deterministic noise such as tonal noise, where very high reduction is expected. Linear feedforward systems in such cases are unable to cope with higher harmonics generated because of nonlinearity. Moreover, nonlinearities, if not properly tackled with, may cause divergence of an adaptive control system. In this paper a feedforward ANC system reducing sound transmitted through a vibrating plate is presented. The ANC system uses nonlinear control filters to suppress negative effects of nonlinearies in the system. Filtered-error LMS algorithm, found more suitable than usually used Filtered-reference LMS algorithm, is employed for updating parameters of the nonlinear filters. The control system is experimentally verified and obtained results are reported.

⋆ ⋆ ⋆

Computer simulation of active sound intensity vector field in enclosure of irregular geometry

Meissner Mirosław

Institute of Fundamental Technological Research
Polish Academy of Sciences
Pawińskiego 5B, 02-106 Warszawa, Poland

The modal expansion method has been used to formulate expressions for real and imaginary parts of the complex sound intensity inside enclosures. Based on theoretical results, the computer program has been developed to simulate the active intensity vector field inside L-shaped enclosure. Calculation results have shown that a distribution of the active intensity is strongly influenced by the modal localization and the typical objects in the active intensity field are energy vortices and saddle points positioned irregularly inside the room. It was found that an increase in a sound attenuation results in the change of vortex positions and can cause the formation of new vortices. An influence of the wall impedance on the quantitative relation between the active and reactive intensities was also studied and it was concluded that for very small sound damping the behavior of the sound intensity is basically only oscillatory.

⋆ ⋆ ⋆

Music-induced vibrations in a concert hall and a church

Merchel Sebastian
Altinsoy M. Ercan

Chair of Communication Acoustics
TU Dresden 01062 Dresden, Germany

Sound and vibrations are often perceived via the auditory and tactile senses simultaneously, e.g., in a car or train. During a rock concert, the body vibrates with the rhythm of the music. Even in a concert hall or a church, sound can excite vibrations in the ground or seats. These vibrations might not be perceived separately because they integrate with the other sensory modalities into one multimodal perception.

This paper discusses the relation between sound and vibration for frequencies up to 1 kHz in an opera house and a church. Therefore, the transfer function between sound pressure and acceleration was measured at different exemplary listening positions. A dodecahedron loudspeaker on the stage was used as a sound source. Accelerometers on the ground, seat and arm rest measured the resulting vibrations. It was found that vibrations were excited over a broad frequency range via airborne sound. The transfer function was measured using various sound pressure levels. Thereby, no dependence on level was found.

⋆ ⋆ ⋆

Measurements of the CMDP and DPOAE signals in guinea pigs

Michalski Wojciech[1], Kutynia Andrzej[1]
Bochnia Marek[2], Dziewiszek Wojciech[3]

[1] Technical University of Wrocław
Wybrzeże Wyspiańskiego 27, 50-370 Wrocław, Poland
[2] Medical University of Wrocław
Department of Pharmacology
Mikulicza-Radeckiego 2, 50-345 Wrocław, Poland
[3] Faculty of Dentistry
Department of Otolaryngology
Borowska 213, 50-556 Wrocław, Poland

Acoustic wave excitation of the cochlea consisting of two tones with frequencies f_1 and f_2 evokes the answer of the hair cells in the form of the cochlea electrical signal CMDP (Cochlear Microphonic Distortion Product) and the acoustic signal DPOAE (Distortion Product OtoAcoustic Emission). The frequency of these signals was $f_3 = 2f_1 - f_2$. For many years the DPOAE signals is used in experimental examinations of the cochlea of the inner ear, as well as in clinical diagnosis. Only in a few articles you can find information on the use of CMDP signals. Simultaneous measurement of both signals, for different parameters of stimulation, offers new opportunities for cognitive physiology of the inner ear. The article presents the first results of measurements of the both signals (CMDP and DPOAE). Measurements were performed in three young, healthy guinea pigs. The results show clear evidence of significant differences between the DPOAE-gram and CMDP-gram in the studied range o f frequency f_3 [500 Hz, 5310 Hz].

⋆ ⋆ ⋆

Acoustic properties of classrooms in primary schools – estimating the speech transmission index from the reverberation time

Mikulski Witold

Central Institute for Labour Protection
– National Research Institute
Czerniakowska 16, 00-701 Warszawa, Poland

Among the parameters determining the acoustic properties of classrooms, the speech transmission index STI is

the most correlated with the subjective feeling of speech intelligibility. However it is not widely used because of the time consuming method of measurement and the need for specialized equipment. The most commonly used parameter characterizing room acoustics is reverberation time. The relationship between these two parameters is not clear and it is still not specified for the considered rooms. The article presents the relationship between speech transmission index STI and the reverberation time in octave frequency bands, based on data from 126 primary school classrooms.

⋆ ⋆ ⋆

New acoustical parameters and measurement methods of floor coverings

Mirowska Marianna, m.mirowska@itb.pl
Ciszewski Radosław, r.ciszewski@itb.pl

Building Research Institute (ITB)
Departments of Acoustics
Ksawerów 21, 02-656 Warszawa, Poland

This paper presents two new laboratory measurement methods of walking noise, which is being radiated during walking from the floor into the room containing the test sample. Mentioned methods are as follows:

1. Developed by European Producers of Laminate Flooring described in paper EPLF 012019-6.
2. Described in European standard proposal Fpr EN 16205:2011.

Floor covering parameters related to radiated sound of walking derived using abovementioned methods have been discussed, as well as several results of test measurement conducted according to the Fpr EN 16205:2011 method have been presented.

⋆ ⋆ ⋆

Effect of climate change in a small room on the results of acoustic measurements

Mleczko Dominik
Kleczkowski Piotr

AGH University of Science and Technology
Faculty of Mechanical Engineering and Robotics
Department of Mechanics and Vibroacoustics
al. A. Mickiewicza 30, 30-059 Kraków, Poland

Computer programs are increasingly used in designing room acoustics, but the problem of determining the reliability of these simulations are so far unresolved. It is necessary to determine both the acoustic measurement and simulation results uncertainties in order to determine the degree of divergence of simulation results with actual values measured in the room. The essential input data for modeling room acoustics are climate conditions (temperature and relative humidity). These values are often variable and therefore their exact definition is difficult and sometimes even impossible. Therefore, it is useful to know about how the final result of modeling is influenced by an uncertainty of the determination of these input values. The hereby paper examined how changes in temperature and humidity affect on the results of measurements parameters: T30, EDT, C80, D50, STI and SPL.

⋆ ⋆ ⋆

Varieties of masking of speech: energetic, modulation and informational

Moore Brian C.J.

University of Cambridge
Department of Experimental Psychology
Downing Street, Cambridge CB2 3EB, UK

There are often situations where it is necessary to listen to speech in the presence of background sounds. Such sounds can reduce speech intelligibility, which will be referred to as partial masking of the speech. The masking of speech can take three forms: (1) "energetic" – the masker "swamps" the internal response to parts of the speech; (2) "modulation" – the amplitude fluctuations in the masker make it more difficult to detect and analyse the information-bearing amplitude fluctuations in the target speech; (3) "informational" – the auditory system has problems in deciding which parts of the input sound emanated from the target speech and which parts emanated from the background. In experimental work, a commonly used masker is a notionally steady noise with the same long-term-average spectrum as speech. This has traditionally been regarded as an energetic masker. However, Stone, Füllgrabe and Moore (2012) showed that the inherent random amplitude fluctuations in such a noise play a critical role, and that such noise is more appropriately described as a modulation masker. A truly steady but energetically similar masker, composed of multiple inharmonically spaced tones, produces much less masking than a noise masker. Informational masking of speech occurs most commonly when the background consists of one or more competing talkers. However, such masking can occur for non-speech backgrounds with speech-like characteristics (Chen *et al.*, 2012). Also, the informational masking produced by a background talker can be small when the target speech material has a highly predictable structure (Lunner *et al.*, 2012).

References

1. Chen J., Li H., Li L., Moore B.C.J., Wu X. (2012), *Informational masking of speech produced by speech-like sounds without linguistic content*, J. Acoust. Soc. Am., 131, 2914–2926.

2. Lunner T., Hietkamp R.K., Andersen M.R., Hopkins K., Moore B.C.J. (2012), *Effect of spee ch material on the benefit of temporal fine structure information in speech for young normal-hearing and older hearing-impaired participants*, Ear Hear., 33, 377–388.

3. Stone M.A., Fullgrabe C., Moore B.C.J. (2012), *Notionally steady background noise acts primarily as a modulation masker of speech*, J. Acoust. Soc. Am., 132, 317–326.

⋆ ⋆ ⋆

Investigation of physical phenomena in two-dimensional phononic crystals using ultrasonic waves

Mróz Agnieszka
Gudra Tadeusz
Opieliński Krzysztof

Wroclaw University of Technology
Instituite of Telecomunications, Teleinformatics and Acoustics
Wybrzeże Wyspiańskiego 27, 50-370 Wrocław, Poland

In this paper an experimental approach to the usage of phononic crystals as focusing lenses by investigating both the negative refraction effect and existence of phononic band-gaps in two-dimensional structures consisting of steel rods immersed in water is presented. The negative refraction behavior has been demonstrated for both square and triangular lattices. Achieved results allow considering further studies in the field of both focusing and imaging using phononic crystals.

⋆ ⋆ ⋆

Ultrasonic transmission tomography imaging of CIRS Model 059 Breast Biopsy Phantom structure in comparison with USG, CT and MRI

Opieliński Krzysztof J.[1], Gudra Tadeusz[1]
Pruchnicki Piotr[1], Podgórski Przemysław[2]
Kraśnicki Tomasz[2], Kurcz Jacek[2],
Sąsiadek Marek[2]

[1] Wroclaw University of Technology
Institute of Telecommunications, Teleinformatics and Acoustics
Wybrzeże Wyspiańskiego 27, 50-370 Wroclaw, Poland
[2] Wroclaw Medical University
Department of Radiology
Borowska 213, 50-556 Wrocław, Poland

In the paper, the results of the ultrasound transmission tomography imaging (UTT) of the internal structure of CIRS Model 059 Breast Biopsy Phantom were analysed and compared with the imaging results by means of the ultrasonography (USG), the computerized X-ray tomography (CT) and the magnetic resonance tomography (MRI). It is impossible to observe any differentiation of the internal structure of that phantom on USG images. The obtained results of the investigations indicated, that the applied ultrasound transmission tomography (UTT) method can be used for the detection and diagnosing of tumor changes in the women breast.

⋆ ⋆ ⋆

A right time and place for pitch perception?

Oxenham Andrew J.

University of Minnesota, Department of Psychology – Twin Cities
240 Williamson Hall, 231 Pillsbury Drive S.E.
Minneapolis, MN 55455-0213

Pitch is a primary auditory percept, and one that has been studied extensively for well over a century. The quest to understand the neural mechanisms of pitch has gained more urgency recently, as pitch deficits are often particularly in striking in people with hearing loss and cochlear implants. This talk will provide a survey of research into pitch perception, and will highlight recent progress in the field that relates to the long-standing question of how tonotopic (place) and temporal (timing) information in the auditory periphery is used in pitch perception.

⋆ ⋆ ⋆

An attempt to identify the acoustic quality in urban environment

Paszkowski Waldemar

Silesian University of Technology
Production Engineering Institute
Roosevelta 26-28, 41-800 Zabrze, Poland

The subject discussed here is a continuation of the research on identifying the features of soundscapes in the Urban environment. The idea of soundscapes has been gaining a greater interest in the approach to acoustic ecology, which to a significant extent makes use of the aspect of perceiving sound as a subjective assessment of noise nuisance. In this context, the condition of noise threat is a resultant of a qualitative and quantitative representation of acoustic and non-acoustic features of an urban environment. The research done in this field shows that the qualitative features of representing and assessing the environment are not well recognised. Research on the acoustic quality of the environment using the entropy method is presented in this paper. The paper presents an example of the method of examining the emotions induced by sound sources using the entropy method, taking into consideration the sensory stimuli.

⋆ ⋆ ⋆

The auditory filter representation of cochlear processing in humans: past, present and future

Patterson Roy D.

PDN, University of Cambridge
Cambridge UK

This paper describes the progress of auditory scientists over the years in their attempts to specify the shape of human auditory filter, that is, the frequency resolution of the auditory system at each point along the tonotopic dimension of the cochlea. Early, behavioural experiments revealed that the auditory filter had a rounded top flanked by exponential skirts – a roex auditory filter. Physiological experiments with cats suggested that the impulse response of the filter had a gamma envelope with a sinusoidal carrier – a gamma-tone auditory filter. Subsequently, behavioural and physiological experiments revealed that the filter shape changes with sound level, which led to the conclusion that the carrier under the gamma envelope must chirp – a gammachirp auditory filter. Finally, the efforts of auditory scientists prompted research on the mathematics of auditory frequency analysis, and we now know that the gammachirp auditory filter is mathematically optimal in the sense that it provides minimal uncertain in linear-time, log-frequency analysis, just as the Gabor function provides minimal uncertain in linear-time, linear-frequency analysis. The fact that the auditory system uses log rather than

linear frequency suggests that it is more concerned with the source-size information in sounds than with frequency per se.

⋆ ⋆ ⋆

Nonlinear features of sound propagation in relaxing media

Perelomova Anna[1], anpe@mif.pg.gda.pl
Kuśmirek Magdalena[2], magdalena.kusmirek@cto.gda.pl

[1] Gdansk University of Technology
Faculty of Applied Physics and Mathematics
Narutowicza 11/12, 80-233 Gdańsk, Poland
[2] Ship Design and Research Center
Wały Piastowskie 1, 80-958 Gdańsk, Poland

Nonlinear features of sound in relaxing fluids are studied. Among other, viscoelastic biological media described by the Maxwell model of the viscous stress tensor, gases with excited degrees of oscillatory freedom of molecules, and chemically reacting media belong to this type of flu-ids. The governing equation of sound is derived by means of the special linear combining of conservation equations in the differential form, which allows to reduce all non-acoustic terms in the linear part of final equation and to hold only dominative non-linear terms associated with sound. It is discovered, that while propagation of the high-frequency sound, the parameter of nonlinearity of the Maxwell fluid increases.

⋆ ⋆ ⋆

Alternative methods for data collection to elaborate acoustic maps

Pierchała Marek, mpierchala@komag.eu

KOMAG Institute of Mining Technology
Pszczyńska 37, 44-101 Gliwice, Poland

Acoustic maps are the basic instruments to assess and manage the level of noise in the environment. On their basis plans of actions are worked out. Those plans are the basis in management of noise issues, which includes conducting the organisational operations as well as implementing the technical measures for noise limiting. All those actions require significant expenditures. Therefore, it is important to guarantee proper deduction on the basis of prepared acoustic maps. This idea is directly connected with collection of correct and up-to-date input data. Among them spatial information should be mentioned. This area of data includes Digital Surface Models (DSM). Generally they are elaborated on the basis of Orthophotomaps. The accuracy and timeliness of DSM depend on precision of Ortophotomaps. Generally the process of obtaining Ortophotomaps is realized with use of Aerial or Satellite Imagery. Unmanned Aerial Vehicle (UAV) is a new alternative method for that. It provides fast and cheaper process of collection of data about terrain. Legal regulations connected with application of UAV are presented. What is more, basic requirements related to preparation of Ortophotomaps are discussed. The range and the method of testing are also given.

⋆ ⋆ ⋆

The influence of well's bottom shape on effectiveness of Schroeder diffusers

Pilch Adam
Kamisiński Tadeusz
Rubacha Jarosław

AGH University of Science and Technology
al. A. Mickiewicza 30, 30-059 Kraków, Poland

Phase grating sound diffusers (QRD) were invented by Schroeder in 1979. Thanks to omnidirectional characteristic of directivity of reflected sound and very easy design, they became very popular. Nowadays they are used in small spaces like control rooms as well as in a big concert halls. Acousticians wanted to obtain wideband diffusion, what lead them to construct very deep and narrow wells, which give big absorption at low and medium frequencies. Because of that, a great area of wideband QRD cannot be used in concert halls. Other popular way of widening the range of effective diffusion of QRD is to shape properly the bottom of their wells to make a kind of fractal diffuser. In the paper some methods of shaping the bottom of wells are shown and its influence on directional sound diffusion coefficient d is presented. The analysis of results shows, that presented methods significantly improves diffusion coefficient especially for mid and high frequency.

⋆ ⋆ ⋆

A software system for off-site timbre solfege with remote results management capability

Pluta Marek, Kleczkowski Piotr

AGH University of Science and Technology
Department of Mechanics and Vibroacoustics
al. A. Mickiewicza 30, 30-059 Kraków, Poland

This paper describes a flexible networked system that combines testing and training of auditory abilities. The system consists of two parts: a user-side test unit ("a client") and a remote data storage unit. For efficient data storage and analysis the system uses remotely accessed MySQL database. The client-side program performs the actual listening tests and connects to a database server through the Internet to upload user results. The client is a standalone Windows application designed to run on various personal computers, including netbooks, and is capable of working with a wide range of computer audio interfaces. An unlimited number of listeners, each using his/her own copy of the test unit, can be trained or tested, even at home, in a convenient time, while their performance is under control of an instructor or experimenter, and the progress of training over time can be monitored easily, by accessing data storage module. Results stored in a database can be browsed us ing general-purpose MySQL clients, which provide various methods of data manipulation useful to select interesting subsets of the listeners' results. At present three types of tests are fully implemented: test of sound equalization recognition, frequency and waveform recognition, as well as dynamic range compression. Each area consists of various tasks, either with predefined difficulty levels or with freely adjustable parameters.

⋆ ⋆ ⋆

Ultrasonic noise – determination of exposure levels at workplaces with ultrasonic welders

Radosz Jan

Central Institute for Labour Protection
– National Research Institute
Czerniakowska 16, 00-701 Warszawa, Poland

One of the most common ultrasonic devices in the working environment are ultrasonic welders. They emit impulse noise very often with high levels exceeding MAI values. The level of ultrasonic noise exposure at workplaces with welders is closely related to the number of produced components, and the sound pressure levels during welding. The paper presents some problems of determining the level of exposure to ultrasonic noise at workplaces with ultrasonic welders including the measurement uncertainties.

⋆ ⋆ ⋆

The concept of the underwater encrypted communication system

Rodwald Przemysław

Polish Naval Academy
Śmidowicza 69, 81-103 Gdynia, Poland

This article presents the initial concept of the underwater encrypted communication system. A block diagram of the system We be presented and reflections on the various functional blocks will be discussed. An overview of underwater acoustic modems available on the market will be shown as well.

⋆ ⋆ ⋆

Analysis of the influence of uncertainty determination of sound absorption coefficient of the audience on the accuracy of prediction of the reverberation time in concert halls

Rubacha Jarosław
Kamisiński Tadeusz
Pilch Adam

AGH University of Science and Technology
Faculty of Mechanical Engineering and Robotics
Department of Mechanics and Vibroacoustics
al. A. Mickiewicza 30, 30-059 Kraków, Poland

In the paper, analysis of dependences that allow to calculate uncertainty of determination of the reverberation time in rooms was carried out. Based on the propagation of uncertainty, dependence of the maximum sound absorption coefficient of the audience on the assumed tolerance range of room reverberation time was determined as well as the range of its application. Basing on presented dependences, method for calculating sound absorption coefficient of the audience and determination of its variation range for assumed tolerance of reverberation time was proposed. Presented method allow to select seats for the audience at the stage of designing interior acoustics. Analysis of the application was conducted based on three concert halls.

⋆ ⋆ ⋆

Simulation studies of planar microphone arrays

Rudno–Rudziński Krzysztof, Dziechciński Paweł
Jakubów Maciej, lba@pwr.wroc.pl

Wroclaw University of Technology, Institute of Telecommunication, Teleinformatics and Acoustics
Wybrzeże Wyspiańskiego 27, 50-370 Wrocław, Poland

The results of computer simulations of irregular planar microphone arrays have been shown. Arrays were studied consisting of 64 microphones on a frame-like square with sides of about 1.9 m. The simulations have shown that it is possible to adjust parameters of the arrays to the metrological requirements, in particular a resolution, a dynamic range, an angular extent of essential noise sources and a frequency spectrum of a signal.

⋆ ⋆ ⋆

Compression of auditory space during uniformly-accelerated forward self-motion

Sakamoto Shuichi[1], Teramoto Wataru[1,2]
Furune Fumimasa[1], Suzuki Yôiti[1], Gyoba Jiro[3]

Tohoku University
[1] Research Institute of Electrical Communication
[2] Graduate School of Arts and Letters
[3] Department of Psychology
Kawauchi, Aoba-ku, Sendai 980-8576, Japan

Spatial inputs from the auditory periphery can be changed with listener's various movements relative to the sound source. Nevertheless, humans can perceive a stable auditory environment and appropriately react to a sound source. This suggests that the inputs are reinterpreted in the brain, while being integrated with information on the movements. Little is known, however, about how these movements modulate auditory perceptual processing. We investigate the effect of the linear acceleration on auditory space representation. Participants were passively transported forward/backward at constant accelerations An array of loudspeakers was aligned parallel to the motion direction. A short noise burst was presented during the self-motion from one of the loudspeakers when the listener's coronal plane reached the location of one of the speakers (null point). The results of the experiments showed that the sound position aligned with the subjective coronal plane was displaced ahead o f the null point only during forward self-motion and that the magnitude of the displacement increased with increasing the acceleration. These suggest a distortion of the auditory space in the direction of movement during forward self-motion.

⋆ ⋆ ⋆

Doppler effect in underwater acoustic system

Salamon Roman

Gdansk University of Technology
Faculty of Ocean Engineering and Ship Technology
Narutowicza 11/12, 80-233 Gdańsk, Poland

The paper contains an overview of the Doppler effect in underwater acoustic systems. Review is preceded by a discussion of the Doppler effect in the category of time compression. Subsequently the Doppler methods used to measure the velocity and position of the observed objects are

presented. Afterwards the Doppler phenomenon in the synthetic aperture sonars is described. In the second part of the paper the negative consequences of the Doppler effect and methods of their limitations in conventional and silent sonars are discussed.

⋆ ⋆ ⋆

Sonodynamically induced in vitro C6 glioma cancer cells damage enhanced by aminolevulinic acid (ALA)

Secomski Wojciech[1], Bilmin Krzysztof[2]
Kujawska Tamara[1], Nowicki Andrzej[1]
Grieb Paweł[2]

[1] Institute of Fundamental Technological Research
Polish Academy of Sciences
Pawińskiego 5B, 02-106 Warszawa, Poland
[2] Mossakowski Medical Research Centre
Polish Academy of Sciences
Pawińskiego 5, 02-106 Warszawa, Poland

Sonodynamic therapy is expected to be a novel therapeutic technique for glioma tumors. To determine the effect of ultrasound and aminolevulinic acid (ALA) on the cancer cell damage, we exposed C6 glioma cells to 1 MHz ultrasound at intensities 0.94, 1.88 and 3.77 W/cm^2 for 3 min. We found that combined ALA + ultrasound therapy (15%–13% living cells) is more efficient than ultrasound alone (41%–27%) at intensities 0.94 and 1.88 W/cm^2. 3.77 W/cm^2 ultrasound was efficient to kill most cells independently on ALA added. Standing wave was observed increasing acoustical intensity by factor $7\times - 10\times$. The results might be useful for efficient sonodynamic tumor therapy.

⋆ ⋆ ⋆

Investigation of ultrasonic emulsifying processes of linseed oil and water mixture

Skumiel Andrzej[1], Józefczak Arkadiusz[1]
Heller Krzysztof[2]

[1] Adam Mickiewicz University, Institute of Acoustics
Umultowska 85, 61-614 Poznań, Poland
[2] Institute of Natural Fibres and Medicinal Plants
Wojska Polskiego 71b, 60-630 Poznań, Poland

Ultrasonic emulsifying processes of immiscible liquids can be used to obtain stable emulsions. The authors used ultrasonic sandwich head with energy concentrator to obtain suitable value of energy density necessary for ultrasonic cavitation emerge. Two piezoelectric rings (D_{ext} = 50 mm) transducers Pz-26 type produced by FERROPERM were used to design of ultrasonic sandwich head. The frequency ultrasonic wave was 18.4 kHz and time of ultrasonic transducer exiting 5 and 10 minutes. Visible bubbles during generation of ultrasonic waves in mixture appeared after exceed cavitation threshold. The authors determined also cavitation threshold by measure electrical voltage conducted to transducers. To receive durable emulsion the electrical voltage attained 300 V_{peak}. The dispersion dependence on time emulsifying was determined. Emulsion of linseed oil and water was stable through some months without surfactants.

⋆ ⋆ ⋆

Exposure to ultrasonic noise at metal finishing workstations

Smagowska Bożena

Central Institute for Labour Protection
– National Research Institute
Czerniakowska 16, 00-701 Warszawa, Poland

This article contains a measurement method and criteria for assessing exposure to ultrasonic noise at workstations. The results of measuring ultrasonic noise and risk assessment related to occupational exposure to ultrasonic noise are presented to workstations where noise is occurring as unintentional results of production process (so-called not technological sources of ultrasonic noise). The measurements were conducted during external machining of elements and engraving, oxy-acetylene welding, electrical welding, cutting and burning.

⋆ ⋆ ⋆

Tonality as a one of the fundamental properties of music perception

Smolik Damian[1], Damian.Smolik@fis.agh.edu.pl
Snakowska Anna[2], anna.snakowska@agh.edu.pl

[1]AGH University of Science and Technology
Faculty of Physics and Applied Computer Science
al. A. Mickiewicza 30, 30-059 Kraków, Poland
[2] AGH University of Science and Technology
Faculty of Mechanical Engineering and Robotics
al. A. Mickiewicza 30, 30-059 Kraków, Poland

An important feature of the perception of numerous audio waveforms used in music for people with developed relative ears is the dependence of the perception of musical sensation at the given moment on the context preceding the moment. This phenomenon will be referred here to generally as the tonality. Tonality thus understood is, among others, underlying the development of European music of the late nineteenth century and it is conceivable that it is going to play an important, perhaps even a fundamental role in the development of music and music theory in the future. A complete theory of perception of auditory sensations – should such a theory be ever created – should include a mathematical description of tonality perception. The aim of the authors of the article is to provide the most general model of the perception of aforementioned attribute of auditory sensation. The article outlines the characteristics of the created model and provides the prospects for its further development. The paper on the subject of this article will be illustrated by relevant sound examples.

⋆ ⋆ ⋆

Content based audio watermarking in DWT domain

Sonoda Kotaro

Nagasaki University
Nagasaki City 851-2196, Japan

In this report, I propose a digital audio watermarking method based on re-quantization of discrete wavelet coefficients. Re-quantization is applied to the relation of power

averages of the detail coefficients sequence in a certain decomposition level. It is expected that the deviations are not to be varied against the attack as long as sound quality is not severely degrade before attack. Moreover, all of payloads are embedded simultaneously to every position of a certain decomposition level in wavelet packet transform domain. Robustness and perceptibility are evaluated through some computer simulations.

⋆ ⋆ ⋆

Sensitivity analysis of the acoustic field parameters in the room on change the boundary conditions

Suder–Dębska Katarzyna
Czajka Ireneusz
Czechowski Mateusz

AGH University of Science and Technology
Faculty of Mechanical Engineering and Robotics
Department of Power Engineering
and Environmental Protection
al. A. Mickiewicza 30, 30-059 Kraków, Poland

The area of environmental protection concern is to minimize the impact of technical objects to the environment. Usually the most effective action to protect are those made "at source". For this reason, studies are conducted to modify the construction of machines, power machines, in particular, so as to minimize their impact on the environment. In the case of environmental protection from noise is most convenient to carry out tests in an anechoic chamber. Therefore it seems advantageous to develop a method to obtain similar and reliable results as in an anechoic chamber, but in thereverberant field. The main objective of this work is a comprehensive analysis of numerical model of a laboratory designed to acoustic tests of the selected energetic machines. The geometry of the room comprising an area of analysis is easy to project. The main difficulty in modeling the phenomena occurring in the analyzed area can be given a lack of knowledge of boundary conditions. Therefore, the authors have analysed the sensitivity of some acoustic parameters of the room on change of sound absorption coefficient.

⋆ ⋆ ⋆

Role of 4–8 kHz one-octave band component for median plane sound localization

Suzuki Yôiti[1], Iwaya Yukio[2]
Magariyachi Tetsu[1], Otani Makoto[3]

[1] Tohoku University Sendai
Research Institute of Electrical Communicaiton
Graduate School of Information Science
Japan
[2] Tohoku Gakuin Univeristy Tagajô
Faculty of Engineering
Japan
[3] Shinshu University Nagano
Faculty of Engineering
Japan

In contrast to horizontal plane sound localization, for which interaural cues play important roles, median plane localization is mainly determined by spectral cues, which represent the spectral shape inputted to the ears characterized by the incident angle of a sound. To clarify spectral cues involved in HRTF in the median plane, we conducted a sound localization test with broadband noises with different one-octave band levels for 4–8 kHz band. To generate these noises, pink noise was filtered so that the one-octave band level varies from −6 to +6 dB. The noises were radiated via one of two loudspeakers located at 30 and 60 degrees of elevations, respectively, in the median plane. As a result, the perceived elevation was shifted according to the band levels. The changes of perceived elevation resembled those of relative power levels in the HRTFs. This suggests that the spectral dips in the HRTFs whose frequency systematically changes as a function of the elevation would be an indirect perceptual cue but that the relative level of this band would be a direct perceptual cue for elevation perception.

⋆ ⋆ ⋆

Guidelines for the revision of national standards for building acoustics

Szudrowicz Barbara
Mirowska Marianna
Nowicka Elżbieta

Building Research Institute (ITB)
Ksawerów 21, 02-656 Warszawa, Poland

The paper presents trends in a series of amendments and additions to the standards PN-B-02151 "Building acoustics. Protection against noise in buildings". These standards apply to residential buildings, housing and public buildings and currently includes 3 parts:

- general requirements and the technical means of protection against noise in buildings,
- required noise level in rooms
- requirements for sound insulation in buildings (internal and external).

Standards covering the above issues from 1987 and 1999 and a number of provisions contained in these standards has become outdated because of changes in other standards and documents involved. Regardless of your experience with the use of these standards indicate a need for a number of changes and clarifications. A set of standards does not include requirements for the protection of reverberant noise introduced into the polish regulations and requirements for residential buildings with a higher standard acoustic. These issues must be made by the establishment of new parts of PN-B-02151.

⋆ ⋆ ⋆

Proposed acoustical classification of sound residential buildings (apartments)

Szudrowicz Barbara
Nowicka Elżbieta

Building Research Institute (ITB)
Ksawerów 21, 02-656 Warszawa, Poland

Ensuring adequate acoustic comfort at home is an important social, technical, technological and economic pro-

blem. The needs of individual people in ensuring the acoustic conditions in the apartments are very diverse. In a market economy on the approach to this issue also have a big impact economic aspects, both in terms of the whole country as well as individual families investing in their own apartment. For this reason, the requirements for acoustic comfort should be graded from a level that ensures a minimum (due to physical and mental health of the population) acoustics in the place of residence up to the higher levels corresponding to higher needs in this area. Transfer to a diverse technical language requirements for acoustic comfort at home means to determine acoustic requirements for buildings with a higher (in varying degrees), standard sound and how the acoustic classification of objects according to the adopted higher minimum.

⋆ ⋆ ⋆

Assessment of left ventricular model strain measurement obtained by means of ultrasonic speckles tracking method

Trawiński Zbigniew[1]
Olszewski Robert[2]
Wójcik Janusz[1]
Nowicki Andrzej[1]

[1] Department of Ultrasound
Institute of Fundamental Technological Research
Polish Academy of Sciences
Pawińskiego 5B, 02-106 Warszawa, Poland
[2] Department of Cardiology and Internal Medicine
Military Institute of Medicine
Szaserów 128, 04-141 Warszawa, Poland

In the contemporary ultrasound elastography exists the problem of the repeatability of the parameters measured by using the ultrasound apparatus made by different producers. In this work the new method for assessment of the quality of the ultrasonic speckles tracking method is proposed. Experiments were carried out using Artida Toshiba ultrasonograph with probe 3.5 MHz. The hydraulic model was based on the SuperPump (Vivitro Systems Inc. Canada). The Left Ventricular (LF) phantom (Fig. 1–2) is made as 10% solution of the POLY(VINYL ALCOHOL), 99% HYDROLYZED (M. 1,000 1.219,34/EA 1.219,34 23,0) (longitude 10 cm, inner diameter 3 cm, outer diameter 5 cm). During cycle of the pump, the Sample Volume (SV) of water is going to the inside of the LF phantom and return to the pump, providing changing the inner and outer diameters of the LV phantom. The SV was changed 8, 16 and 24 ml. Heart rate was changed from 40 to 120 b.p.m. for each SV. The parameters examined were: Radial Strain, Circumferential Strain, for two positions of LV phantom: 1) 0 deg and 2) after turn left the LV phantom of 25 deg. The nonparametric U-test Mann-Whitney was used for confirmation that for 0 deg and 25 deg not exist any significant statistical difference between measured parameters. For all cases the level of the coefficient of significance was $p > 0.05$. The results of statistical analysis indicate that the change of the acquisition angle not influences on measured above parameters. It may authenticate the applied ultrasonic speckles tracking method implemented in ultrasound.

This work was supported in part by Polish National Centre of Science (project N N518 292340).

⋆ ⋆ ⋆

Comparison of efficiency of homogeneus and two-layer piezo elements in plates vibration reduction – numerical study

Trojanowski Roman, Wiciak Jerzy

AGH University of Science and Technology
Department of Mechanics and Vibroacoustics
al. A. Mickiewicza 30, 30-059 Kraków, Poland

This paper presents the results of numerical studies on efficiency of different structures of piezo elements used as actuators. For this purpose numerical models were created with ANSYS software that contained steel plate clamped on all sides with piezo elements attached. Four elements as sensors, one for vibration excitation and four as actuators. For each model sensor and actuators are always cuboid elements, while actuators differ in shape and structure for different models. Harmonic analyses shown that, two-layer piezo elements can be much more efficient in reducing the vibration than homogeneous ones independently of the shape of elements used.

⋆ ⋆ ⋆

Virtual room acoustics

Vorländer Michael

RWTH Aachen University, Institute of Technical Acoustics
Neustrasse 50, 52066 Aachen, Germany

Room acoustic auralization has been developed from simulation algorithms and binaural technology in a historic process of more than 20 years. Full-immersive Virtual Reality (VR) systems, such as CAVE-like environments, have been in use for about 15 years. The link between simulation and auralization is the representation of the problem in the signal domain and the treatment of sound and vibration by signal processing. Apart from the simulation process, the so-called called "rendering", the development of audio reproduction of acoustic stimuli in VR is now at a stage where integration of 3D sound is in the focus of general interest. This applies to binaural synthesis as well as to full room-acoustic simulation algorithms and to various applications of 3D sound stimuli. In this presentation the state of the art is summarized, and the contribution of the Institute of Technical Acoustics in Aachen to this field is illustrated in examples.

⋆ ⋆ ⋆

Sound intensity methods and laser anemometry techniques in the studies of sound emission in cases of acoustic disturbed flow

Weyna Stefan[1], Mickiewicz Witold[2]
Pyła Michał[1], Jabłoński Michał J.[2]

West Pomeranian University of Technology
[1] Faculty of Marine Technology and Transport
[2] Electrical Faculty
al. Piastów 19, 70-310 Szczecin, Poland

The birth of sound in hydro and aeroacoustics flow is still not clearly described theoretically and verified experi-

mentally. The paper will present the current views on the origins of sound occurring in physical systems, which typically examine the numerical modeling (numerical study of a group of models, CFD, FSI and CAA) adapted to the theory of Vortex Sound Theory. It will show the results of acoustic studies of flow fields generated in limited systems (acoustic waveguides) and the acoustic near-field regions, where the reactions are the effects of nonlinear wave amplitude-phase compounds. Performed experimental studies on the graphic description of the vector of parameters of the acoustic field generated by the flow of acoustic waves in regions of the obstacles and ambiguous. Research is conducted using the measurement of sound intensity (SI) and the currently developed non-invasive methods of laser anemometry (PIV – Particle Image Velocimetry and LDA – Laser Doppler Anemometry) adjusttion to the study of acoustic (A-PIV, A-LDA). The use of laser methods for testing acoustic flow is shown as the own preliminary results. The results of experimental tests parameters of the acoustic wave vectors (sound intensity and particle velocity) showing the energetic phenomena occurring in the acoustics flow fields confirm the crucial importance of innovative measurement techniques in the development of knowledge of the sound theory and point to their usefulness in conducting validation of the theoretical results of numerical models.

⋆ ⋆ ⋆

Effect of contralateral speech-in-noise on the level of the distortion product otoacoustic emissions (DPOAES)

Wicher Andrzej

Adam Mickiewicz University
Institute of Acoustics
Umultowska 85, 61-614 Poznań, Poland

The main objective of this study was to determine the influence of contralateral speech-in-noise on the level of distortion product otoacoustic emissions (DPOAEs). Two types of contralateral signals (CS) were used in the study: speech presented against a babble masking noise and the babble noise without speech signal. The CS was presented at a level of 60 dB SPL. The signal-to-noise ratio (SNR) was a speech reception threshold (SRT). The primary tones with frequencies f_1 and f_2 ($f_2/f_1 = 1.21$) were generated at levels of $L_1 = 60$ dB SPL and $L_2 = 50$ dB SPL. Ten normal hearing subjects participated in the study. The CS produced a decrease in the level of the DPOAEs (suppression effect) in 88% of cases for f_2 changing from 1000 to 8000 Hz. The suppression effect was higher for babble noise without speech signal than for speech against a babble masking noise. A within-subject analysis of variance (ANOVA) revealed a significant effect of CS type:

$$F(1, 9) = 9.66, \qquad p = 0.013.$$

This work was supported by a grant from the National Science Centre No. N N518 405438.

⋆ ⋆ ⋆

Application of shape memory elements to excitations or reduce vibrations of mechanical structures an example cantilever beam

Wiciak Jerzy
Dąbrowski Kamil

AGH University of Science and Technology
Department of Mechanics and Vibroacoustics
al. A. Mickiewicza 30, 30-059 Kraków, Poland

Materials with shape memory are alloys or polymers capable in certain conditions to return to its previous "Memorized" shape. In engineering practice, most widely used alloy is nitinol, which is alloy of nickel and titanium. It has two stable phase, the shape change occurs by changing the phase low-temperature (martensite) at high temperature (austenite) or *vice versa*. In engineering, the most commonly used of this material: actuators, switches and sensors. The actuator can be used as a vibration exciter, if only enforce its work with the appropriate frequency. In this work the shape memory alloys are used in this way. Performed research has shown the ability to force cantilever steel beams to vibration. Research of controlling the movement was made: offset response structure in the frequency domain and reduce or enhance the movement for a specified range of frequency.

⋆ ⋆ ⋆

Perception and evaluation of sound fields

Wierstorf Hagen
Spors Sascha
Raake Alexander

T-Labs, TU Berlin
Straße des 17. Juni 135, 10623 Berlin, Germany

Sound field synthesis techniques claim to recreate a desired sound field within an extended listening area. In order to investigate the perceptual properties of the synthesized sound field the listener has to be placed at different positions. In practice that can be quite difficult with real loudspeakers. Another possibility to perform listening tests is to present the field via binaural synthesis. This study investigates whether binaural synthesis is perceptually transparent for the purpose of localization studies for sound field synthesis. A localization test is performed comparing real loudspeakers to two different binaural synthesis configurations using non-individual head-related transfer functions (HRTFs), once with and once without reflections. The results show only slight differences between real speakers and HRTFs-based synthesis, resulting in a one degree greater localization blur for the HRTFs without reflections than for the other two cases.

⋆ ⋆ ⋆

Spherical sound panorama

Wierzbicki Jacek, wierzbic@agh.edu.pl

AGH University of Science and Technology
Department of Mechanics and Vibroacoustics
al. A. Mickiewicza 30, 30-059 Kraków, Poland

Directivity of sound field in measurement place is one of the most important characteristic during environmental measurements in open space. The detection of arriving

sound direction is a first step in data pre-selection in automatic monitoring system. Such technique can be used to follow e.g. airplanes or car traces and indication of their influence on measured noise. It is necessary to use specialized microphones in order to receive spatial information about sound sources localization. Results from SoundField ST 350 microphone system recordings are presented on spherical panoramas where each type of noise source is indicated using different shape and color. For evaluation of spatial recordings and for noise measurements documentation the 16 loudspeakers auralization system is proposed. A complete 3D sound measurement, visualization and reproduction system with procedures of data acquisition, processing and visualization will be the main results of investigations. The idea of such system and first results are presented in the paper.

The work was financed by The National Centre for Research and Development (project no NR03 0030 06/2009).

⋆ ⋆ ⋆

The effect of a mode of playing on spectral parameters of the clarinet sound

Wilczyński Tomasz
Kleczkowski Piotr

AGH University of Science and Technology
Department of Mechanics and Vibroacoustics
al. A. Mickiewicza 30, 30-059 Kraków, Poland

Seventeen notes were played on the clarinet, each at five different sound levels corresponding to its five modes of playing. The steady state portions of the recorded 85 sounds were analysed. Sounds with most salient features were analysed using the Short-Time Fourier Transform (STFT). A specific algorithm was used to derive a set of parameters characterising the harmonic structure of each sound from the STFT. A quantitative analysis of harmonic structures of all sounds was performed. It revealed some effects of sound level on that structure.

⋆ ⋆ ⋆

Measurement of vibration in a model of the soundboard of Viola Organista instrument with Laser Vibrometer

Wilczyński Tomasz
Kleczkowski Piotr

AGH University of Science and Technology
Department of Mechanics and Vibroacoustics
al. A. Mickiewicza 30, 30-059 Kraków, Poland

Twenty four points were precisely spread over the soundboard of a model of Viola Organista instrument. The measurement was based on three realizations, each related to the specific construction of a particular component of the soundboard. The sounds were generated by three strings tuned in quint, mounted on the bridge, which sticked to the soundboard. Each string was stimulated by a cello bow three times in the same time period for every recorded signal. The Laser Vibrometer, calibrated to a specific range, was used to measure vibration. It was plugged into the spectrum analyser. The values of signal energy were obtained from analyser output, after appropriate processing. The maps of energy of signal vibration were obtained with the use of soundboard geometry.

⋆ ⋆ ⋆

Cumulative method of the image reconstruction in synthetic aperture. Experimental results

Wójcik Janusz, Trots Ihor, Lewandowski Marcin

Institute of Fundamental Technological Research
Polish Academy of Sciences
Pawińskiego 5B, 02-106 Warszawa, Poland

An analytical model of imaging using synthetic aperture (SA) methods is presented. This model takes into account: fundamental features of an environment, of an electric transmission/reception path and a description of SA structure – possible schemes of transmission, reception and image formation. Then two schemes are analyzed: a proposed cumulative synthetic transmit aperture (CSTA) and for comparison of the standard STA schemes. For both methods identical basic parameters – equal sequences of transmit and receive transducers were applied. The distinctive feature of CSTA is gathering (summing up) echoes of subsequent transmissions in one acquisition matrix sufficient for image reconstruction. In traditionally applied STA methods a separate acquisition matrix for each transmission is created. Therefore there are a dozen to several dozen more matrices and the time of image reconstruction is at least several times longer than in CSTA. The presented experimental results ob tained using wire and tissue mimicking phantoms have shown the comparable imaging quality in both methods.

⋆ ⋆ ⋆

The relationship between the subjective and objective measurement of sound intensity leveling between the violin strings

Wrzeciono Piotr

Warsaw University of Life Sciences
Faculty of Applied Informatics and Mathematics
Nowoursynowska 159, 02-776 Warszawa, Poland

The sound intensity leveling between the violin strings is an important property of this instrument. This property is evaluated during the violin making competitions because this parameter has high influence on a playing technique. This paper presents the relationship between the objective parameters which describe the sound intensity leveling and the evaluation made by jurors of the 10th International Henryk Wieniawski Violin Making Competition. The parametrization of sound intensity leveling was realized with using the method based on searching for low energy modes below 198 Hz in the recordings of violin sounds. The arithmetic mean of the modules of differences of the sound intensity between the violin strings: G-D, D-A and A-E was used as the main objective parameter describing the violin strings leveling. The mentioned arithmetic mean was compared with the evaluations made by the jurors of the violin making competition. In this research the AMATI multimedia database was used.

⋆ ⋆ ⋆

The analysis of the objective possibility of reconstruction of the baroque violin timbre aesthetics

Wrzeciono Piotr
Orłowski Arkadiusz

Warsaw University of Life Sciences
Faculty of Applied Informatics and Mathematics
Nowoursynowska 159, 02-776 Warszawa, Poland

At present, the Baroque music is becoming more and more popular. A historical performance of Baroque music is also a subject of interdisciplinary research and the need of making the good replicas of historical music instruments is still growing. But in this case, the main problem is the inability to direct research of original musical instruments sound. The reason for this are the changes in material structure related to aging of wood. Thus, the sound of the preserved historical bow instruments is different from the original state. The developing of method to recreate the original sound of historical violins is very important.

During the work we plan to use the results of latest researches related to the automatic evaluation of the quality of sound of musical instruments and develop new classifiers of this kind.

We want to achieve this aim by using information technology, especially MIR (Music Information Retrieval). It is also needed to make interdisciplinary studies on acoustics, psychoacoustics and Baroque music aesthetics. The results of mentioned researches will be used to develop methods to build excellent replicas of baroque violin and write a computer application to support the violin makers.

⋆ ⋆ ⋆

Uncertainty assessment for airborn sound reduction index measuremets with reduced size of the sample

Wszołek Tadeusz

AGH University of Science and Technology
al. A. Mickiewicza 30, 30-059 Kraków, Poland

The problems with reproducibility of sound reduction index measurement results, not only for inter-laboratory research but also in the same laboratory, evidence of the occurrence of some factors that increase measurement uncertainty. The origins might lie in the inhomogenities of the acoustic field in the both rooms and reverberation time in the receiving room. Further factors include the flanking transmission, the background noise, especially at high values of insulation, the way of mounting the samples within the window and the reduced dimensions of the window as well a proper sample sealing. Using the propagation uncertainty law, uncertainty analysis of partial above mentioned factors have been made as well their impact on the expanded uncertainty in 1/3 octave bands and sound reduction index Rw. The analysis indicates the most influential factors on the final accuracy of measurements, including the impact of deviations from ISO standards, especially the reduced size of the sample and increased the reverberation time.

⋆ ⋆ ⋆

Methods of cognitive categorization for analysis of pathological speech

Wszołek Wiesław

AGH University of Science and Technology
Faculty of Mechanical Engineering and Robotics
al. A. Mickiewicza 30, 30-059 Kraków, Poland

The presented article discusses the results of studies aimed at an attempt to systematize the methods used in construction of intelligent systems for medical diagnosis, based on the analysis of acoustic speech signal. New, original acoustic speech signal parameters have been proposed (called relative power coefficients), which introduce additional information concerning the changes of the voice channel parameters (treated as a sound source), and manifested by deformations of the speech signal. A new, original approach has been presented, based on the concept of automatic understanding. In general the understanding is distinguished from recognition by the fact that it is strongly knowledge based. In the meaning considered here the term"automatic understanding" denotes such an analysis of the deformed speech signal, which is oriented towards revealing the origins of the observed signal deformations. The practical importance of the cognitive methodology proposed in the paper follows from the growing importance of correct diagnosis for a wide variety of pathologies, manifesting by improper structure of the speech signal produced by the examined patient. In principle the problem is mainly of medical nature, but it seems also plausible to have in mind its social aspects.

⋆ ⋆ ⋆

A self-organizing map in supporting air traffic noise monitoring systems

Wszołek Wiesław
Kłaczyński Maciej
Batko Wojciech

AGH University of Science and Technology
Faculty of Mechanical Engineering and Robotics
al. A. Mickiewicza 30, 30-059 Kraków, Poland

Acoustic phenomena generated by various systems (biological, technical, related to environment, etc.) can be relatively precisely recorded and investigated by extracting acoustic parameters. However, at attempts of practical applications a large number of difficulties – related to the interpretation of recorded data according to the practical needs – arise. Tasks of analysis and recognition of sound signals, which – as a residual process – are emitted by technical objects are very difficult. Standard methods of processing and classification of acoustic signals applied in diagnostics are disappointing in all problems, in which we have to assess the noise arduousness, not the noise itself. Application of an artificial intelligence can be included in those information methods, which are able to combine the possibilities of the traditional acoustic measurements technique with the requirements of modern monitoring systems of air noises. The concept of the application of advance d methods of artificial intelligence as analytical tools at monitoring air traffic noises – is presented in the hereby paper.

⋆ ⋆ ⋆

Efficient phantom source widening

Zotter Franz
Frank Matthias

University of Music and Performing Arts
Institute of Electronic Music and Acoustics
Leonhardstraße 15, 8010 Graz, Austria

A suitably controlled pair of loudspeakers symmetrically arranged with regard to the listener allows to create an auditory event of adjustable width. This auditory event, the so-called phantom source, is usually narrowest when both loudspeakers are driven with the same signal. It is generally known that the phantom source can be adjusted to a variable direction in between the loudspeakers by controlling broadband time-delay and/or level differences of the loudspeaker signals. Moreover, the literature about (pseudo-)stereophony describes that nonuniform level differences or time-delay differences over frequency are suitable to widen the phantom source. A recently presented time-delay based method seems to be efficient, but seems to be restricted to the central listening spot. This contribution investigates an alternative comb filter structure that creates pure level differences instead and compares the time-delay and level-difference based approaches on central and shifted listening positions based on the interaural cross correlation coefficient and third-octave levels to assess coloration.

⋆ ⋆ ⋆